Microscopic 2D-Modeling of Driver Behavior based on Trajectory Data from Real Traffic, Driving Simulation and Traffic Simulation

Von der Fakultät für Bauingenieurwesen
der Rheinisch-Westfälischen Technischen Hochschule Aachen
zur Erlangung des akademischen Grades eines Doktors der Ingenieurwissenschaften
genehmigte Dissertation

vorgelegt von

Moritz Berghaus

Berichter: Universitätsprofessor Dr.-Ing. habil. Markus Oeser
Universitätsprofessor Dr. rer. nat. Michael Herty
Universitätsprofessor Dr. Alvaro García Hernandez

Tag der mündlichen Prüfung: 26.09.2025

Acknowledgments

This dissertation was written during the time of my employment at the Institute of Highway Engineering at RWTH Aachen University.

First and foremost, I would like to express my sincere gratitude to my supervisor, Prof. Markus Oeser, for his invaluable input, his continued trust in me, and his motivating words — even beyond his tenure as head of the institute. His guidance has played a crucial role throughout my doctoral journey. I am also deeply grateful to Prof. Michael Herty for agreeing to serve as the second examiner of this dissertation and for the many stimulating discussions we shared over the years as part of our collaboration in two research projects. I would like to thank Prof. Alvaro Garcia Hernandez, who succeeded Prof. Oeser as head of the institute, for giving me the freedom to continue working on my research topics and for the trust he placed in me during this time. I also wish to thank the project partners with whom I had the pleasure to collaborate during the research projects in the context of which this dissertation was developed: Niklas Kolbe, Anna-Lena Köhler, Vincent de Waal and Giuseppe Visconti.

I am very grateful to my former colleagues at the institute for the strong sense of community and team spirit — both professionally and personally — that made working there such a rewarding and enjoyable experience. A special thanks goes to my research group leaders Adrian, Serge and Dirk for their support, guidance, and encouragement along the way.

To my parents, Bärbel and Friedrich, I owe my deepest thanks for making it possible for me to pursue higher education and for sparking my interest in science from an early age. Your constant support has been the foundation of everything I have achieved.

Above all, my greatest thanks go to my partner Hannah. Her incredible support during the final and most intense years of this journey — her patience, her understanding, and her ability to carry me through moments of stress — meant more to me than words can express. Thank you for always being there.

Abstract

Microscopic traffic flow models are an essential tool for understanding how driver behavior influences the safety and efficiency of road traffic, and how road infrastructure can be designed to support safe and efficient driving behavior.

Microscopic traffic flow models describe a vehicle's trajectory in two dimensions - longitudinal and lateral - depending on surrounding traffic and road layout. To reduce modeling complexity, different model types focus on specific influencing factors. Car-following models primarily consider the effect of the leading vehicle on driver behavior, without accounting for road layout or vehicles in adjacent lanes. Speed prediction models describe speed choice based on road geometry, without incorporating surrounding traffic. Lane change models capture driver behavior before and during lane changes, taking into account vehicles in the current and adjacent lanes, but not the road layout.

To calibrate and validate microscopic traffic flow models, various sources of trajectory data can be used. Real-world trajectory data yield the most realistic representation of actual driving behavior, but they do not allow for the study of behavior under controlled conditions. Driving simulator data, on the other hand, make it possible to investigate such controlled conditions. Additionally, synthetic trajectory data from traffic simulations can be used to analyze model properties under idealized or specific conditions.

This dissertation investigates how trajectory data from real-world driving, driving simulation, and traffic simulation can contribute to more accurate modeling of driver behavior in two dimensions. The overarching research question is divided into five sub-questions, each addressing specific challenges associated with individual model types and data sources. For car-following models, a calibration and validation method was developed that enables the investigation of individual differences between drivers as well as their behavior in extreme traffic situations using a driving simulator. A speed prediction model was applied to evaluate a speed reduction measure in freeway off-ramps based on real-world trajectory data. For the modeling of driver behavior in freeway on-ramps, a lane change model was developed and validated using both real-world and simulated trajectory data. Furthermore, data processing methods and quality assessment procedures were developed for real-world trajectory data, enabling their use in real-time applications as well as for model calibration and validation.

The models and methods developed in this dissertation can be applied in traffic simulations to predict traffic conditions, evaluate planned infrastructure or traffic control measures, or assess the impact of automated driving on traffic flow and safety. They thus make a valuable contribution towards the development of safe, efficient, and future-ready road systems.

Kurzfassung

Mikroskopische Verkehrsflussmodelle sind ein zentrales Werkzeug, um zu verstehen, wie das Verhalten der Fahrer*innen die Sicherheit und Effizienz des Straßenverkehrs beeinflusst, und wie die Straßeninfrastruktur so gestaltet werden kann, dass sie sicheres und effizientes Fahrverhalten fördert.

Mikroskopische Verkehrsflussmodelle beschreiben die Trajektorie eines Fahrzeugs in zwei Dimensionen - Längs- und Querrichtung - in Abhängigkeit vom umgebenden Verkehr und dem Straßenverlauf. Um die Komplexität der Modellierung zu reduzieren, konzentrieren sich verschiedene Modelltypen auf unterschiedliche Einflussgrößen. Bei Fahrzeugfolgemodellen liegt der Fokus auf dem Einfluss des vorausfahrenden Fahrzeugs auf das Fahrverhalten ohne Berücksichtigung des Straßenverlaufs und der Fahrzeuge auf benachbarten Fahrstreifen. Geschwindigkeitsvorhersagemodelle beschreiben die Wahl der Geschwindigkeit in Abhängigkeit vom Straßenverlauf ohne den Einfluss des umgebenden Verkehrs. Fahrstreifenwechselmodelle beschreiben das Fahrverhalten vor und während eines Fahrstreifenwechsels unter Berücksichtigung der Fahrzeuge auf dem aktuellen und dem benachbarten Fahrstreifen.

Zur Kalibrierung und Validierung von mikroskopischen Verkehrsflussmodellen können Trajektoriendaten aus verschiedenen Quellen genutzt werden. Trajektoriendaten aus dem realen Verkehr bilden das Fahrverhalten am realistischsten ab, sie ermöglichen jedoch keine Untersuchung des Fahrverhaltens unter kontrollierten Bedingungen. Hierfür sind Trajektoriendaten aus dem Fahrsimulator geeignet, wo solche kontrollierten Bedingungen hergestellt werden können. Um die Eigenschaften von Verkehrsflussmodellen zu untersuchen, können Trajektoriendaten aus Verkehrssimulationen genutzt werden.

In dieser Dissertation wurde untersucht, wie Trajektoriendaten aus realem Verkehr, Fahrsimulation und Verkehrssimulation zu einer genaueren Modellierung des Fahrverhaltens in zwei Dimensionen beitragen können. Diese übergeordnete Forschungsfrage wurde in fünf Teilfragen untergliedert, in denen die spezifischen Herausforderungen der einzelnen Modelltypen und Datenquellen genauer betrachtet wurden. Für Fahrzeugfolgemodelle wurde eine Kalibrierungs- und Validierungsmethode entwickelt, mit der im Fahrsimulator sowohl individuelle Unterschiede zwischen Fahrer*innen als auch ihr Verhalten in extremen Verkehrssitu-

ationen untersucht werden konnten. Mit Hilfe eines Geschwindigkeitsvorhersagemodelles wurde eine Maßnahme zur Geschwindigkeitsreduktion in Autobahnausfahrten anhand von Trajektoriendaten aus realem Verkehr evaluiert. Zur Beschreibung des Fahrverhaltens in Autobahnauffahrten wurde ein Fahrstreifenwechselmodell entwickelt und anhand von Trajektoriendaten aus realem Verkehr und Verkehrssimulationen validiert. Für Trajektoriendaten aus realem Verkehr wurden außerdem Methoden zur Datenbearbeitung und Bewertung der Datenqualität entwickelt, die eine Nutzung der Daten sowohl für Echtzeit-Anwendungen als auch für die Modellkalibrierung und -validierung ermöglichen.

Die in dieser Dissertation entwickelten Modelle und Methoden können beispielsweise in Verkehrssimulationen zur Vorhersage der Verkehrslage, zur Bewertung geplanter Infrastruktur- oder Verkehrssteuerungsmaßnahmen oder zur Abschätzung der Auswirkungen des automatisierten Fahrens auf den Verkehrsfluss und die Verkehrssicherheit angewendet werden. Sie leisten somit einen wichtigen Beitrag zur Entwicklung sicherer, effizienter und zukunftsfähiger Straßen.

Contents

1 Introduction

1.1 Motivation

Traffic systems fulfill a fundamental human need: the ability to travel from one place to another. However, traffic also has significant negative effects in terms of crashes, environmental impacts, and traffic jams. All these effects are associated with substantial socio-economic costs. To reduce these impacts, traffic systems must be designed to be as safe and efficient as possible. To this end, traffic flow models, also known as driver behavior models, are an important tool to understand how the behavior of the system's users (drivers, cyclists, pedestrians etc.) impacts the safety and efficiency of the entire system and, vice versa, how the traffic system can be designed to induce safe and efficient behavior. With almost 3,000 fatalities on German roads [1], approximately 500,000 traffic jams on German freeways [2], and 150 million tons of traffic-related CO_2-equivalent emissions in Germany every year [3], it becomes clear that road traffic still faces major challenges. These challenges demonstrate the significant need for research in the field of traffic flow models.

Traffic flow models are used for various applications. In the short term, they predict the traffic conditions on a specific road or a road network in response to fluctuations in traffic demand or disruptions such as crashes or work zones. This information helps road operators implement appropriate traffic management measures, such as variable speed limits or detour recommendations, and allows road users to plan their routes and estimate arrival times. In the long term, traffic flow models are essential for traffic simulations, which assist in the assessment of planned changes in the road infrastructure in terms of safety and efficiency. Thus, traffic flow models enable an economical infrastructure that is neither underutilized nor congested. Traffic flow models also play a crucial role in the context of automated driving. To behave safely and efficiently in all conceivable traffic situations, automated vehicles require an integrated traffic flow model. The development of such automated driving features relies on learning from human driving behavior. With traffic flow models for human drivers and automated vehicles, the impact of an increasing spread of automated vehicles on traffic safety and efficiency can be analyzed.

Vehicles move on a two-dimensional road surface, which means that traffic flow must be

modeled in two dimensions. Both the surrounding vehicles and the road layout influence driver behavior and should therefore be taken into account in a traffic flow model. To reduce complexity, models usually focus on one of these elements. Car-following models [4], for example, focus on the influence of the preceding vehicle ("leader") on the driver behavior, neglecting the road layout and the vehicles in adjacent lanes. Speed prediction models [5], on the other hand, describe the influence of the road layout on the speed of vehicles, neglecting surrounding traffic. Lane change models [6] focus on the driver behavior before and during a lane change taking into account surrounding vehicles in both the current and the adjacent lane, but neglecting the road layout. Lane change models are often integrated with car-following models.

The choice of the most suitable model type depends on the specific road section being analyzed. For straight road sections between intersections with few lane changes, car-following models are most suitable. Car-following models are well advanced compared to the other two model types. However, they might not capture driver behavior in risky situations accurately, for example when the leader suddenly brakes. For curved road sections with little traffic, e.g. freeway off-ramps[1], speed prediction models are most suitable. The main challenge of this model type is isolating the effect of the curve on vehicle speed from other factors such as weather, daylight and traffic conditions. As such, speed prediction models are crucial for evaluating the effectiveness of speed reduction measures. For road sections with frequent lane changes, e.g. freeway on-ramps[2], lane change models are most suitable. Modeling lane changes at on-ramps can be complex due to the large speed differences and short time headways, which are associated with risky behavior that differs from typical car-following behavior.

The development and validation of traffic flow models relies on data regarding driver behavior. Advances in sensor and computer vision technologies in recent years have made detailed trajectory data from real traffic more accessible, thereby supporting the development of new models and the evaluation of existing models. In real traffic, however, driver behavior cannot be measured under controlled conditions. To study driver behavior in specific scenarios that might not be included in real-world data, data from driving simulators are useful. Driving simulator studies also enable the analysis of individual differences in driver behavior and the impact of these differences on traffic flow. Furthermore, the properties of traffic flow models can be explored in traffic simulations, where controlled conditions can also be created. These three data sources – real traffic data, driving simulator data, and traffic simulations – complement each other in the development and validation of traffic flow models.

Despite the technological advances in trajectory data collection, the data quality remains

[1] British English: motorway exit or motorway slip road

[2] British English: motorway access or slip road

a significant challenge. False positive or false negative detections of vehicles result in incomplete trajectories, while inaccurate detections lead to position errors, which multiply when speed and acceleration are computed from the positions. To improve data quality, traditional processing techniques like smoothing or filtering can be applied, along with assumptions on the physical plausibility of vehicle movements. Data processing is particularly challenging when information from the trajectories needs to be extracted in real-time, e.g. for adaptive speed reduction measures, as only past data points are available in real-time applications.

1.2 State of the Art

In the context of road traffic, driving behavior can be defined as the driver's response to both external stimuli, such as the road conditions and surrounding traffic, and internal stimuli, including the driver's experience, skills and personality. These response manifest through actions like pressing the gas or brake pedal and moving the steering wheel. These actions are often described using kinematics, focusing on the resulting movements of the vehicle rather than the driver's direct actions. The movement of a vehicle's position over time is referred to as its *trajectory*. Thus, the most intuitive way to model driving behavior is by representing a vehicle's trajectory as a function of the external and internal stimuli mentioned above. Since this approach focuses on individual vehicles, it is called microscopic. Although a trajectory is a time-continuous function, it is typically discretized into time steps for most applications.

For macroscopic models, on the other hand, multiple trajectories are aggregated over time and space. As a result, traffic is considered as a fluid with properties such as flow, density and (average) velocity [7]. This approach can be more practical for certain applications for three main reasons. First, macroscopic traffic properties are easier to measure than individual vehicle trajectories. However, recent advancements in computer vision and sensor technology have significantly increased the availability of trajectory data that can be used to develop microscopic driver behavior models. Second, macroscopic models are more computationally efficient, which is relevant for modelling large-scale road networks. Third, the efficiency of a traffic system is typically defined by the capacity, which is the maximum achievable flow, i.e. a macroscopic property. Microscopic models, in contrast, may introduce biases when predicting macroscopic properties like capacity, as small inaccuracies in trajectory predictions can accumulate at the macroscopic scale. However, this effect can be mitigated if the microscopic model is calibrated and/or validated at the macroscopic scale.

1.2.1 Microscopic Models

Due to the complexity of the external and internal stimuli influencing driving behavior, different microscopic models focus on different stimuli. **Car-following models** describe the longitudinal component of a vehicle's trajectory depending on the vehicle directly ahead. Hence, the influence of all other surrounding vehicles is neglected. All other external and internal stimuli are incorporated into model parameters, such as desired speed or maximum acceleration. These parameters are constant within a limited road section and can be either constant for all drivers (deterministic) or different for each individual driver (stochastic). The model equations of car-following models are derived from different assumptions. Only the most important models or classes of models are described in the following. The **Optimal Velocity Model** is based on the assumption that the velocity of a vehicle is a function of the distance to its leader [8]. In its simplest form, the velocity increases linearly with the distance, up to the desired speed. The **Safety Distance Models**, e.g. Gipps' model, assume that drivers select their speed such that there is a positive minimum distance if the leader suddenly performs an emergency braking and the follower reacts with an emergency braking after some reaction time [9]. **Social Force Models** (or generalized force models) are based on the assumption that vehicles are subject to different forces that define the movement of the vehicle, e.g. a repulsive force by other vehicles [10]. **Psycho-physical Models**, e.g. the Wiedemann model, assume that drivers cannot perfectly estimate their own speed and the distance to the leader, leading to fluctuations around an equilibrium speed and distance [11].

Speed prediction models describe the trajectory of a vehicle depending on the road layout and other environmental conditions. Hence, the influence of traffic is neglected, and it is assumed that vehicles drive on an empty road. Whilst car-following models are primarily kinematic models, speed prediction models are mostly data-driven predictive models with curvature, gradient etc. as input variables and speed as output variable. Internal stimuli, e.g. the vehicle type, can be incorporated as additional input variables. Various statistical and machine learning techniques including Mixed Effect Models [5] and Deep Learning [12] have been used in the literature to develop this model type.

Lane change models describe the lateral component of a vehicle's trajectory. When combined with a car-following model, they can describe the complete vehicle trajectory in two dimensions. These models account for the influence of all other surrounding vehicles (leader in the current lane as well as the leader and follower in adjacent lanes). Other external and internal stimuli are incorporated into model parameters, some of which overlap with those in car-following models. However, the values of the parameters may differ, as driver behavior during lane changes differs from standard car-following behavior. Lane change models

usually focus on the decision of whether or not to initiate a lane change. This decision can be modelled with different approaches, including game theory [13], logistic regression [14] or neural networks [15].

1.2.2 Trajectory Data

Empirical trajectory data play a crucial role in the development and validation of traffic flow models, particularly microscopic models. One of the most widely used datasets is the NGSIM (Next Generation Simulation) dataset collected on freeways in the United States, which has been the foundation for numerous studies on traffic flow. Subsequently, several studies have analyzed the quality of the NGSIM data and proposed methods for detecting and correcting implausible data [16–18]. Trajectory data quality is primarily affected by two main sources of error. The first source is inaccurate position measurements, i.e. when the detected vehicle position deviates from the true position. These errors propagate if the speed and acceleration is calculated from the position. To mitigate this, trajectory data must be smoothed. However, the challenge is that over-smoothing the trajectories inhibits the detection of short-term acceleration changes, making it difficult to capture sudden driving maneuvers. The second source of error is false positive or false negative detections, which lead to incomplete trajectories. They often result from occlusions by other vehicles or a small contrast between vehicle and the road surface in the background. Addressing these challenges is essential for ensuring reliable trajectory data, which in turn improves the accuracy of traffic flow models.

In recent years, an increasing number of trajectory datasets have become available. These datasets are mostly extracted from camera images using deep learning methods such as Yolo [19] or Mask R-CNN [20]. Additionally, light detection and ranging (LiDAR) [21] and radar sensors [22] can be used to detect vehicles and extract their trajectories. Compared to cameras, the strength of LiDAR lies in the three-dimensional detection of vehicles, which allows for a better vehicle classification. The strength of radar lies in the high accuracy of the speed measurement based on the Doppler effect. Nevertheless, cameras are the most widely used method due to their cost-efficiency and the advanced developments in image recognition technology.

1.2.3 Calibration and Validation of Microscopic Models

Model calibration aims to optimize the model parameters that reflect driver behavior by minimizing the model's prediction error. The literature on this topic discusses three main aspects, which must be considered in the calibration procedure. First, the objective function, i.e. the quantity to be minimized, must be defined. Common quantities include the headway error,

velocity error, or acceleration error [23, 24]. The second aspect is the decision whether the model is calibrated locally or globally. In a local calibration, the model errors are assessed at each time step individually, whilst in a global calibration, the model errors are accumulated over multiple time steps [25–27]. The third aspect concerns the completeness of the dataset, which means that the dataset should include both free-flow and congested traffic conditions for a more comprehensive calibration [28].

Model validation aims to demonstrate that the model accurately represents the characteristics of real traffic. These characteristics can be either macroscopic or microscopic. Macroscopic validation focuses on large-scale traffic characteristics including flow, density and mean speed. Microscopic validation ensures that individual driver behavior, such as accelerations, gaps between vehicles or lane-change decisions, aligns with empirical trajectory data [29–31].

1.2.4 Influences on Driver Behavior

Driver behavior is influenced by a complex interplay of external and internal stimuli. External stimuli include factors such as traffic conditions, road layout, and environmental conditions, while internal stimuli include human factors and vehicle properties. Depending on the model type, these stimuli are either considered as a constant or variable input.

The influence of traffic conditions on driver behavior can be categorized into longitudinal and lateral traffic. Longitudinal traffic refers to other vehicles within the same lane. If the preceding vehicle maintains a constant speed, the following vehicle intends to match that speed while keeping a constant distance, which depends on the speed. If the preceding vehicle accelerates or decelerates, the following vehicle responds by adjusting its speed accordingly. Lateral traffic becomes relevant in three different situations. First, if a vehicle can increase its speed by changing lanes (tactical lane change), it will take into account the speeds and distances of vehicles in the adjacent lane to decide whether to initiate a lane change. Second, if a vehicle cannot continue its route on its current lane, e.g. because the current lane ends (mandatory lane change), it will also take into account the vehicles in the adjacent lane to plan a lane change. Third, if a vehicle obstructs the lane change of another vehicle, it may facilitate this lane change by performing a lane change itself (courtesy lane change) [32].

The road layout affects the driver behavior mainly through the desired speed of the driver. The desired speed increases with the lane width, as wider lanes provide additional margin for lateral position variations, which are associated with larger speeds [33]. Narrow lanes also discourage some drivers from passing other vehicles, particularly in road work zones [34]. Small curve radii also reduce the desired speed due to the lateral forces, which are increasing with the square of the speed and are limited by the friction between tires and road

[35]. Additionally, the road gradient can impact both the desired speed and the maximum acceleration due to limited engine power [36, 37]. As a result, the road layout can contribute to the formation of a bottleneck, where congestion can occur [38].

Environmental conditions include weather, daylight, and road surface quality. Rainy conditions reduce desired speeds due to wet road surfaces and decreased visibility. The longer braking distances associated with wet road surfaces also require larger time headways between vehicles [39]. Similarly, drivers tend to adopt smaller desired speeds at night due to limited visibility [40]. Additionally, damages in the road surface such as potholes might cause abrupt speed reductions [41].

Human factors are the main reason why different drivers behave differently even under identical external conditions. Age and driving experience significantly impact driver behavior. Young drivers tend to take more risks, which corresponds to larger desired speeds or smaller time headways [42], whereas old drivers drive more cautiously but typically have longer reaction times [43]. Gender is another factor that influences driver behavior, with men generally driving more riskily than women [44]. Additionally, personality and emotions, such as stress or anger, can also affect driver behavior [45]. These human factors play an important role in the overall heterogeneity of traffic. However, integrating human factors into traffic flow models is challenging, as different model parameter values, which can also be time-dependent, must be assigned to each driver. Driver heterogeneity can be studied in driving simulator studies, where a good correlation between self-reported and observed driver behavior has been found [46]. This finding contributes to the validity of driving simulator studies.

Vehicle properties also contribute to the heterogeneity of traffic. In some situations, not the desired speed or maximum acceleration of the driver is the limiting factor, but the power of the vehicle engine. A key example is the difference in maximum speeds between cars and trucks. For modelling purposes, the vehicle length is also relevant, although it does not directly influence the driver behavior. Traffic flow models typically require the net gap between two vehicles, whilst only the gross gap can be derived from trajectory data if the vehicle length is unknown.

1.3 Research Objectives

Building on the motivation and the introduction to the relevant state of the art, the research question of this thesis can be formulated.

How can trajectory data from real traffic, driving simulation, and traffic simulation contribute to model driver behavior in two dimensions more accurately?

This overarching research question addresses multiple dimensions of driver behavior mod-

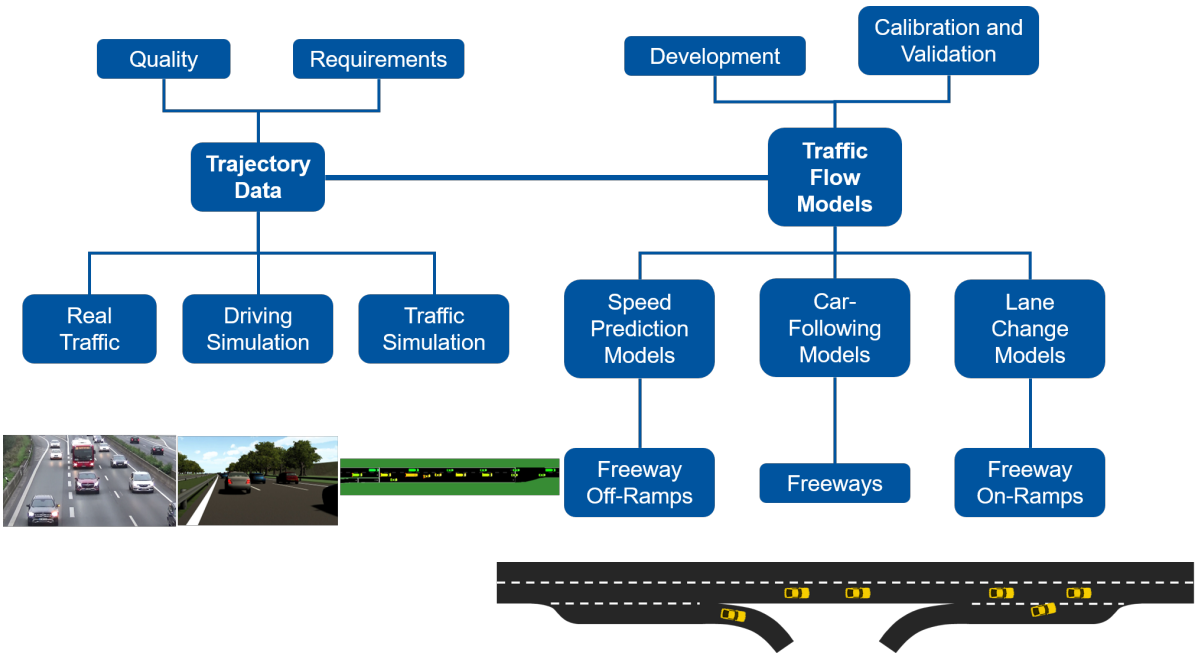

Figure 1.1: Overview of the research framework of this thesis with different data sources, model types and modeling approaches.

eling by incorporating trajectory data from three different sources, as well as three different types of traffic flow models and their development, calibration, and validation (see Figure 1.1). However, a comprehensive investigation of all potential data sources, model types, and modeling stages would exceed the scope of a single dissertation. Therefore, the overarching research question is divided into five selected sub-questions, each addressing specific research gaps in the field of driver behavior modeling and trajectory data. Three of these sub-questions cover a specific combination of data source, model type, and modeling stage, while two sub-questions focus solely on data, specifically their quality and the requirements they must fulfill.

The five sub-questions, which are addressed in the following chapters of this thesis, are as follows:

1. How can car-following models be calibrated based on trajectory data from driving simulations and what are the benefits of this type of data?

2. What are the requirements for trajectory data from real traffic when used in real-time applications?

3. How can the effectiveness of a speed reduction measure be evaluated using a speed prediction model based on trajectory data from real traffic?

Table 1.1: Mapping of the sub-questions to aspects of the overarching research question.

Sub-Question		1	2	3	4	5
Trajectory Data	Real Traffic		X	X	X	X
	Driving Simulation	X				
	Traffic Simulation					X
	Quality				X	
	Requirements		X			
Traffic Flow Models	Car-Following Model	X				
	Speed Prediction Model			X		
	Lane Change Model					X
	Development			X		X
	Calibration and Validation	X		X		X

4. How can the quality of trajectory data from real traffic be improved and evaluated?

5. How can lane changes at on-ramps be modeled more accurately and how can this lane change model be validated using trajectory data from real traffic and traffic simulations?

Table 1.1 provides an overview of which aspects of the overarching research question are addressed in each sub-question.

1.4 Methodology

In the following, the motivation to divide the overarching research question into these sub-questions and the methodology to address these sub-questions are elaborated on.

1.4.1 Sub-Question 1

This sub-question focuses on **car-following models** for **freeways** and their **calibration** using **trajectory data from driving simulations**. The large number of different car-following models in the literature suggests that the primary research need in this field is to evaluate and refine existing models rather than developing new models. While numerous studies assess whether car-following models can reproduce different properties of the efficiency of traffic flow, such as the Capacity Drop, fewer studies focus on their ability to reproduce the frequency and severity of risky driving situations. If car-following models are to be used for road safety analyses, they must be valid not only in regular car-following situations, but also in risky situations,

for example if the leader suddenly brakes or if a vehicle from an adjacent lane is suddenly cutting in. These situations are not included in data from real traffic, and they cannot be provoked in real traffic. Instead, driving simulations, where crashes do not have any consequences, allow for the creation and controlled study of such situations. Furthermore, trajectory data from driving simulators are useful to analyze how properties of drivers (internal stimuli) influence the driver behavior. To address this, a **driving simulator study** is conducted in which participants drive on freeways and encounter one of the risky situations mentioned above. The trajectories of the participants and their leaders are recorded and used to **calibrate four different car-following models** with individual parameter values for each participant. **Statistical tests** are then applied to identify significant relationships between driver characteristics and car-following model parameters.

1.4.2 Sub-Question 2

This sub-question focuses on the **requirements for trajectory data from real traffic** if these data must be available in real-time. A possible application is a speed reduction measure at a **freeway off-ramp** that influences drivers individually only if they are driving unsafely. To implement such a measure, this unsafe behavior must be identified in real-time. This requires the speed and the position of vehicles, i.e. the trajectory, in real-time. To capture the trajectories of vehicles, the vehicles must be detected by sensors, e.g. cameras. Computer vision algorithms yield the positions of vehicles in image coordinates. These image coordinates must then be converted into world coordinates using a **rotation matrix and translation vector**. Since traffic engineers are usually interested in vehicle positions relative to the road, the world coordinates must be converted into local road coordinates. The road geometry as a continuous function is obtained from discrete measurement points using **polynomial regression**. The **Newton-Raphson method** is then applied to transform the vehicle positions from world coordinates into local road coordinates.

To compensate for measurement errors, the resulting trajectories must be processed. While previous studies on processing of trajectory data have only focused on post-processing, real-time processing presents additional challenges. The key difference is that post-processing utilizes trajectory data from all time steps, allowing for an effective smoothing of position inaccuracies. In contrast, real-time processing can only use past time steps, limiting the ability to correct position errors. As a result, the speeds, which are computed from the positions using a **moving average filter**, might be less accurate. Another challenge arises if the trajectories are gathered by more than one camera, and if the fields of vision of these cameras do not overlap. In this case, the speeds are also required to extrapolate the position of the vehicle

when it is between the fields of vision.

1.4.3 Sub-Question 3

This sub-question focuses on the **development, calibration, and validation** of a **speed prediction model** based on **trajectory data from real traffic**. The speed prediction model is applied to evaluate a speed reduction measure on a **freeway off-ramp**. To evaluate the measure, it is not sufficient to compare the mean speed with and without the measure because the speed of a vehicle is affected by multiple external factors including weather, daylight or traffic conditions. To account for these factors, a speed prediction model is required, which describes the speed as a function of the position. With this model, the speeds with and without the measure can be compared. The trajectory data used to calibrate the model are processed by **fitting a smoothing spline** to the position measurements and removing incomplete and implausible trajectories. The other influencing variables are pre-processed using **mean centering** and **dummy coding**. The speed prediction model is then built as a **multiple linear regression model** with weather, daylight, traffic conditions, and scenario (variant of the speed reduction measure) as input variables, and speed as an output variable. The coefficients of the scenario variable provide an estimate of the speed reduction effect.

1.4.4 Sub-Question 4

This sub-question focuses on evaluating and improving the **quality of trajectory data from real traffic**. Unlike in the second sub-question, the focus is on the use of trajectory data for traffic flow models. Before trajectory data can be used for the development and validation of traffic flow models, its accuracy and plausibility must be assured. Whilst there are standardized metrics for evaluating the performance of computer vision methods on image level, no such metric exists at the trajectory level. False detections on image level can be identified at the trajectory level because they often produce physically unrealistic trajectories. By **detecting and removing** these **outliers** and by **fitting a smoothing spline** to the remaining position measurements, plausible trajectories with realistic velocities and accelerations are obtained. Additionally, the accuracy of velocities and accelerations is evaluated by **benchmarking against reference sensors** (induction loops and vehicle-based accelerometer).

1.4.5 Sub-Question 5

This sub-question focuses on **lane change models** for **freeway on-ramps**. A lane change model is **developed, calibrated, and validated** based on **trajectory data from real traf-**

fic, and its properties are analyzed through **traffic simulations**. Whilst car-following models are well-established and extensively validated, lane change models still have substantial limitations, particularly in the modeling of complex merging behavior at freeway on-ramps. To address this gap, there is a need for a novel traffic flow model for on-ramps. This model must describe both longitudinal and lateral behavior, i.e. it must be a combined car-following and lane change model. The model is **derived from kinematic equations** that describe the time headway between the merging vehicle and its leader. The principles of car-following models and their calibration are adapted to the lane change model. The calibration of the model parameters is conducted by means of **optimization algorithms**. Additionally, a **sensitivity analysis** is performed to assess the robustness of the calibrated parameters. Different **microscopic and macroscopic traffic parameters from real traffic and simulated traffic** are then compared to validate the model.

1.5 Thesis Structure

The work presented in this thesis aims to contribute to a more accurate and applicable modeling of driver behavior in two dimensions based on trajectory data from different sources. Each model type and each data source bears different challenges and research gaps that this thesis addresses. The thesis is structured into five main chapters (Chapters 2 to 6), each corresponding to a peer-reviewed scientific article that covers one of the five sub-questions derived above.

Chapter 2 (Sub-Question 1) introduces a methodology for calibrating and validating car-following models for freeways based on trajectory data from driving simulations. The study explores two possible applications of this methodology. The first application is analyzing the influence of driver characteristics on driver behavior. The second application is investigating the driver behavior in extreme situations that are usually not included in trajectory data from real traffic.

Chapter 3 (Sub-Question 2) defines the requirements for trajectory data from real traffic in real-time applications. The study explores methods for real-time processing of trajectory data to ensure these requirements are met.

Chapter 4 (Sub-Question 3) presents a speed prediction model to evaluate a speed reduction measure for freeway off-ramps. This study describes the set-up and data collection method of the field test to investigate this speed reduction measure. It then describes the development and calibration of the speed prediction model considering multiple influences on driver behavior.

Chapter 5 (Sub-Question 4) examines the quality of trajectory data from real traffic and

presents a methodology to process the data in order to enhance its accuracy and reliability.

Chapter 6 (Sub-Question 5) presents a lane change model that describes the driver behavior at freeway on-ramps. This study describes the model development based on kinematic equations and introduces a methodology for calibrating and validating the model based on trajectory data from real traffic and traffic simulations.

The main chapters are followed by a conclusion (Chapter 7) that synthesizes the key findings and discusses potential directions for further research.

References

[1] Bundesministerium für Digitales und Verkehr. Straßenverkehrssicherheit - Alles tun für #DeinLeben: Jedes Opfer eines Verkehrsunfalls ist eines zu viel., 2025. URL https://bmdv.bund.de/DE/Themen/Mobilitaet/Strasse/Strassenverkehrssicherheit/strassenverkehrssicherheit.html.

[2] ADAC. ADAC Staubilanz 2024: So viel Stillstand gab es auf den Autobahnen, 2025. URL https://www.adac.de/news/staubilanz-2024/.

[3] Umweltbundesamt. Klimaschutz im Verkehr, 2024. URL https://www.umweltbundesamt.de/themen/verkehr/klimaschutz-im-verkehr.

[4] M. Treiber, A. Hennecke, and D. Helbing. Congested traffic states in empirical observations and microscopic simulations. *Physical Review E*, 62(2):1805–1824, 2000. ISSN 1063-651X. doi: 10.1103/PhysRevE.62.1805.

[5] H. Farah, W. Daamen, and S. Hoogendoorn. How do drivers negotiate horizontal ramp curves in system interchanges in the Netherlands? *Safety Science*, 119:58–69, 2019. ISSN 09257535. doi: 10.1016/j.ssci.2018.09.016.

[6] W. J. Schakel, V. L. Knoop, and B. van Arem. Integrated Lane Change Model with Relaxation and Synchronization. *Transportation Research Record: Journal of the Transportation Research Board*, 2316(1):47–57, 2012. ISSN 0361-1981. doi: 10.3141/2316-06.

[7] G. Bretti, R. Natalini, and B. Piccoli. A Fluid-Dynamic Traffic Model on Road Networks. *Archives of Computational Methods in Engineering*, 14(2):139–172, 2007. ISSN 1134-3060. doi: 10.1007/s11831-007-9004-8.

[8] M. Bando, K. Hasebe, A. Nakayama, A. Shibata, and Y. Sugiyama. Dynamical model of traffic congestion and numerical simulation. *Physical Review E*, 51(2):1035–1042, 1995. ISSN 1063-651X. doi: 10.1103/PhysRevE.51.1035.

[9] P. G. Gipps. A behavioural car-following model for computer simulation. *Transportation Research Part B: Methodological*, 15(2):105–111, 1981. ISSN 01912615. doi: 10.1016/0191-2615(81)90037-0.

[10] D. Helbing and B. Tilch. Generalized force model of traffic dynamics. *Physical Review E*, 58(1):133–138, 1998. ISSN 1063-651X. doi: 10.1103/PhysRevE.58.133.

[11] R. Wiedemann. *Simulation des Straßenverkehrsflusses*, volume 8 of *Schriftenreihe des Instituts für Verkehrswesen der Universität Karlsruhe*. Karlsruhe, 1974.

[12] J. Lemieux and Y. Ma. Vehicle Speed Prediction Using Deep Learning. In *2015 IEEE Vehicle Power and Propulsion Conference (VPPC)*, pages 1–5. IEEE, 2015. ISBN 978-1-4673-7637-2. doi: 10.1109/VPPC.2015.7353037.

[13] H. Kita. A merging–giveway interaction model of cars in a merging section: a game theoretic analysis. *Transportation Research Part A: Policy and Practice*, 33(3-4):305–312, 1999. ISSN 09658564. doi: 10.1016/S0965-8564(98)00039-1.

[14] F. Marczak, W. Daamen, and C. Buisson. Merging behaviour: Empirical comparison between two sites and new theory development. *Transportation Research Part C: Emerging Technologies*, 36(4):530–546, 2013. ISSN 0968090X. doi: 10.1016/j.trc.2013.07.007.

[15] C. Dong, H. Wang, Y. Li, X. Shi, D. Ni, and W. Wang. Application of machine learning algorithms in lane-changing model for intelligent vehicles exiting to off-ramp. *Transportmetrica A: Transport Science*, 17(1):124–150, 2021. ISSN 2324-9935. doi: 10.1080/23249935.2020.1746861.

[16] B. Coifman and L. Li. A critical evaluation of the Next Generation Simulation (NGSIM) vehicle trajectory dataset. *Transportation Research Part B: Methodological*, 105:362–377, 2017. ISSN 01912615. doi: 10.1016/j.trb.2017.09.018.

[17] V. Punzo, M. T. Borzacchiello, and B. Ciuffo. On the assessment of vehicle trajectory data accuracy and application to the Next Generation SIMulation (NGSIM) program data. *Transportation Research Part C: Emerging Technologies*, 19(6):1243–1262, 2011. ISSN 0968090X. doi: 10.1016/j.trc.2010.12.007.

[18] T. T. Zhang, P. J. Jin, B. Piccoli, and M. Sartipi. Deep spatial–temporal embedding for vehicle trajectory validation and refinement. *Computer-Aided Civil and Infrastructure Engineering*, 39(11):1597–1615, 2024. ISSN 1093-9687. doi: 10.1111/mice.13160.

[19] X. Shi, D. Zhao, H. Yao, X. Li, D. K. Hale, and A. Ghiasi. Video-based trajectory extraction with deep learning for High-Granularity Highway Simulation (HIGH-SIM). *Communications in Transportation Research*, 1:100014, 2021. doi: 10.1016/j.commtr.2021.100014.

[20] A. Clausse, S. Benslimane, and A. de La Fortelle. Large-Scale extraction of accurate vehicle trajectories for driving behavior learning. In *2019 IEEE Intelligent Vehicles Symposium (IV)*, pages 2391–2396. IEEE, 2019. ISBN 978-1-7281-0560-4. doi: 10.1109/IVS.2019.8814095.

[21] C. Creß, W. Zimmer, L. Strand, V. Lakshminarasimhan, M. Fortkord, S. Dai, and A. Knoll. A9-Dataset: Multi-Sensor Infrastructure-Based Dataset for Mobility Research.

[22] J. Wang, T. Fu, J. Xue, C. Li, H. Song, W. Xu, and Q. Shangguan. Realtime wide-area vehicle trajectory tracking using millimeter-wave radar sensors and the open TJRD TS dataset. *International Journal of Transportation Science and Technology*, 12(1):273–290, 2023. ISSN 20460430. doi: 10.1016/j.ijtst.2022.02.006.

[23] A. Kesting and M. Treiber. Calibrating Car-Following Models by Using Trajectory Data. *Transportation Research Record: Journal of the Transportation Research Board*, 2088 (1):148–156, 2008. ISSN 0361-1981. doi: 10.3141/2088-16.

[24] V. Punzo and M. Montanino. Speed or spacing? cumulative variables, and convolution of model errors and time in traffic flow models validation and calibration. *Transportation Research Part B: Methodological*, 91:21–33, 2016. ISSN 01912615. doi: 10.1016/j.trb.2016.04.012.

[25] M. Treiber and A. Kesting. Microscopic Calibration and Validation of Car-Following Models – A Systematic Approach. *Procedia - Social and Behavioral Sciences*, 80:922–939, 2013. ISSN 18770428. doi: 10.1016/j.sbspro.2013.05.050.

[26] B. Ciuffo, V. Punzo, and V. Torrieri. Comparison of Simulation-Based and Model-Based Calibrations of Traffic-Flow Microsimulation Models. *Transportation Research Record: Journal of the Transportation Research Board*, 2088(1):36–44, 2008. ISSN 0361-1981. doi: 10.3141/2088-05.

[27] L. Li, X. Chen, and L. Zhang. A global optimization algorithm for trajectory data based car-following model calibration. *Transportation Research Part C: Emerging Technologies*, 68:311–332, 2016. ISSN 0968090X. doi: 10.1016/j.trc.2016.04.011.

[28] A. Sharma, Z. Zheng, and A. Bhaskar. is more always better? the impact of vehicular trajectory completeness on car-following model calibration and validation. 2019.

[29] M. Treiber and A. Kesting. validation of traffic flow models with respect to the spatiotemporal evolution of congested traffic patterns. 2012.

[30] E. Brockfeld, R. D. Kühne, and P. Wagner. Calibration and Validation of Microscopic Models of Traffic Flow. *Transportation Research Record: Journal of the Transportation Research Board*, 1934(1):179–187, 2005. ISSN 0361-1981. doi: 10.1177/0361198105193400119.

[31] M. Kontorinaki, A. Spiliopoulou, C. Roncoli, and M. Papageorgiou. first-order traffic flow models incorporating capacity drop: Overview and real-data validation. 2017.

[32] V. Knoop. *Introduction to Traffic Flow Theory*. Delft University of Technology, 2nd edition edition, 2018.

[33] S. Liu, J. Wang, and T. Fu. effects of lane width, lane position and edge shoulder width on driving behavior in underground urban expressways: A driving simulator study. 2016.

[34] S. Yousif, Z. Nassrullah, and S. H. Norgate. Narrow lanes and their effect on drivers' behaviour at motorway roadworks. *Transportation Research Part F: Traffic Psychology and Behaviour*, 47:86–100, 2017. ISSN 13698478. doi: 10.1016/j.trf.2017.04.016.

[35] C. Dias, T. Oguchi, and K. Wimalasena. Drivers' Speeding Behavior on Expressway Curves: Exploring the Effect of Curve Radius and Desired Speed. *Transportation Research Record: Journal of the Transportation Research Board*, 2672(17):48–60, 2018. ISSN 0361-1981. doi: 10.1177/0361198118778931.

[36] S. Yagar and M. van Aerde. Geometric and environmental effects on speeds of 2-lane highways. *Transportation Research Part A: General*, 17(4):315–325, 1983. ISSN 01912607. doi: 10.1016/0191-2607(83)90094-8.

[37] H. Liu, M. O. Rodgers, and R. Guensler. The impact of road grade on vehicle accelerations behavior, PM2.5 emissions, and dispersion modeling. *Transportation Research Part D: Transport and Environment*, 75:297–319, 2019. ISSN 13619209. doi: 10.1016/j.trd.2019.09.006.

[38] B. S. Kerner and S. L. Klenov. A theory of traffic congestion at moving bottlenecks. *Journal of Physics A: Mathematical and Theoretical*, 43(42):425101, 2010. ISSN 1751-8113. doi: 10.1088/1751-8113/43/42/425101.

[39] M. M. Ahmed and A. Ghasemzadeh. The impacts of heavy rain on speed and headway Behaviors: An investigation using the SHRP2 naturalistic driving study data. *Transportation Research Part C: Emerging Technologies*, 91:371–384, 2018. ISSN 0968090X. doi: 10.1016/j.trc.2018.04.012.

[40] W. Brilon and M. Ponzlet. Variability of Speed-Flow Relationships on German Autobahns. *Transportation Research Record*, 1555(1):91–98, 1996. doi: 10.1177/0361198196155500112.

[41] Z. H. Khan, A. B. Altamimi, W. Imran, M. Alsaffar, K. S. Khattak, and F. F. Alfaisal. Macroscopic Traffic Modelling on the Impact of Road Surface Potholes: Development and Numerical Solution. *IEEE Access*, 12:81718–81735, 2024. doi: 10.1109/ACCESS.2024.3411303.

[42] B. A. Jonah. Accident risk and risk-taking behaviour among young drivers. *Accident; analysis and prevention*, 18(4):255–271, 1986. ISSN 0001-4575. doi: 10.1016/0001-4575(86)90041-2.

[43] B. Chen, X. Zhao, Y. Li, J. Gong, and X. Liu. How does older and younger drivers' risk cognition affect the safety performance: A driving simulator study of sudden lane-changing of the leading vehicle. *Journal of Transportation Safety & Security*, 16(6):633–654, 2024. ISSN 1943-9962. doi: 10.1080/19439962.2023.2246017.

[44] E. Ericsson. Variability in urban driving patterns. *Transportation Research Part D: Transport and Environment*, 5(5):337–354, 2000. ISSN 13619209. doi: 10.1016/S1361-9209(00)00003-1.

[45] K. Steinhauser, F. Leist, K. Maier, V. Michel, N. Pärsch, P. Rigley, F. Wurm, and M. Steinhauser. Effects of emotions on driving behavior. *Transportation Research Part F: Traffic Psychology and Behaviour*, 59:150–163, 2018. ISSN 13698478. doi: 10.1016/j.trf.2018.08.012.

[46] B. Reimer, L. A. D'Ambrosio, J. E. Coughlin, M. E. Kafrissen, and J. Biederman. Using self-reported data to assess the validity of driving simulation data. *Behavior research methods*, 38(2):314–324, 2006. ISSN 1554-351X. doi: 10.3758/BF03192783.

2 Car-Following Model Calibration Based on Driving Simulator Data to Study Driver Characteristics and to Investigate Model Validity in Extreme Traffic Situations

This paper was published under:

Berghaus, Moritz; Kalló, Eszter and Oeser, Markus (2021). Car-Following Model Calibration Based on Driving Simulator Data to Study Driver Characteristics and to Investigate Model Validity in Extreme Traffic Situations. Transportation Research Record, 2675(12), 1214-1232. https://doi.org/10.1177/03611981211032650

Individual contributions:

M. Berghaus: study conception and design; data collection; analysis and interpretation of results; draft manuscript preparation.
E. Kalló: study conception and design; data collection; draft manuscript preparation (with a particular focus on the planning and execution of the driving simulator study, Section 2.3.3).
M. Oeser: study conception and design; supervision.

2.1 Abstract

In this paper we use traffic data from a driving simulator study to calibrate four different car-following models. We also present two applications for which the calibration results can be used. The first application relied on the advantage that driving simulator data also contain information on driver characteristics, for example, age, gender, or the self-assessment of driver behavior. By calibrating the models for each driver individually, the resulting model parameters could be used to analyze the influence of driver characteristics on driver behavior. The analysis revealed that certain characteristics, for example, self-identification as an aggressive driver, were reflected in the model parameters. The second application was based on the capability to simulate dangerous situations that require extreme driving behavior, which is often not included in datasets from real traffic and cannot be provoked in field studies. The model validity in these situations was analyzed by comparing the prediction errors of normal and extreme driving behavior. The results showed that all four car-following models underestimated the deceleration in an emergency braking scenario in which the drivers were momentarily shocked. The driving simulator study was validated by comparing the calibration results with those obtained from real trajectory data. We concluded that driving simulator data were suitable for the two proposed applications, although the validity of driving simulator studies must always be regarded.

2.2 Introduction

Car-following models are an essential component of traffic flow analysis as they describe longitudinal driving behavior and explain traffic phenomena. The calibration of these models relies on traffic data from different sources. One possible source is trajectory data, such as the NGSIM dataset, which are gathered by cameras and computer vision algorithms and contain the trajectories of vehicles passing through a relatively short road section. Another source is naturalistic driving data or floating car data, which are generated by in-vehicle sensors and contain the trajectories of a small percentage of vehicles on a large road network. Both data sources have been used to calibrate car-following models in different studies [1–5]. Moreover, Hoogendoorn and Hoogendoorn combined driving simulator data with real trajectory data to calibrate different car-following models [6]. Although they studied how the fusion of these two data sources can improve calibration results, the focus of our paper is the calibration procedure specific to driving simulator data and the possible applications of this type of data.

Driver behavior is influenced by external factors, that is, the surrounding traffic and road design, and internal factors, that is, the characteristics of the driver. The interaction between

these factors increases the complexity in modeling driver behavior. Driving simulator studies allow researchers to observe driver behavior under controlled conditions and therefore analyze these factors separately. The surrounding traffic in a driving simulator is typically controlled by traffic simulation software that creates the desired traffic conditions [7, 8]. The road design, for example, in work zones, can systematically be varied to find the safest design [9]. The influence of driver characteristics, such as age or experience, on driver behavior has been analyzed extensively in the literature [10–12]. In addition, Reimer et al. have shown that driver behavior in the simulator correlates with statements made by the participants regarding their own driving behavior [13].

Driving simulator studies are also suitable for analyzing driver behavior in potentially dangerous situations that cannot be otherwise provoked in field studies. Oeser et al. investigated the reaction of participants to wrong-way drivers and evaluated different warning systems [14]. The impact of using smartphones while driving has been studied by Basacik et al. [15]. Another application of driving simulator studies is the analysis of interactions between human drivers and advanced driver-assistance systems [16, 17] or the comparison between human and automated driving behavior [18].

In this study, we collected driving simulator data to calibrate the optimal velocity model (OVM), which is a simple car-following model, the generalized force model, and the full velocity difference model, which are both extensions of the OVM, and the intelligent driver model. During model calibration, we focused on three aspects that have been discussed in the literature. The first was the choice of an objective function. For car-following models, this objective function can either be the error of headway, velocity, or acceleration. For a discussion on the choice of objective function and a review of papers dealing with this issue, we refer the reader to Sharma et al. [19]. The second aspect was the choice between local (model-based) and global (simulation-based) calibration. Local calibration uses the trajectories of leader and follower at each time step as an initial condition to predict the follower's trajectory at the subsequent time step. Global calibration uses only the first available time step of the two trajectories as an initial condition to predict the trajectory of the follower at all subsequent time steps [1]. Although the global calibration is computationally extremely expensive [20], it yields more reliable results [1]. The third aspect is referred to as trajectory completeness; car-following models consist of few equations that are supposed to describe driver behavior in every traffic situation, from standstill to free flow. To obtain valid model parameters, the data used for calibration must contain all of these traffic situations [19]. Although trajectory data from real traffic do not necessarily contain all traffic situations, the surrounding traffic in driving simulator studies can be controlled in such a way that every traffic situation occurs. In this paper we discuss how the three above-mentioned aspects can be addressed in a driving sim-

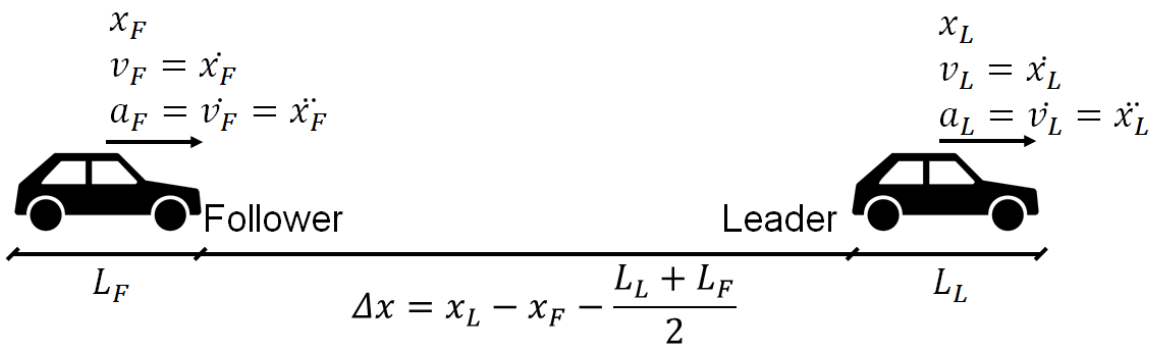

Figure 2.1: Definition of a vehicle pair.

ulator study. We also investigate the validity of the simulator study using real trajectory data from a German motorway as a reference. Furthermore, we analyze the influence of driver characteristics on driver behavior by calibrating the models for each driver individually. Lastly, we study the model validity in dangerous situations compared with normal traffic conditions.

2.3 Methods

2.3.1 Car-Following Models

In general, car-following models describe the dynamic behavior of a vehicle ("follower") by predicting its trajectory. For the prediction, the trajectory of its preceding vehicle ("leader") and the follower's initial position on the observed road section have to be known. Most models assume that the trajectory of the follower is determined only by the vehicle directly in front of it. This means, that lateral movements and lane changes are neglected. The one-dimensional vehicle dynamics of leader and follower can be described in relation to the longitudinal position of their centroid x, their length L, velocity v, and acceleration a (see Fig. 2.1).

Optimal Velocity Model

OVM consists of an optimal velocity function that returns the velocity of the follower given the headway of the leader-follower pair,

$$v_{opt} = f(\Delta x) \tag{2.1}$$

Despite its simplicity, the OVM adequately represents macroscopic traffic phenomena such as congestion waves [21, 22].

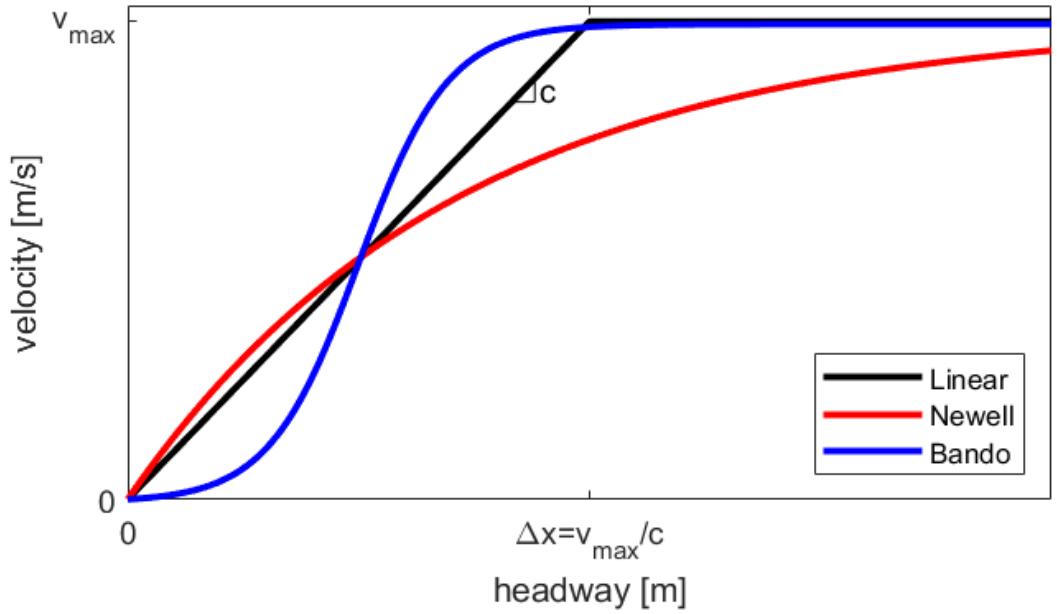

Figure 2.2: Comparison of the optimal velocity functions by Bando [22] and Newell [23] and the linear optimal velocity function used in this paper.

The theory that a vehicle's velocity is determined only by the (net) spatial headway, Δx, was first suggested by Newell [23]. Newell proposed an exponential optimal velocity function (see Fig. 2.2):

$$v_{opt,Newell} = v_{max}\left[1 - exp\left(\frac{\lambda}{v_{max}}(\Delta x - \Delta x_{min})\right)\right] \tag{2.2}$$

In this function λ represents the rate at which the function converges to the desired velocity v_{max}, and Δx_{min} is the minimum headway at standstill.

Bando et al. introduced a similar model using the term "legal velocity" [21] and later established the term "optimal velocity" [22]. The optimal velocity function of Bando et al. contains a hyperbolic tangent that results in an S-shaped curve [22] (see Fig. 2.2),

$$v_{opt,Bando} = V_0(tanh(m(\Delta x - b_f)) - tanh(m(\Delta x_{min} - b_f))) \tag{2.3}$$

The shape of the "S" is governed by the parameters V_0, m and b_f.

Wilson [24] showed that Gipps' car-following model [25], which uses the concept of safe distances, can also be simplified to an OVM in the case of uniform flow.

Since one goal of this paper is to interpret the model parameters with respect to driver characteristics, a simple optimal velocity function with a few comprehensible parameters is

preferred. Hence, in this paper we propose a piecewise linear optimal velocity function (see Fig. 2.2) with only two parameters,

$$v_{opt,linear} = min(c \cdot \Delta x, v_{max}) \tag{2.4}$$

where v_{max} is the desired speed at which the driver wants to drive in free flow, and describes how aggressively or riskily the driver wants to drive. The larger c is, the higher the vehicle speed for a given headway, hence the riskier the driver behavior. This function implies that in the case that the headway is smaller than the maximum velocity divided by parameter c ($\Delta x < v_{max}/c$), the speed is proportional to the headway. For headways larger than this term, the speed is constant. Hence, on a macroscopic scale, this optimal velocity function corresponds to a triangular fundamental diagram.

If the velocity of the follower differs from the optimal velocity at a given moment, the follower does not adopt the optimal velocity immediately, as this would require extreme acceleration. To take account of this, the model requires a sensitivity parameter that indicates how sensitively the follower reacts to deviations between its current velocity and the optimal velocity [21]. Like Kesting and Treiber [26], in our acceleration function (see Equation 2.5) we also use adaptation time, τ, which is the inverse of Bando's sensitivity parameter, a, [22] which might be confused with the acceleration.

$$a_F = \frac{v_{opt}(\Delta x) - v_F}{\tau} \tag{2.5}$$

Note that τ neither represents the reaction time of the follower, nor the time until the optimal velocity is reached because both v_{opt} and v_F change during the acceleration process. It rather describes the sensitivity to the difference between the optimal and current velocity. To understand the influence of τ, let us consider a case in which a vehicle approaches a slower vehicle. For a very low τ, the driver decelerates sharply as soon as the headway falls below v_{max}/c and reaches the velocity of the slower vehicle immediately. In contrast, if τ is very large, the driver does not decelerate enough to reach the velocity of the leading vehicle, which results in an accident. Neither extremes are desirable.

Generalized Force Model

The main shortcoming of the OVM is that the optimal velocity depends only on the headway between leader and follower and neglects the velocity of the leader. Hence, the model does not reflect that drivers decelerate more when they are approaching a slower vehicle. Helbing and Tilch overcame this shortcoming by introducing an additional term in the acceleration function that only comes into effect if the speed difference between follower and leader is

positive [27]. In their model, the acceleration of a driver is governed by the superposition of two "forces," hence the name generalized force model (GFM). The first force is called the acceleration force, f_{acc}, which makes drivers accelerate toward their desired velocity, v_{max}. The second force is called the interaction force, f_{int}, which causes drivers to decelerate if the optimal velocity, v_{opt}, is below v_{max}, if there is a positive speed difference, or if both conditions are found. The model equation is as follows:

$$a_F = f_{acc} + f_{int} \tag{2.6}$$

with

$$f_{acc} = \frac{v_{max} - v_F}{\tau_1} \tag{2.7}$$

$$f_{int} = \frac{v_{opt}(\Delta x, v_F) - v_{max}}{\tau_1} - \frac{\Delta v \Theta(\Delta v)}{\tau_2} e^{-\frac{\Delta x - s(v_F)}{R_2}} \tag{2.8}$$

$$s(v_F) = \Delta x_{min} + v_F T \tag{2.9}$$

$$v_{opt}(\Delta x, v_F) = v_{max} \cdot \left(1 - e^{-\frac{\Delta x - s(v_F)}{R_1}}\right) \tag{2.10}$$

$$\Delta v = v_F - v_L \tag{2.11}$$

where

Θ = Heaviside function,

τ_1 = acceleration time,

τ_2 = braking time,

R_1 = range of the acceleration interaction,

R_2 = range of the deceleration interaction, and

T = safe time headway.

In the case of $v_L > v_F$, the GFM is identical to the OVM with an optimal velocity function similar to that of Newell (Equation 2.2). By using two different sensitivity values, τ_1 and τ_2, and ranges, R_1 and R_2, for accelerating and decelerating respectively, the GFM can represent the different acceleration and braking capabilities of vehicles.

Full Velocity Difference Model

Jiang et al. argue that the speed difference between follower and leader influences the driver behavior regardless of whether it is positive or negative [28]. The observation that drivers accept smaller headways when the leading vehicle accelerates is not represented either by the OVM or the GFM. Hence, Jiang et al. introduced the full velocity difference model (FVDM), which extends the OVM in a simpler way than the GFM. In the FVDM, acceleration is governed by two terms. The first term is identical to the OVM, that is, it contains the difference between the optimal and the current velocity. The second term contains the speed difference between leader and follower,

$$a_F = \frac{v_{opt}(\Delta x) - v_F}{\tau} - \lambda \cdot \Delta v \tag{2.12}$$

where λ is the sensitivity to speed differences between the leader and the follower. Note that unlike in the original publication, we use a negative sign in front of the second term to have a consistent definition of Δv. In principle, the FVDM can be used with any optimal velocity function. In this paper, we use the same optimal velocity function as for the OVM (see Equation 2.4).

Although the FVDM extends the GFM in cases in which the leader is faster than the follower, it uses the same sensitivity for both acceleration and deceleration. In return, the FVDM has fewer parameters than the GFM. A major shortcoming of the model is that the sensitivity to speed differences between the leader and follower does not depend on the headway.

Intelligent Driver Model

The intelligent driver model (IDM) proposed by Treiber et al. picks up on some ideas from the GFM, but the implementation is slightly different [29]. In both models, the acceleration decreases as drivers approach the desired velocity, but in the IDM the acceleration is determined by the ratio of v_F and v_{max} rather than their difference. Furthermore, both models use the notion of a desired headway $s = \Delta x_{min} + v_F T$. The model equation of the IDM is as follows:

$$a_F = a \cdot \left(1 - \left(\frac{v_F}{v_{max}}\right)^{\delta} - \left(\frac{s(v_F, \Delta v)}{\Delta x}\right)^2\right) \tag{2.13}$$

with

$$s(v_F, \Delta v) = \Delta x_{min} + max\left(0, v_F T + \frac{v_F \Delta v}{2\sqrt{ab}}\right) \tag{2.14}$$

where

a is maximum acceleration,

b is comfortable deceleration, and

δ is an exponent that describes how drivers reduce their acceleration as they approach the desired velocity.

In Treiber et al. [29] and Kesting and Treiber [2], it is assumed that δ is a constant ($\delta = 4$) rather than a parameter.

The IDM distinguishes three driving situations with smooth transitions in between. The first situation is acceleration with a large distance to the leading vehicle ($s << \Delta x$). In this case, drivers accelerate toward the desired velocity. The second situation is following a slow leader with constant speed and constant headway ($a_F = 0$, $v_F << v_{max}$, $\Delta v = 0$). The headway is then approximately equal to $\Delta x_{min} + v_F T$. The third situation is deceleration when approaching a slower vehicle ($\Delta v > 0$, $s > \Delta x$). In this case, the desired headway, s, becomes larger than the actual headway, Δx, and the resulting a_F becomes negative.

The IDM produces realistic acceleration profiles in all driving situations and its parameters are easy to interpret as they correspond to values that can be directly measured in their respective driving situations.

2.3.2 Model Calibration

The goal of calibration is to identify those model parameters that describe the driver behavior best. In other words, the calibration seeks to minimize the prediction error of the car-following model. This section discusses three main aspects that must be considered in the calibration procedure. The three aspects are objective function, local versus global calibration, and trajectory completeness. This section also proposes how the specifics of driving simulator studies can be taken into account in these three aspects.

Objective Function

The choice of the objective function is not intuitive and may have a large impact on the calibration result. For example, it is not possible to minimize only the velocity or acceleration error as this would result in a systematic error in the headway. Kesting and Treiber [2] and Punzo and Montanino [30] propose minimizing only the headway error, which automatically reduces the velocity and acceleration errors. However, this could lead to undesired results in situations in which the observed headway differs from the headway predicted by the model. In this case, if the headway error is minimized, the model seeks to reach the observed headway as quickly as possible, which results in unrealistic and even physically impossible acceleration values. As a result, the model parameters τ in the OVM and FVDM, τ_1 and τ_2 in the GFM, and b in the

IDM might become very small, and a in the IDM might become very large. To avoid this scenario, in this paper we use the sum of headway, velocity, and acceleration root-mean-square error (RMSE) as an objective function. Since these three error values do not have the same units and magnitudes, they are normalized using the range of their observed values.

$$ObjectiveFunction = \frac{RMSE_{\Delta x}}{\Delta x_{max,Obs.} - \Delta x_{min,Obs.}} + \frac{RMSE_v}{v_{max,Obs.} - v_{min,Obs.}} + \frac{RMSE_a}{a_{max,Obs.} - a_{min,Obs.}} \tag{2.15}$$

Local Versus Global Calibration

The local calibration method evaluates the model error at each time step individually. For each time step, the model uses the observed trajectory of the leader and the observed trajectory of the follower to predict the trajectory of the follower at the next time step (see Equation 2.16). The global calibration method does this only at the first time step as an initial condition. At the subsequent time steps it uses the predicted trajectory of the follower instead of the observed one (see Equation 2.17).

$$a_{F,Mod.,Local}(t + \Delta t) = f\left([x, v, a]_{L,Obs.}(t), [x, v, a]_{F,Obs.}(t)\right) \tag{2.16}$$

$$a_{F,Mod.,Global}(t + \Delta t) = f\left([x, v, a]_{L,Obs.}(t), [x, v, a]_{F,Mod.}(t)\right) \tag{2.17}$$

Local calibration essentially "resets" the model error after each time step, whereas the global calibration "allows" the model error to accumulate over all time steps. As a result, the global calibration method enables a better comparison of different model parameters. However, it is only suitable for "long" trajectories (with several time steps) since the difference between the observed and the predicted trajectory at the first time step is zero per definition and takes a few time steps to increase enough to get meaningful values. Since the trajectories from the driving simulator study were sufficiently long and the computational effort of a global calibration was acceptable for our amount of data, we utilized the global calibration method in this study.

In general, the calibration of a car-following model is an optimization problem in mathematical terms. To solve this problem we used a direct search algorithm [31], which has been applied in previous studies to calibrate car-following models [32]. Since this algorithm finds a local minimum that is not necessarily the global minimum of the objective function (Equation 2.15), we ran the algorithm several times with different initial values to increase the probability of obtaining the global minimum.

Trajectory Completeness

Sharma et al. define six different driving regimes: free acceleration (toward the desired speed), cruising (driving at the desired speed), acceleration (behind a faster vehicle), deceleration (behind a slower vehicle), following (constant speed behind another vehicle), and standstill [19]. If the trajectories used for calibration contain all these driving regimes, they are referred to as "complete." However, the impact of missing driving regimes on calibration errors depends on the car-following model. Table 2.1 shows which model parameters are relevant in which driving regime. Most model parameters appear in more than one driving regime, that is, the models can in theory be calibrated even if there is one driving regime missing. Furthermore, most driving regimes are governed by more than one model parameter. There are a three counterintuitive appearances worth mentioning. The first is that λ (FVDM), which represents sensitivity to faster or slower leaders, is relevant in free acceleration and cruising although the headway goes to infinity. The second is that b (IDM), which describes comfortable deceleration, is not only relevant in deceleration but also in acceleration. However, this only applies if the leader is not much faster than the follower, such that the term $v_F T + \frac{v_F \Delta v}{2\sqrt{ab}}$ is still positive. The third appearance is that OVM and FVDM (at least for the optimal velocity functions used in this paper) do not have a parameter for the headway at standstill, that is, these models assume that the net headway at standstill is zero.

To consider the aspect of trajectory completeness in the design of the driving simulator study, the surrounding traffic should be controlled in such a way that every participant experiences each driving regime. At the same time, the participant should perceive the surrounding traffic to be as realistic as possible, hence a fixed sequence and strict separation of driving regimes should be avoided. Instead of controlling the driving regime directly by manipulating the behavior of the leading vehicle, we varied the traffic density and created stop-and-go waves. As a result, the different traffic regimes occurred in a realistic sequence.

2.3.3 Description of the Driving Simulator

The car utilized in the driving simulator was an E.Go passenger car (see Figure 2.3a). The simulator car was static, which means there was no imitation of movements in the driving cabin. The vehicle was instrumented to obtain data from the response of the steering wheel, gas and braking pedals, and the turn signal actuation. Furthermore, there was an incorporated sound effect that imitated the noise of the engine depending on the acceleration of the car. The engine was replaced by a computer that controlled these features and communicated through a self-developed interface with another computer responsible for the simulation. The surrounding traffic was controlled by the microscopic traffic simulation software PTV Vissim.

Driving regime	Definition	OVM	GFM	FVDM	IDM
Free acceleration	$v_F < v_{max}$ $\Delta x \to \infty$ $a_F > 0$	v_{max}, τ	v_{max}, τ_1	v_{max}, τ, λ	a, v_{max}
Cruising	$v_F = v_{max}$ $\Delta x \to \infty$ $a_F = 0$	v_{max}	v_{max}	v_{max}, λ	v_{max}
Acceleration	$v_F < v_{max}$ $\Delta v < 0$ $a_F > 0$	c, τ	v_{max}, τ_1, Δx_{min}, T, R_1	c, τ, λ	a, v_{max}, Δx_{min}, T, b
Deceleration	$\Delta v > 0$ $a_F < 0$	c, τ	v_{max}, τ_1, τ_2, Δx_{min}, T, R_1, R_2	c, τ, λ	a, v_{max}, Δx_{min}, T, b
Following	$\Delta v = 0$ $a_F = 0$	c	v_{max}, Δx_{min}, T, R_1	c	v_{max}, Δx_{min}, T
Standstill	$v_F = 0$ $a_F = 0$	N/A	Δx_{min}	N/A	Δx_{min}

Table 2.1: Relevant Model Parameters in the Different Driving Regimes. Note: OVM = optimal velocity model; GFM = generalized force model; FVDM = full velocity difference model; IDM = intelligent driver model; N/A = not applicable.

(a) (b)

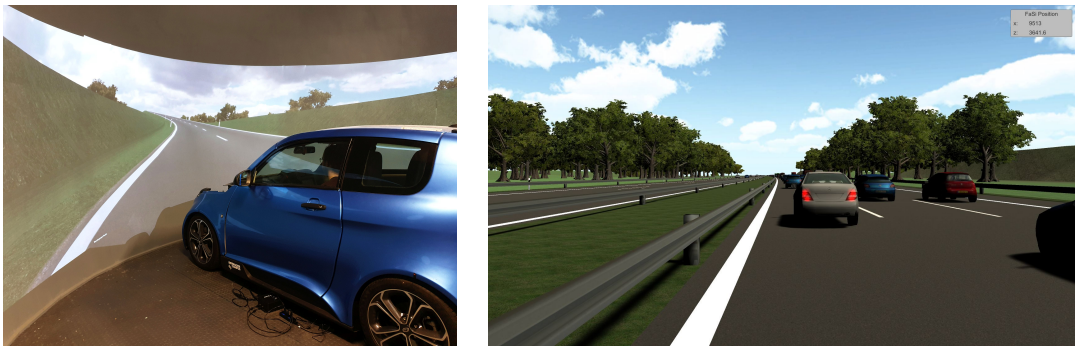

Figure 2.3: (a) Simulator car and (b) screenshot of the simulation environment.

The interface allowed for the continuous exchange of the simulator car's position data between the computer inside the car and the simulation computer. For the visualization of the simulation the game software Unity was used. The traffic was displayed by three projectors on a 180° curved wall that surrounded the simulator car. The traffic behind the simulator car was shown on a screen to the reverse of the vehicle, so all the mirrors could be used as well.

In our study, we exchanged the integrated simulation model of Vissim in a longitudinal direction with a new microscopic traffic flow model developed by Herty et al. [33]. For the driving simulator study, we designed two motorway sections with the commercial drawing software AutoCAD. Both roads had three 3.75-m wide lanes in each direction, and both led through curved and straight sections. The first road was 12.5 km long and had the role of helping the participants to get used to driving in a simulator before the actual study. The second road was the test motorway used for the study, which was 4.5 km long and had an 800-m long entry lane at the beginning, where each participant started the simulation. The speed limit on the main road was 100 km/h, just like on the motorway section where we obtained real traffic data from videos with image processing methods [34, 35]. The entry lane had a speed limit of 80 km/h.

In total, 49 participants over the age of 18 with a Category B driving license (passenger car) participated in our study. Three of the participants could not finish the study owing to simulator sickness, therefore their results were not included in our analysis. The study included three questionnaires and a secondary task during driving. The study started with the first questionnaire before the participants started to drive. This questionnaire aimed to collect information about the drivers' characteristics, which were grouped in four categories: gender, age, duration of possession of a driving license, and yearly mileage. After answering the first questionnaire, the participants started with the test trial on the first road without simulated traffic to familiarize themselves with the simulator. After that, each participant drove twice on

No.	Question: How would you describe your driver behavior?	
1	Fast (“I like driving fast if it’s allowed”)	Slow (“I prefer driving slowly even if a higher speed is allowed”)
2	Aggressive (“I insist on my right of way”)	Defensive (“I give in even if I have right of way”)
3	Secure (“I feel secure while driving”)	Insecure (“I have doubts about my driving skills”)
4	Careful (“I approach situations carefully”)	Fearless (“I take situations as they come”)
5	Calm (“I let nothing get me excited”)	Stressed (“I get easily excited in traffic”)
6	Good (“I’m a good driver”)	Bad (“I’m a bad driver”)
7	Distractible (“I’m distractible e.g., by radio, smartphone, co-driver, landscape”)	Focused (“I focus only on driving”)

Table 2.2: Questionnaire with Self-Assessment of Driver Behavior

the second road through different traffic conditions simulated on the road. During the first test measurement, the participants had to perform a secondary task. The participants were asked to estimate the time-to-collision (TTC) between themselves and the vehicle in front of them at certain moments. The test leader had explained the meaning of TTC to the participants beforehand. During the second test measurement the test leader filled out the second questionnaire based on the participants’“either or” answers. The questionnaire focused on the participants’ self-assessment of their driving behavior in real driving situations (see Table 2.2). The self-assessment was used to study the influence of driver characteristics on driver behavior. The third questionnaire was answered after the second test measurement. The questions were repeated from the second questionnaire but were in reference to the participants’ driving behavior in the driving simulator in simulated traffic [36].

During both test measurements, we simulated different dangerous traffic situations and traffic jams. The scenarios were happening ahead of the participant, which were “emergency braking” (velocity of the leader reduced to 0 km/h), “strong braking” (velocity of the leader reduced to 20 km/h), and “sudden lane change” (vehicle changes from an adjacent lane directly in front of the participant). During the study, each participant was involved in two different traffic scenarios and most of the time a traffic jam was also present on the road. These scenarios enabled the analysis of driver behavior in dangerous situations, which cannot be provoked in real traffic [36].

2.3.4 Data Quality and Data Preparation

The traffic simulation software recorded the position, velocity, and acceleration of the surrounding vehicles every 0.1 s. To each vehicle an ID, vehicle type, length, and width were assigned. Owing to limited computational resources, the position and velocity were rounded to one decimal place and the acceleration to two decimal places. For the simulator car, only the position was logged, but with higher precision. To compute the velocity and acceleration of the simulator car, we fitted a smoothing spline to the position data with a smoothing parameter of 0.99.

Car-following models only describe longitudinal driver behavior, which means lateral behavior, that is, lane changing, was ignored. Therefore, the recorded data of each participant had to be prepared before using them to calibrate the car-following models. For example, lane changes of both the participant and the preceding vehicle were removed from the data. All time steps during which the boundaries of a vehicle were closer than 0.20 m to the lane marking were considered to be part of a lane change. Consequently, the scenario "sudden lane change" was not analyzed within the scope of this paper. Besides lane changing, redundant data also had to be removed from the data: when both the participant and its preceding vehicle were in a traffic jam and their speeds were zero, their trajectories were still recorded every 0.1 s. The redundant data points in these situations were not considered in the calibration procedure.

With regard to the simulation of surrounding traffic, further data preparation was needed. The surrounding vehicles do not always react to the simulator vehicle correctly and sometimes behave unrealistically. This might lead to very small headways or even negative headways, that is, accidents. Therefore, all data points with negative headways and data points where the speed values were larger than three times the headway values ($v[m/s] > 3\Delta x[m]$) were also removed. All remaining data points consisting of v_F, a_F, v_L, and Δx were used as input for the model calibration.

2.3.5 External Validity

In the context of driving simulator studies, the term external validity describes the extent to which conclusions drawn from the driving behavior in the simulator are also valid in real traffic (see Reimer et al. for a detailed discussion on the validity of driving simulator studies [13]). For a car-following model this means that calibrations with simulator data and with real trajectory data should give the same model parameters. In our case, data on the driver behavior in real traffic were not available for the participants who took part in the driving simulator study. Instead, we designed the road used in the simulator study in such a way that it resembled

the German motorway for which a trajectory dataset was available [35]. Both roads had three lanes and a speed limit of 100 km/h. Because of a nearby onramp, the real data contained some congested traffic on the right and middle lanes whereas there was almost only free flow on the left lane. The left lane therefore lacked trajectory completeness and was not suitable for a model calibration. Just as for the simulator data, we removed all lane changes and obviously false data. The road of the real dataset was in a tunnel, which could not be implemented in the simulator study. It was also shorter (100 m covered per camera) than the road in the simulator study. Therefore, we used both local and global calibration for comparison.

2.4 Results and Discussion

2.4.1 Calibration of Driving Simulator Data

We calibrated the model parameters of the four car-following models described above for each participant individually. To obtain physically realistic values, we used lower and upper bounds for the model parameters (see Table 2.3). Figure 2.4 shows the distribution of the parameters. We tested the distribution of each parameter for normal and log-normal distribution using the Anderson–Darling test. Most parameters that cannot be assumed to be normally or log-normally distributed have a peak at the lower or upper bound, or both. The parameter values close to the lower or upper bound were evenly distributed over the partipicants, hence there is no evidence that the data of some participants were unsuitable for calibration. There is also no evidence that these parameter values are associated with large prediction errors. Apparently, the models can compensate for unrealistic values of one parameter with the values of the other parameters without producing unrealistic driver behavior.

According to the OVM, most participants had a v_{max} below the speed limit of 100 km/h (27.8 m/s) although the traffic conditions would have allowed each participant to reach their desired speed. However, participants reported having difficulties estimating their speed in the static driving simulator. They could only rely on the relative movements in their surroundings (reflector posts next to the road every 50 m) or the speedometer. Participants may also have been influenced by the instruction to comply with the speed limit. This instruction was necessary because participants unintentionally tend to drive too fast. Therefore, speeds in a static driving simulator should always be treated with caution.

Parameter c represents the slope of the optimal velocity function and can be interpreted as the “riskiness” of the driver behavior. A frequently used rule of thumb states that one should maintain a constant time headway of 2 s, which corresponds to $c = 0.5$. Most participants had a lower c, meaning that their driver behavior was less risky.

Car-following model	Model parameter	Unit	Lower bound	Upper bound
OVM	v_{max}	m/s	10	45
	c	s^{-1}	0.2	2
	τ	s	0.5	10
GFM	v_{max}	m/s	10	45
	τ_1	s	0.1	10
	τ_2	s	0.1	10
	Δx_{min}	m	0	10
	T	s	0.2	3
	R_1	m	0	20
	R_2	m	0	200
FVDM	v_{max}	m/s	10	45
	c	s^{-1}	0.2	2
	τ	s	0.5	10
	λ	s^{-1}	0.1	10
IDM	a	m/s^2	0.1	5
	v_{max}	m/s	10	45
	Δx_{min}	m	0	10
	T	s	0.2	3
	b	m/s^2	1	6

Table 2.3: Lower and Upper Bounds of Model Parameters. Note: OVM = optimal velocity model; GFM = generalized force model; FVDM = full velocity difference model; IDM = intelligent driver model.

(a)

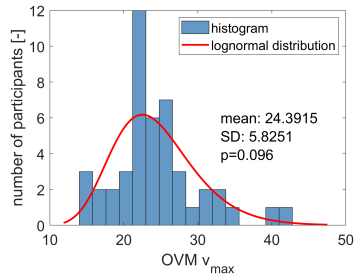

(b)

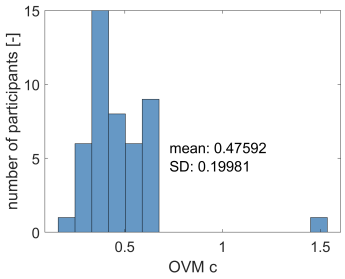

(c)

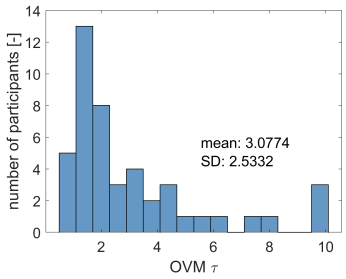

(d)

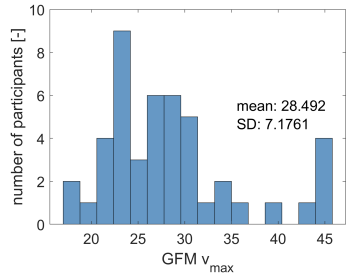

(e)

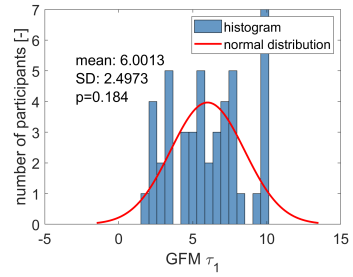

(f)

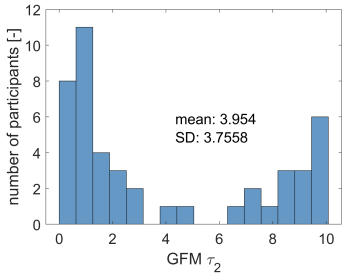

(g)

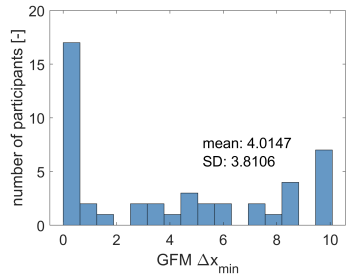

(h)

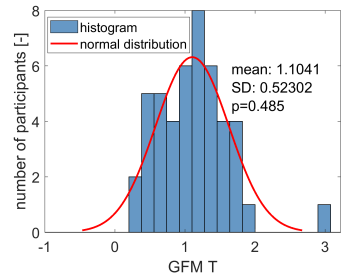

(i)

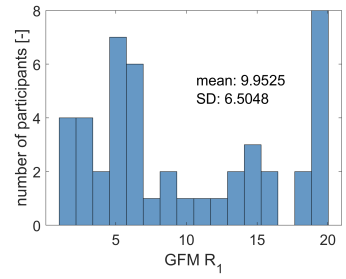

(j)

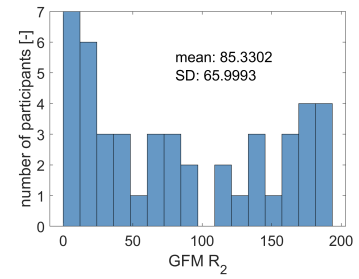

(k)

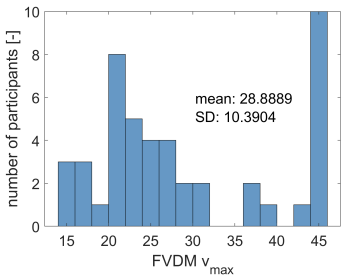

(l)

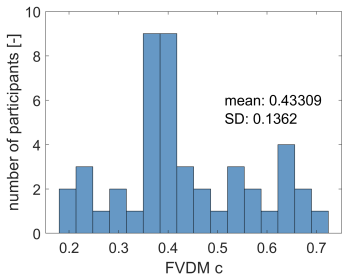

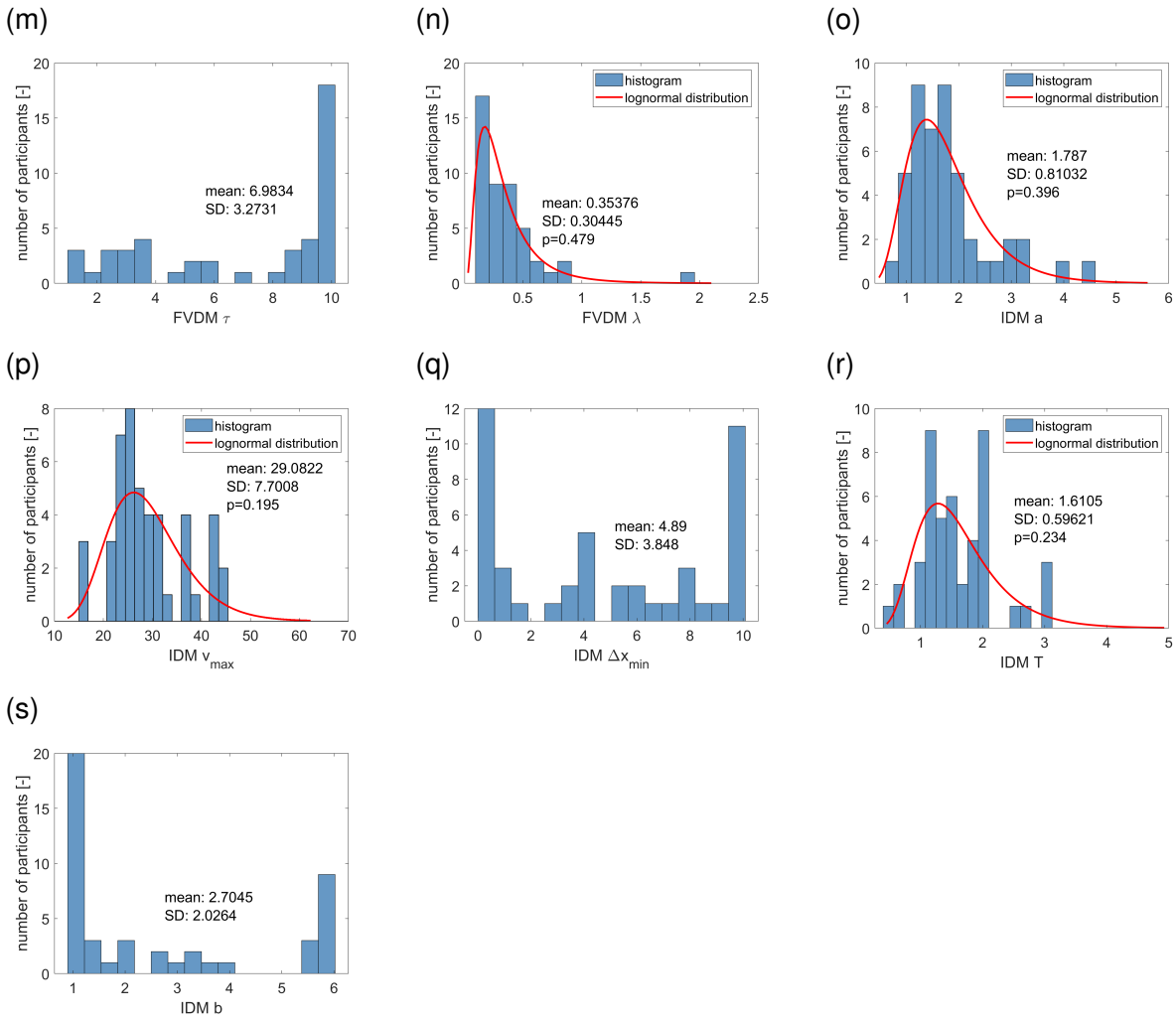

Figure 2.4: Distribution of calibrated model parameters with mean, standard deviation (SD) and p-value of the Anderson–Darling test where applicable.

Parameter τ describes how sensitively the driver reacts to differences between the current and the optimal velocity. The results showed that τ was in a reasonable range ($\tau \approx 1$) for most drivers, with few outliers with very large values.

The FVDM yielded similar results to the OVM for parameter c, but it had several outliers with very large v_{max} and/or very large τ values. Large values of τ mean that the first term of the model equation (Equation 2.12) ($(v_{opt} - v_F)/\tau$) is very small, large values of v_{max} mean that the optimal velocity can become very large, so the first term of the model equation becomes very large. Both cases can partly be compensated by the second term of the model equation ($-\lambda\Delta v$), such that the model produces realistic acceleration even if the parameters are unrealistic.

For the GFM, the distributions of v_{max} and T were plausible with only a few drivers with a very large v_{max}. The values of τ_1 were mostly larger than τ_2, that is, drivers reacted more sensitively when they braked than when they accelerated, which is plausible and in line with the findings of Helbing and Tilch [27]. The values of Δx_{min} were very small (less than 1 m) for several drivers, but it should be recalled that Δx_{min} is not only relevant in the standstill driving regime. R_1 and R_2 were almost evenly distributed within their lower and upper bounds. Since these parameters do not have a physical representation, it is hard to decide whether this is reasonable.

The IDM yielded plausible distributions for a, v_{max}, and T, although v_{max} and T had more outliers in both directions than the same in the GFM. Parameter Δx_{min} in the IDM had a very similar distribution as the same parameter in the GFM. Most values of b were close to either the lower or the upper bounds. This indicates that in the deceleration driving regime driver behavior is not only governed by b.

Figure 2.5 shows two examples of the observed trajectories and the trajectories predicted by each model. In general, all models described the observed driver behavior in all driving regimes properly. Since the models were calibrated for each participant individually, there were no large errors in the headway, speed, or acceleration. The acceleration and deceleration values were realistic, but the short-term fluctuations in the acceleration (Figure 2.5a) and the time and intensity of braking (Figure 2.5b) could not be reproduced by the models.

Figure 2.6 shows the RMSEs of headway, velocity, and acceleration for each participant. The IDM had the smallest errors for headway, velocity, and acceleration, and the OVM had the largest errors. The errors can be explained mainly by two aspects. First, every car-following model is only an approximation of real driver behavior. Second, drivers do not show deterministic behavior, that is, even under the same conditions their driving behavior varies from time to time.

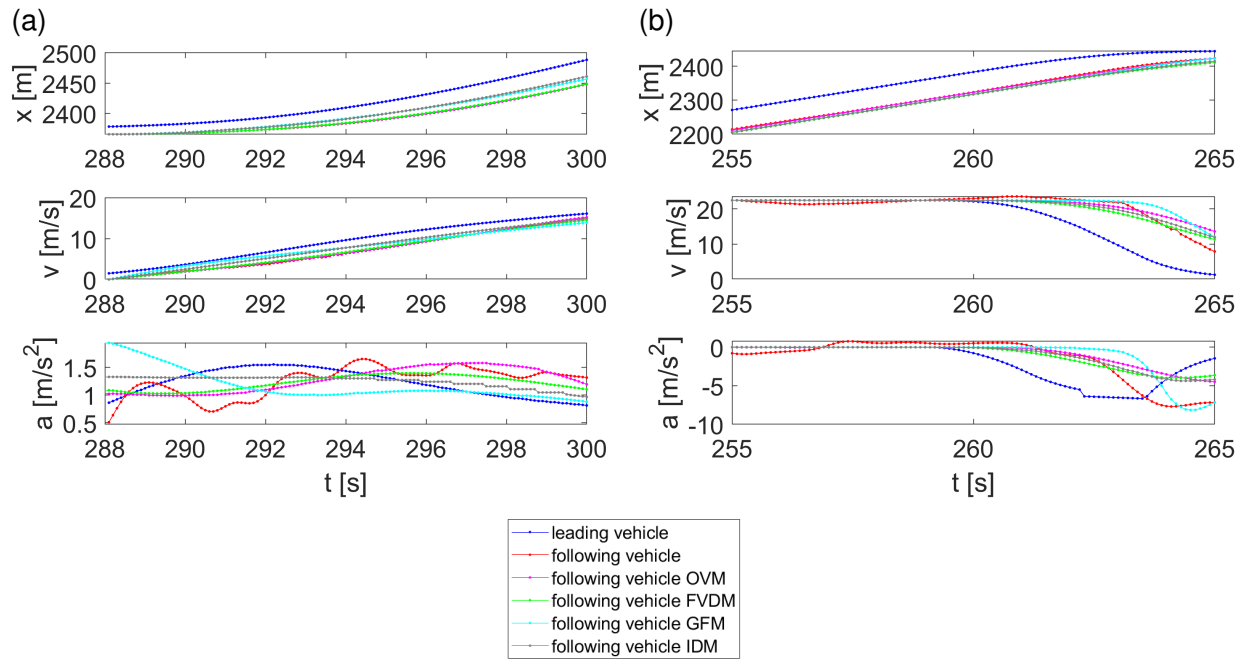

Figure 2.5: Excerpts of the trajectories of two participants with different driving regimes: (a) acceleration and (b) following and deceleration.

2.4.2 Calibration of Real Trajectory Data

The external validity of a driving simulator study can be evaluated by comparing the calibration results with the calibration results from real trajectory data. Compared with the driving simulator data, the real trajectory data contained driver behavior of many different drivers with unknown characteristics. Therefore, we compared the model parameters obtained from the real trajectory data with the median model parameters obtained from the simulator study, rather than the model parameters of each participant individually. Since the real trajectory data covered a road section of only 100m, a global calibration might not have been suitable (see Model Calibration). Hence, we performed both local and global calibrations.

Both calibration methods showed some shortcomings when applied to real data (see Table 2.4). The most obvious shortcoming was that the parameters τ (OVM, FVDM) or τ_1 and τ_2 (GFM) reached the value of the upper bound, hence the resulting acceleration was small. This can be explained by the broad scatter of the data. If a single optimal velocity function is assumed for all drivers, there can be large differences between the optimal and the actual velocity. In this case the models predict that the drivers accelerate or decelerate to reach the optimal velocity, although drivers might not want to accelerate or decelerate in reality because they do not perceive their current velocity as being far from optimum in reality. The models

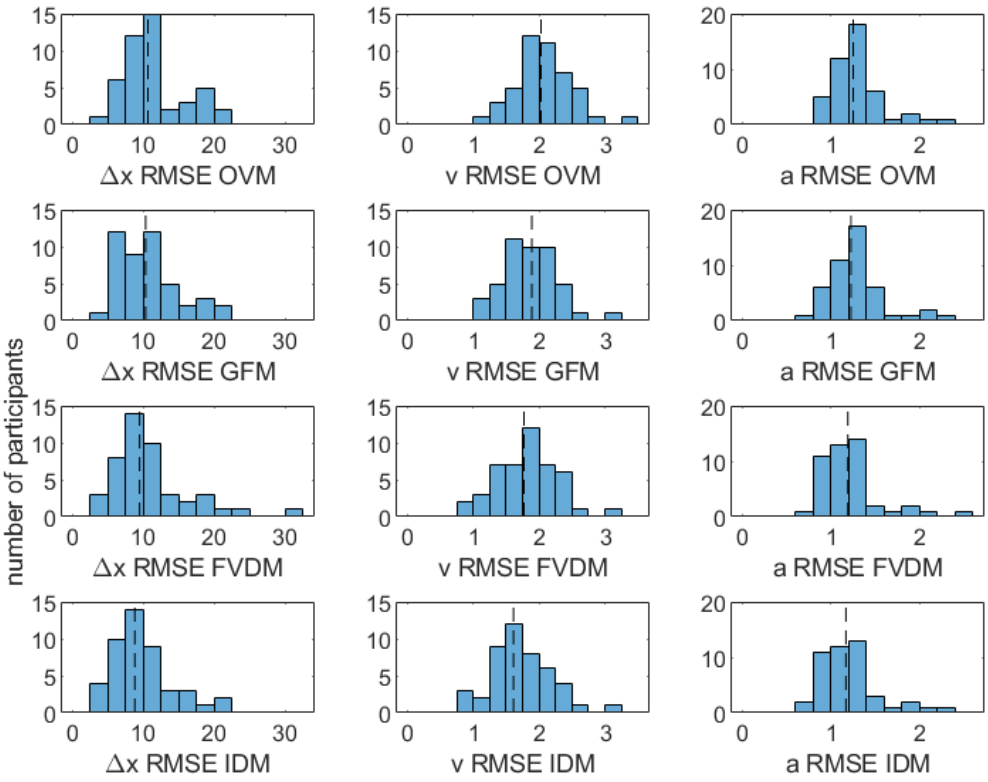

Figure 2.6: Root-mean-square error (RMSE) of headway, velocity, and acceleration of each participant. The dashed vertical lines represent the median values.

compensate for this difference between predicted and observed acceleration with a large τ. The broad scatter in the data also indicates that it is not appropriate to assume the same model parameters for each driver.

The values of v_{max} in the OVM, FVDM, and GFM were consistent with the results of the simulator data in spite of the slightly different road characteristics. In the IDM, however, the values of v_{max} were close or equal to the upper bound and larger than the maximum observed speed in the dataset. In all driving regimes except cruising, this could be compensated for by the other model parameters. The cruising driving regime was underrepresented in the dataset as it was associated with large headways, which could not be included in a dataset that covers a road section of only 100 m.

The parameter c (OVM, FVDM) varied in the two lanes and the two calibration methods. However, all values were larger than the values observed in the driving simulator, which means that drivers drive more riskily in real traffic. The same conclusion can be drawn from the parameter T (GFM, IDM), which was smaller in real traffic. One possible explanation might be that participants tend to show socially desirable behavior (in this case safe driving) in experimental studies, a phenomenon known as social desirability bias [37]. Another possible explanation is that in real traffic drivers might want to drive efficiently and utilize the available road capacity in an optimal way.

The parameters R_1 and R_2 in the GFM, the parameter in the FVDM, and the parameters a and b in the IDM also had significantly different values in the driving simulator study than in the real trajectory data.

The differences in the model parameters were not only caused by the different driver behavior in the simulator, but also by shortcomings in the real trajectory dataset. First, the driving regimes were not evenly distributed in the real trajectory dataset and, second, the real trajectory data were inaccurate, especially the acceleration values. These shortcomings led to unrealistic values of the model parameters, which implies that they are a limited benchmark for the model parameters obtained by the driving simulator study. Therefore, it is difficult to draw conclusions about the external validity of the driving simulator study.

2.4.3 Driver Characteristics

The first application of the individually calibrated model parameters was to analyze whether the driver characteristics were reflected in the model parameters. The participants were divided into groups according to their characteristics and their self-assessments of driver behavior (see Table 2.2). The distribution of the model parameters of the four models were then compared for each pair of groups. The group of elderly people was excluded from the anal-

Model	Parameter	Median driving simulator data	Global calibration Lane 1 real data	Global calibration Lane 2 real data	Local calibration Lane 1 real data	Local calibration Lane 2 real data
OVM	v_{max}	23.16	27.75	26.08	24.60	25.13
	c	0.42	0.82	1.37	0.92	1.66
	τ	1.98	10	10	10	10
GFM	v_{max}	27.28	31.66	31.70	28.03	30.55
	τ_1	5.86	10	10	10	10
	τ_2	2.04	10	0.61	10	0.69
	Δx_{min}	3.52	2.78	0	0	0.27
	T	1.13	0.2	0.2	0.2	0.2
	R_1	7.07	17.72	2.70	15.30	0.99
	R_2	74.57	1.82	25.89	0.05	23.18
FVDM	v_{max}	24.92	25.13	23.82	22.79	24.27
	c	0.40	0.73	1.21	0.94	1.60
	τ	8.86	10	10	10	10
	λ	0.30	0.50	0.31	0.14	0.1
IDM	a	1.63	0.64	0.93	0.47	0.69
	v_{max}	27.90	45	36.84	45	42.89
	Δx_{min}	4.35	6.35	2.52	5.14	2.97
	T	1.52	0.42	0.45	0.2	0.2
	b	1.55	1.11	3.16	2.12	6

Table 2.4: Comparison of Model Parameters Obtained from the Calibration of the Driving Simulator Data and the Real Trajectory Data.
Note: OVM = optimal velocity model; GFM = generalized force model; FVDM = full velocity difference model; IDM = intelligent driver model.

ysis owing to the low number of participants ($n = 5$). The category driving experience was also excluded since there was a strong correlation with the age category. Welch's t-test was performed to test the hypotheses that the model parameters for each pair of groups had equal means without assuming equal variance. Figure 2.7 shows all cases where the hypotheses were rejected at the 5% significance level, meaning that the means were significantly different.

The following driver characteristics were reflected in the model parameters.

OVM and FVDM:

- Participants who stated that they drove fast drove faster than participants who stated that they drove slowly. This is not a surprising insight, but it indicates that driver behavior in the simulator resembled the behavior in real traffic.
- Men drove more riskily than women.
- Participants who stated that they drove aggressively drove more riskily than participants who stated that they drove defensively.

Only OVM:

- Participants who stated that they drove aggressively drove faster than participants who stated that they drove defensively.

GFM:

- Participants who stated that they drove fast had a smaller τ_2 than participants who stated that they drove slowly. This finding is surprising as τ_2 is only relevant in the deceleration driving regime in which drivers cannot choose their speed freely.
- Participants who stated that they drove aggressively had a smaller R_1 than participants who stated that they drove defensively. This finding is plausible as small values of R_1 lead to large optimal velocity values for a given headway.
- Participants who stated that they drove carefully had a larger R_1, that is, a smaller optimal velocity for a given headway, than participants who stated that they drove fearlessly.

IDM:

- Participants who stated that they drove aggressively had greater acceleration than participants who stated that they drove defensively.
- Men maintained smaller time headways than women, that is, they drove more riskily, which is in line with the statement derived by c in the OVM and FVDM.

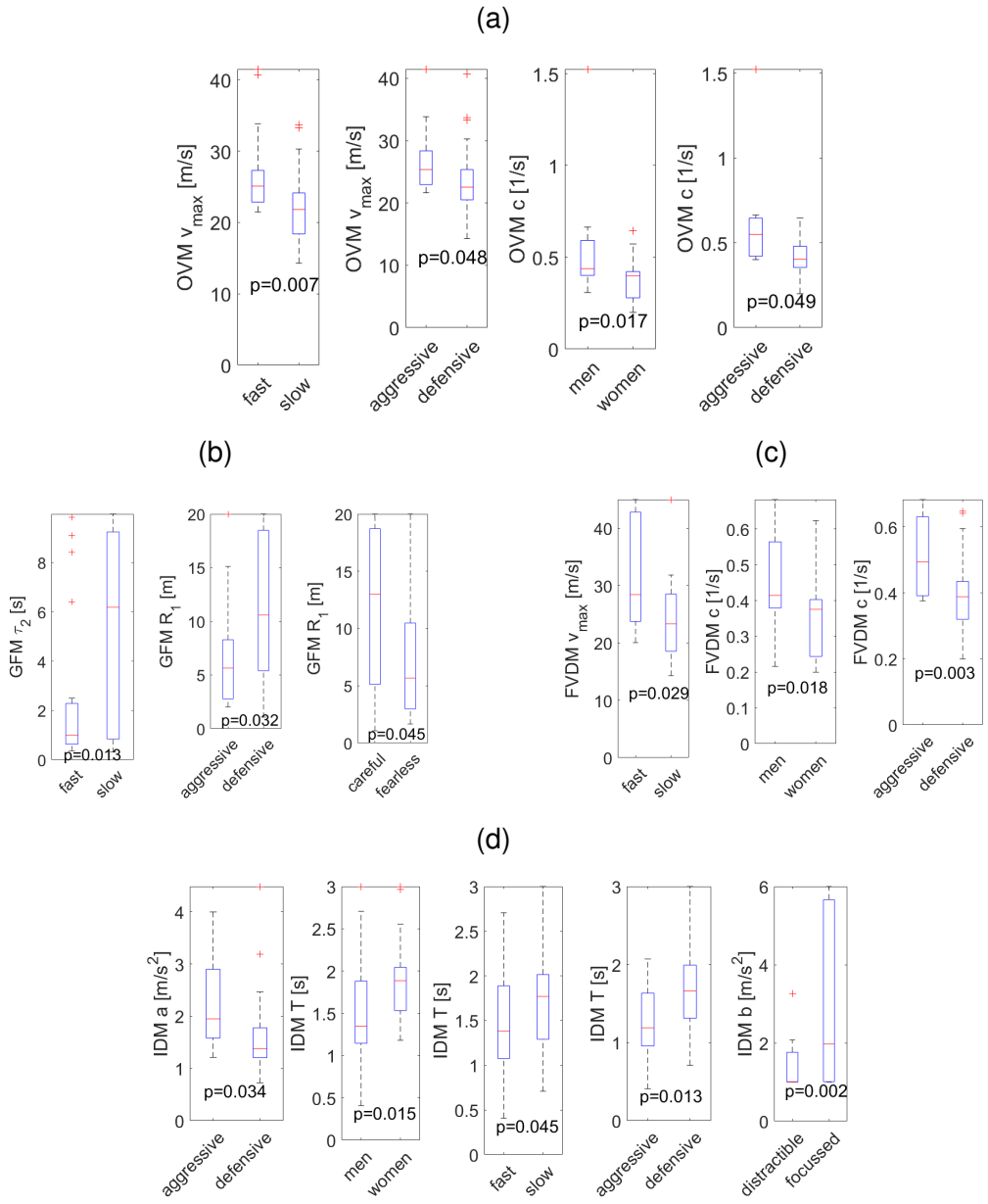

Figure 2.7: Distribution of the model parameters that are significantly influenced by driver characteristics (see Table 2.2).

- Participants who stated that they drove fast maintained smaller time headways than participants who stated that they drove slowly. Since the parameter T is only relevant in driving regimes in which drivers cannot select their speed freely, this finding is surprising.
- Participants who stated that they drove aggressively maintained smaller time headways than participants who stated that they drove defensively.
- Participants who stated that they were focused on driving had larger comfortable decelerations than participants who stated that they were distractible. This indicates that distractible drivers might keep a larger safety margin between the comfortable deceleration in normal situations and the maximum deceleration in dangerous situations.

It is worth noting not only which driver characteristics were reflected in the model parameters, but also which were not. For example, the parameter v_{max} indicated how fast drivers wanted to drive only in the OVM and the FVDM, not in the GFM and IDM. A possible explanation for this is that v_{max} is only relevant in the driving regimes free acceleration and cruising in the OVM and FVDM, whereas it is also relevant in all other driving regimes except standstill in the GFM and IDM.

All other driver characteristics that have not been mentioned above either did not have an influence on driver behavior or the number of participants was too small to show a significant influence. Note that the focus of this study was to perform a calibration of car-following models based on driving simulator data. The above findings should be treated with caution as they only demonstrate a possible application of the calibration results.

2.4.4 Driver Behavior in Extreme Situations

For the second application of the driving simulator data, the participants were brought into dangerous situations to investigate the validity of the models in such circumstances. The scenarios “emergency braking” and “strong braking” began when the desired speed of the leading vehicle was set to zero and it started decelerating. The scenario ended when both the leading vehicle and the participant have come to a standstill. An example with the trajectory of the leading vehicle, the observed trajectory of the participant, and the trajectory predicted by the models is given in Figure 2.8.

The acceleration profile shown in Figure 2.8 was typical of several participants. After the reaction time (in this case $\approx 2s$) the participants started braking and reached a maximum deceleration, dependent on the pressure applied to the brake pedal. Usually, this deceleration was higher than necessary to avoid a collision, so the participants released the brake until they stopped a few meters behind the leading vehicle. The short period of high deceleration

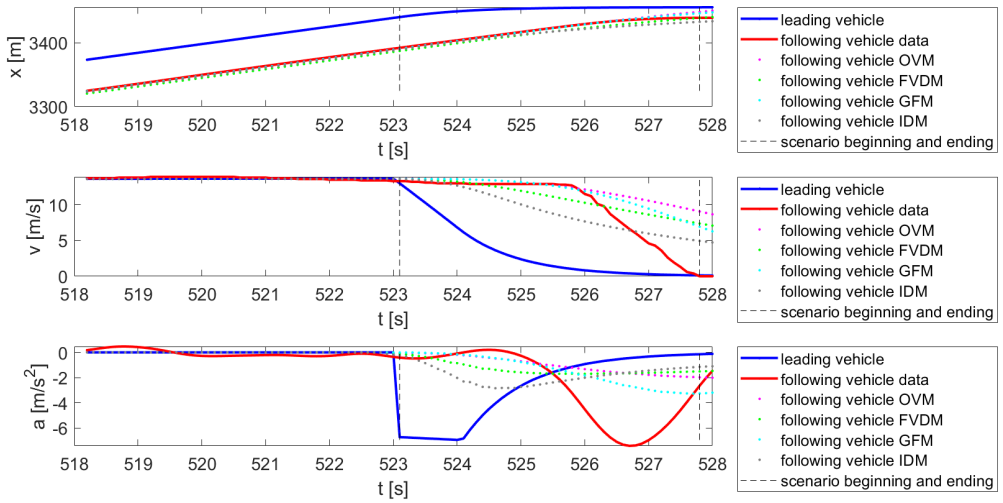

Figure 2.8: Example trajectory of Participant 30 (observed and modeled) and its leading vehicle during the scenario "emergency braking." The scenario begins at $t = 523.1s$ when the leading vehicle suddenly brakes.

can be interpreted as a moment of shock when faced with the sudden braking of the leading vehicle. After this moment of shock, the participants were able to adjust their deceleration to a more comfortable level. Figure 2.8 also shows that the models did not predict this strong deceleration. Instead, they predicted that the driver would decelerate more steadily. Figure 2.9 shows that this applied to almost all participants and all four models.

The models were also incapable of predicting the time when the participants reached the maximum value of the deceleration. The maximum value was reached later according to the OVM and GFM (median differences 1.0 s and 0.4 s respectively). The IDM predicted that drivers would reach the maximum deceleration earlier than they actually did (median difference -0.7 s), and the FVDM had no clear tendency (median difference 0.0 s). As a result, the velocity error and acceleration error during the scenario were substantially higher compared with normal driving (see Figure 2.10). However, the headway error did not substantially differ between normal and extreme driving situations. The ratio of the errors during the scenario to the errors in normal driving was roughly equal for all four models, so it is not possible to reach a conclusion about which model performed best in extreme driving situations. None of the models are able to appropriately describe driver behavior in extreme situations, despite their inclusion in the data used for calibration.

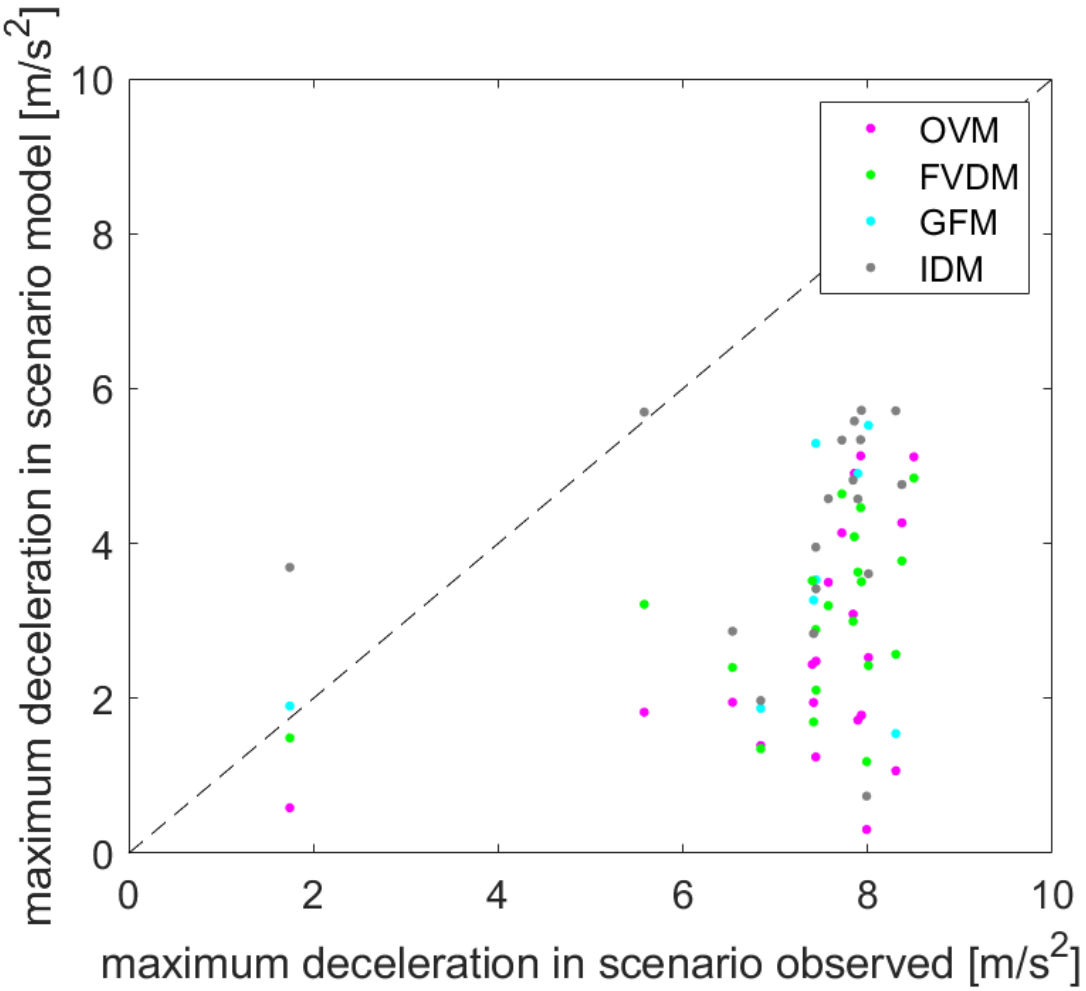

Figure 2.9: Maximum deceleration of each participant during the scenarios “emergency braking” and “strong braking” observed and predicted by the models.
Note: OVM = optimal velocity model; GFM = generalized force model; FVDM = full velocity difference model; IDM = intelligent driver model.

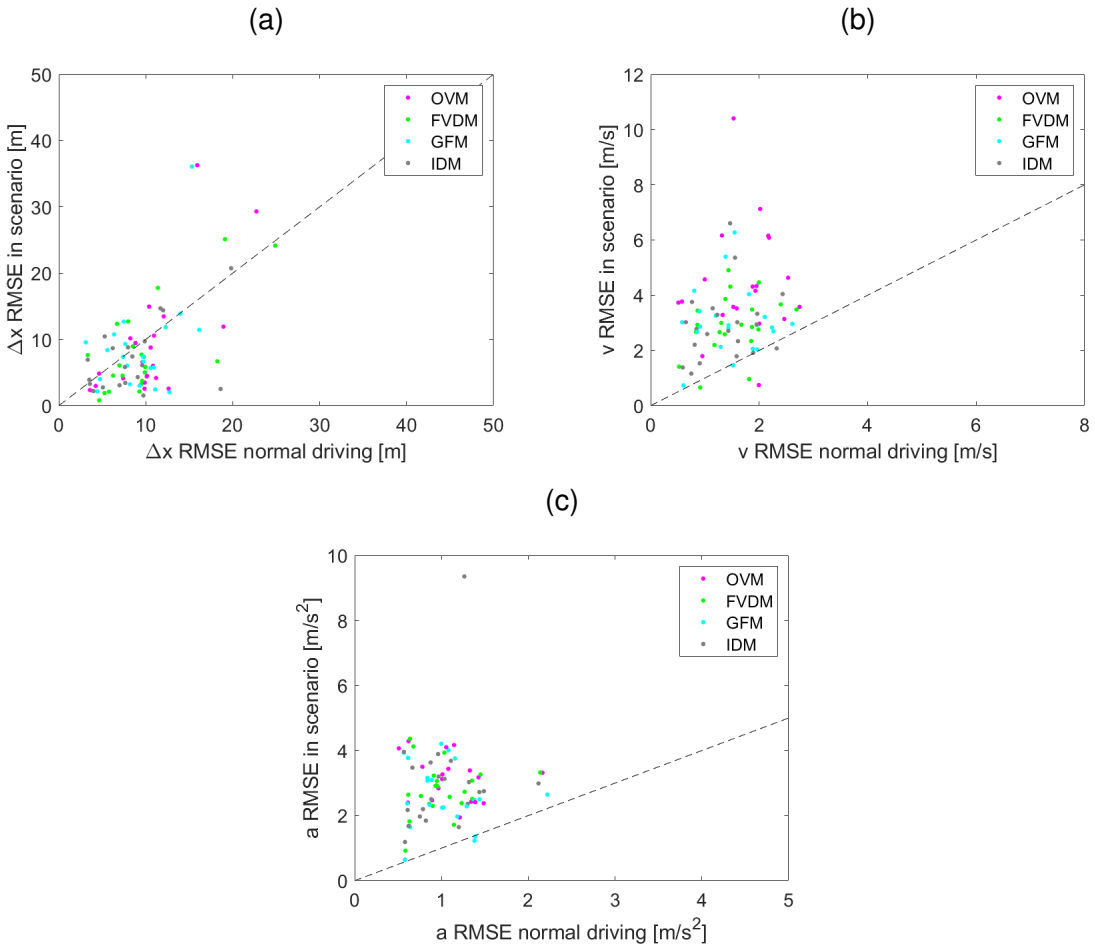

Figure 2.10: Root-mean-square error (RMSE) of the headway, velocity, and acceleration of each participant during normal driving and during the scenarios “emergency braking” and “strong braking.”

Note: OVM = optimal velocity model; GFM = generalized force model; FVDM = full velocity difference model; IDM = intelligent driver model.

2.5 Conclusions

In this paper we have calibrated four car-following models based on driving simulator data. The obtained parameters were mostly in a realistic range, and they reproduced individual driver behavior well. We have shown that the calibration results were valid with regard to speed, but that the participants drove less riskily than drivers on a similar road in real traffic.

We have presented two applications for which driving simulator data can be used and are more suitable than data from real traffic. By calibrating the model for each participant individually, the influence of driver characteristics on driving behavior can be analyzed. Some significant effects have been identified that need to be confirmed by an experimental design that focuses more on the systematic variation of driver characteristics. However, it can be concluded that the analysis of driver characteristics might help in understanding the stochastic nature of traffic flow.

Driving simulators allow the investigation of dangerous situations with extreme driver behavior that is not included in most datasets from real traffic. We have shown that model validity is weaker in these situations since the models cannot predict sudden, strong braking in a moment of shock. Car-following models must be developed further to have the capacity to describe both normal and extreme driver behavior. Driving simulator studies are particularly suitable for this purpose as participants can be put into dangerous situations in a controlled manner.

The analyses in this paper should also be extended to lane changes and especially to merging and weaving traffic where small headways and large velocity differences occur. The dynamics during lane changes cannot be described by the same model parameters used for normal car-following situations.

Despite the advantages of driving simulator data over real trajectory data, one must not ignore the shortcomings of driving simulators. Participants do not feel acceleration and cannot estimate their own speed as well as in real traffic. Moreover, they are aware of being in a simulated environment and of participating in an experiment, so they might not drive in the same way as in real traffic. One must decide carefully which conclusions drawn from simulator studies are valid.

Acknowledgments

The authors would like to thank Richard Schulte Holthausen, Jessica Balog, and Philipp-Armand Klee from RWTH Aachen University for their valuable support and dedication in enabling the driving simulator study. The authors would also like to thank Michael Herty from

RWTH Aachen University and Giuseppe Visconti from Sapienza University of Rome for their helpful advice and many insightful discussions.

References

[1] M. Treiber and A. Kesting. Microscopic Calibration and Validation of Car-Following Models – A Systematic Approach. *Procedia - Social and Behavioral Sciences*, 80:922–939, 2013. ISSN 18770428. doi: 10.1016/j.sbspro.2013.05.050.

[2] A. Kesting and M. Treiber. Calibrating Car-Following Models by Using Trajectory Data. *Transportation Research Record: Journal of the Transportation Research Board*, 2088 (1):148–156, 2008. ISSN 0361-1981. doi: 10.3141/2088-16.

[3] M. Pourabdollah, E. Bjarkvik, F. Furer, B. Lindenberg, and K. Burgdorf. Calibration and evaluation of car following models using real-world driving data. In *IEEE ITSC 2017*, pages 1–6, Piscataway, NJ, 2017. IEEE. ISBN 978-1-5386-1526-3. doi: 10.1109/ITSC.2017.8317836.

[4] J. Sangster, H. Rakha, and J. Du. Application of Naturalistic Driving Data to Modeling of Driver Car-Following Behavior. *Transportation Research Record: Journal of the Transportation Research Board*, 2390(1):20–33, 2013. ISSN 0361-1981. doi: 10.3141/2390-03.

[5] S. Ossen and S. P. Hoogendoorn. Validity of Trajectory-Based Calibration Approach of Car-Following Models in Presence of Measurement Errors. *Transportation Research Record: Journal of the Transportation Research Board*, 2088(1):117–125, 2008. ISSN 0361-1981. doi: 10.3141/2088-13.

[6] S. Hoogendoorn and R. Hoogendoorn. Calibration of microscopic traffic-flow models using multiple data sources. *Philosophical transactions. Series A, Mathematical, physical, and engineering sciences*, 368(1928):4497–4517, 2010. ISSN 1364-503X. doi: 10.1098/rsta.2010.0189.

[7] J. J. Olstam, J. Lundgren, M. Adlers, and P. Matstoms. A framework for simulation of surrounding vehicles in driving simulators. *ACM Transactions on Modeling and Computer Simulation*, 18(3):1–24, 2008. ISSN 10493301. doi: 10.1145/1371574.1371575.

[8] V. Punzo and B. Ciuffo. Integration of Driving and Traffic Simulation: Issues and First Solutions. *IEEE Transactions on Intelligent Transportation Systems*, 12(2):354–363, 2011. ISSN 1524-9050. doi: 10.1109/TITS.2010.2095846.

[9] C. Scotti, D. Kemper, M. Oeser, M. Haberstroh, F. Welter, S. Jeschke, and E.-M. Skottke. Psychologische Wirkungen von Arbeitsstellenlängen, -staffelung und -gestaltung auf den Verkehrsteilnehmer (Psychological effects of work-zone length, design and staggered alignment thereof on traffic participants).

[10] A. Ikeda. Study of driver characteristics using driving simulator considerations on difference in accident avoidance performance due to age. *JSAE Review*, 23(2):219–222, 2002. ISSN 03894304. doi: 10.1016/S0389-4304(02)00164-9.

[11] A. K. Pradhan, K. R. Hammel, R. DeRamus, A. Pollatsek, D. A. Noyce, and D. L. Fisher. Using eye movements to evaluate effects of driver age on risk perception in a driving simulator. *Human factors*, 47(4):840–852, 2005. ISSN 0018-7208. doi: 10.1518/001872005775570961.

[12] V. Cantin, M. Lavallière, M. Simoneau, and N. Teasdale. Mental workload when driving in a simulator: effects of age and driving complexity. *Accident; analysis and prevention*, 41(4):763–771, 2009. doi: 10.1016/j.aap.2009.03.019.

[13] B. Reimer, L. A. D'Ambrosio, J. E. Coughlin, M. E. Kafrissen, and J. Biederman. Using self-reported data to assess the validity of driving simulation data. *Behavior research methods*, 38(2):314–324, 2006. ISSN 1554-351X. doi: 10.3758/bf03192783.

[14] M. Oeser, T. Volkenhoff, D. Kemper, and C. Wietfeld. Wrong Way Driving on German Motorways – Safety Gain by a Low Cost Detection System. *TRB 94th Annual Meeting Compendium of Papers*, 2015.

[15] D. Basacik, N. Reed, and R. L. Robbins. Smartphone Use While Driving: A Simulator Study.

[16] S. Banerjee. *Evaluation and Validation of the Effect of Connected and Automated Vehicle Safety Applications on Driver Behavior - A Driving Simulator Approach: Dissertation*. Baltimore, MD, 2019.

[17] C.-Y. Chang and Y.-R. Chou. Development of Fuzzy-Based Bus Rear-End Collision Warning Thresholds Using a Driving Simulator. *IEEE Transactions on Intelligent Transportation Systems*, 10(2):360–365, 2009. ISSN 1524-9050. doi: 10.1109/TITS.2009.2020204.

[18] P. Nilsson, L. Laine, and B. Jacobson. A Simulator Study Comparing Characteristics of Manual and Automated Driving During Lane Changes of Long Combination Vehicles. *IEEE Transactions on Intelligent Transportation Systems*, 18(9):2514–2524, 2017. ISSN 1524-9050. doi: 10.1109/TITS.2017.2664890.

[19] A. Sharma, Z. Zheng, and A. Bhaskar. Is more always better? The impact of vehicular trajectory completeness on car-following model calibration and validation. *Transportation Research Part B: Methodological*, 120:49–75, 2019. ISSN 01912615. doi: 10.1016/j.trb.2018.12.016.

[20] B. Ciuffo, V. Punzo, and V. Torrieri. Comparison of Simulation-Based and Model-Based Calibrations of Traffic-Flow Microsimulation Models. *Transportation Research Record: Journal of the Transportation Research Board*, 2088(1):36–44, 2008. ISSN 0361-1981. doi: 10.3141/2088-05.

[21] M. Bando, K. Hasebe, A. Nakayama, A. Shibata, and Y. Sugiyama. Dynamical model of traffic congestion and numerical simulation. *Physical review. E, Statistical physics, plasmas, fluids, and related interdisciplinary topics*, 51(2):1035–1042, 1995. ISSN 1063-651X. doi: 10.1103/physreve.51.1035.

[22] M. Bando, K. Hasebe, K. Nakanishi, A. Nakayama, A. Shibata, and Y. Sugiyama. Phenomenological Study of Dynamical Model of Traffic Flow. *Journal de Physique I*, 5(11):1389–1399, 1995. ISSN 1155-4304. doi: 10.1051/jp1:1995206.

[23] G. F. Newell. Nonlinear Effects in the Dynamics of Car Following. *Operations Research*, 9(2):209–229, 1961. ISSN 0030-364X. doi: 10.1287/opre.9.2.209.

[24] R. E. Wilson. An analysis of Gipps's car-following model of highway traffic. *IMA Journal of Applied Mathematics*, 66(5):509–537, 2001. ISSN 0272-4960. doi: 10.1093/imamat/66.5.509.

[25] P. G. Gipps. A behavioural car-following model for computer simulation. *Transportation Research Part B: Methodological*, 15(2):105–111, 1981. ISSN 01912615. doi: 10.1016/0191-2615(81)90037-0.

[26] A. Kesting and M. Treiber. How Reaction Time, Update Time, and Adaptation Time Influence the Stability of Traffic Flow. *Computer-Aided Civil and Infrastructure Engineering*, 23(2):125–137, 2008. ISSN 10939687. doi: 10.1111/j.1467-8667.2007.00529.x.

[27] D. Helbing and B. Tilch. Generalized force model of traffic dynamics. *Physical review. E,*

Statistical physics, plasmas, fluids, and related interdisciplinary topics, 58(1):133–138, 1998. ISSN 1063-651X. doi: 10.1103/PhysRevE.58.133.

[28] R. Jiang, Q. Wu, and Z. Zhu. Full velocity difference model for a car-following theory. *Physical review. E, Statistical, nonlinear, and soft matter physics*, 64(1 Pt 2):017101, 2001. ISSN 1539-3755. doi: 10.1103/PhysRevE.64.017101.

[29] M. Treiber, A. Hennecke, and D. Helbing. Congested traffic states in empirical observations and microscopic simulations. *Physical review. E, Statistical physics, plasmas, fluids, and related interdisciplinary topics*, 62(2 Pt A):1805–1824, 2000. ISSN 1063-651X. doi: 10.1103/PhysRevE.62.1805.

[30] V. Punzo and M. Montanino. Speed or spacing? Cumulative variables, and convolution of model errors and time in traffic flow models validation and calibration. *Transportation Research Part B: Methodological*, 91:21–33, 2016. ISSN 01912615. doi: 10.1016/j.trb.2016.04.012.

[31] R. Hooke and T. A. Jeeves. Direct Search" Solution of Numerical and Statistical Problems. *Journal of the ACM*, 8(2):212–229, 1961. ISSN 0004-5411. doi: 10.1145/321062.321069.

[32] L. Li, X. Chen, and L. Zhang. A global optimization algorithm for trajectory data based car-following model calibration. *Transportation Research Part C: Emerging Technologies*, 68(5):311–332, 2016. ISSN 0968090X. doi: 10.1016/j.trc.2016.04.011.

[33] M. Herty, S. Moutari, and G. Visconti. Macroscopic Modeling of Multilane Motorways Using a Two-Dimensional Second-Order Model of Traffic Flow. *SIAM Journal on Applied Mathematics*, 78(4):2252–2278, 2018. ISSN 0036-1399. doi: 10.1137/17M1151821.

[34] A. Fazekas and M. Oeser. Performance Metrics and Validation Methods for Vehicle Position Estimators. *IEEE Transactions on Intelligent Transportation Systems*, pages 1–11, 2019. ISSN 1524-9050. doi: 10.1109/TITS.2019.2920973.

[35] E. Kallo, A. Fazekas, S. Lamberty, and M. Oeser. Microscopic traffic data obtained from videos recorded on a German motorway.

[36] J. Balog. *Untersuchung der Auswirkungen der Fahrereigenschaften auf das Fahrverhalten anhand einer Fahrsimulatorstudie (Analysis of the effect of driver characteristics on driver behaviour by means of a driving simulator study)*. Master Thesis at Institute of Highway Engineering, RWTH Aachen University, 2019.

[37] P. Grimm. Social Desirability Bias. In *Wiley International Encyclopedia of Marketing (eds J. Sheth and N. Malhotra)*, volume 50, page 537. doi: 10.1002/9781444316568.wiem02057.

3 Technical requirements for real-time traffic detection and dynamic infrastructure measures for safer behaviour

This conference paper was published under:

Berghaus, Moritz; Fazekas, Adrian and Oeser, Markus (2020). Technical requirements for real-time traffic detection and dynamic infrastructure measures for safer behaviour. 8th Transport Research Arena, Helsinki, Finland.
https://publications.rwth-aachen.de/record/815515/files/815515.pdf

Individual contributions:

M. Berghaus: study conception and design; analysis and interpretation of results; draft manuscript preparation (with a particular focus on the introduction, overview of the infrastructure measure and data processing, Sections 3.2, 3.3, 3.4.1, 3.4.2)
A. Fazekas: study conception and design; data collection; draft manuscript preparation (with a particular focus on the trajectory extraction, Sections 3.4.3, 3.5).
M. Oeser: study conception and design; supervision.

3.1 Abstract

One of the main reason for road accidents is unsafe driving behaviour due to wrong perception of the road. Infrastructure-based road safety measures are most effective if they only target those drivers that drive unsafely. In order to influence individual drivers towards safer behaviour, their behaviour must be captured and evaluated in real-time. This requires the collection of vehicle trajectory data. We present a system that detects vehicle positions and speeds using thermal cameras and computer vision algorithms. The system uses the concept of nudging to reduce the vehicles' speeds and guide them along a safe trajectory. In order to nudge unsafe drivers individually and in real-time, the detection system needs to fulfil several requirements which we discuss in this work. Furthermore, we present methods of data acquisition able to fulfil these requirements.

3.2 Introduction

Although most road accidents occur due to human errors, road design is often responsible for these errors. Roads should be designed in such a way that they match the expectations of the drivers. As a result, drivers automatically drive safely. This design principle is called "self-explaining road" [1]. Many aspects of this principle have been implemented in national road design guidelines. One example is the rule that the radii of two subsequent curves should not differ too much. However, this rule cannot be applied on motorway exits. On the motorway itself the radii are large, while in the exit smaller radii are required. Although drivers are aware that they have to decelerate in front of an exit, they might overestimate the curve radius and underestimate their speed. The system presented in this paper aims at reducing speeds in front of the exit in order to increase safety in the exit.

There are several approaches to make driver behaviour safer. Road safety campaigns aim at enhancing traffic safety usually by means of mass media [2]. The goal is to change driver behaviour in general, without focusing on those road sections where unsafe behaviour frequently occurs. Speed limit enforcement cameras can effectively reduce speeds at specific road sections, but they often lack acceptance as they are often perceived as "rip-off" rather than a means of increasing safety. Soft measures such as speed indicator devices contain radar detectors to measure vehicle speeds and give a visual feedback to each individual driver whether their speed is safe, without enforcing speeding. Walter and Knowles [3] found that these devices can reduce mean vehicle speeds by 1.4 mph (2.2 km/h) in free flow conditions. Taylor et al. [4] argue that 1 mph (1.6 km/h) of speed reduction reduces accident frequencies by 3 % on higher speed urban roads. However, Quddus [5] states that the average speed

has no significant effect on accident rates, but a smaller variation in speed can reduce the accident rates. This indicates that it is most effective to target only the drivers with the highest speeds and slow them down.

For this purpose, the vehicle positions and speeds of all vehicles taking the motorway exit must be known at any given time. Radar sensors used in speed indicator devices are not suitable for this as they are only able to measure the speed of one vehicle at a time without measuring its position. Video systems are however able to provide trajectories of all vehicles within their field of view [6]. The trajectories are evaluated in real-time to decide which drivers are driving unsafely.

Informing drivers about their current speed is only effective when drivers make a conscious decision to drive more safely. In complex driving situations such as motorway exits, the driver might not have the cognitive capacity to make this decision. Instead, we use a more subtle approach called nudging. A nudging intervention works on an intuitive level and can therefore evoke safer behaviour without requiring the driver's awareness. [7]

The remainder of this paper is structured as follows: Section 3.3 gives an overview of the infrastructure measure that we propose to make driver behaviour safer, and presents the field test location. In section 3.4 and 3.5 we focus on the methods to detect and track vehicles in real-time, which is essential for the presented infrastructure measure. Section 3.4 describes the necessary steps to transform image coordinates into road coordinates. Section 3.5 explains how the vehicle positions and speeds are estimated, and discusses the challenges associated with this infrastructure measure and the field test location. Unfortunately, we cannot present results on the effectiveness of the infrastructure measure since the field test is still ongoing, but we give an outlook in section 3.6.

3.3 Overview of the infrastructure measure

The case study location for this infrastructure measure is a motorway exit in Eindhoven, the Netherlands. The motorway leads from the motorway ring around Eindhoven into the city centre. The speed limit decreases from 80 km/h in front of the exit to 70 km/h at the beginning of the exit down to 50 km/h in the curve itself. Before the implementation of the infrastructure measure, the speed distribution and the traffic volume have been measured by simple radar sensors. On the straight part of the exit lane, the average speed was 82 km/h, at the beginning of the curve (where the speed limit of 50 km/h begins) it was 57 km/h and in the middle of the curve it was 56 km/h. On the main lanes, the average daily traffic volume adds up to 30,000 vehicles, while 4,700 vehicles per day use the exit. The ratio of heavy goods vehicles (HGV) is approximately 2 %. This ratio is characteristic for a road with predominantly urban traffic.

The main goal of the infrastructure measure is to influence those vehicles driving unsafely and nudge them towards safer behaviour. From this main goal, the technical and functional requirements for the whole system are derived backwards. In order to influence unsafe drivers exclusively, the driving behaviour of each vehicle has to be evaluated in terms of safety and the unsafe drivers have to identified. To achieve this, the positions and speeds of all vehicles must be captured. This leads to three main steps that are conducted in real-time:

1. Detecting vehicle positions and speeds
2. Identifying vehicles driving unsafely
3. Influencing those drivers to make their behaviour safer

In this section we describe the three steps in some detail. We start with the chronologically last step (3) as this is logically the first step in the design of the infrastructure measure.

The infrastructure measure aims at reducing vehicle speeds and make their trajectories along a curve safer. Drivers are influenced by a dynamic light pattern using the principle of nudging. The lights are state-of-the-art LED road studs embedded in the road surface. In order to avoid a haptic effect when driving over the road studs, the road studs are placed along the edge of the exit lane on top of the road marking. Each road stud must be controlled individually to create the desired pattern. The pattern must be shown only in front of the driver who is to be influenced to avoid influencing other drivers ahead or behind who drive safely. That means the light pattern is dynamic in space. Since the light pattern has a certain length, it cannot be shown if two vehicles follow each other too closely. This means the infrastructure measure cannot influence all unsafe drivers. However, it can be argued that small headways occur more frequently at low speeds.

Before influencing the drivers, their current behaviour must be assessed in terms of safety (step 2). Only those vehicles driving unsafely must be nudged. For this purpose, we define a speed threshold that is depending on the position along the exit lane. In front of the curve, the speed threshold decreases, while it is constant in the curve. The speed threshold is above the speed limit and above the average speed in order to target only the fastest drivers. If a vehicle is above the threshold, the light pattern will turn on and the driver will be nudged. If drivers change their speed along the road and pass the threshold between safe and unsafe, the light pattern has to react to this by turning accordingly on or off. At a later stage, more elaborate criteria for unsafe behaviour can be used by taking into account a combination of speed, longitudinal and lateral acceleration, and lateral deviation from the centre of the lane.

In order to show the light pattern at the right position and to the right drivers, the positions and speeds of all vehicles on the whole road section must be known (step 1). Cross-section

based sensors such as radar detectors or inductive loops are not suitable for this because they cannot adapt to changes in speed early enough. Instead, a set of cameras are installed along the road, each covering a section of up to 100 m. In curves the range of a camera may be lower due to vegetation next to the road. With multiple cameras, vehicles can be tracked along the road, so their positions and speeds are known at any given time. For the case study, we use thermal cameras as they can detect vehicles also at night. An additional very important aspect is that number plates are not visible in thermal imaging, so there are no privacy concerns with this technique.

The remainder of this paper focuses on the detection of the vehicles (step 1). A more detailed description of the whole infrastructure measure can be found in [8].

3.4 Road Geometry and Coordinate Systems

In the process of detecting the positions of vehicles on the road using cameras, there are three different coordinate systems involved. The cameras use an image coordinate system, the road alignment is described in a global coordinate system, and the vehicle positions relative to the road are described in a local coordinate system. The correct transformation between these coordinate systems is crucial for the accuracy of the detection.

3.4.1 Global Road Coordinate System

The horizontal alignment of the road is described in a global coordinate system, e.g. UTM. The road can be described either as a sequence of straight lines, circles and clothoids or as a polygonal chain. If plans of the road are not available, a polygonal chain can be extracted from a map of orthophotos from satellites. The points of the polygonal chain can then be fitted to a continuous line, e.g. a polynomial of k-th degree. The polynomial is two-dimensional and gives the North- and East-coordinate as a function $N(x)$ and $E(x)$, where x is the distance to some reference point, measured along the road.

$$\begin{bmatrix} E(x) \\ N(x) \end{bmatrix} = \begin{bmatrix} \sum_{i=0}^{k} p_{E,i} x^i \\ \sum_{i=0}^{k} p_{N,i} x^i \end{bmatrix} \tag{3.1}$$

For the case study road, we manually extracted the coordinates of 104 points along the road edge from satellite images. We then divide the road in four sections, each approximately 90 m long, and fit a 3rd degree 2D polynomial to the road coordinates of each section. The

Table 3.1: Goodness of fit for fitting the road coordinates to a set of polynomials

	Section 1	Section 2	Section 3	Section 4
RMSE East Coordinates [m]	0.060	0.076	0.300	0.039
RMSE North Coordinates [m]	0.015	0.021	0.126	0.067

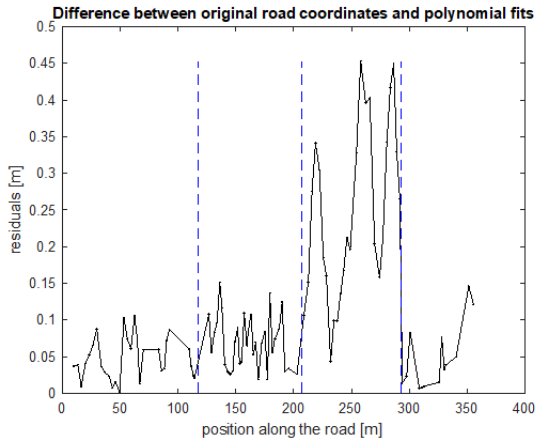

Figure 3.1: Residuals of the polynomial fits computed as the Euclidian distance between the road points and the corresponding points of the polynomials

sections overlap each other by 10 m to ensure that the transition between the polynomials is smoother. The goodness of fit in terms of the Root-Mean-Square Error (RMSE) is listed in Table 3.1 and the residuals are shown in Fig. 3.1.

At the transition between the four sections, the gaps between the polynomials are 0.033 m, 0.188 m and 0.142 m respectively. Hence, this method gives a good approximation of the road alignment, even if the accuracy of the input data is low.

3.4.2 Local Road Coordinate System

The positions of vehicles are described in a local coordinate system, i.e. in coordinates relative to the road. The x-coordinate is the position along the road. The y-coordinate is the orthogonal distance to the (right) edge of the road (see Fig. 3.2). This enables to describe the trajectory of a vehicle relative to the road. The transformation from local to global coordinates is simple and efficient if the road is represented by a polynomial. The normalised normal vector of the polynomial is required to account for the distance to the road edge.

$$\begin{bmatrix} x \\ y \end{bmatrix} \rightarrow \begin{bmatrix} E \\ N \end{bmatrix} : \begin{bmatrix} E(x,y) \\ N(x,y) \end{bmatrix} = \begin{bmatrix} E(x) \\ N(x) \end{bmatrix} + y * \begin{bmatrix} -N'(x) \\ E'(x) \end{bmatrix} / \left\| \begin{array}{c} -N'(x) \\ E'(x) \end{array} \right\| \tag{3.2}$$

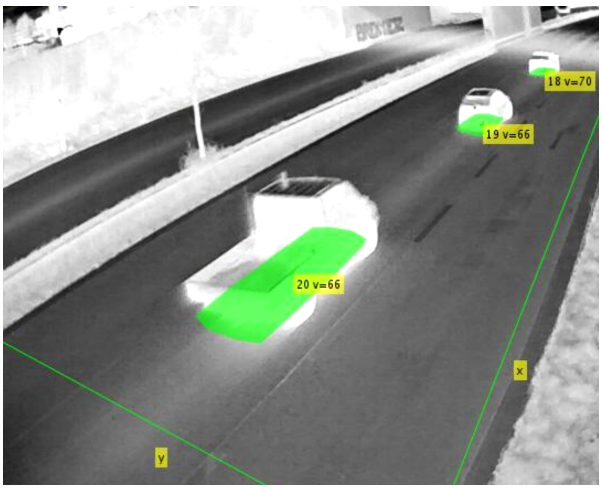

Figure 3.2: Detection of vehicle positions and speeds in a local coordinate system, where the x-coordinate is the (longitudinal) position along the road and the y-coordinate is the lateral position, i.e. the orthogonal distance of the vehicle to the right edge of the road

The transformation from global to local coordinates requires computing the distance between a point and a polynomial curve. Whether this is algebraically possible depends on the degree of the polynomial [9]. However, a numerical solution, e.g. with the Newton-Raphson method, is much easier to implement.

3.4.3 Image Coordinate System and Camera Calibration

The vehicle positions are detected in image coordinates. The transformation between image coordinates and the global road coordinates requires an internal and external calibration of the cameras. For the internal calibration, the Matlab Camera Calibration Toolbox [10] is used. To estimate the camera parameters, usually a grid of black and white squares or circles is filmed from different orientations [11]. Since thermal cameras cannot distinguish colours, we use a laminated aluminium plate with circular holes that is heated up to make it visible for the thermal camera. For the external calibration we use a point cloud with characteristic points of the road and its surrounding, e.g. road markings, lampposts, traffic signs or trees. The points can be extracted from an aerial image. Six characteristic points serve to compute a first approximation of the rotation matrix and the translation vector. Afterwards, a manual fine adjustment is conducted by projecting the whole point cloud into the camera image.

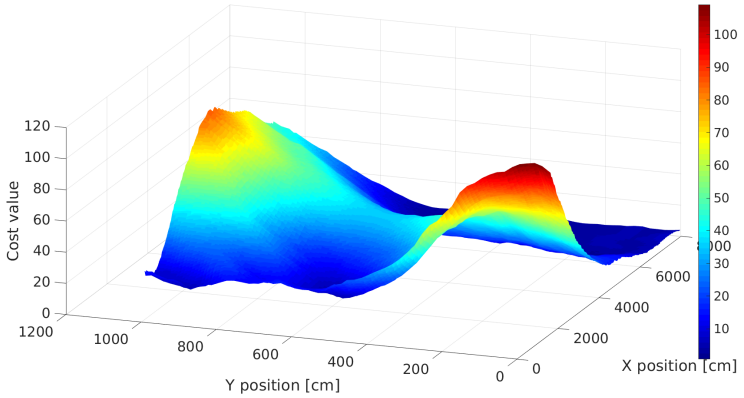

Figure 3.3: Cost function representing the probability of the presence of a vehicle [12]

3.5 Vehicle Detection and Tracking

In order to determine the position and velocity of a vehicle, two steps are necessary. Firstly, the detection of the vehicle in the area, in which the vehicles enter the field of vision. Each vehicle is represented by a point cloud that describes the corners and edges of the vehicle. The comparison of this projection to the distinctive features of the image enables the calculation of the probability of a car's presence on different positions in space (see Fig. 3.3) [12].

As soon as the presence of a vehicle is detected, its position is tracked in the following images. For this, the sequential Monte Carlo method, also called particle filter [13, 14], is used. A certain number of states that represent the movement of the vehicle in spaces is created. For each state the corresponding position of the vehicle in the next time step is translated to image coordinates using the methods presented in section 3.4. Thus for each state a hypothesis how the vehicles boundaries should be visible in the image is proposed. By comparing the postulated boundaries to the actual image features these hypotheses are assessed. This method is referred to as Chamfer-Matching [15]. For the state with the highest compliance, the corresponding position in the street system of coordinates is marked as the position of the vehicle. The speed is then computed as the derivative of the position with respect to time. Since inaccuracies in the position increase in the derivative, a moving average filter over the period of 1 second is used to smooth the speed values. This procedure is repeated until the vehicle leaves the field of vision of the camera.

In order to track vehicles over a longer period, multiple cameras are installed in a row. In the gaps between those cameras, the movements of the cars have to be calculated by extrapolation. Once a vehicle leaves the field of vision of one camera, it is assumed that the vehicle maintains the speed that was last detected by the camera. If the gaps between the

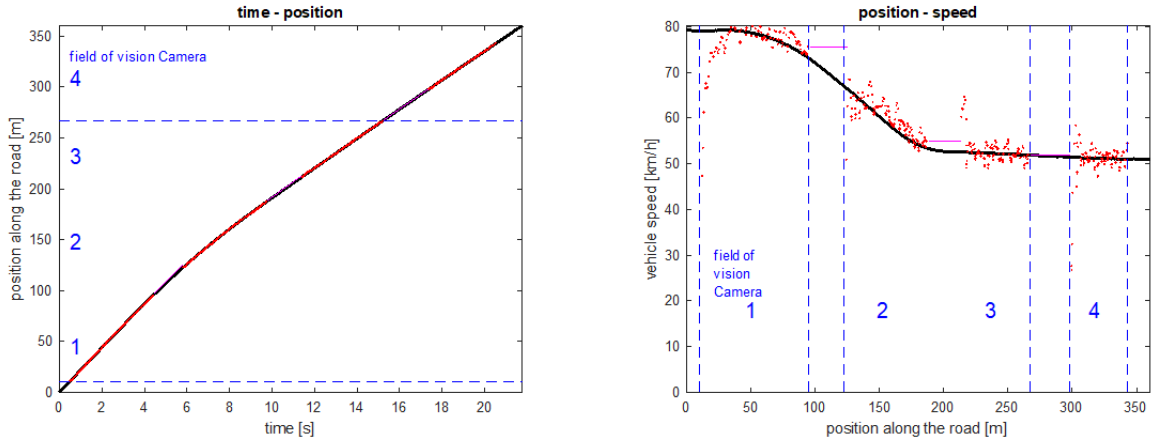

Figure 3.4: Example trajectory with true positions and speeds (black line), detected positions (assuming a normally distributed position error of 0.5 m) and computed speeds (red dots), and extrapolated positions and speeds (magenta line)

cameras are sufficiently small, the exact time when the car enters the field of vision of the next camera is predicted reliably (see Fig. 3.4). Hence, each vehicle is assigned a distinct ID that relates to all cameras. This allows us to analyse driver behaviour over a longer distance.

As a result of the above-mentioned method, vehicle trajectories over the course of the exit are obtained. This method is efficient enough to be implemented in real-time and yet robust against measurement errors. The trajectories are used for two purposes. On the one hand, the Processing Unit receives the current position and velocity of each vehicle in real time and decides whether to nudge that vehicle. Due to the measurement errors, a hysteresis is implemented in order to avoid that the nudging turns on and off too frequently if the vehicle speed is close to the threshold. On the other hand, in order to evaluate the efficiency of the nudging measure, the trajectories of the field test are analysed.

3.6 Conclusions and Outlook

In this paper, we have presented a system that is able to detect vehicle speeds and positions along a motorway exit in order to individually nudge those vehicles driving unsafely. Computer vision algorithms are used to track vehicles in thermal images and translate image coordinates into road coordinates. Since the system operates in real-time, both the tracking and the coordinate transformation must be computationally efficient. We therefore use a polynomial model of the road rather than a polygonal chain or the correct alignment. This allows a fast generation and evaluation of states during the tracking process, which is crucial for an

accurate position estimation. The system is robust enough to identify the vehicles driving above the speed threshold reliably.

The system has been developed and implemented on a motorway exit in Eindhoven, the Netherlands. A long term field test with different nudging scenarios is currently conducted. Afterwards the effectiveness of the infrastructure measure will be evaluated by analysing the vehicle trajectories. In the future, the system can be adapted for different locations where other safety interventions have not worked or are not applicable. It would especially be interesting to validate the system in several countries, where obedience rates to traffic signs can be very different. The prospect of connecting the system to a centralized Advanced Traffic Management System (ATMS) would enable a higher level of adaption to external factors like weather conditions and traffic diversion. This would result in a more flexible Cooperative-ITS solution.

Acknowledgments

This work is part of the project MeBeSafe which has received funding from the European Union's Horizon 2020 research and innovation programme under grant agreement No 723430.

References

[1] J. Theeuwes and H. Godthelp. Self-explaining roads. *Safety Science*, 19:217–225, 1995.

[2] T. Hoekstra and F. Wegman. Improving the effectiveness of road safety campaigns: Current and new practices. *IATSS Research*, 34(2):80–86, 2011. ISSN 0386-1112. doi: https://doi.org/10.1016/j.iatssr.2011.01.003. URL https://www.sciencedirect.com/science/article/pii/S0386111211000045.

[3] L. K. Walter and J. Knowles. Effectiveness of Speed Indicator Devices on reducing vehicle speeds in London: Published Project Report 314.

[4] M. C. Taylor, D. A. Lynam, and A. Baruya. The effects of drivers' speed on the frequency of road accidents: Prepared for Road Safety Division, Department of the Environment, Transport and the Regions.

[5] M. Quddus. Exploring the Relationship Between Average Speed, Speed Variation, and Accident Rates Using Spatial Statistical Models and GIS. *Journal of Transportation Safety & Security*, 5(1):27–45, 2013. doi: 10.1080/19439962.2012.705232.

[6] M. Bommes, A. Fazekas, T. Volkenhoff, and M. Oeser. Video Based Intelligent Transportation Systems – State of the Art and Future Development. *Transportation Research Procedia*, 14:4495–4504, 2016. ISSN 2352-1465. doi: https://doi.org/10.1016/j.trpro.2016.05.372. URL https://www.sciencedirect.com/science/article/pii/S2352146516303787. Transport Research Arena TRA2016.

[7] M. Karlsson, R. Brouwers, F. Fahrenkrog, T. Hof, A. Köhler, M. Ljung Aust, A. Selvefors, I. van Schagen, A. Sprajcer, A. Toffetti, D. Twisk, A. af Wåhlgren, and J. Ziegler. Delivery report for MeBeSafe. Measures for behaving safely in traffic: Integrated Framework. Deliverable D1.1. https://www.mebesafe.eu//wp-content/uploads/2018/04/MeBeSafe_D1.1_Integrated-framework.pdf (accessed 30 June 2019), 2017.

[8] A. Köhler, O. Op den Camp, M. van Mierlo, S. Ladwig, and M. Schwalm. Nudging Drivers

Towards Higher Safety Margins - Applications of the H2020-Project MeBeSafe. In *13th ITS European Congress, Brainport, The Netherlands, 3rd-6th June 2019*, 2019.

[9] C. Lennerz and E. Schömer. Efficient distance computation for quadratic curves and surfaces. In *Geometric Modeling and Processing. Theory and Applications. GMP 2002. Proceedings*, pages 60–69, 2002. doi: 10.1109/GMAP.2002.1027497.

[10] J. Bouguet. Camera Calibration Toolbox for Matlab. Computational Vision at the California Institute of Technology, 2015.

[11] Z. Zhang. A flexible new technique for camera calibration. *IEEE Transactions on pattern analysis and machine intelligence*, 22(11):1330–1334, 2000.

[12] A. Fazekas and M. Oeser. Performance metrics and validation methods for vehicle position estimators. *IEEE Transactions on Intelligent Transportation Systems*, 21(6):2853–2863, 2019.

[13] D. A. Forsyth and J. Ponce. *Computer Vision - A Modern Approach, Second Edition.* Pitman, 2012. ISBN 978-0-273-76414-4.

[14] A. Fazekas, M. Bommes, and M. Oeser. Vehicle Tracking using 3D Particle Filter in Tunnel Surveillance and Incident Detection. In *Models and Technologies for Intelligent Transportation Systems 2013*. IEEE, 2013.

[15] G. Borgefors. Hierarchical chamfer matching: A parametric edge matching algorithm. *IEEE Transactions on pattern analysis and machine intelligence*, 10(6):849–865, 1988.

4 Speed Reduction Measure Based on Nudging Using Real-Time Vehicle Trajectory Acquisition With Thermal Cameras

This paper was published under:

Berghaus, Moritz; Fazekas, Adrian; Lukas, Kristina; Schwalm, Maximilian and Oeser, Markus (2024). Speed Reduction Measure Based on Nudging Using Real-Time Vehicle Trajectory Acquisition With Thermal Cameras. IEEE Transactions on Intelligent Transportation Systems, 25(8), 8429 - 8443. https://doi.org/10.1109/TITS.2024.3366289

Individual contributions:

M. Berghaus: study conception and design; data collection; analysis and interpretation of results; draft manuscript preparation (with a particular focus on the introduction, literature review, field test setup, data processing, results, and conclusions, Sections 4.2, 4.3.1, 4.3.2, 4.4.1, 4.4.3, 4.5, 4.6).

A. Fazekas: study conception and design; data collection; draft manuscript preparation (with a particular focus on the literature review and trajectory extraction, Sections 4.3.3, 4.4.2).
K. Lukas: analysis of results; input to draft manuscript preparation (with a particular focus on the literature review, data processing, and results, Sections 4.3.1, 4.4.3, 4.5).
M. Schwalm: study conception and design.
M. Oeser: study conception and design; supervision.

4.1 Abstract

Accident risk and severity are closely associated with speeding. Reducing vehicles' speeds can contribute to road traffic safety. Conventional speed reduction measures, such as speed limit enforcement or speed indicator devices, only have a local effect, so they are not suitable for longer road stretches with varying speed limit, e.g. narrow curves in motorway exits. We present a novel speed reduction measure based on the concept of "nudging". The measure consists of LEDs embedded in the road marking that light up in front of vehicles which exceed a predefined speed threshold. The speeds and positions of the vehicles are gathered in real-time by thermal cameras and computer vision algorithms in order to target and follow only the speeding vehicles without distracting other drivers. The speed reduction measure was implemented and evaluated at a motorway exit with a narrow curve in Eindhoven, the Netherlands. The effectiveness was analyzed using linear regression models in order to take external influences on the speed (e.g. daylight, weather) into account. The mean speed was reduced by up to 2.7 km/h and the ratio of speeding vehicles by up to 40%. The most substantial speed reduction was observed on the straight part of the exit lane, which means that drivers decelerate earlier in front of the curve rather than in the curve, where longitudinal and lateral acceleration would overlap.

4.2 Introduction

Speeding is one of the main causes for road accidents [1]. The risk of speeding increases when drivers are inattentive or misperceive the road alignment. At road sections where speeding frequently occurs, the accident risk should be reduced by speed reduction measures. Several measures against speeding have been implemented by road authorities and evaluated by researchers. Road safety campaigns, for example, aim at enhancing traffic safety by means of mass media [2]. The goal of these campaigns is to change driver behavior in general, but they do not focus on the road sections with high accident risk. Speed enforcement cameras can effectively reduce speeds at specific road sections, but they lack public acceptance as they are often perceived as "rip-off" devices rather than as a means of increasing safety [3]. While speed limit enforcement increases drivers' attentiveness, it does not tackle drivers' misperception of the road alignment. Soft measures such as speed indicator devices use radar detectors to measure vehicle speeds and give visual feedback to individual drivers whether their speed is safe, e.g. with a "smiley", without enforcing the speed limit. Both speed enforcement cameras and speed indicator devices influence the drivers' behaviors only based on the speed limit and only at their specific, fixed locations. They are not suitable for longer

road stretches with varying speed limit.

In this paper, we present a measure that “nudges” drivers towards safer behavior. The term nudging originates from behavioral science and is defined as influencing someone’s behavior on an intuitive level without legislation or enforcement [4]. In our study, the drivers are nudged by a LED light pattern along the road markings if they exceed a predefined speed threshold. The light pattern adapts to the current position and speed of the individual vehicles, so it is only visible in front of the driver without distracting other drivers.

A crucial system component of this measure is a real-time trajectory acquisition system which is able to evaluate the position and speed of individual drivers. Radar sensors used in speed indicator devices are unsuitable for this purpose as they are only able to measure the speed of one vehicle at a time without measuring its position. Video systems are, however, able to provide trajectories of all vehicles within their field of vision [5]. Image processing consists of a 3D-model based vehicle detection in combination with a full camera calibration, which yields initial pose and position estimation in a world coordinate system. Trajectory estimation through tracking in world coordinates is conducted with a Bayesian approach, namely a sequential Monte-Carlo simulation. The data acquisition requires real-time capabilities with a limited time delay. In our system, we use thermal cameras as they are also capable of detecting vehicles at night and in adverse weather conditions, when normal RGB cameras only see the headlights of the vehicles. Since number plates are not visible in thermal images there are no data privacy concerns associated with this technology.

The system was implemented at a motorway exit in Eindhoven, the Netherlands. The motorway itself has large curve radii, while the exit lane has a small curve radius with short sight distances, which causes many drivers to approach the curve too fast or to inadvertently decelerate too late. Three cameras gathered vehicle trajectories over a road stretch of several hundred meters. The data of consecutive cameras were fused by object matching on the basis of the temporal dynamics of the tracked vehicles.

The remainder of this paper is structured as follows: Section 4.3 gives an overview of related work in the fields of traffic safety, driver behavior and computer vision. In Section 4.4, we describe the methodology of our proposed speed reduction measure and its evaluation. Section 4.5 presents the results of the field test.

4.3 Related Work

4.3.1 Speed and Road Safety

It is widely recognized that speed has an influence on accident rates and accident severity. Roads with a larger mean speed also exhibit higher accident rates [6, 7]. The Power Model developed by Nilsson in 1981 [8] states that in Sweden the ratio of fatal accidents before and after a speed reduction measure can be predicted by the 4th power (3rd power for personal injury accidents, 2nd power for all police reported accidents) of the ratio of mean speeds before and after. Several studies have confirmed the validity of the Power Model and refined the power values for other countries or different types of roads, e.g. [9–11]. In addition to the mean speed, a higher speed variance also leads to higher accident rates [12]. The fastest vehicles have a larger individual accident risk [13]. Thus, the effectiveness of a speed reduction measure can be evaluated based on both the change in mean speed and the ratio of speeding vehicles.

In horizontal curves, more accidents occur than on straight roads. Small curve radii and large distances to adjacent curves result in larger accident rates, e.g. [14]. Small radii cause drivers to decelerate later with respect to the center of the curve [15]. As a result, the deceleration occurs within the curvature [16]. In this case, tangential and radial acceleration overlap, which reduces the margin of safety, i.e. the difference between friction supply and demand [17]. Hence, it is safer to decelerate in front of the curve and maintain a constant speed within the curve.

Speed limit enforcement unquestionably contributes to a reduction in average speeds, the ratio of speeding vehicles, and accident rates, e.g. [18–21]. However, most drivers only comply with the speed limit at the specific location of the enforcement camera and reaccelerate behind it [22]. Some countries use average speed enforcement with two enforcement cameras and an automatic number plate recognition system [23]. Whilst this method can reduce speeds on a longer road stretch, it can only be applied at road sections with a constant speed limit. Speed indicator devices can reduce mean speeds by 1.4 mph (2.2 km/h) in free flow conditions, but the effect does not persist behind the sign [24].

Other speed reduction or traffic calming measures, such as warning signs, which can also be combined with flashing beacons, rumble strips, and lane narrowing, can also be applied to horizontal curves [25–28]. These measures either warn the drivers of the curve or direct their attention to the curve. Although these measures are effective in reducing speed without enforcement, they are not adaptive to the speeds of individual drivers. All drivers receive the same warning regardless of whether it is necessary to reduce their speed or whether they are already slow enough.

In-vehicle speed reduction measures, e.g. visual or acoustic warnings which are triggered when the speed limit is exceeded [29], are adaptive to individual driver behavior. However, these interventions are limited to drivers in vehicles equipped with such technology.

In order to analyze the effect of a speed reduction measure, other factors that influence the speeds at a specific road section have to be taken into account. Some factors such as the road design are not affected by the measure, so their effect does not have to be modelled. Other factors such as driver characteristics, which cause a large variation in the distribution of speeds, cannot be controlled by the experimental design, but it can be assumed that they are unaffected by the speed reduction measure. The effect of external factors such as weather, traffic conditions and light conditions can be modelled if data are available.

Several studies have confirmed that precipitation has a negative effect on speed and that a larger precipitation intensity leads to a larger speed reduction [30–33]. Other studies suggest that drivers reduce their speed in rainy conditions not due to wet road surfaces, but due to limited sight distances, which means that only high rainfall intensities lead to a significant speed reduction [34, 35]. On the contrary, drivers increase their speed when visibility is impaired due to fog as the perceived speed is lower in foggy conditions according to [36].

The influence of traffic on speed is given by the fundamental diagram of traffic flow [37]. There are many different mathematical relationships between traffic density and speed proposed in the literature, e.g. [38–41], corresponding to different shapes of the fundamental diagram. They all have in common that larger densities are associated with lower speeds due to the smaller distances between vehicles.

The differences in speed between day and night have been studied by [42]. The authors found that drivers drive significantly slower in darkness compared to daylight. Other studies indicate that the effect of light conditions on vehicle speeds depends on other factors such as weather and the speed limit [43].

4.3.2 Influencing Driver Behavior Using Nudging

Nudging has been defined by behavioral economists Thaler and Sunstein as a concept to influence people's behavior subconsciously without prohibiting alternative behaviors [4]. There are several examples where the concept has been applied to road design in order to increase traffic safety. For example, transverse road markings with decreasing spacings in front of curves or intersections can reduce speeds by increasing the perceived speed [44]. The same effect can also be achieved by trees next to the road [45]. Not only the distance between the trees can be reduced, but also the distance of the trees to the road, which creates the illusion of a narrowing road [45]. Measures that increase the salience and direct the drivers' attention,

such as red colored cycle lanes, are also considered as nudging [46].

4.3.3 Computer Vision

Camera based vehicle tracking has been of great interest in the research community in the last decades. Many different methods have been proposed for 2D, pixel-based tracking such as background modelling based on Gaussian Mixture Models [47], saliency descriptors within a framework like the Scale-Invariant Feature Transform (SIFT) [48], Histogram of Oriented Gradients (HOG) [49] or Haar Features [50]. Most recent research activities have introduced the use of deep learning solutions, like R-CNN (Region Based Convolutional Neural Networks) [51], but despite their good detection capabilites, even substantial computational resources cannot yet enable low latency applications like the nudging system introduced in this paper.

To generate 3D world coordinates from image coordinates, camera calibration techniques have early been introduced [52]. Nevertheless, the capabilities of capturing positions in world coordinates are very limited due to the maximal height of the installed cameras and the resulting perspective of the vehicles in the image. A more practical approach is the use of 3D model-based methods, which have also long been explored by various research groups. One of the early contributions in this domain include [53] and [54]. The authors used simple manually generated 3D models of vehicles in combination with a pinhole camera model to be able to project the 3D vehicle models onto the road plane. The models are then matched to image features such as edges by measuring their distance to the lines of the projected model. Combined, the results of the two research groups offer a comprehensive solution for the problem of 3D vehicle tracking. While the work of [53] is more focused on generating an initial pose and class hypothesis on the ground plane, in [54] the assumption is that the vehicle class and an initial position and orientation is known, primarily focusing on three-dimensional vehicle tracking. Hence, it has already been formulated at that time, that the two concepts could be linked in a way, that the initial position and pose estimation could serve as a front-end to the tracking system. Nevertheless, the real-time capabilities of such a combined system have not been investigated and would probably have been limited due to the lower computational capacity available at that time. The 3D model-based vehicle detection and tracking has since been greatly enhanced in more recent works, including [55] or [56]. A significant improvement was achieved by employing high-resolution CAD-based vehicle models, with an appropriate derivation of the 3D edges potentially present in the image. Furthermore, the images used for the feature matching exhibit a significantly higher quality in terms of resolution and contrast, leading to a more accurate position estimation.

More recent research activities regarding static, roadside vehicle tracking focus on the use

of LIDAR sensors [57–59]. While the results of the detection are promising, there is limited understanding regarding the applicability of the point cloud processing in real-time, low-latency scenarios and the influence of adverse weather conditions, which should not be overlooked when planning an extended validation period.

Additionally to tracking vehicles within single cameras or sensors, vehicle objects need to be passed from camera to camera for our application. One well known method already demonstrated by [60] is the use of features, specifically Haar-Like-features to match vehicles between tunnel surveillance cameras. Other approaches also use spatiotemporal cues to identify vehicles between pairs of cameras [61].

To the best of our knowledge, no studies have been conducted on the use of 3D vehicle tracking for real-time, low-latency ITS applications over time periods of several weeks under different illumination and weather conditions.

4.4 Methodology

In this paper, we present a speed reduction measure based on the concept of nudging [4]. Drivers are nudged if their speed exceeds a predefined threshold. The measure consists of LEDs installed along the road markings, so they are located in the drivers' natural field of view and are therefore not expected to cause distractions. The measure was first tested in a driving simulator study and then in a field test. Since the driving simulator study lies beyond the scope of this paper, we refer to [62–64] for more information. Vehicle trajectories are gathered using thermal cameras and computer vision algorithms.

4.4.1 Field Test Setup

A motorway exit in Eindhoven, the Netherlands (see Fig. 4.1), was selected for the field test based on accident risk, feasibility and support of the road authority. The motorway connects the ring motorway of Eindhoven with its city center. At the exit, the road category changes from motorway (NL: Autosnelweg) to dual carriageway (NL: Autoweg) without a visible change in road design, yet the speed limit drops from 80 km/h to 70 km/h. The curve radii on the motorway are large ($>$ 1000 m), which implies that the road alignment may not effectively discourage drivers from exceeding the speed limit. The exit is a half cloverleaf junction (NL: halfklaverbladaansluiting) with a minimum curve radius of 50 m (estimated from satellite images) and a speed limit of 50 km/h. The average daily traffic volume recorded by radar detectors over three work days in January 2018 was 30,000 vehicles per day on the two through lanes and 4,700 vehicles per day on the exit lane. The ratio of heavy goods vehicles

Figure 4.1: Field test location: motorway exit in Eindhoven, the Netherlands

(HGV) is about 2%, under the assumption that every vehicle longer than 10 m is a HGV.

The setup of the field test is shown in Fig. 4.3. Four thermal cameras were installed to record the trajectories of vehicles on the right through lane and the exit lane. The number of cameras was selected based on the length of the exit lane and the cameras' field of vision (FOV). The cameras were attached to existing lampposts, approximately 6 m above the road surface. Only the first three cameras were used for the field test due to limited CPU load. Vehicles on the left through lane were neglected as they are unlikely to change to the exit lane. Vehicle positions are represented in a road coordinate system with the longitudinal position $x\ [m]$ and the lateral position $y\ [m]$ (distance to the right edge of the road). Based on the current and previous positions, the speeds of the vehicles are computed. The positions and the speeds are used to check whether the criteria for nudging are fulfilled. The most important criterion is that only fast drivers are intended to be nudged. The speed threshold above which drivers are nudged depends on the position and it was defined based on the desired driver behavior, i.e. decelerating in front of the curve and driving with constant speed in the curve. The threshold is at 80 km/h at the start of the exit lane ($x \leq 80m$) and it decreases linearly to 55 km/h at the beginning of the curve ($x \geq 160m$, see Fig. 4.2). The threshold is given by the following equation:

$$v_{thr}(x) = \begin{cases} 80 & \forall x \in [40, 80] \\ 80 - \frac{x-80m}{160m-80m} \cdot (80-55) & \forall x \in (80, 160] \\ 55 & \forall x \in (160, 260] \end{cases} \tag{4.1}$$

where v_{thr} is the threshold speed in km/h.

The other nudging criteria are listed in Table 4.1. If a vehicle fulfils the nudging criteria, a light pattern is displayed in front of it. To this end, 80 LED road studs, 40 on each side of the exit lane with a spacing of 6 m, were installed along the road marking. The first pair of

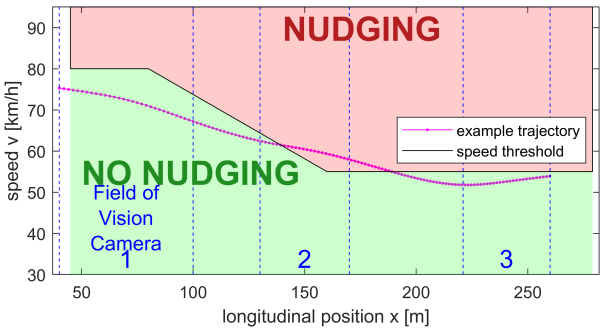

Figure 4.2: Speed threshold depending on the current position of the vehicle. If a vehicle's current position and speed is in the red area, it is nudged (if the other nudging criteria are fulfilled as well, see Table 4.1)

LEDs was located close to the start of the exit lane, and the last pair of LEDs was located approximately at the point with the smallest curve radius because the driving simulator study showed that most drivers have reached the speed limit (50 km/h) at this point [62, 63].

The following positions (rounded to the nearest 5 m) are of importance (see also Fig. 4.3):

x = 0 Location of camera 1

x = 40 Start of the exit lane

x = 40 Start of FOV camera 1

x = 45 Position of first LED

x = 50 Start of speed limit 70 km/h

x = 125 Through lanes and exit lane are separated by a double marking

x = 205 Start of speed limit 50 km/h

x = 260 End of FOV camera 3

x = 280 Position of last LED

In order to identify the most effective way to nudge the drivers, the LEDs showed different light patterns, hereafter referred to as *scenarios*. The light patterns were tested in a driving simulator study and the most effective ones were selected for the field test. For the derivation of the light patterns and an overview of the driving simulator study, we refer to [62–64]. In some scenarios, the lights were controlled to create an impression of movement towards the driver (*moving*), in the other scenarios, the lights did not move (*static*). The moving lights were

Table 4.1: Criteria for Nudging

Criterion	Explanation
$v(x) \geq v_{thr}(x)$	The current speed of the vehicle is above the speed threshold at its current position
$40m \leq x \leq 260m$	The vehicle is within the FOV of the first three cameras
$y(x) \leq ExitLaneWidth(x) - \frac{VehicleWidth}{2}$	The center of the vehicle is within the edges of the exit lane
$y(x = 40m) \leq 6m$	The vehicle is on the exit lane or on the right through lane at the start of the exit lane
$\Delta x \geq 90m$ (or 96 m depending on the scenario)	The headway to the leading vehicle is at least 90 m (or 96 m depending on the scenario)

expected to increase the perceived speed, while the static lights were expected to increase drivers' awareness. Light patterns moving in the same direction as the driver were excluded from the field test since participants in the driving simulator study perceived them as least appropriate for speed reduction [63]. Scenario 0 (lights inactive) served as a baseline to analyze driver behavior without the speed reduction measure. In scenario 8, the lights were inactive as well in order to analyze whether the effect of the measure persists. The color of the lights was red across all scenarios as this was found to be the most effective and most comprehensible color in the driving simulator study [62, 63]. Each scenario typically remained active for one week. The scenarios used in the field test are presented in Table 4.2. The speed reduction measure from a driver's perspective is shown in Fig. 4.4.

The positions of the active lights changes with the position of the vehicle so other drivers are not distracted. The light pattern is displayed by the 15 (16 in scenarios 3, 4 and 11) LEDs directly in front of the driver. As a result, drivers can only be nudged if the headway to their leading vehicle is at least 90 m (96 m in scenarios 3, 4 and 11; 15 or 16 lights with 6 m spacing). This restriction is acceptable as vehicles with a smaller headway have to adopt the speed of the leading vehicle, so their risk of speeding is lower.

Since the measure is inactive in scenarios 0 and 8, vehicles are not nudged in these scenarios even when fulfilling all the nudging criteria.

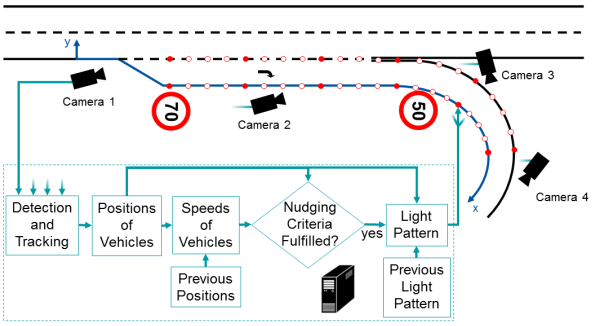

Figure 4.3: Setup and functionality of the field test (not to scale)

Figure 4.4: The speed reduction measure from a driver's perspective

4.4.2 Trajectory Acquisition

The trajectory acquisition is implemented through computer vision software applied to thermal imaging. In order to ensure a long-term validation over several months, the development of the trajectory estimation was focused on usability, ease of applicability and computational complexity. In this context, some simplifications have been used to increase the robustness of the data acquisition.

The idea behind the trajectory acquisition consists of three main concepts: (1) calibration [65] of the thermal cameras, (2) chamfer matching [66] to validate vehicle positions hypothesis and (3) particle filter [67] for fast 3D vehicle tracking and hypothesis generation. These methods are well known in the scientific community. The abstraction of the hypothesis generation and hypothesis verification in the context of applying particle filters in vehicle tracking has already been described in [68]. Thus, in this paper we only focus on the system specific adaptation of the algorithms in order to present a comprehensive overview to the reader.

Since a vast majority of the vehicles targeted for nudging at the test site were passenger cars, only one 3D model has been used for the chamfer matching evaluations. After calibrating the camera and making the simplification that the road segment lies on a flat plane, the process of validating positions by chamfer matching consists of projecting the 3D car model

Table 4.2: Description of the scenarios used in the field test

Scenario No.	**Light movement**	**Light pattern**	**Number of vehicles using the exit**	**Remark**
0		Lights inactive	19,030	
1	moving 50 km/h (2.31 Hz)	○○●○○●○○●○○●○○●	10,059	Less vehicles due to software issues
2	Static	○○●○○●○○●○○●○○●	18,458	
3	moving 50 km/h (2.31 Hz)	○○○●○○○●○○○●○○○●	19,417	
4	Static	○○○●○○○●○○○●○○○●	19,211	
5	moving 50 km/h (2.31 Hz)	○○●○○●○○●○○●○○●	79,198	Identical to scenario 1. 5 weeks (during Christmas holidays)
6	moving 20 km/h (0.93 Hz)	○○●○○●○○●○○●○○●	19,492	
7	moving 80 km/h (3.70 Hz)	○○●○○●○○●○○●○○●	19,181	
8		Lights inactive	18,780	
9	moving 50 km/h (2.31 Hz)	○●●○●●○●●○●●○●●	6,189	Less vehicles due to software issues
10	Static	○●●○●●○●●○●●○●●	28,702	
11	moving 50 km/h (2.31 Hz)	○○●●○○●●○○●●○○●●	19,790	

to specific locations on the street and evaluating the distance transform against the edge information of images. For the detection of vehicles, this has been carried out on a predefined grid on the lane with a specified orientation, which results in a cost value distribution shown in Fig. 4.5.

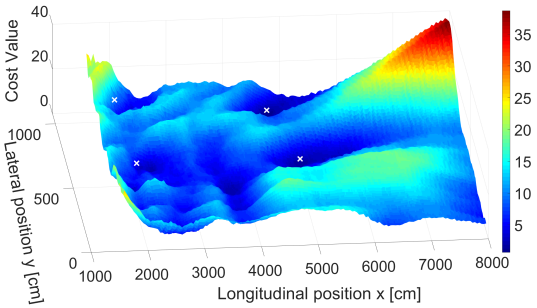

Figure 4.5: Chamfer Matching of a 3D model of a car, conducted on a grid of locations. The white crosses represent the ground truth positions which are used as reference to validate the cost value function

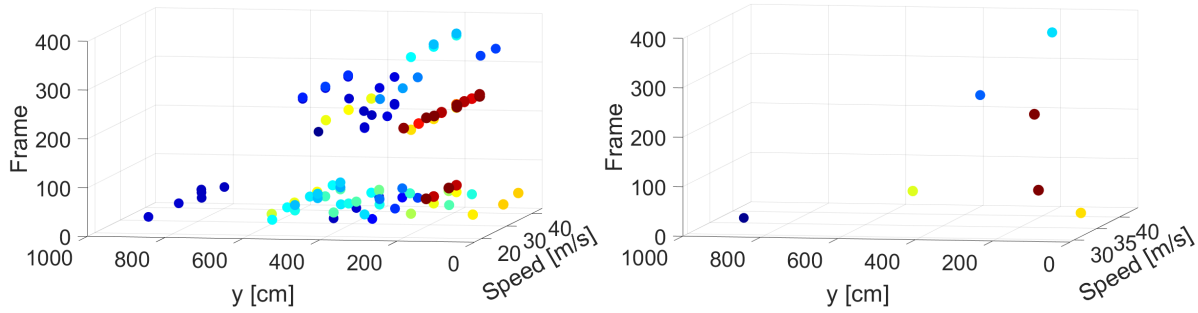

(a) (b)

Figure 4.6: (a) Local minima of chamfer matching trajectories with specific speed. (b) Result of applying a non-maximum suppression on the local minima with the information of a 3D car model

Vehicle detections are carried out by evaluating predefined hypothesized trajectories for different speeds within the detection grid and finding local minima of these hypothesized trajectories (see Fig. 4.6a). To avoid conflicting detections in the 3D space, we also apply a non-maxima suppression with the information of the 3D model size (see Fig. 4.6b).

After detecting individual vehicles, the 3D models are passed on to a Sequential Monte Carlo Simulation which tracks the vehicles by sequentially generating and evaluating the 3D pose and positions on the basis of the 3D car model and its image projection. The results of this tracking are time-sampled tracking data of the 3D models translated to the surface of the investigated exit lane (Fig. 4.7).

Vehicle hand-over between adjacent cameras along the exit lane is carried out by extrapolating vehicle positions beyond the limits of the cameras' FOV. When a vehicle leaves the

Figure 4.7: Snapshot of thermal camera 3 with the x-axis of the road coordinate system (green line with yellow labels) and the detected vehicle positions and speeds (green shapes with yellow labels)

camera's FOV, it is passed over to a simple simulation involving position updates based on mean speed and last known position. The resulting position of the simulated vehicle is taken as a mean of a bivariate normal distribution, where the standard deviation is increasing over time. The vehicles detected by the following camera are then matched using Maximum a-posteriori estimation, so the detected vehicles are matched to the most probable ones from the previous camera, based on the ellipsoid resulting from the simulated position distribution.

4.4.3 Data Processing

The available raw data provided by the computer vision algorithms consist of

- Vehicle ID
- Timestamp t ($\approx 30Hz$)
- Position $x(t)$, $y(t)$ ($\approx 30Hz$)

The time when a vehicle enters the FOV of camera i is noted as $t_{i,min}$, the time when a vehicle leaves the FOV of camera i is noted as $t_{i,max}$.

Data processing has to be performed in two distinct phases of the field test. During the field test, the data are processed in real-time to evaluate whether a vehicle fulfils the nudging criteria and to control the LEDs in order to nudge the right vehicles at the right positions. In the offline analysis, the data are used to evaluate the effectiveness of the measure.

Real-Time Data Processing

The main requirement in real-time data processing is an efficient and robust estimation of speed and position based only on the previous positions. Two cases have to be distinguished:
(1) the vehicle is within the FOV of one of the cameras, i.e. $t_{i,min} \leq t \leq t_{i,max}$, and
(2) the vehicle is between the FOVs of the cameras, i.e. $t_{i,max} < t < t_{i+1,min}$.

In case (1), the position is known and the speed has to be derived from the position:

$$v(t) = \frac{x(t) - x(t - \Delta t)}{\Delta t} \tag{4.2}$$

In order to make the speed estimation more robust against position errors, a relatively large Δt is used if available:

$$\Delta t = min(1sec, t - t_{i,min}) \tag{4.3}$$

In case (2), both position and speed are unknown and need to be extrapolated from the last known position and speed. It is assumed that vehicles maintain their speed and lateral position:

$$v(t) = v(t_{i,max}) \tag{4.4}$$

$$x(t) = x(t_{i,max}) + v(t_{i,max}) \cdot (t - t_{i,max}) \tag{4.5}$$

$$y(t) = y(t_{i,max}) \tag{4.6}$$

Offline Data Processing

To analyze the effectiveness of the measure, a more thorough offline data processing was performed. The accuracy of the speed and position estimation can be increased by smoothing the data using all available positions. Furthermore, obvious errors in the data and implausible trajectories can be removed from the analysis.

The following steps were conducted:

- Remove the trajectories of vehicles that have not taken the motorway exit as they are not relevant for the analysis.
- Smooth the trajectories in order to obtain realistic speed and acceleration values. The extrapolated position values between the FOVs of the cameras were not used. Since the accuracy of the positions depends on the distance to the camera, the position values were weighted according to this distance:

$$w(t) = 1 - 0.5 \cdot \frac{x(t) - x(t_{i,min})}{x(t_{i,max}) - x(t_{i,min})} \tag{4.7}$$

where $w(t)$ is the weight assigned to $x(t)$.

A smoothing spline is then fitted to the positions in both x and y-direction separately using MATLAB's Curve Fitting Toolbox [69]. The selected smoothing parameter was 0.1 in x and 0.8 in y-direction. The speed and acceleration can then be computed as the first and second derivative of the smoothed positions.

- Compute the headway Δx between consecutive vehicles.
- Remove the trajectories of vehicles that have not been tracked until the end of camera 3.
- Check the plausibility of the data according to the following criteria:
  - $min(\Delta x) < 0m$

    If negative headways occur, both the leading and the following vehicle are removed from the analysis.
  - $max(\Delta x) < 40m$

    In order to exclude trucks that have been falsely detected as two passenger cars, vehicles with a headway of less than 40 m throughout the whole exit are removed from the analysis.
  - $min(y) < 0m$ or $y(x) > RoadWidth(x)$

    Trajectories that lie outside the bounds of the road are removed from the analysis.
  - $|\frac{x(t_{i,max})-x(t_{i,min})}{t_{i,max}-t_{i,min}} - \frac{x(t_{i+1,min})-x(t_{i,max})}{t_{i+1,min}-t_{i,max}}| > 10m/s$

    or

    $|\frac{x(t_{i,min})-x(t_{i-1,max})}{t_{i,min}-t_{i-1,max}} - \frac{x(t_{i,max})-x(t_{i,min})}{t_{i,max}-t_{i,min}}| > 10m/s$

    or

    $|\frac{y(t_{i,max})-y(t_{i,min})}{t_{i,max}-t_{i,min}} - \frac{y(t_{i+1,min})-y(t_{i,max})}{t_{i+1,min}-t_{i,max}}| > 2m/s$

    or

    $|\frac{y(t_{i,min})-y(t_{i-1,max})}{t_{i,min}-t_{i-1,max}} - \frac{y(t_{i,max})-y(t_{i,min})}{t_{i,max}-t_{i,min}}| > 2m/s$

    Vehicles with a large velocity difference between two consecutive segments (a segment is either the FOV of a camera or the gap between two adjacent FOVs) are removed from the analysis. If a trajectory contains a large velocity difference, it is likely that the trajectory belongs to two vehicles that have falsely been matched between the cameras.

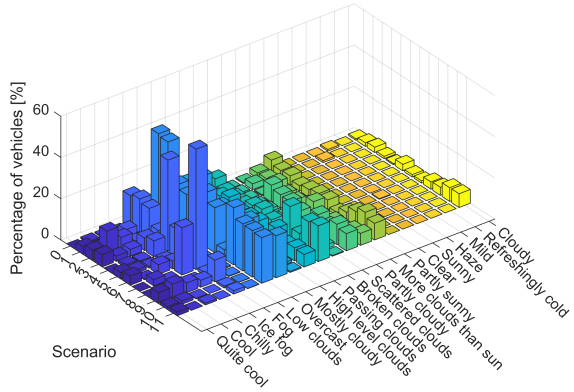

Figure 4.8: Distribution of weather conditions (sky descriptor) in each scenario

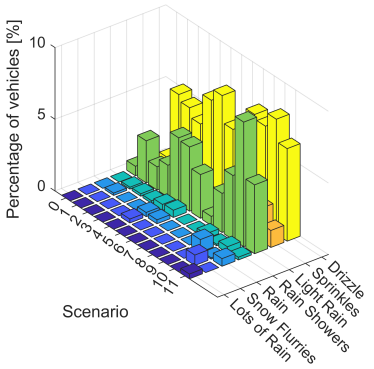

Figure 4.9: Distribution of weather conditions (precipitation) in each scenario. The bars for ”no precipitation” are not included in the figure.

The selection of these plausibility criteria involves a small chance of confusing extreme driving behavior with errors in the data. Since no ground truth is available, the plausibility criteria cannot be validated. However, we do not assume that the selection of these criteria creates any biases in the data that would affect the results.

Weather Data

In order to study the influence of weather conditions on the speed, we use a weather dataset provided by CustomWeather [70] which contains the daylight status (day or night), a sky descriptor, a precipitation descriptor and the temperature in $[°C]$. Since the scenarios were tested one at a time, the weather conditions are not evenly distributed over the scenarios (see Fig. 4.8 and 4.9).

4.5 Results

The speed reduction measure was evaluated from October 2019 to March 2020. During this time, the trajectories of 2,329,211 vehicles ($\approx$ 16,600 per day) on the exit lane and the right through lane were gathered. Since no data of vehicles on the left through lane were collected, the number of detected vehicles does not reflect the actual traffic volume. 727,299 of the vehicles used the exit lane, i.e. 31.2% of all detected vehicles and about 5,200 vehicles per day. 374,449 (51.5%) of these vehicles passed the thorough offline data processing, the rest was removed for the following reasons: 26.9% were not tracked until the end of camera 3, 4.7% had a negative headway, 9.3% had a small headway throughout the exit, and 7.5% had implausible trajectories. 295,843 (79.0%) vehicles could be used for the evaluation; the remainder was detected during periods when the nudge system was inactive or faulty. This sample of vehicles will be used in the following analysis steps if not stated otherwise. 198,666 (67.2%) vehicles fulfilled the nudging criteria for at least a short period of time. Note that this number is not equal to the number of vehicles that were actually nudged for two reasons: (1) In the scenarios 0 and 8, which were used as a baseline, vehicles were not nudged regardless of their speed, (2) some vehicles fulfilled the nudging criteria in the real-time data processing, but were excluded from the analysis in the offline data processing.

4.5.1 Descriptive Statistics

Mean Speed

At first, we analyze the mean speed along the motorway exit in the different scenarios. Note that the mean speed includes vehicles that do not meet all nudging criteria. As a result, the change in mean speed provides only preliminary insight into the effectiveness of the measure. Baseline scenario 0 (no lights) exhibited the highest mean speed beyond $x = 115$ (see Fig. 4.10). In the scenarios with nudging, the mean speed was up to 2.1 km/h (3.7%) lower ($x = 205$, scenario 4). However, speeds in scenario 8 are also lower than in scenario 0 although both scenarios are identical. It is also noteworthy that the mean speed at the beginning of the exit ($x = 50$) differs between the scenarios. This cannot directly be attributed to the measure as it is only 5 m behind the first light. Two potential explanations exist for this phenomenon: (1) drivers using the exit regularly become aware of the measure and adapt their speed accordingly or (2) external factors such as weather or traffic conditions influence the speed. Option (1) would affect the conclusion as to which scenario is the most effective one as the data do not reveal which driver experiences the measure for the first time and which uses the exit frequently. In order to control for the external factors, we build a statistical

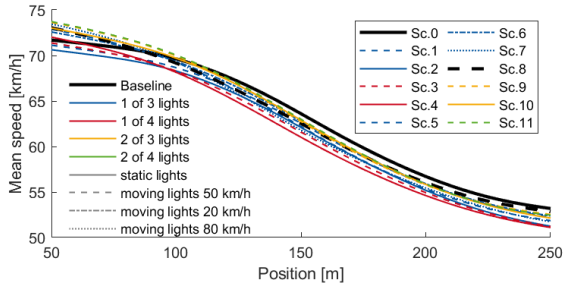

Figure 4.10: mean speed of all vehicles (both nudged and not nudged) in each scenario

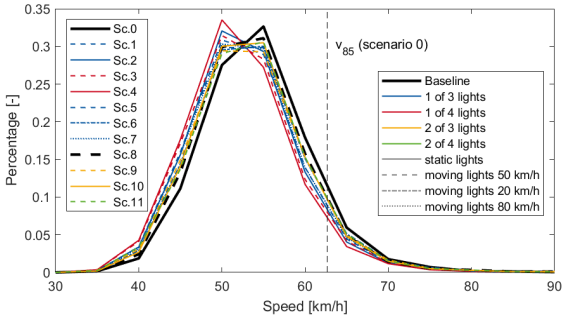

Figure 4.11: Speed distribution in each scenario at $x = 200$. The ratio of speeding vehicles is represented by the area under the curves to the right of the vertical dashed line

model for the initial speed at $x = 50$ (see Section 4.5.2), and for the speed throughout the exit lane (see Sections 4.5.3 and 4.5.4) to separate the effects of the external factors and the scenarios on the speed.

Speed Variance

The distribution of the speeds at the beginning of the curve ($x = 200$) (see Fig. 4.11) shows that the speed variance is large in all scenarios. The standard deviation ranges between 6.3 km/h at the beginning of the curve ($x = 200$) and 9.3 km/h near the start of the exit lane ($x = 50$). There are no considerable differences among the scenarios (between 8.6 and 9.3 km/h at $x = 200$).

Ratio of Speeding Vehicles

Since a speed reduction measure only targets speeding vehicles, the ratio of speeding vehicles is also an important criterion to evaluate the measure. First of all, we have to define

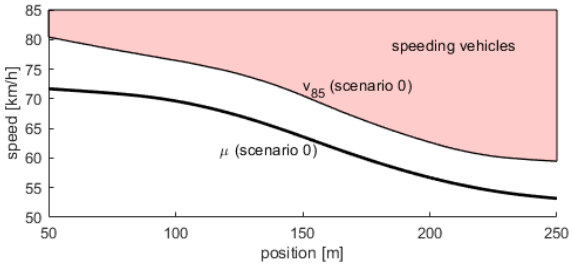

Figure 4.12: Definition of a speeding vehicle based on v_{85} of scenario 0 (no nudging)

what the term *speeding* refers to. The speed limit is not a suitable criterion in this case as the sudden change from 70 km/h to 50 km/h does not reflect realistic driver behavior. Instead, we adopt the 85% quantile of speeds (v_{85}), which is frequently used in road design [71]. Fig. 4.12 shows the v_{85} values in scenario 0, which we use as baseline. We assume that by definition 15% of all vehicles are speeding in scenario 0. Although this assumption is rough and arbitrary, it provides a suitable metric to compare the different scenarios. We then compute the ratio of speeding vehicles at each position, which can be illustrated by the area under the curves to the right of the vertical dashed line in Fig. 4.11.

The ratios of speeding vehicles in the different scenarios at each position are shown in Fig. 4.13. All scenarios have a lower ratio of speeding vehicles for $x \geq 115$. Although the speed distribution varies among the scenarios due to the external factors, the ratio of speeding vehicles decreases from the beginning of the exit lane ($x = 50$) to the end of the road section under study ($x = 250$) in every scenario. In scenario 4, the ratio of speeding vehicles decreases to 9%, which is equal to a reduction of 40% compared to scenario 0 (15%). This reduction does not significantly change if a different speed quantile (80% or 90%) was used. This shows that the measure is effective in slowing down speeding vehicles and thus reducing their ratio.

4.5.2 Model for Initial Speed

Both the mean speed and the ratio of speeding vehicles vary significantly over the scenarios at $x = 50$. To understand the reasons behind these differences, we build a model that incorporates both the effects of the scenarios and the effects of external factors. The model predicts the speed of the vehicles at $x = 50$, i.e. the beginning of the exit lane. We select a linear regression model of the form:

$$y_i = b_0 + b_1 \cdot x_{i1} + ... + b_k \cdot x_{ik} + \epsilon_i \tag{4.8}$$

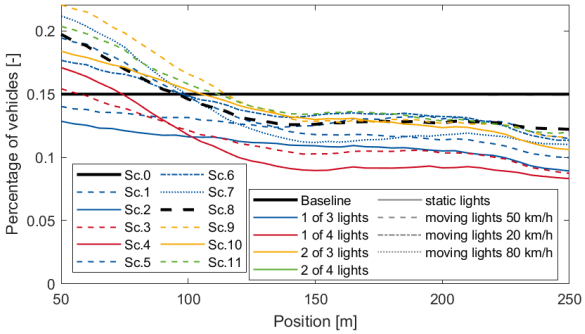

Figure 4.13: Ratio of speeding vehicles in each scenario, i.e. the ratio of vehicles faster than the 85% quantile of speeds in the baseline scenario 0

where y_i is the speed of vehicle i at $x = 50$, x_{ij} is the i-th observation of the explanatory variable j with $j = 1, \ldots, k$, b_j is the regression coefficient of variable j and ϵ_i denotes the error of the i-th observation. The following explanatory variables are considered:

- *Density* (continuous): the traffic density $[veh/km]$ is computed in one minute intervals as traffic flow divided by mean speed. Note that the traffic flow also includes vehicles that have not used the motorway exit. The density is included as vehicles have to adapt their speed to the speed of the other vehicles in dense traffic.
- *Scenario* (categorical): the scenario that was active while vehicle i passed the site. This variable allows to estimate the speed reduction effect in each scenario.
- *Night* (binary): 1 if vehicle i passed the site at night (between sunset and sunrise), 0 if it passed during the day. This variable is included because the literature review has shown that vehicles are slower at night [42]. This variable also allows to estimate whether the speed reduction measure is more effective at night, when the lights are better visible than during the day.
- *Rain* (binary): 1 if precipitation was recorded while vehicle i has passed the site, 0 otherwise. This variable is included because precipitation leads to smaller speeds according to the literature, e.g. [30].
- *Heavy Rain* (binary): 1 for either “rain showers”, “rain” or “snow flurries”, 0 for either “drizzle”, “sprinkles”, “light rain” or no precipitation. This variable is included additionally to the variable *Rain* because the literature review has shown that the speed reduction due to rain depends on the rainfall intensity, e.g. [30]. Since the weather data only contain qualitative descriptions of the rainfall intensity, only *Rain* and *Heavy Rain* are distinguished.

- *Fog* (binary): 1 if fog (sky descriptors “fog”, “ice fog” or “haze”) was recorded while vehicle i has passed the site, 0 otherwise. This variable is included because the literature indicates that speeds are surprisingly larger in foggy conditions [36]. This variable is also included to investigate whether the speed reduction effect is smaller in foggy conditions, when the lights might be less visible.

- *Temperature* (continuous): the temperature $[℃]$ recorded while vehicle i passed the site. Although there is no evidence in the literature that the temperature has a direct effect on the speed, we included this variable because it might act as a surrogate for the brightness, which is not fully represented in the binary variable *Night*, i.e. the speeds are lower in the middle of the night (lower temperature) than right after sunset (higher temperature).

All continuous variables are mean centered to avoid multicollinearity when interactions between explanatory variables are incorporated in the model. This step also allows an easier interpretation of the regression results. The categorical variable *Scenario* is dummy coded, i.e. there is one separate binary variable for each scenario.

In order to obtain a sparse model, we use a forward stagewise approach, i.e. we start with a trivial model with no explanatory variables. We then add the explanatory variables and interactions between them to the model one by one. The order is determined by the F value of an ANOVA. To prevent excessive model complexity, we exclude a variable x_j if its inclusion results in a higher Bayes' Information Criterion (BIC) than the model without x_j:

$$BIC = -2 \cdot log(L) + m \cdot log(N) \tag{4.9}$$

where $log(L)$ is the log-likelihood of the model, m is the number of estimated parameters and N is the number of observations.

To reduce the influence of outliers on the model parameters, we perform a robust regression using M-estimation. Additionally, outliers in terms of speed (vehicles faster than 5 standard deviations above the mean speed: 0.14% of the data) and traffic flow (traffic flow larger than 3,600 vehicles per hour: 0.02% of the data) are removed before fitting the model.

Table 4.3 presents the coefficients of the regression model, while Fig. 4.14 illustrates the BIC values for each stage. The variable *Heavy Rain* is not contained in the model as it increased the BIC. The coefficient b_0 means that vehicles drive on average 20.2 m/s under conditions of mean density ($15veh/km$), mean temperature ($7.3℃$), daytime, without rain and fog. The coefficient of the variable *Density* is negative, indicating that vehicles drive slower at large densities, which is in line with the fundamental diagram. At the maximum observed density ($104veh/km$), the estimated speed is 6.8 m/s lower than at the mean density. The

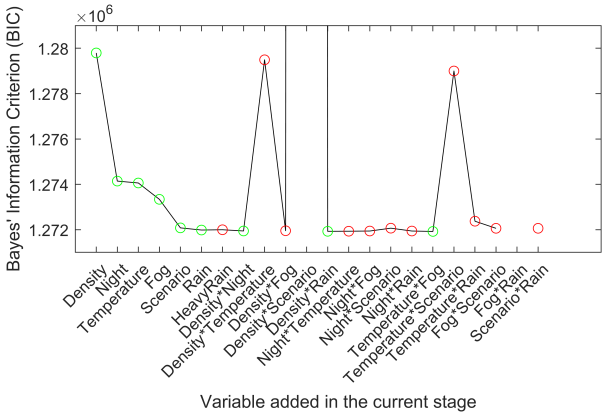

Figure 4.14: Stagewise regression for the initial speed. If the BIC decreases in the current stage, the variable is added to the model (green circles). If the BIC increases, the variable is not added to the model (red circles). A missing circle indicates that the variable is not significant.

coefficient of the variable *Night* shows that vehicles drive on average 0.69 m/s slower at night than during the day. At the maximum temperature ($20\,°C$), the estimated speed is 0.4 m/s higher than at the mean temperature. This finding supports the hypothesis that the variable *Temperature* acts as a surrogate for the brightness, which is not fully represented in the binary variable *Night*. It is worth noting that both the variable *Fog* and the variable *Rain* have positive coefficients, which means that vehicles drive faster in foggy and rainy conditions, which is to some extent in line with previous studies as mentioned in Section 4.3.1 [34] [35] [36]. Only some scenarios have a nonzero coefficient and the coefficients are both positive and negative, hence it remains unclear whether drivers who frequently use the exit adjust their speed in anticipation of the measure. Three interaction terms (*Density* * *Night*, *Density* * *Rain*, *Fog* * *Temperature*) are contained in the model, but they are practically irrelevant as their coefficients are close to zero. All other interaction terms were excluded as they either increased the BIC or were not significant. The adjusted coefficient of determination (R^2) of the model is 0.064, which shows that only a small fraction of the speed variance can be explained by external factors. The remaining speed variance arises from individual differences in driver behavior. Nevertheless, there is no clear evidence that drivers using the exit frequently reduce their speed in anticipation of the measure.

It has also to be noted that there is an autocorrelation in the residuals. As a result, it cannot be assumed that the residuals are independent of each other. This leads to larger standard errors of the regression coefficients and to larger p values. Since the p values are well below the 5% threshold, we do not expect the autocorrelation to impact the choice of the

Table 4.3: Coefficients of the regression model for the initial speed

	Estimate $[m/s]$	Standard Error	t	p
(Intercept)	20.209	0.011	1866.275	0
Density	-0.077	0.001	-65.737	0
Night=1	-0.687	0.01	-70.181	0
Temperature	0.033	0.002	21.141	0
Fog=1	0.543	0.018	30.589	0
Scenario=1	0	0		
Scenario=2	-0.418	0.019	-21.422	0
Scenario=3	-0.06	0.019	-3.145	0.002
Scenario=4	0	0		
Scenario=5	0.165	0.012	13.64	0
Scenario=6	0.175	0.019	9.121	0
Scenario=7	0	0		
Scenario=8	0	0		
Scenario=9	0	0		
Scenario=10	0.191	0.017	11.201	0
Scenario=11	0.346	0.019	17.869	0
Rain=1	0.196	0.015	13.065	0
Density * Night	-0.008	0.001	-5.389	0
Density * Rain	0.012	0.002	5.564	0
Fog * Temperature	0.014	0.003	4.126	0

explanatory variables. Moreover, the coefficients of the explanatory variables are not biased by the autocorrelation.

4.5.3 Model for Speed Reduction in front of the Curve

In this section, we analyze the speed reduction in front of the curve ($50 \leq x \leq 205$) caused by the measure and by external conditions. The form of the model is the same as in Eq. 4.8. For now, y_i is the speed of vehicle i at $x = 205$, which is the start of the 50 km/h speed limit, but we extend the model to other positions later. The initial speed is now an explanatory variable, but we neglect the factors that influence the initial speed. The explanatory variables of the previous model are still considered as they might also influence how much drivers reduce their speed in front of the curve or in the curve. Only the variable *Density* is not used in this model as it includes also vehicles that do not use the exit. These vehicles are not assumed

to have an influence on the speeds on the exit lane. Instead, the variable *Headway* is used, which represents the distance to the preceding vehicle in meters. The following explanatory variables x_j are considered:

- *Initial Speed* (continuous): the speed $[m/s]$ of vehicle i at $x = 50$
- *Headway* (continuous): the distance $[m]$ of vehicle i to the preceding vehicle on the exit lane at $x = 205$. Since the headway cannot be computed for vehicles without a preceding vehicle, these vehicles are assigned a headway value of 250 m.
- *Scenario* (categorical), *Night* (binary), *Rain* (binary), *Heavy Rain* (binary), *Fog* (binary), *Temperature* (continuous): see description in Section 4.5.2

Again, continuous variables are mean-centered, categorical variables are dummy coded, outliers are removed, and a robust forward stagewise regression is performed. The order of the variables is again determined by the results of an ANOVA.

The adjusted R^2 of the model is 0.302. Table 4.4 presents the coefficients of the regression model, while Fig. 4.15 illustrates the corresponding BIC values. Again, the variable *Heavy Rain* yields a larger BIC and is therefore not included in the model. The same applies to the variable *Headway*, which can be explained by the large proportion of vehicles without a preceding vehicle. All other explanatory variables are contained in the model along with several interaction terms. Under normal conditions (all variables $x_j = 0$, i.e. mean initial speed, mean temperature, daytime, no nudging, no rain, and no fog), the estimated speed at $x = 205$ equals 15.9 m/s or 57.3 km/h, which significantly exceeds the speed limit of 50 km/h. This highlights the necessity of a speed reduction measure at this motorway exit. Vehicles with a larger *Initial Speed* remain faster at $x = 205$ (coefficient of *Initial Speed* is positive), but they do reduce their speed more than vehicles with a lower initial speed (coefficient is smaller than one). In every scenario with nudging, the estimated speeds are lower, up to 0.54 m/s = 2.0 km/h in scenario 4, which shows that the speed reduction measure is effective. Note that the coefficients of the variable *Scenario* represent the average speed reduction, which also includes vehicles that did not fulfil the nudging criteria. It would be too complex to isolate the effect of the measure on the speed as the measure was activated at different positions and for different durations for each individual vehicle according to its speed and headway profile. Moreover, the measure appears to have a long-term effect as the coefficient of scenario 8 is nonzero although the lights were turned off in this scenario. For this reason, the coefficients of the variable *Scenario* only allow limited conclusions as to which scenario was the most effective one. The interaction between *Initial Speed* and *Scenario* is not contained in the model due to an increased BIC, hence the model does not reveal that the effect of the measure

depends on the speed. In adverse conditions (*Night*, *Rain* or *Fog*), vehicles reduce their speed between $x = 50$ and $x = 205$ more than in favorable conditions (day, no rain and no fog). The *Temperature* has a negligible influence on the speed at $x = 205$. Compared to the model for initial speed, the model for speed reduction contains more interaction terms, particularly interactions with the *Scenario* variable. However, many of these interaction terms are not significant or have a negligible effect size (coefficients close to zero). Note that the positive coefficients of the interaction terms, e.g. *Night* * *Scenario*, do not show that the measure is less effective at night. Small positive coefficients indicate in this case that the effect of the measure at night is smaller than the sum of the effect of the measure itself and the effect of the night itself. The interactions of *Night*, *Rain* and *Fog* with the *Scenario* are further analyzed in the following section, where we extend the model to other positions.

Table 4.4: Coefficients of the regression model for the speed reduction. Only the significant interactions are included

	Estimate $[m/s]$	Standard Error	t	p
(Intercept)	15.924	0.017	964.449	0
Initial Speed	0.35	0.002	203.579	0
Night=1	-0.609	0.024	-25.259	0
Rain=1	-0.671	0.1	-6.687	2.29e-11
Fog=1	-0.117	0.03	-3.872	0
Scenario=1	-0.211	0.027	-7.951	1.86e-15
Scenario=2	-0.312	0.022	-14.272	0
Scenario=3	-0.425	0.022	-19.029	0
Scenario=4	-0.545	0.026	-20.733	0
Scenario=5	-0.471	0.018	-26.011	0
Scenario=6	-0.396	0.022	-18.344	0
Scenario=7	-0.492	0.031	-16.07	0
Scenario=8	-0.363	0.021	-17.24	0
Scenario=9	-0.516	0.029	-18.004	0
Scenario=10	-0.455	0.02	-23.324	0
Scenario=11	-0.499	0.021	-24.299	0
Temperature	-0.013	0.001	-10.04	1.03e-23
Initial Speed * Night	0.013	0.002	5.872	4.31e-09
Initial Speed * Rain	-0.036	0.003	-10.405	2.39e-25
Initial Speed * Fog	-0.021	0.003	-7.73	1.08e-14
Rain * Night=1	0.13	0.018	7.086	1.38e-12
Night * Scenario=2	0.177	0.032	5.55	2.86e-08
Night * Scenario=3	0.089	0.032	2.82	0.005
Night * Scenario=5	0.248	0.026	9.412	4.88e-21

Continued on next page...

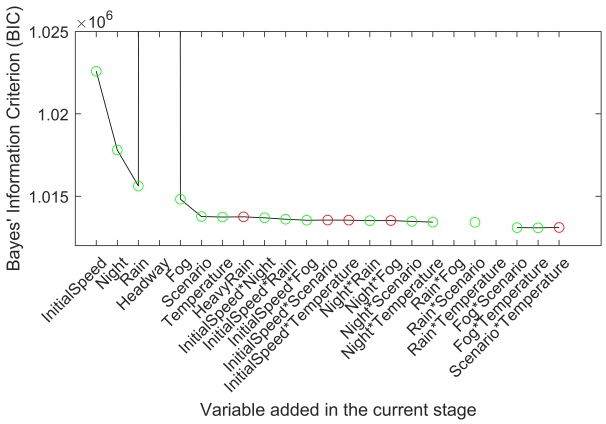

Figure 4.15: Stagewise regression for the speed reduction. If the BIC decreases in the current stage, the variable is added to the model (green circles). If the BIC increases, the variable is not added to the model (red circles). A missing circle indicates that the variable is not significant.

	Estimate $[m/s]$	Standard Error	t	p
Night * Scenario=6	0.252	0.031	8.076	6.70e-16
Night * Scenario=7	0.287	0.035	8.111	5.04e-16
Night * Scenario=8	0.184	0.031	5.9	3.65e-09
Night * Scenario=9	0.372	0.045	8.348	6.99e-17
Night * Scenario=10	0.202	0.03	6.668	2.59e-11
Night * Scenario=11	0.284	0.032	8.853	8.54e-19
Night * Temperature	0.012	0.002	7.084	1.41e-12
Rain * Scenario=7	0.322	0.145	2.223	0.026
Rain * Scenario=8	0.254	0.105	2.424	0.015
Rain * Scenario=10	0.273	0.102	2.671	0.008
Fog * Scenario=1	0.157	0.059	2.653	0.008
Fog * Scenario=3	0.095	0.047	2.002	0.045
Fog * Scenario=4	0.122	0.041	2.975	0.003
Fog * Scenario=5	-0.213	0.035	-6.045	1.50e-09
Fog * Scenario=6	0.203	0.049	4.116	3.86e-05
Fog * Scenario=8	-0.526	0.093	-5.632	1.78e-08
Fog * Scenario=9	-0.225	0.093	-2.416	0.016
Fog * Scenario=10	-0.341	0.094	-3.609	3.08e-04
Fog * Scenario=11	-1.129	0.087	-12.956	2.23e-38
Fog * Temperature	0.012	0.003	4.71	2.48e-06

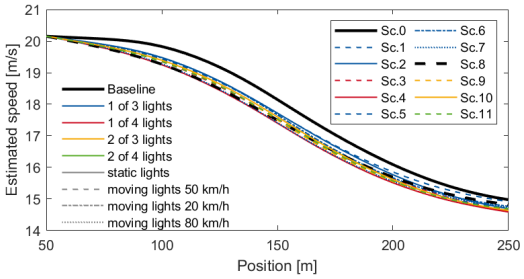

Figure 4.16: Estimated speeds for each scenario under normal conditions (mean initial speed, mean temperature, day, no rain and no fog)

4.5.4 Model for Speed Throughout the Exit Lane

In this section, we use the same approach as in the previous section in order to model the speed at all positions between $x = 50$ and $x = 250$ every 5 m. Naturally, not only the coefficients will depend on the position, but also the significance of the variables. For example, at positions close to $x = 50$, the speed is predominantly influenced by the initial speed, and all other variables have a negligible effect. To achieve consistent models, we use the same variables and interactions contained in the model for $x = 205$ for the other positions as well even if they are not significant or yield a larger BIC. Fig. 4.16 shows the estimated speed in each scenario under normal conditions. In all nudging scenarios, speeds are lower than in the baseline scenario 0. The largest speed difference occurs in the straight part of the exit lane while the speed reduction in the curve is smaller. This implies that the measure effectively prompts drivers to decelerate early, which has two safety benefits: (1) mitigating abrupt deceleration in case the drivers overestimate the radius of the curve, and (2) increasing the safety margin within the curve, where the friction available for longitudinal acceleration is lower due to the radial acceleration. Scenario 4 yields the largest overall speed reduction compared to scenario 0 (-0.75 m/s = -2.7 km/h at $x = 140$). The maximum speed reduction in the curve ($x = 250$) is -0.39 m/s = -1.4 km/h. Note that even a small speed reduction in the curve reduces the radial acceleration ($Speed^2/Radius$) considerably. Again, the estimated speeds in scenario 8 are lower than in scenario 0 although vehicles are not nudged in both scenarios.

To visualize the effect of the measure in rainy and foggy conditions and at night, we select only scenario 0 and 4 in the following figures. The effects in the other scenarios are similar if not mentioned otherwise. In rainy conditions, the estimated speeds are lower than in dry conditions, see Fig. 4.17a. This holds for every scenario and every position between $x = 50$ and $x = 250$. Note that the *Initial Speed* is an explanatory variable here, which means the

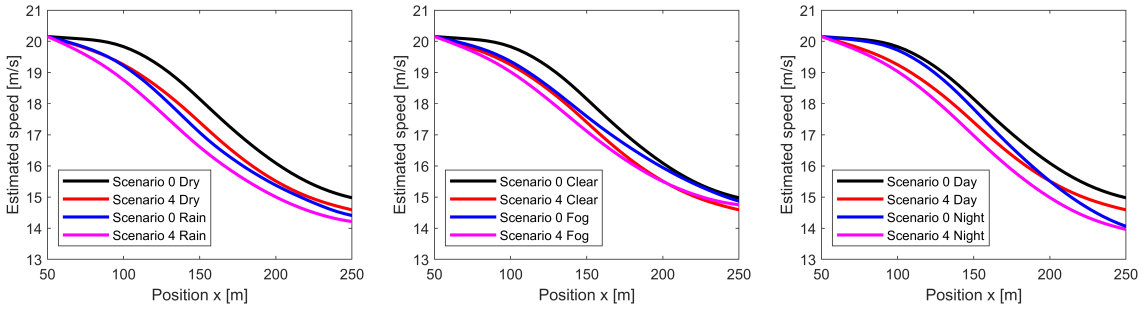

(a) (b) (c)

Figure 4.17: Effect of *Rain* (a), *Fog* (b) and *Night* (c) on estimated speeds in scenarios 0 and 4.

effect of *Rain* on the *Initial Speed* (see Section 4.5.2) is neglected in these models.

The speed differences between fog and clear sight are larger on the straight part of the exit lane than in the curve, see Fig. 4.17b. However, the speed differences between scenario 0 and 4 are larger in clear sight than in foggy conditions, which implies that the measure is less effective in foggy conditions. This can be explained by the worse visibility of the lights in foggy conditions. In scenario 4, the estimated speed in foggy conditions is slightly larger than in clear sight, but still smaller than in foggy conditions in scenario 0, where drivers are not nudged. However, the estimated speeds in foggy conditions in scenarios 1 and 6 are slightly larger than in foggy conditions in scenario 0 ($\approx$ 0.9 km/h), but these two scenarios cause only a small speed reduction even under normal conditions.

The speed differences between day and night are larger in the curve than on the straight part of the exit lane, see Fig. 4.17c. This shows that drivers are more cautious in the curve at night, but they decelerate late as it is more difficult to estimate the curve radius (and thus the appropriate speed in the curve) correctly at night. The speed difference at night between scenarios 0 and 4 is larger on the straight part of the exit lane than in the curve. Hence, the measure does not distinctly reduce the speed in the curve, but it does make the drivers decelerate earlier, which is desirable in terms of traffic safety. In scenarios 1, 2 and 5 to 11, the estimated speeds at night in the curve ($x > 225$) are slightly larger (up to 0.8 km/h) than in scenario 0 at night, but the earlier deceleration in front of the curve occurs in all scenarios. However, not all of these differences are significant.

As mentioned above, the models contain the same variables for each position even if the variables are not significant. Since the model for the speed at $x = 50$ is a trivial model (the model predicts the initial speed using the *Initial Speed* as an explanatory variable), this position is neglected. If $p > 0.05$, the null hypothesis that the coefficient of the variable is equal

to zero cannot be rejected, i.e. the variable does not significantly contribute to the power of the model. In our models, the variable *Temperature* and the interactions *Initial Speed* * *Night*, *Night* * *Temperature* and *Fog* * *Temperature* are not significant at some positions. These variables are not important for the interpretation of the models anyway, and we do not expect that including the insignificant variables notably affects the coefficients of the other variables. The interactions with the *Scenario* are significant as a whole, but the coefficients of some scenarios of the interactions *Rain* * *Scenario* and *Fog* * *Scenario* are not significant at some positions. This is due to the uneven distribution of weather conditions over the scenarios. Therefore, the conclusions drawn from these interaction terms should be treated with caution. The value decreases from $R^2 = 1$ at $x = 50$ (trivial model) to $R^2 = 0.21$ at $x = 250$. The reduced R^2 value indicates that each individual driver has their own comfortable speed in the curve, which does not necessarily match the speed on a straight road. This individual behavior cannot be incorporated into the model. Nevertheless, the model can verify that the speed reduction measure is effective throughout the exit lane.

4.6 Conclusion

In this paper, we have presented a speed reduction measure based on the concept of nudging. The measure targets only fast vehicles and influences the drivers individually according to their current speed and position measured by thermal cameras. The results have shown that the speed reduction measure successfully reduces the vehicles' speeds by up to 2.7 km/h on average and the ratio of speeding vehicles by up to 40%. Since lower speeds are associated with fewer accidents and since fast vehicles have a larger individual accident risk according to the literature, it can be concluded that the proposed measure can contribute to traffic safety. However, the duration of the field test was too short to demonstrate that the measure can reduce the number of accidents.

The largest effects were achieved with four static lights on each side of the lane with a spacing of 24 m. Both static and moving lights are able to increase drivers' awareness and therefore prevent speeding in the motorway exit. However, it is difficult to compare the effects of the different light patterns due to the study design. The scenarios were tested one after another mostly for one week, and all drivers who use the exit frequently have experienced the scenarios in the same order. It can therefore not be ruled out that the effect of the measure persists, i.e. drivers become used to the measure and reduce their speed even if they were not nudged. The speed reduction effect in scenario 8, in which the measure was inactive, supports this assumption. Nevertheless, we do not expect that the study design leads to an overestimation of the effect of the measure. If different light patterns are investigated in future

field tests, a randomized study design is recommended to control external influences and to study long-term effects. It is also recommended to compare the presented speed reduction measure based on nudging with other conventional speed reduction measures.

The speed reduction in the straight part of the exit lane was larger than in the curve. This shows that drivers decelerate earlier if they are nudged, which contributes to traffic safety. This effect is particularly beneficial at night, when drivers decelerate later than at daytime. The measure is also effective in rainy conditions, but the effect in foggy conditions is smaller due to the reduced visibility of the lights.

The computer vision technology using thermal cameras has been demonstrated to provide trajectories in real-time with sufficient accuracy during both daytime and nighttime. In order to increase the sensitivity of the system and to obtain more plausible trajectories, the gaps between consecutive cameras should be reduced in future applications of this technology.

In further research, the presented speed reduction measure can be applied to other locations where speeding is an issue and where conventional speed reduction measures are not suitable. It is also recommended to analyze the effect on traffic safety as measured by accidents in a long-term study.

Acknowledgment

The research presented in this paper is part of the project MeBeSafe (Measures for Behaving Safely in Traffic), which has received funding from the European Union's Horizon 2020 research and innovation programme under grant agreement No 723430.

The authors would like to thank Anna-Lena Köhler and Stefan Ladwig (both Institute for Automotive Engineering, RWTH Aachen University) and the late Vincent de Waal (Heijmans Infra BV) for the fruitful collaboration within the project.

The authors would also like to thank CustomWeather, Inc. for providing the weather data.

References

[1] NHTSA's National Center for Statistics and Analysis. Traffic Safety Facts: 2018 Data, 2020. URL https://crashstats.nhtsa.dot.gov/Api/Public/ViewPublication/812932.

[2] T. Hoekstra and F. Wegman. Improving the effectiveness of road safety campaigns: Current and new practices. *IATSS Research*, 34(2):80–86, 2011. ISSN 03861112. doi: 10.1016/j.iatssr.2011.01.003.

[3] R. Tay. Speed Cameras: Improving Safety or Raising Revenue? *Journal of Transport Economics and Policy*, 44:247–257, 2010.

[4] R. Thaler and C. Sunstein. *Nudge: Improving Decisions About Health, Wealth, and Happiness*. Penguin, New York, 2009.

[5] M. Bommes, A. Fazekas, T. Volkenhoff, and M. Oeser. Video Based Intelligent Transportation Systems – State of the Art and Future Development. *Transportation Research Procedia*, 14(2):4495–4504, 2016. ISSN 23521465. doi: 10.1016/j.trpro.2016.05.372.

[6] D. J. Finch, P. Kompfner, C. R. Lockwood, and G. Maycock. Speed, Speed Limits and Accidents.

[7] M. C. Taylor, D. A. Lynam, and A. Baruya. The effects of drivers' speed on the frequency of road accidents: Prepared for Road Safety Division, Department of the Environment, Transport and the Regions.

[8] G. Nilsson. Effects of speed limits on traffic accidents in Sweden, .

[9] G. Nilsson. Traffic Safety Dimensions and the Power Model to Describe the Effect of Speed on Safety, .

[10] R. Elvik. The Power Model of the relationship between speed and road safety: Update and new analyses.

[11] A. Baruya, editor. *Speed-Accident Relationships on European Roads*, 1998.

[12] N. Garber and R. Gadiraju. Factors Affecting Speed Variance and Its Influence on Accidents. *Transportation Research Record*, (1213):64–71, 1989.

[13] L. Aarts and I. van Schagen. Driving speed and the risk of road crashes: a review. *Accident Analysis and Prevention*, 38(2):215–224, 2006. doi: 10.1016/j.aap.2005.07.004.

[14] R. Elvik. International transferability of accident modification functions for horizontal curves. *Accident Analysis and Prevention*, 59:487–496, 2013. doi: 10.1016/j.aap.2013.07.010.

[15] A. Montella, F. Galante, F. Mauriello, and M. Aria. Continuous Speed Profiles to Investigate Drivers' Behavior on Two-Lane Rural Highways. *Transportation Research Record*, 2521(1):3–11, 2015. doi: 10.3141/2521-01.

[16] A. Palmberg, J. Imberg, Selpi, and R. Thomson. The Effect of Curve Geometry on Driver Behaviour in Curves by Using Naturalistic Driving Data. *Proceedings of the 3rd International Symposium on Future Active Safety Technology Towards zero traffic accidents*, pages 155–160, 2015.

[17] J. Glennon. State of the Art Related to Safety Criteria for Highway Curve Design: Research Report Number 134-4.

[18] C. Wilson, C. Willis, J. K. Hendrikz, and N. Bellamy. Speed enforcement detection devices for preventing road traffic injuries. *The Cochrane database of systematic reviews*, (2):CD004607, 2006. doi: 10.1002/14651858.CD004607.pub2.

[19] L. J. Mountain, W. M. Hirst, and M. J. Maher. Costing lives or saving lives: a detailed evaluation of the impact of speed cameras. *Traffic, Engineering and Control*, 45(8):280–287, 2004.

[20] C. Goldenbeld and I. van Schagen. The effects of speed enforcement with mobile radar on speed and accidents. An evaluation study on rural roads in the Dutch province Friesland. *Accident Analysis and Prevention*, 37(6):1135–1144, 2005. doi: 10.1016/j.aap.2005.06.011.

[21] D. W. Soole, B. C. Watson, and J. J. Fleiter. Effects of average speed enforcement on speed compliance and crashes: a review of the literature. *Accident Analysis and Prevention*, 54:46–56, 2013. doi: 10.1016/j.aap.2013.01.018.

[22] M. Elliott and J. Broughton. How methods and levels of policing affect road casualty rates: Prepared for Transport for London: TRL Report TRL637.

[23] K. Charlesworth. The effect of average speed enforcement on driver behaviour. In *IET Road Transport Information and Control Conference and the ITS United Kingdom Members' Conference (RTIC 2008)*, page 65. Institution of Engineering and Technology, 20-22 May 2008. ISBN 978-0-86341-920-1. doi: 10.1049/ic.2008.0794.

[24] L. K. Walter and J. Knowles. Effectiveness of Speed Indicator Devices on reducing vehicle speeds in London: Published Project Report 314.

[25] A. Montella, F. Galante, F. Mauriello, and L. Pariota. Low-Cost Measures for Reducing Speed at Curves on Two-Lane Rural Highways. *Transportation Research Record*, 2472 (1):142–154, 2015. doi: 10.3141/2521-01.

[26] A. Vest, N. Stamatiadis, A. Clayton, and J. Pigman. Effect of Warning Signs on Curve Operating Speeds, 2005.

[27] H. Gonzalo-Orden, M. Rojo, H. Pérez-Acebo, and A. Linares. Traffic Calming Measures and their Effect on the Variation of Speed. *Transportation Research Procedia*, 18:349–356, 2016. ISSN 2352-1465. doi: https://doi.org/10.1016/j.trpro.2016.12.047. Efficient, Safe and Intelligent Transport. Selected papers from the XII Conference on Transport Engineering, Valencia (Spain) 7-9 June.

[28] A. Akbari and F. Haghighi. Traffic calming measures: An evaluation of four low-cost TCMs' effect on driving speed and lateral distance. *IATSS Research*, 44(1):67–74, 2020. ISSN 0386-1112. doi: https://doi.org/10.1016/j.iatssr.2019.07.002.

[29] K. Brookhuis and D. de Waard. Limiting speed, towards an intelligent speed adapter (ISA). *Transportation Research Part F*, 2(2):81–90, 1999. doi: 10.1016/S1369-8478(99)00008-X.

[30] A. T. Ibrahim and F. L. Hall. Effect of adverse weather conditions on speed-flow-occupancy relationships. *Transportation Research Record*, (1457):184–191, 1994.

[31] R. Hranac, E. Sterzin, D. Krechmer, H. Rakha, and M. Farzaneh. Empirical Studies on Traffic Flow in Inclement Weather.

[32] H. Mohammed Alhassan and J. Ben-Edigbe. Highway Capacity Prediction in Adverse Weather. *Journal of Applied Sciences*, 11(12):2193–2199, 2011. ISSN 18125654. doi: 10.3923/jas.2011.2193.2199.

[33] N. Mashros, J. B. Edigbe, S. A. Hassan, N. Abdul Hassan, and N. Z. Mohd Yunus. Impact of Rainfall Condition on Traffic Flow and Speed: A Case Study in Johor and Terengganu. *Jurnal Teknologi*, 70(4), 2014. ISSN 0127-9696. doi: 10.11113/jt.v70.3490.

[34] R. Lamm, E. M. Choueiri, and T. Mailaender. Comparison of Operating Speeds on Dry and Wet Pavements of Two-Lane Rural Highways. *Transportation Research Record*, (1280):199–207, 1990.

[35] Z. Sándor. How does the rainfall influence the traffic parameters of the motorways? *Conference on Effective Road Safety Campaigns*, 2014.

[36] R. J. Snowden, N. Stimpson, and R. A. Ruddle. Speed perception fogs up as visibility drops. *Nature*, 392(6675):450, 1998. ISSN 0028-0836. doi: 10.1038/33049.

[37] M. J. Lighthill and G. B. Whitham. On kinematic waves II. A theory of traffic flow on long crowded roads. *Proceedings of the Royal Society of London. Series A. Mathematical and Physical Sciences*, 229(1178):317–345, 1955. ISSN 0080-4630. doi: 10.1098/rspa.1955.0089.

[38] Greenshields. B.D., J. R. Bibbins, W. S. Channing, and H. H. Miller. A Study of Traffic Capacity. *Proceedings of the Fourteenth Annual Meeting of the Highway Research Board*, 14:448–477, 1935.

[39] H. Greenberg. An Analysis of Traffic Flow. *Operations Research*, 7(1):79–85, 1959. ISSN 0030-364X. doi: 10.1287/opre.7.1.79.

[40] R. T. Underwood. Speed, Volume, and Density Relationships. Quality and Theory of Traffic Flow. *Bureau of Highway Traffic*, (141-188), 1961.

[41] L. C. Edie. Car-Following and Steady-State Theory for Noncongested Traffic. *Operations Research*, 9(1):66–76, 1961. ISSN 0030-364X. doi: 10.1287/opre.9.1.66.

[42] W. Brilon and M. Ponzlet. Variability of Speed-Flow Relationships on German Autobahns. *Transportation Research Record*, 1555(1):91–98, 1996. doi: 10.1177/0361198196155500112.

[43] A. K. Jägerbrand and J. Sjöbergh. Effects of weather conditions, light conditions, and road lighting on vehicle speed. *SpringerPlus*, 5:505, 2016. ISSN 2193-1801. doi: 10.1186/s40064-016-2124-6.

[44] E. Arnold and K. Lantz. Evaluation of Best Practices in Traffic Operations and Safety: Phase I: Flashing LED Stop Sign and Optical Speed Bars, 2007.

[45] E. Avineri. Nudging Safer Road Behaviours, 2014.

[46] A. Fyhri, K. Karlsen, and H. Sundfor. Paint It Red - A Multimethod Study of the Nudging Effect of Coloured Cycle Lanes. *frontiers in psychology*, 12(662679), 2021.

[47] B. T. Morris and M. M. Trivedi. Learning, modeling, and classification of vehicle track patterns from live video. *IEEE Transactions on Intelligent Transportation Systems*, 9(3): 425–437, 2008.

[48] X. Ma and W. E. L. Grimson. Edge-based rich representation for vehicle classification. In *Tenth IEEE International Conference on Computer Vision (ICCV'05) Volume 1*, volume 2, pages 1185–1192. IEEE, 2005.

[49] S. Tuermer, F. Kurz, P. Reinartz, and U. Stilla. Airborne vehicle detection in dense urban areas using HoG features and disparity maps. *IEEE Journal of Selected Topics in Applied Earth Observations and Remote Sensing*, 6(6):2327–2337, 2013.

[50] Y. Tang, C. Zhang, R. Gu, P. Li, and B. Yang. Vehicle detection and recognition for intelligent traffic surveillance system. *Multimedia tools and applications*, 76(4):5817–5832, 2017.

[51] H. Zhang, M. Liptrott, N. Bessis, and J. Cheng. Real-time traffic analysis using deep learning techniques and uav based video. In *2019 16th IEEE International Conference on Advanced Video and Signal Based Surveillance (AVSS)*, pages 1–5. IEEE, 2019.

[52] E. K. Bas and J. D. Crisman. An easy to install camera calibration for traffic monitoring. In *Proceedings of Conference on Intelligent Transportation Systems*, pages 362–366, Nov 1997. doi: $10.1109/\mathrm{ITSC}.1997.660502$.

[53] G. Sullivan. Model-based vision for traffic scenes using the ground-plane constraint. *Real-time Computer Vision*, pages 93–115, 1994.

[54] M. Haag and H.-H. Nagel. Combination of edge element and optical flow estimates for 3D-model-based vehicle tracking in traffic image sequences. *International Journal of Computer Vision*, 35(3):295–319, 1999.

[55] M. J. Leotta and J. L. Mundy. Vehicle surveillance with a generic, adaptive, 3D vehicle model. *IEEE transactions on pattern analysis and machine intelligence*, 33(7):1457–1469, 2011.

[56] M. Hödlmoser, B. Micusik, M. Pollefeys, M.-Y. Liu, and M. Kampel. Model-based vehicle pose estimation and tracking in videos using random forests. In *3D Vision-3DV 2013, 2013 International Conference on*, pages 430–437. IEEE, 2013.

[57] Z. Zhang, J. Zheng, H. Xu, and X. Wang. Vehicle detection and tracking in complex traffic circumstances with roadside LiDAR. *Transportation research record*, 2673(9):62–71, 2019.

[58] J. Zhang, W. Xiao, B. Coifman, and J. Mills. Image-based vehicle tracking from roadside lidar data. *ISPRS Geospatial Week 2019*, 2019.

[59] J. Zhao, H. Xu, H. Liu, J. Wu, Y. Zheng, and D. Wu. Detection and tracking of pedestrians and vehicles using roadside LiDAR sensors. *Transportation research part C: emerging technologies*, 100:68–87, 2019.

[60] R. R. Cabrera, T. Tuytelaars, and L. Van Gool. Efficient multi-camera detection, tracking, and identification using a shared set of haar-features. In *Computer Vision and Pattern Recognition (CVPR), 2011 IEEE Conference on*, pages 65–71. IEEE, 2011.

[61] H.-T. Chen, M.-C. Chu, C.-L. Chou, S.-Y. Lee, and B.-S. Lin. Multi-camera vehicle identification in tunnel surveillance system. In *2015 IEEE International Conference on Multimedia & Expo Workshops (ICMEW)*, pages 1–6. IEEE, 2015.

[62] A.-L. Köhler, O. Op den Camp, M. van Mierlo, S. Ladwig, and M. Schwalm. Nudging Drivers Towards Higher Safety Margins - Applications of the H2020-Project MeBeSafe. *13th ITS European Congress*, 2019.

[63] A.-L. Köhler, A. Aslan, M. Berghaus, F. Fahrenkrog, A. Fazekas, M. Klatt, S. Ladwig, M. van Mierlo, L. Plum, M. Schnelle, and V. de Waal. Report Infrastructure measures: Delivery Report for MeBeSafe. Measures for Behaving Safely in Traffic. D3.2, 2019.

[64] A.-L. Köhler, I. Koch, and S. Ladwig. Guiding drivers towards safer driving speed: Exploiting visual dominance in speed adaptation. *Transportation Research Part F: Traffic Psychology and Behaviour*, 90:438–450, 2022. ISSN 1369-8478. doi: https://doi.org/10.1016/j.trf.2022.09.011.

[65] Z. Zhang. A flexible new technique for camera calibration. *IEEE Transactions on pattern analysis and machine intelligence*, 22(11):1330–1334, 2000.

[66] G. Borgefors. Hierarchical chamfer matching: A parametric edge matching algorithm. *IEEE Transactions on pattern analysis and machine intelligence*, 10(6):849–865, 1988.

[67] D. Forsyth and J. Ponce. *Computer vision: A modern approach.* Prentice hall, 2011.

[68] A. Fazekas and M. Oeser. Performance metrics and validation methods for vehicle position estimators. *IEEE Transactions on Intelligent Transportation Systems*, 21(6):2853–2863, 2019.

[69] The MathWorks, Inc. MATLAB Curve Fitting Toolbox, 2021. URL `https://de.mathworks.com/help/curvefit/index.html`.

[70] CustomWeather, Inc. URL https://customweather.com/.

[71] C. Lippold. Zur Geschwindigkeit V85 als Projektierungsgroesse im Strassenentwurf. *Straßenverkehrstechnik*, 43(1), 1999.

5 Vehicle Trajectory Dataset from Drone Videos Including Off-Ramp and Congested Traffic – Analysis of Data Quality, Traffic Flow and Accident Risk

This paper was published under:

Berghaus, Moritz; Lamberty, Serge; Ehlers, Jörg; Kalló, Eszter and Oeser, Markus (2024). Vehicle trajectory dataset from drone videos including off-ramp and congested traffic – Analysis of data quality, traffic flow, and accident risk. Communications in Transportation Research, 4, 100133. https://doi.org/10.1016/j.commtr.2024.100133

Individual contributions:

M. Berghaus: study conception and design; data collection; analysis and interpretation of results; draft manuscript preparation (with a particular focus on the introduction, data processing, macroscopic comparison with induction loop data, traffic flow analysis, and conclusions, Sections 5.2, 5.4.1, 5.4.3, 5.5.1, 5.6.1, 5.7)
S. Lamberty: study conception and design; data collection; analysis and interpretation of results; draft manuscript preparation (with a particular focus on the trajectory extraction, Sections 5.3.1, 5.3.2, 5.4.2).
J. Ehlers: study conception and design; data collection; analysis and interpretation of results; draft manuscript preparation (with a particular focus on the microscopic comparison with in-vehicle sensors, Section 5.5.2).
E. Kalló: study conception and design; data collection; analysis and interpretation of results; draft manuscript preparation (with a particular focus on the accident risk analysis, Section 5.6.2).

M. Oeser: study conception and design; supervision.

5.1 Abstract

Vehicle trajectory data have become essential for many research fields, such as traffic flow, traffic safety, and automated driving. To make trajectory data useable for researchers, an overview of the included road section and traffic situation as well as a description of the data processing methodology is necessary. In this paper, we present a trajectory dataset from a German highway with two lanes per direction, an off-ramp and congested traffic in one direction, and an on-ramp in the other direction. The dataset contains 8,648 trajectories and covers 87 min and an $\sim$1,200 m long section of the road. The trajectories were extracted from drone videos using a posttrained YOLOv5 object detection model and projected onto the road surface via three-dimensional (3D) camera calibration. The postprocessing methodology can compensate for most false detections and yield accurate speeds and accelerations. The trajectory data are also compared with induction loop data and vehicle-based smartphone sensor data to evaluate the plausibility and quality of the trajectory data. The deviations of the speeds and accelerations are estimated at 0.45 m/s and 0.3 m/s^2, respectively. We also present some applications of the data, including traffic flow analysis and accident risk analysis.

5.2 Introduction

Vehicle trajectory data or microscopic traffic data are highly valuable for a wide range of applications. The oldest application, starting with the famous Greenshields' study [1], was the analysis of traffic flow and the development and validation of traffic flow models. Treiterer [2] was among the first researchers to collect vehicle trajectories using aerial images. The second application emerged in the 1980s with the Swedish Traffic Conflict Technique, which uses vehicle trajectories to evaluate traffic safety based on surrogate safety measures (SSMs), e.g., time to collision (TTC) [3]. While vehicle movements were analyzed manually in the beginning, image processing methods helped to automatically compute SSMs and identify traffic conflicts [4]. The most recent application is the development of automated driving systems, which rely on naturalistic driving data to ensure that these systems interact safely with human drivers in every possible situation [5]. All these applications benefit from a wide variety of trajectory datasets with different road characteristics and traffic situations.

With the increasing number of applications, progress in computer vision technology has led to a growing number of trajectory datasets. The interest in publicly available datasets, such as the NGSIM dataset [6], has shown that these datasets can be used for more than the application they were created for.

Most datasets contain only limited information on the data collection methodology and qual-

ity. Commonly used metrics in object detection, such as the mean average precision (mAP), represent only the quality of the position measurements, while most applications require velocity and acceleration. With appropriate postprocessing of the raw trajectory data, accurate velocities and accelerations can be achieved even with noisy position measurements. However, there is no standardized metric for evaluating the quality of processed trajectories. The trajectory dataset presented in this paper is compared with data from an induction loop and data from a smartphone sensor that was present in one of the vehicles included in the trajectory data. By comparing the speeds and accelerations, we can estimate the accuracy of the speed and acceleration values.

Although the purpose of publishing trajectory datasets is to make them useable for other researchers, it is often difficult for them to assess whether a dataset contains a suitable road section and suitable traffic scenarios for their research question. We therefore conduct a traffic flow analysis with time–space diagrams, fundamental diagrams, and time series of flow, density, and mean speed.

The trajectory dataset presented in this paper originates from a German highway with two lanes per direction, an off-ramp and congested traffic in one direction, and an on-ramp in the other direction. Based on the information on data quality, road characteristics, and traffic situations provided in this paper, researchers can evaluate whether the dataset meets their requirements.

The remainder of this paper is structured as follows. In Section 5.3, we provide an overview of other publicly available trajectory datasets. In Section 5.4, we present the data collection and data processing methodology. Section 5.5 contains the description of the data and an evaluation of the data quality. In Section 5.6, we present two possible applications of the dataset.

5.3 Related Work

5.3.1 Vehicle trajectory datasets

When searching for comparable datasets, the high requirements in the area of traffic safety analysis and the complex boundary conditions that allow an evaluation of the infrastructure should not be neglected. The investigated datasets are compared and analyzed in this section.

The first category of datasets is generated from infrastructure-based sensors [6–8]. Here, the focus does not lie in the generation of particularly diverse data. Rather, with this kind of data generation, large amounts of data can be collected easily, e.g., for training vehicle

behavior models. As the first large dataset of its kind, NGSIM [6] demonstrated the possibility of microscopic traffic data collection by placing cameras on buildings, understandably with a small amount of data and noncomparable accuracy. The dataset presented in [7] comes from a large test site of the A9 highway in Germany, which covers a 3 km stretch of highway and is captured with lidar and cameras. A similar approach using radar was taken by Wang et al. [8], where a dataset of several kilometers of highway in China was created. All three datasets and their corresponding methodologies show promising results but are too complex and expensive to perform on many different routes or have little lead time and low cost.

The remaining datasets used a similar approach as in this work: flying drones at a very high altitude either above or directly next to the highway. For example, Krajewski et al. [9] acquired $\sim$16.5 h of trajectory data from straight highway sections, and Moers et al. [10] supplemented these data with on-ramp and off-ramp trajectories. The AUTOMATUM DATA dataset also provides a good basis for many applications with 30 h of material [11]. The MAGIC dataset focuses on using a large number of drones simultaneously and uses a commercial service to extract the trajectories, which are detrimentally longer than those of any other dataset because of the large number of drones [12].

Although all of these works are very relevant and the data can be considered for many use cases, there is still room for improvement. These studies generally rely on a road surface consisting of a single flat area with no change in elevation. However, this approach works only when simple road geometries are used. The more complex the road infrastructure is, the larger the resulting errors will be. In contrast, this work uses three-dimensional (3D) models for the infrastructure, which allows these inaccuracies to be avoided.

5.3.2 Trajectory extraction methods

The generation of trajectory data has been a research topic for many years, such that a whole series of works is available. Various sensors and evaluation algorithms are used, often depending on the use case and users. For example, several laser scanners are fused for trajectory data [13], and several lidar sensors [14] are used to capture trajectories at intersections. Furthermore, camera systems installed in the infrastructure can be used for recording trajectories. For example, in [15], a general framework with a method based on Mask R–CNN was presented for the extraction of 3D trajectories for the use of traffic cameras.

However, even when focusing on the acquisition of trajectories from drone videos, a multitude of works have attempted different methods with varying success. Azevedo et al. [16] recognized the possibilities of a drone-based approach early on and extracted vehicle trajectories through background subtraction and a k-shortest disjoint path algorithm for tracking at

a speed of two frames per second without classification. Apeltauer et al. [17] used the AdaBoost classifier with multiblock local binary pattern (MB-LBP) for detection followed by the sequential Monte Carlo method to track vehicles through an intersection. Khan et al. [18] used the Lucas–Kanade optical flow algorithm to detect and track vehicles in combination with background extraction. Zhao and Li [19] used Mask R–CNN for detection combined with a semiautomatic extraction of different lanes but lacked a description of the method for camera calibration. Kim et al. [20] compared the results from the aggregated channel feature (ACF) and Faster R–CNN methods for the tracking of vehicles in congested traffic situations and achieved promising results despite some problems with false positive detection. Ahmadi and Mohammadzadeh [21] extracted vehicle trajectories from spaceborne videos using background subtraction with a much larger field of view but with no classification and a lower precision due to the lower resolution of the videos. Masouleh and Shah-Hosseini [22] developed a new algorithm for the semantic segmentation of vehicles from UAV-based thermal infrared imagery using a Gaussian–Bernoulli restricted Boltzmann machine (GB-RBM) with improvements compared to other semantic segmentation networks. Feng et al. [23] included pedestrians and cyclists in their YOLOv3-based approach and can therefore be used to record scenes on urban roads with all traffic participants, with an accuracy of approximately 92% for motor vehicles. Shi et al. [24] used videos made from multiple helicopters to capture a larger section of a highway, and simultaneously, trajectory extraction with YOLOv3 automatically detected lane markings and calculated vehicle motion characteristics. Yeom and Nam [25] approached the detection problem through the difference between two consecutive images for a driving vehicle and tracked the detected vehicles using a Kalman filter, sadly only using their method on a total of 22 vehicles in the recorded videos.

Furthermore, there are methods already listed in Section 5.3.1 that have already proven their potential with the publication of large datasets. As one of the first applications of neural networks for the extraction of vehicle trajectories from drone videos, Krajewski et al. [9] used U-Net for the detection of vehicles and further started the extraction of parameters of interest for the automotive industry, such as maneuver classification. Using the same method, trajectories from intersections and exits were recorded in subsequent years [9, 10].

Since the number of works on this topic is too large to cite them all in this work, the interested reader can refer to two reviews. In their review paper on drone-based road traffic monitoring systems, Bisio et al. [26] presented additional approaches and datasets and compared different detection and tracking algorithms. Unfortunately, there is no mention of the different calibration methods used in the reviewed papers. Butilă and Boboc [27] provide a systematic overview of 34 works on drone-based trajectory extraction, categorizing the works according to aim and feasibility.

Figure 5.1: Aerial views of the filmed road section. (a) Western region and (b) eastern region.

5.4 Methods

In this section, we describe the workflow used to obtain the trajectory data presented in this paper. Section 5.4.1 contains all relevant information on the study area and the collection of the videos. Section 5.4.2 describes how the trajectories are extracted from the drone videos, including video stabilization, camera calibration, and vehicle detection. Section 5.4.3 contains the necessary steps of data processing to achieve a high-quality trajectory dataset.

5.4.1 Study area and material collection

The dataset presented in this paper was collected at the highway A43 near Münster, Germany. The highway has two lanes in each direction, with a two-lane off-ramp in direction 1 (west to east) and a one-lane on-ramp in direction 2 (east to west). The dataset covers an $\sim$1,200 m long stretch of road during the morning peak hour (7:11 to 8:38) on September 6, 2021. Direction 1 is partly congested during this time due to a nearby on-ramp. The data were collected at two locations using DJI Mavic Pro drones. Two drones per location were used alternately due to limited battery capacity. As a result, there are some temporal overlaps and gaps in the videos, which must be considered during data processing. The drones flew 500 m above ground and each covered more than 600 m of the road with a spatial overlap of $\sim$50 m. The videos were recorded with 4K resolution (3,840 × 2,160) at 25 frames per second, which corresponds to a vehicle size of approximately 30 × 12 pixels. Fig. 5.1 shows two aerial views of the filmed road section.

To check the plausibility of the vehicle trajectories derived from drone data, additional measurements were taken with a vehicle that was traveling on the highway section during the time of video recording. A smartphone's GPS sensor and inertial measurement unit captured the vehicle's position, speed, and acceleration at frequencies of 1 Hz (position and speed) and 100 Hz (acceleration), respectively. The smartphone was mounted on a flat surface approxi-

mately at the center of the vehicle to ensure that it remained aligned in the vehicle coordinate system at all times. The data were collected with an iPhone X and the app PhyPhox, which allows the recording of raw sensor data [28]. To ensure that the vehicle was easily visible in the video images, an orange van (VW Transporter) was used. This ensures that the drone data can be correctly assigned to this vehicle and that the drone and vehicle data can be compared correctly.

5.4.2 Trajectory extraction

Stabilization

The first step in evaluating drone images is usually video stabilization. Since the calibration step explained in the next section can only be performed on the first frame of each video, each subsequent frame in the video is transformed to match this first frame. The stabilization is performed based on a standard pipeline using feature detection from Shi and Tomasi [29], the Lucas–Kanade feature tracking method presented in [30], and the computation of a homography via RANSAC. If the computation of the homography is successful, the current image can be deformed accordingly. In the case of particularly abrupt movements of the drone or continuous displacement of the image and thus too large a deviation, stabilization is interrupted, and the video is split, removing up to 2 s of video to eliminate any blurred images. Editing of the video is initiated in the event that less than 5% of the features found can be recovered by homography.

Calibration

Calibration of the video corresponds to the process of finding a transformation matrix for converting two-dimensional (2D) image coordinates to 3D world coordinates. The intrinsic camera parameters (focal length and distortion) of the drone were computed in preparation for the evaluation and used for the extrinsic calibration process.

For the extrinsic calibration, the first step is to create a 3D model of the road markings using publicly available geodata (georeferenced orthophotos and an elevation model from laser scanner data) from North Rhine–Westphalia [31] (Fig. 5.2). Since the resulting model does not show a single straight road surface as in other works but rather a more realistic 3D surface, it is approximated with triangulation. Instead of calculating a single transformation for the entire road surface, as is usually the case; in our case, each triangulation surface receives a separate transformation. With the 3D model, reference points can be captured, and the different transformations can be computed in a final step.

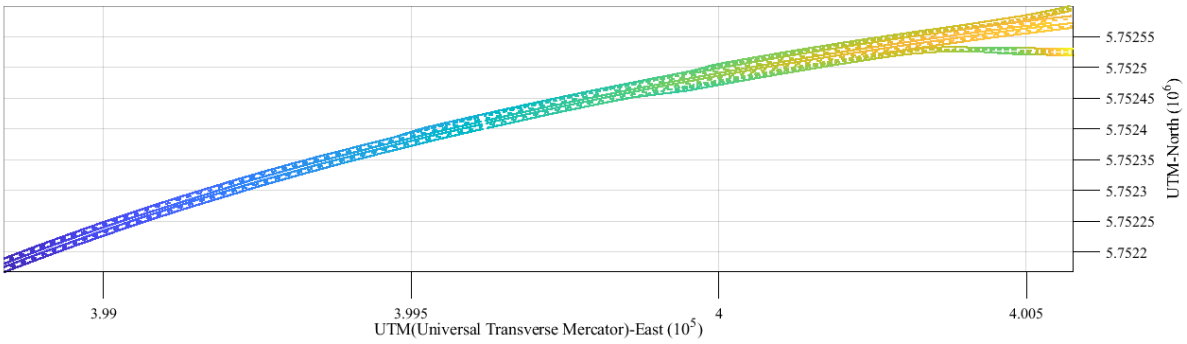

Figure 5.2: 3D-street model of the recorded highway segment, color-coded according to the z-axis.

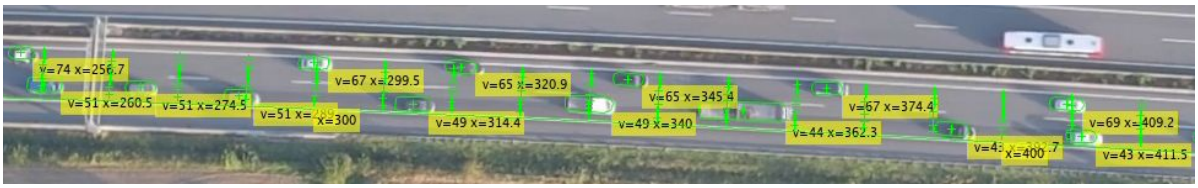

Figure 5.3: Snapshot of a drone video with vehicle detections.

Detection and tracking

The detection of vehicles in single frames is performed with a posttrained model based on YOLOv5 [32]. For this purpose, several minutes of video footage were labeled by hand and used via transfer learning to adapt an existing model. The trained model provides excellent results in detecting vehicles (mAP@0.5 of 95%). A slight tendency toward false-positive results can be remedied in the future via further training; in our case, false detections are reliably eliminated by tracking and postprocessing of the trajectories. Accordingly, in the present work, not single detections are a criterion of the data quality but rather the complete trajectories (see Section 5.5). These trajectories are created in the first step by matching the positions and the driving direction. In all further steps, the distance between two detections is no longer determined, but the distance between the current position and the position is predicted on the basis of the speed recorded thus far. Munkres [33] is used as the matching algorithm. Even if a vehicle is covered by a bridge or gantry for a short period, this algorithm can track it in most cases. Fig. 5.3 shows a snapshot of a drone video with the vehicle detections reprojected into the image.

5.4.3 Data processing

Data processing ensures that the vehicle trajectories are plausible and that the trajectories extracted from each video are combined into a single dataset.

The first step is to convert the vehicle positions from world coordinates to road coordinates, i.e., a coordinate system where the x-axis lies on the right edge of the rightmost lane and the y-axis is orthogonal to the x-axis. Thus, the x value represents the distance traveled by a vehicle, and the y value represents the distance to the right edge of the road, which can be used to determine the lane on which the vehicle drives. This coordinate system is convenient for most applications involving interurban roads, where all vehicles drive in the same direction, and mostly only the velocities and accelerations in the driving direction are relevant. The road markings were extracted as polygonal chains from georeferenced orthophotos (see Section 5.4.2) and then smoothed.

The road coordinates are also useful for checking the plausibility of the data. It can be assumed that vehicles only drive forward, i.e., the velocity in the x-direction must not be smaller than zero. It can also be assumed that the velocity has an upper bound. Therefore, the difference between two subsequent x values (Δx) is a criterion for plausibility. The difference between two subsequent y values should be limited more strictly because lateral velocities are usually much smaller than longitudinal velocities. A large time gap between two subsequent data points of the same vehicle is another criterion that has also proven to be a criterion for implausibility. The implausible points are removed from the data to remove all single outliers. The plausibility is checked again with the remaining data points. This procedure is applied until multiple subsequent outliers are removed. To identify data points of a trajectory that do not belong to the same vehicle, the trajectory is split if implausible points remain after several iterations. In this case, a new vehicle ID is assigned to one part of the trajectory. Fig. 5.4 shows that most obvious errors in the data can be removed by this method. Most of these errors result from vehicle tracks that are matched to a nonmoving false positive detection, e.g., the shadow of a tree.

To obtain realistic velocities and accelerations, the trajectories are then smoothed by fitting a smoothing spline to the data. The smoothing parameter must be selected depending on the magnitude of the outliers that have not been removed during the plausibility check. In our dataset, smoothing parameters of 0.2 in the x-direction and 0.5 in the y-direction were shown to be suitable. Fig. 5.5 shows that this process can successfully remove the outliers.

Next, the trajectories extracted from different videos are combined. Since the timestamps of the videos are not perfectly synchronized, the trajectories must be shifted temporally by a few seconds. Since the number of videos is not too high, this step can be performed manually.

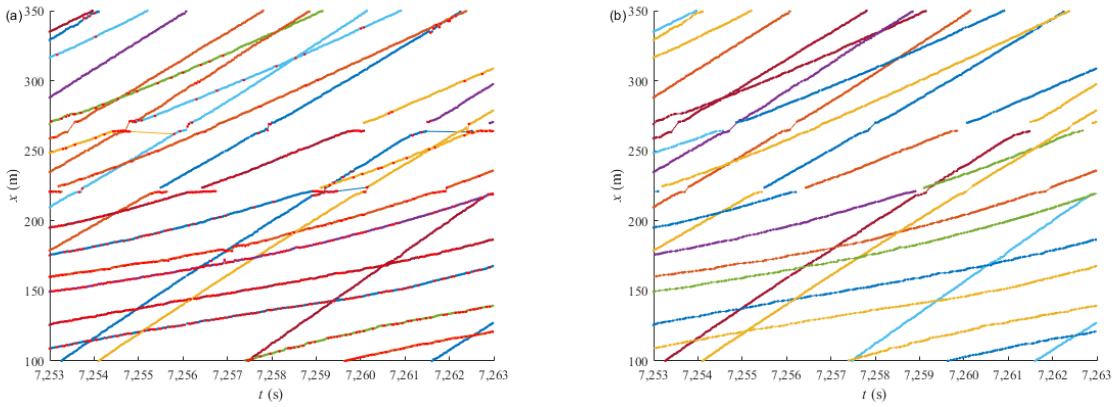

Figure 5.4: (a) Raw data with implausible points marked in red. (b) Data after removal of implausible points.

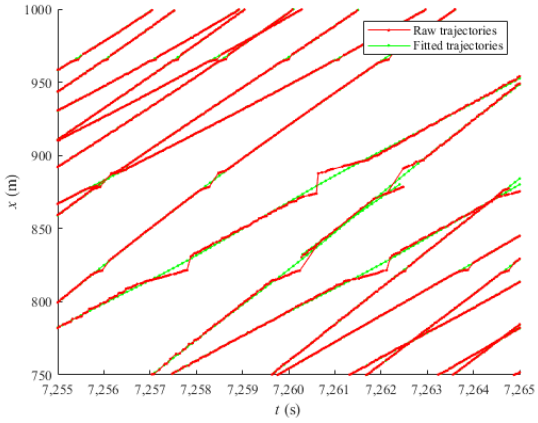

Figure 5.5: Comparison of raw trajectories (after removing implausible points) and fitted trajectories.

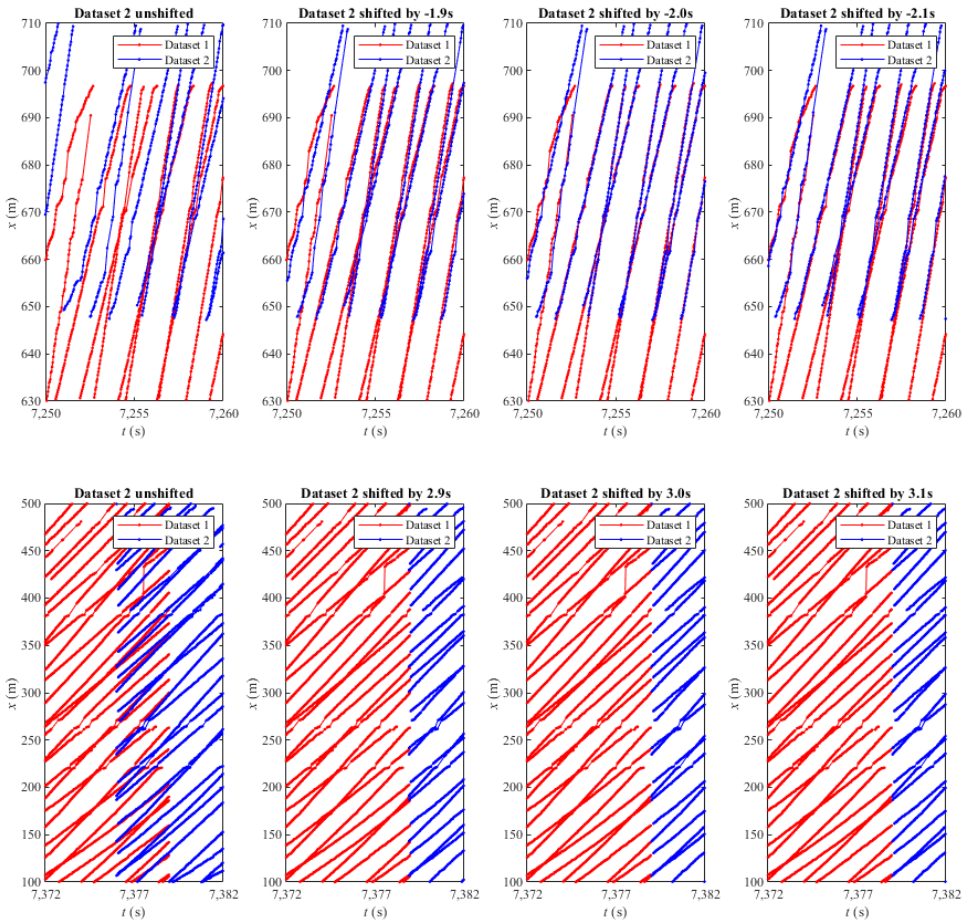

Figure 5.6: Identifying the shift between two adjacent (temporal or spatial) videos.

The trajectories of two adjacent (spatially or temporally) videos are plotted with different shift values, and the best fit is selected (Fig. 5.6).

Many vehicles are represented in the raw data by more than one trajectory either because they are not tracked correctly (Fig. 5.4) or because they appear in more than one video (Fig. 5.6). Therefore, overlapping or adjacent trajectories that belong to the same vehicle must be identified and joined. If the distance in the x-direction is smaller than 5 m and the distance in the y-direction is smaller than 2.5 m, the trajectories are considered to overlap. In this case, one of the trajectories is removed. If the last point of one trajectory and the first point of another trajectory are closer than 10 m in the x-direction and 3 m in the y-direction, they are joined because they likely belong to the same vehicle (Fig. 5.7). With this method, vehicles can be tracked even in situations where the Kuhn–Munkres algorithm fails. The joined trajectories are then smoothed again. Short trajectories ($<$ 3 s) are removed from the dataset because they are likely false positive detections, as mentioned above.

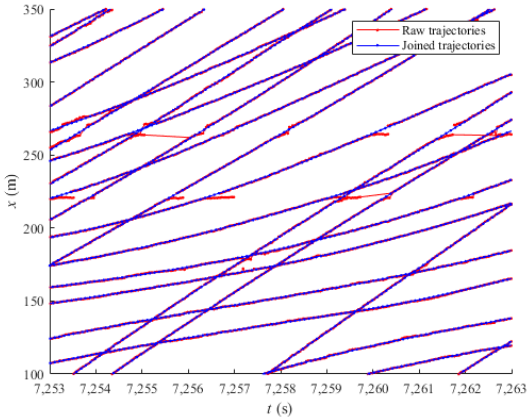

Figure 5.7: Raw data (red) and trajectories after all data processing steps (blue).

5.5 Description and evaluation of the dataset

The dataset contains 5,016 trajectories in direction 1 and 3,632 trajectories in direction 2. Regarding the sensitivity of the recorded data, a random sample analysis of approximately 450 vehicles showed that only approximately 0.45% of the vehicles actually present were not detected. These vehicles are gray; hence, their contrast to the road pavement is very small. False detections could not be identified in the sample, mainly due to trajectory postprocessing, which removes any trajectories that are too short. In direction 1, 3,993 trajectories (79.5%) are longer than 90% of the length of the filmed road section (direction 2: 2,928 trajectories, 80.6%). The remaining vehicles are represented in the dataset by two or more shorter trajectories with small gaps that cannot be filled by the data processing methodology. These shorter trajectories can still be used for traffic flow and accident risk analyses.

We provide the data in two different formats: for MATLAB users in .mat format and for all other users in .csv format.

In .mat format, the data are provided in a cell array where each cell contains the data of a single vehicle. The data of a single vehicle are organized in a structure array (“struct”). The struct contains time-dependent and time-independent data. The time-independent data include the vehicle ID, a description of the vehicle category (passenger car, bus, truck, etc.), a corresponding ID of the vehicle category, the vehicle length and width in (m), and the 2D contour (n-by-2 table, where X = 0 and Y = 0 are the vehicle centroid). The time-dependent data include the trajectory. The original (unprocessed) trajectory is an n-by-6 table with a vehicle ID, 2D positions in the road coordinate system in (m) (x is the direction along the road, y is orthogonal to x), a timestamp in (s) (starting at September 6, 2021, 6 a.m.), and

2D positions in the global UTM coordinate system. The fitted (processed) trajectory is an n-by-3 table with 2D positions in the road coordinate system and timestamps, an n-by-3 table with 2D speeds in the road coordinate system and timestamps, and an n-by-3 table with 2D accelerations in the road coordinate system and timestamps.

For MATLAB users, we also provide a small toolbox that enables some basic analyses and visualizations.

In the .csv format, the data are provided in a table with the following columns: timestamp in (s) (starting at September 6, 2021, 6 a.m.), timestamp in "yyyy-MM-dd HH:mm:ss.s", vehicle ID, a description of the vehicle category (passenger car, bus, truck, etc.), vehicle length and width in (m), and the fitted (processed) trajectory with the 2D-positions in (m), 2D-speeds in (m/s) and 2D-accelerations in (m/s^2) in the road coordinate system in (m) (x is the direction along the road, y is orthogonal to x).

The dataset and the MATLAB toolbox can be downloaded at https://data.isac.rwth-aachen.de [34].

5.5.1 Macroscopic comparison with induction loop data

Using data from nearby induction loops provided by the road operator Die Autobahn GmbH des Bundes [35], the flow and mean speeds computed with our dataset can be compared to the flow and mean speeds measured by the induction loops. First, we use data from two induction loops (one on each lane, only direction 1) that are located in the middle of the filmed road section. Fig. 5.8 shows that both the flows and the mean speeds from the drone dataset are consistent with the flows and mean speeds from the induction loop data. However, the flows from the drone dataset are mostly slightly smaller, which indicates that not all vehicles have been detected. The root mean square (RMS) deviation of the flows is 2.2 vehicles per minute in lane 1 and 3.1 vehicles per minute in lane 2. The speeds from the drone data are also generally slightly lower. The RMS deviation of the speeds is 0.78 m/s (2.8 km/h) in both lanes. Since the accuracy of the speed measurement of the induction loops is unknown, it cannot be concluded which values are more accurate.

The data from the adjacent induction loops can be used to interpolate the mean speeds in the filmed road section. Due to the propagation of shock waves (forward in free flow conditions and backward in congested flow conditions), linear interpolation is not appropriate. Instead, we use the adaptive smoothing method (ASM) proposed by Treiber and Helbing [36], which takes the propagation of shock waves into account. Fig. 5.9 shows good agreement between the mean speeds obtained from the trajectory data and the interpolated mean speeds obtained from the induction loop data.

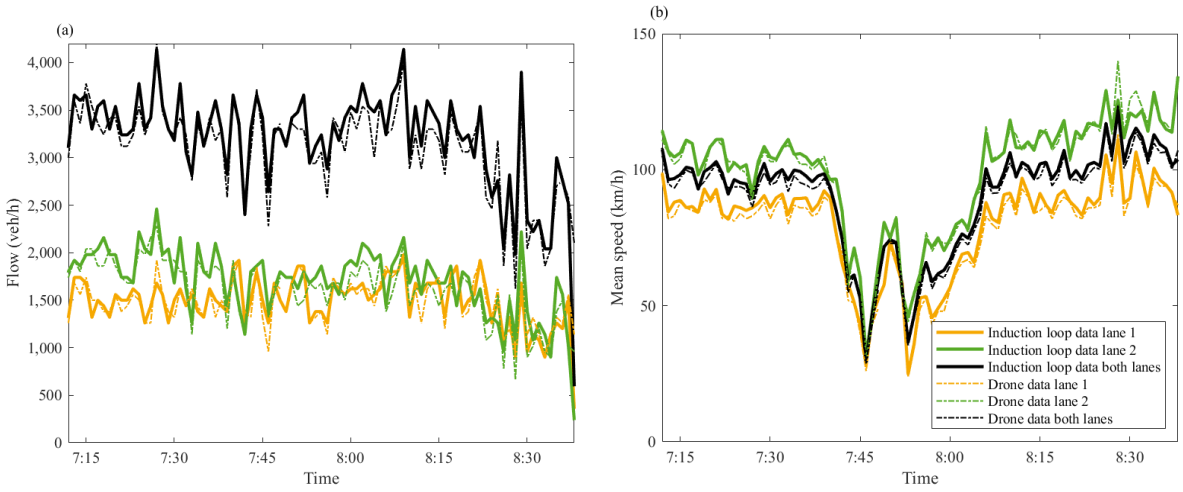

Figure 5.8: Comparison of induction loop data and drone data with respect to (a) flow and (b) mean speed in 1-min-intervals.

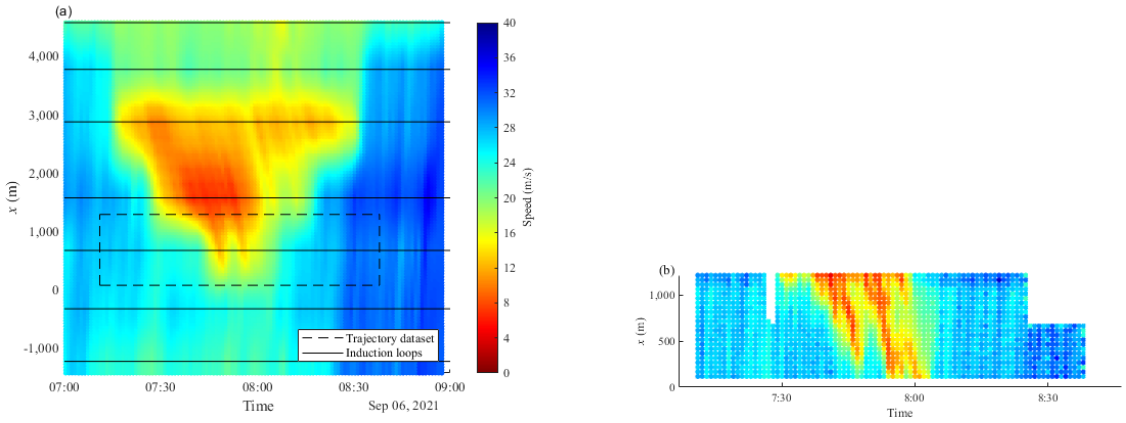

Figure 5.9: Comparison of (a) mean speeds obtained from induction loop data and the adaptive smoothing method and (b) the mean speeds obtained from our trajectory data.

The induction loops categorize the vehicle flows into passenger cars and trucks. In direction 1, the truck ratio is 8.2% (direction 2: 10.5%) according to the induction loop data and 12.3% (direction 2: 11.5%) according to the trajectory data. These differences indicate that some passenger cars might have been falsely labeled as trucks in the trajectory data. However, the accuracy of vehicle categorization in induction loop data cannot be validated.

5.5.2 Microscopic comparison with in-vehicle sensors

To check the plausibility of the calculated speeds and accelerations obtained from drone data, eight test runs with in-vehicle sensors were performed, four in each direction. Similar to the drone data, in-vehicle data were smoothed to reduce signal noise. A smoothing spline with break points of 0.5 s for the accelerometer and 2 s for the GPS was used. These parameters were chosen to filter out sensor noise without compromising the validity of the data. For a valid comparison between drone data and in-vehicle data, the clocks of both data sources were aligned based on the position data. The signals of the in-vehicle sensors were shifted by the time difference between the drone and in-vehicle sensor data at the position where the measurement vehicle was first detected by the drone.

Fig. 5.10 shows good agreement between the speeds derived from drone data and the speeds obtained from in-vehicle sensors. The deviations between the signals of the two data sources are normally distributed, with a mean of 0.01 m/s and a standard deviation of 0.47 m/s. Thus, no systematic deviation can be identified. The mean correlations between the signals are 0.99 (direction 1) and 0.90 (direction 2). The RMS deviations between the signals are on average 0.43 m/s (direction 1) and 0.46 m/s (direction 2).

The travel direction (x-direction) and direction orthogonal to the travel direction (y-direction) of acceleration are compared. The general patterns of the drone data and in-vehicle sensor data are similar in both x-direction (Fig. 5.11) and y-direction (Fig. 5.12), which is also indicated by low average RMS deviations (Table 5.1). However, high-frequency changes in acceleration cannot be detected in the drone data. This is particularly noticeable in y-direction. Lane changes are clearly recognizable as peaks with in-vehicle data, while the signal derived from drone data is substantially smoothed. This is also reflected in a low correlation in y-direction between the two data sources. In addition, there is an offset in x- and y-directions, which changes between runs. This could be due to small movements of the smartphone mount between runs, as the offset is constant during each test run.

Compared to the speed differences between induction loops and drone data, the differences between in-vehicle data and drone data are substantially smaller. This indicates that the induction loops on this section of the road might not be well calibrated for speed mea-

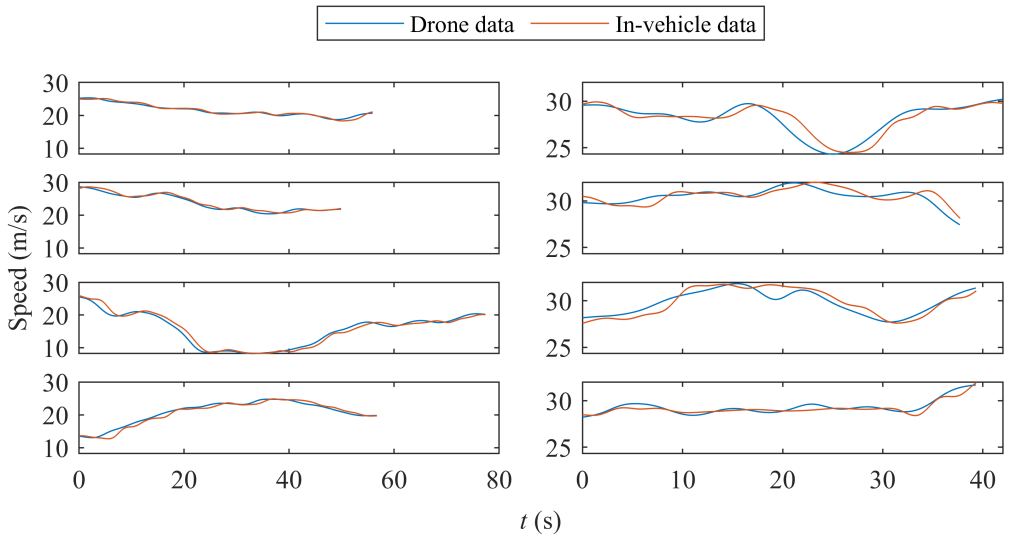

Figure 5.10: Comparison of the speeds of the measurement vehicle obtained from drone data (blue lines) and from in-vehicle data (orange lines) of eight test runs (left: direction 1, right: direction 2).

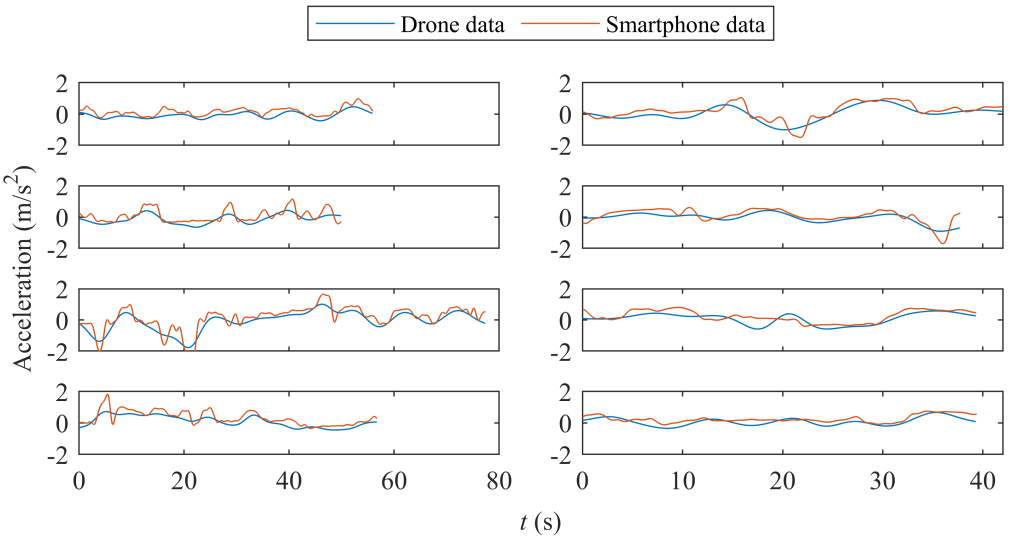

Figure 5.11: Comparison of the accelerations along the road (x-direction) of the measurement vehicle obtained from drone data (blue lines) and from in-vehicle data (orange lines) from eight test runs (left: direction 1, right: direction 2).

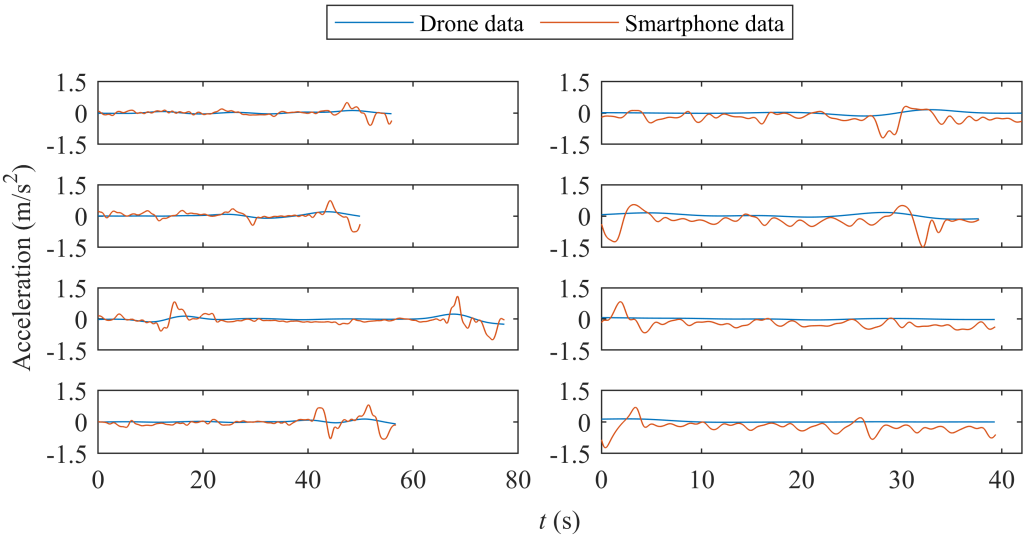

Figure 5.12: Comparison of the accelerations orthogonal to the road (y-direction) of the measurement vehicle obtained from drone data (blue lines) and from in-vehicle data (orange lines) from eight test runs (left: direction 1, right: direction 2).

Table 5.1: Parameters for comparing acceleration data derived from drone data and acceleration data obtained from the in-vehicle sensor.

Signal		**Mean of Deviations (m/s^2)**	**Std.-Dev. (m/s^2)**	**Correlation**	**Average RMS deviations (m/s^2)**
Acceleration in X	Direction 1	0.23	0.25	0.83	0.33
	Direction 2	0.16	0.23	0.80	0.28
Acceleration in Y	Direction 1	-0.03	0.20	0.45	0.20
	Direction 2	-0.24	0.26	0.36	0.26

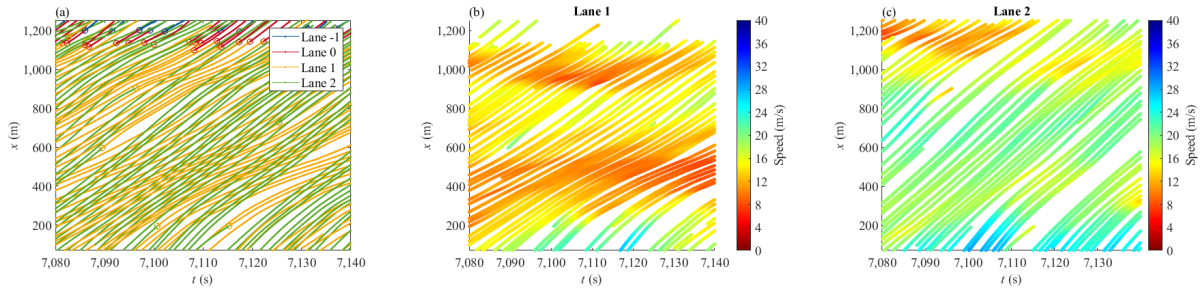

Figure 5.13: Time–space diagrams with (a) color-coded lanes and speeds in lanes (b) 1 and (c) 2.

surements. Therefore, the comparison with the in-vehicle data confirms the high quality of the drone data.

5.6 Possible applications of the dataset

5.6.1 Traffic flow analysis

In the following, we present a microscopic and macroscopic traffic flow analysis based on trajectory data. Fig. 5.13 shows two time–space diagrams of an excerpt of the data. The color-coding of the lanes (Fig. 5.13a) illustrates the frequency and locations of lane changes, the gaps between vehicles and the speed differences between the lanes. The color coding of the speed (Fig. 5.13b) illustrates the propagation of shock waves.

The time series of flow, density, and mean speed in 1-min interval (Fig. 5.14) allow the identification of congestion and the distribution of vehicles between lanes. There are two stop-and-go waves (7:46 and 7:53) with large densities and low speeds in both lanes. Due to the small length of these stop-and-go waves, the flow does not decrease significantly. As expected, the mean speed in lane 2 is greater than that in lane 1 due to the presence of fewer trucks in lane 1.

The flow–density diagram, speed–flow diagram, and speed–density diagram (Fig. 15) show the capacity, optimal speed, and critical density on this road section, respectively. Again, the small length of the stop-and-go waves leads to densities up to 57 veh/km per lane, which is well below the maximum jam density.

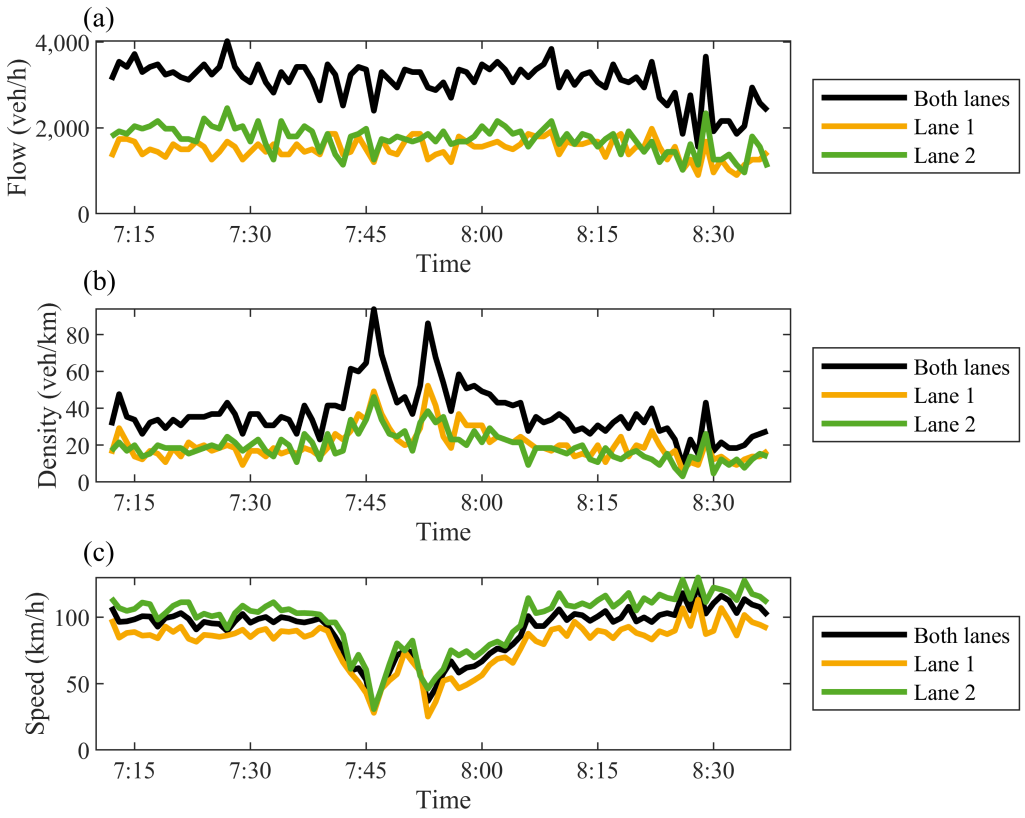

Figure 5.14: Time series of (a) flow, (b) density, and (c) mean speed.

5.6.2 Accident risk analysis

The concept of traffic conflict analysis is based on the assumption that each traffic interaction can lead to a collision. The less likely the participants of a traffic interaction are to react and avoid a crash, the more dangerous the situation is evaluated. To determine this "closeness" to a crash, different surrogate safety measures (SSMs) have been developed in recent decades. According to Mahmud et al. [37], these SSMs can be categorized as follows: (1) temporal-proximal indicators, (2) deceleration-based indicators, and (3) distance-based proximal indicators.

In the first two categories, time-to-collision (TTC) and deceleration rate to avoid crash (DRAC) are two of the most commonly used measures to analyze traffic safety. Both of these SSMs rely on the assumptions that the analyzed traffic participants will maintain their course and momentum from the initial moment until a collision occurs. In this way, the TTC determines the remaining time until the collision from this initial moment, whereas the DRAC estimates the smallest deceleration rate needed to avoid the collision [38, 39].

However, both in inner-city traffic and on highways, acceleration and deceleration of the traffic participants cannot be neglected. Therefore, to evaluate the traffic on the recorded road section, we applied modified versions of these two indicators: We used the modified time-to-collision (MTTC) and deceleration rate to avoid crashes using constant initial acceleration (DCIA). The MTTC was developed by Ozbay et al. [40] and can be calculated as Eq. 5.1:

$$MTTC = \begin{cases} \frac{D}{v_d}, \text{ if } v_d > 0 \text{ and } a_d = 0 \\ \frac{-v_d \pm \sqrt{v_d^2 + 2a_d D}}{a_d}, \text{ if } a_d \neq 0 \end{cases} \tag{5.1}$$

where $v_d = v_F - v_L$ is the initial speed difference between the speed of the follower v_F and the speed of the leader v_L vehicles, $a_d = a_F - a_L$ is the acceleration difference, and D is the initial net distance between the vehicles. MTTC is the smallest positive result. When the MTTC is equal to or lower than 1.5 s, the interaction is considered risky [40].

The DCIA was developed by Fazekas et al. [41] and can be calculated as Eq. 5.2:

$$DCIA = \frac{d_L T + v_L - d_F R - v_F}{T - R}, \text{ if } T > R \tag{5.2}$$

where v_F, v_L, d_F, and d_L are the initial speed and initial deceleration of the follower and leader vehicles, respectively. R is the reaction time of the follower vehicle. T is the time until a crash, which can be calculated as Eq. 5.3:

$$T = \frac{v_F R - v_L R - 2D}{v_L + d_L R - v_F - d_F R}, \text{ if denom.} \neq 0 \tag{5.3}$$

when the DCIA is above 3.4 m/s^2, the interaction is considered dangerous [41].

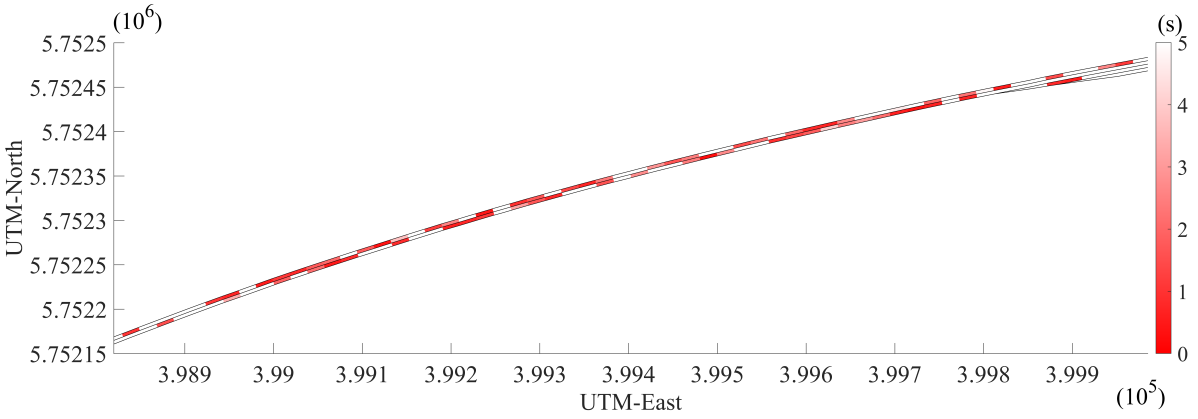

Figure 5.15: Average MTTC values under 5 s in 20 m long sections from the west to the east.

Due to the traffic data collection method described above, SSMs can be calculated at any timestamp in this dataset. This allows us to determine the extreme values of TTC and DCIA between interacting vehicles, which enables the analysis of the whole traffic scene. For this purpose, we built so-called pairs of interacting vehicles (one follower and one leader vehicle) that could collide based on their momentum. In the case of MTTC, we then determined the lowest value of each vehicle pair, whereas for DCIA, we identified the highest deceleration rates between the paired vehicles. In the next step, we located these extreme values on the positions of the follower vehicles on the road. Then, we calculated the average value of these results in each 20 m long section on the analyzed road section for each traffic lane separately. To present only relevant information, we considered only MTTC values under 5 s. Accordingly, Fig. 5.15 shows the average MTTC, and Fig. 5.16 shows the average DCIA values in the west-to-east travel direction. The values are presented with colors: The riskier the interaction based on the SSM is, the darker the red is.

The average MTTC values were less than the threshold value of 1.5 s in the main lane (lane 1) in 23% of the 20 m long road sections, in the passing lane (lane 2) in 27.9% and in the first exit lane (lane 0) in 18.2%. In contrast to the MTTC, the average DCIA values did not reach the threshold value of 3.4 m/s^2 on the road section. In fact, the highest average value present in the data was 1.69 m/s^2, which, although corresponding to stronger braking, still falls within the range of normal occurrences in traffic. The results can be explained by the congested traffic, where vehicles are relatively close to each other; therefore, the time to a crash is low, while due to lower speed values, traffic participants do not need to brake strongly to avoid a collision.

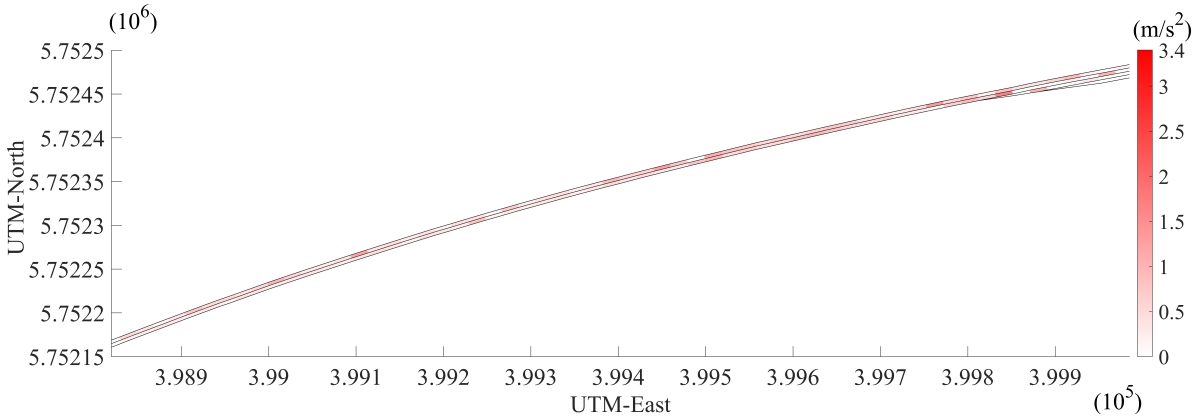

Figure 5.16: Average DCIA values in 20 m long sections from the west to the east.

5.7 Conclusions

This study presented a vehicle trajectory dataset from a German highway with two lanes and an off-ramp as well as the methods implemented to create the dataset. The data contain both free and congested traffic. The data extraction and processing methodology is applicable to other drone videos and, to some extent, to videos from stationary cameras. We performed a traffic flow analysis and an accident risk analysis, which showed that the trajectory data are suitable for these two applications. We also evaluated the plausibility and quality of the data by comparing the speeds, accelerations and flows with the results from induction loop data and smartphone accelerometer data. The results showed good agreement between our dataset and the other sensor data, which indicates good data quality. We therefore conclude that the dataset is useable for traffic flow and traffic safety analyses.

Acknowledgments

The work presented in this study is part of the projects BueLaMo (Bürgerlabor Mobiles Münsterland - Citizens' Laboratory Mobile Münsterland) funded by the German Federal Ministry for Education and Research, FeGis+ (Früherkennung von Gefahrenstellen im Straßenverkehr - Early Detection of Dangerous Areas in Traffic) funded by the German Federal Ministry for Digital and Transport, and NeMo (Neue Ansätze der Verkehrsmodellierung unter Berücksichtigung komplexer Geometrien und Daten - New traffic models considering complex geometries and data) funded by the German Research Foundation (DFG).

References

[1] Greenshields. B.D., J. R. Bibbins, W. S. Channing, and H. H. Miller. A Study of Traffic Capacity. *Proceedings of the Fourteenth Annual Meeting of the Highway Research Board*, 14:448–477, 1935.

[2] J. Treiterer. Investigation of traffic dynamics by aerial photogrammetry techniques. *Transportation Research Record*, 224, 1975.

[3] C. Hydén and L. Linderholm. The swedish traffic-conflicts technique. In E. Asmussen, editor, *International Calibration Study of Traffic Conflict Techniques*, pages 133–139, Berlin, Heidelberg, 1984. Springer Berlin Heidelberg. ISBN 978-3-642-82109-7.

[4] S. Messelodi and C. M. Modena. A computer vision system for traffic accident risk measurement. A case study. *Advances in Transportation Studies*, 7:51–66, 2005.

[5] C. Roesener, J. Sauerbier, A. Zlocki, F. Fahrenkrog, L. Wang, A. Várhelyi, E. de Gelder, J. Dufils, S. Breunig, P. Mejuto, et al. A comprehensive evaluation approach for highly automated driving. In *25th International Technical Conference on the Enhanced Safety of Vehicles (ESV) National Highway Traffic Safety Administration*, 2017.

[6] U.S. Federal Highway Administration. Next generation simulation program (NGSIM), 2006. URL `http://ops.fhwa.dot.gov/trafficanalysistools/ngsim.htm`.

[7] C. Creß, W. Zimmer, L. Strand, M. Fortkord, S. Dai, V. Lakshminarasimhan, and A. Knoll. A9-Dataset: Multi-Sensor Infrastructure-Based Dataset for Mobility Research. In *2022 IEEE Intelligent Vehicles Symposium (IV)*, pages 965–970, 2022. doi: 10.1109/IV51971.2022.9827401.

[8] J. Wang, T. Fu, J. Xue, C. Li, H. Song, W. Xu, and Q. Shangguan. Realtime wide-area vehicle trajectory tracking using millimeter-wave radar sensors and the open TJRD TS dataset. *International Journal of Transportation Science and Technology*, 12(1):273–290, 2023. ISSN 2046-0430. doi: https://doi.org/10.1016/j.ijtst.2022.02.006. URL `https://www.sciencedirect.com/science/article/pii/S2046043022000247`.

[9] R. Krajewski, J. Bock, L. Kloeker, and L. Eckstein. The highD Dataset: A Drone Dataset of Naturalistic Vehicle Trajectories on German Highways for Validation of Highly Automated Driving Systems. In *2018 21st International Conference on Intelligent Transportation Systems (ITSC)*, pages 2118–2125, 2018. doi: 10.1109/ITSC.2018.8569552.

[10] T. Moers, L. Vater, R. Krajewski, J. Bock, A. Zlocki, and L. Eckstein. The exiD Dataset: A Real-World Trajectory Dataset of Highly Interactive Highway Scenarios in Germany. In *2022 IEEE Intelligent Vehicles Symposium (IV)*, pages 958–964, 2022. doi: 10.1109/IV51971.2022.9827305.

[11] P. Spannaus, P. Zechel, and K. Lenz. AUTOMATUM DATA: Drone-based highway dataset for the development and validation of automated driving software for research and commercial applications. In *2021 IEEE Intelligent Vehicles Symposium (IV)*, pages 1372–1377, 2021. doi: 10.1109/IV48863.2021.9575442.

[12] W. Ma, H. Zhong, L. Wang, L. Jiang, and M. Abdel-Aty. MAGIC Dataset: Multiple Conditions Unmanned Aerial Vehicle Group-Based High-Fidelity Comprehensive Vehicle Trajectory Dataset. *Transportation Research Record*, 2676(5):793–805, 2022. doi: 10.1177/03611981211070549. URL https://doi.org/10.1177/03611981211070549.

[13] H. Zhao, J. Cui, H. Zha, K. Katabira, X. Shao, and R. Shibasaki. Sensing an intersection using a network of laser scanners and video cameras. *IEEE Intelligent Transportation Systems Magazine*, 1(2):31–37, 2009.

[14] L. Kloeker, C. Geller, A. Kloeker, and L. Eckstein. High-precision digital traffic recording with multi-lidar infrastructure sensor setups. In *2020 IEEE 23rd International Conference on Intelligent Transportation Systems (ITSC)*, pages 1–8. IEEE, 2020.

[15] A. Clausse, S. Benslimane, and A. de La Fortelle. Large-Scale extraction of accurate vehicle trajectories for driving behavior learning. In *2019 IEEE Intelligent Vehicles Symposium (IV)*, pages 2391–2396, 2019. doi: 10.1109/IVS.2019.8814095.

[16] C. L. Azevedo, J. L. Cardoso, M. Ben-Akiva, J. P. Costeira, and M. Marques. Automatic Vehicle Trajectory Extraction by Aerial Remote Sensing. *Procedia - Social and Behavioral Sciences*, 111:849–858, 2014. ISSN 1877-0428. doi: https://doi.org/10.1016/j.sbspro.2014.01.119. URL https://www.sciencedirect.com/science/article/pii/S1877042814001207. Transportation: Can we do more with less resources? – 16th Meeting of the Euro Working Group on Transportation – Porto 2013.

[17] J. Apeltauer, A. Babinec, D. Herman, and T. Apeltauer. Automatic vehicle trajectory extraction for traffic analysis from aerial video data. volume 40, page 9 – 15, 2015. doi: 10.

5194/isprsarchives-XL-3-W2-9-2015. URL https://www.scopus.com/inward/record.uri?eid=2-s2.0-84925349737&doi=10.5194%2fisprsarchives-XL-3-W2-9-2015&partnerID=40&md5=ef127bd7b5c31d180d4a102bd74f723a. Cited by: 64; All Open Access, Gold Open Access, Green Open Access.

[18] M. A. Khan, W. Ectors, T. Bellemans, D. Janssens, and G. Wets. Unmanned Aerial Vehicle–Based Traffic Analysis: Methodological Framework for Automated Multivehicle Trajectory Extraction. *Transportation Research Record*, 2626(1):25–33, 2017. doi: 10.3141/2626-04. URL https://doi.org/10.3141/2626-04.

[19] D. Zhao and X. Li. Real-World Trajectory Extraction from Aerial Videos - A Comprehensive and Effective Solution. In *2019 IEEE Intelligent Transportation Systems Conference (ITSC)*, pages 2854–2859, 2019. doi: 10.1109/ITSC.2019.8917175.

[20] E.-J. Kim, H.-C. Park, S.-W. Ham, S.-Y. Kho, and D.-K. Kim. Extracting vehicle trajectories using unmanned aerial vehicles in congested traffic conditions. *Journal of Advanced Transportation*, 2019(1):9060797, 2019.

[21] S. A. Ahmadi and A. Mohammadzadeh. A simple method for detecting and tracking vehicles and vessels from high resolution spaceborne videos. In *2017 Joint Urban Remote Sensing Event (JURSE)*, pages 1–4, 2017. doi: 10.1109/JURSE.2017.7924614.

[22] M. K. Masouleh and R. Shah-Hosseini. Development and evaluation of a deep learning model for real-time ground vehicle semantic segmentation from UAV-based thermal infrared imagery. *ISPRS Journal of Photogrammetry and Remote Sensing*, 155:172–186, 2019.

[23] R. Feng, C. Fan, Z. Li, and X. Chen. Mixed Road User Trajectory Extraction From Moving Aerial Videos Based on Convolution Neural Network Detection. *IEEE Access*, 8:43508–43519, 2020. doi: 10.1109/ACCESS.2020.2976890.

[24] X. Shi, D. Zhao, H. Yao, X. Li, D. K. Hale, and A. Ghiasi. Video-based trajectory extraction with deep learning for High-Granularity Highway Simulation (HIGH-SIM). *Communications in transportation research*, 1:100014, 2021.

[25] S. Yeom and D.-H. Nam. Moving Vehicle Tracking with a Moving Drone Based on Track Association. *Applied Sciences*, 11(9), 2021. ISSN 2076-3417. doi: 10.3390/app11094046. URL https://www.mdpi.com/2076-3417/11/9/4046.

[26] I. Bisio, C. Garibotto, H. Haleem, F. Lavagetto, and A. Sciarrone. A Systematic Review of

Drone Based Road Traffic Monitoring System. *IEEE Access*, 10:101537–101555, 2022. doi: 10.1109/ACCESS.2022.3207282.

[27] E. V. Butilă and R. G. Boboc. Urban Traffic Monitoring and Analysis Using Unmanned Aerial Vehicles (UAVs): A Systematic Literature Review. *Remote Sensing*, 14(3), 2022. ISSN 2072-4292. doi: 10.3390/rs14030620. URL https://www.mdpi.com/2072-4292/14/3/620.

[28] S. Staacks, S. Hütz, H. Heinke, and C. Stampfer. Advanced tools for smartphone-based experiments: phyphox. *Physics Education*, 53(4):045009, may 2018. doi: 10.1088/1361-6552/aac05e. URL https://dx.doi.org/10.1088/1361-6552/aac05e.

[29] J. Shi et al. Good features to track. In *1994 Proceedings of IEEE conference on computer vision and pattern recognition*, pages 593–600. IEEE, 1994.

[30] J.-Y. Bouguet et al. Pyramidal implementation of the affine lucas kanade feature tracker description of the algorithm. *Intel corporation*, 5(1-10):4, 2001.

[31] Geoportal.NRW. GEOportal.NRW, 2024. URL https://www.geoportal.nrw/.

[32] G. Jocher, A. Chaurasia, A. Stoken, J. Borovec, Y. Kwon, J. Fang, K. Michael, D. Montes, J. Nadar, P. Skalski, et al. ultralytics/yolov5: v6. 1-tensorrt, tensorflow edge tpu and openvino export and inference. *Zenodo*, 2022. URL https://github.com/ultralytics/yolov5/discussions/6740.

[33] J. Munkres. Algorithms for the assignment and transportation problems. *Journal of the society for industrial and applied mathematics*, 5(1):32–38, 1957.

[34] M. Berghaus, S. Lamberty, J. Ehlers, E. Kalló, and M. Oeser. Vehicle Trajectory Dataset from Drone Videos Including Off-Ramp and Congested Traffic, 2022. URL https://data.isac.rwth-aachen.de/?p=58.

[35] Mobilithek. Querschnittsdaten (Q und v) von Messstellen auf BAB in Nordrhein-Westfalen, 2022. URL https://mobilithek.info/offers/110000000003477001.

[36] M. Treiber and D. Helbing. Reconstructing the spatio-temporal traffic dynamics from stationary detector data. *Cooper@ tive Tr@ nsport@ tion Dyn@ mics*, 1(3):3–1, 2002.

[37] S. S. Mahmud, L. Ferreira, M. S. Hoque, and A. Tavassoli. Application of proximal surrogate indicators for safety evaluation: A review of recent developments and research needs. *IATSS Research*, 41(4):153–163, 2017. ISSN 0386-1112. doi:

https://doi.org/10.1016/j.iatssr.2017.02.001. URL https://www.sciencedirect.com/science/article/pii/S0386111217300286.

[38] S. Almqvist, C. Hyden, and R. Risser. Use of speed limiters in cars for increased safety and a better environment. *Transportation Research Record*, (1318):34–39, 1991.

[39] J. Hayward. *Near misses as a measure of safety at urban intersections*. Pennsylvania Transportation and Traffic Safety Center, 1971.

[40] K. Ozbay, H. Yang, B. Bartin, and S. Mudigonda. Derivation and Validation of New Simulation-Based Surrogate Safety Measure. *Transportation Research Record*, 2083 (1):105–113, 2008. doi: 10.3141/2083-12. URL https://doi.org/10.3141/2083-12.

[41] A. Fazekas, F. Hennecke, E. Kalló, and M. Oeser. A Novel Surrogate Safety Indicator Based on Constant Initial Acceleration and Reaction Time Assumption. *Journal of Advanced Transportation*, 2017, 2017. doi: 10.1155/2017/8376572. URL https://www.scopus.com/inward/record.uri?eid=2-s2.0-85042332321&doi=10.1155%2f2017%2f8376572&partnerID=40&md5=3364808a69d332ef691eee3ca33be3d9. Cited by: 14; All Open Access, Gold Open Access, Green Open Access.

6 Modeling Lane Changes at Freeway On-Ramps with a Novel Car-Following Model Based on Desired Time Headways

This paper was published under:

Berghaus, Moritz; Oeser, Markus (2025). Modeling Lane Changes at Freeway On-Ramps with a Novel Car-Following Model Based on Desired Time Headways. Journal of Advanced Transportation, 2025. https://doi.org/10.1155/atr/9971254

Individual contributions:

M. Berghaus: study conception and design; data collection; analysis and interpretation of results; draft manuscript preparation.
M. Oeser: study conception and design; supervision.

6.1 Abstract

The traffic flow at freeway on-ramps is influenced not only by the lane changes made by merging vehicles but also by the longitudinal behavior of the merging vehicles and vehicles in the main lane. Existing car-following models are not suitable to represent the longitudinal behavior during merging because they are based on the idea that vehicles intend to reach a steady state, that is, constant time headway and zero speed difference, as soon as possible. At on-ramps, however, merging vehicles have time to reach this steady state until they reach the end of the on-ramp. We therefore derive a novel car-following model based on desired time headways that is able to represent this continuous adaptation toward a steady state. From this car-following model, we derive a lane change model for freeway on-ramps with seven parameters. The lane change model includes a leader selection algorithm, which enables merging vehicles to pass or be passed by vehicles in the main lane. The model also includes components to predict the lane change start time based on surrogate safety measures and to describe the lateral behavior during the lane change. Due to the resemblance to car-following models, the methodology to calibrate the lane change model at the microscopic scale can be adopted from car-following models. To validate the model, we conduct traffic simulations and compare the simulated traffic flow with trajectory data from two German freeway on-ramps. The results show that the model accurately represents the longitudinal driving behavior of merging vehicles and their followers, although it slightly overestimates the number of merging vehicles passing a vehicle in the main lane under congested traffic conditions. The simulations yield accurate headway distributions, except in cases of very risky driver behavior, and realistically capture the macroscopic speed-density relationship at the on-ramp.

6.2 Introduction

Microscopic traffic flow models are an important tool to assess road designs and traffic management measures, to help researchers understand traffic flow, and to study the impact of automated driving on traffic flow. They describe the longitudinal and lateral behavior of vehicles in relation to their surrounding vehicles. Microscopic traffic flow models consist of car-following models, which describe the longitudinal driving behavior, and lane change models, which describe the lateral driving behavior. Car-following models predict the acceleration of the following vehicle as a function of the gap to the leading vehicle and the speeds of the leading and following vehicle. Lane change models predict the lane change start time (lane change decision model), as well as the longitudinal and lateral acceleration during the lane change (lane change execution model), considering the positions and speeds of the surrounding vehicles in both the current lane and the target lane.

Lane changes are typically classified into desired, mandatory, and courtesy lane changes [1]. Desired lane changes, also referred to as tactical [2] or discretionary [3] lane changes, occur when a vehicle passes a slower vehicle. Mandatory (or strategic) lane changes occur when the vehicle's current lane ends or is not along its intended route, such as at on-ramps, off-ramps, or weaving sections. Courtesy (or cooperative) lane changes occur when a vehicle changes lanes to allow another vehicle to make a mandatory lane change.

Modeling the merging process at on-ramps is complex due to the different driving maneuvers in addition to the lane change itself. Merging vehicles must accelerate to reach the speed of traffic in the main lane and to reach a gap into which they can merge. This maneuver is commonly referred to as *synchronization* [4]. In dense traffic, merging vehicles accept smaller time headways during the lane change compared to regular car-following behavior, and they increase the time headway after the lane change. This maneuver is called *relaxation* [5]. In some cases, the vehicle in the main lane following the merging vehicle must facilitate the merge by making a courtesy lane change to the left or by decelerating. The former maneuver is called *anticipation* [6], the latter *cooperation* [7]. A lane change model for on-ramps must account for all these maneuvers. van Beinum et al. [8] have shown that the lane change models used in common traffic simulation packages are unable to reproduce all of these maneuvers. van Beinum et al. [8] also pointed out that the calibration of these lane change models is impractical due to the large number of parameters. The driving maneuvers at on-ramps evoke macroscopic traffic features such as the capacity drop, which means that the maximum flow in congested traffic is smaller than in free-flow traffic [9]. Chen et al. [10] have shown that congested traffic at on-ramps is also associated with riskier lane changes due to negative gaps at the start of the lane change.

Many lane change models proposed in the literature are discrete choice models focusing on criteria that must be met to perform a lane change. For example, Kesting, Treiber, and Helbing [11] proposed the MOBIL model, which includes the incentive criterion describing whether a driver intends to change lanes, and the safety criterion describing whether it is safe to change lanes. Another common approach is to model which gap a merging vehicle accepts depending on the surrounding traffic [4, 12]. The decision whether a gap is accepted or not can be described with logistic regression models that predict the probability of gap acceptance depending on the distance to the end of the on-ramp, the size of the gap, and the speed difference between the merging vehicle and its adjacent vehicles [13, 14]. The decision to start a lane change can also be modeled with game-theoretical approaches, which means that drivers intend to maximize a payoff function that depends on collision risk and speed gain [6, 15]. Laval and Leclercq [5] criticized decision-based models for being too complex and inconsistent and proposed a macroscopic lane change model in which the rate of lane changes depends on the density. Choudhury [16] argues that drivers develop a latent merging plan when they enter the on-ramp and choose their acceleration according to this plan. Other concepts to model the interaction between the merging vehicle and adjacent vehicles include lateral friction, which leads to reduced speed [17], and cooperation due to social interactions between drivers [18]. Data-driven models based on neural networks or other machine learning techniques can potentially capture merging behavior more realistically [19, 20]. While they are crucial for the development of autonomous vehicles, these black-box models do not contribute to a deeper understanding of the complexity of merging behavior.

For a complete microscopic traffic flow model that can be used in traffic simulations, lane change models must be combined with car-following models. The main challenge of these combined models is to accurately represent the longitudinal behavior during a lane change, which differs from the behavior during regular car-following [5]. Nevertheless, a regular car-following model can be applied if a vehicle in an adjacent lane can also be regarded as the leader [4, 21]. In the case of on-ramps, this assumption leads to the problem that small gaps between the merging vehicle and the leader in the main lane would result in extreme decelerations, although small gaps are not unsafe before the merging vehicle starts changing lanes. To avoid this undesired behavior, Schakel, Knoop, and van Arem [4] applied boundary conditions on the gap, which result in bounded acceleration values predicted by the car-following model. However, these boundary conditions do not ensure that the merging vehicle gradually adapts to the leader in the main lane. The model for lane changes at on-ramps proposed in this paper achieves this gradual adaptation using the idea that the merging vehicle gradually reaches a desired time headway to the leader until it reaches the end of the on-ramp.

Traffic flow models must be calibrated to find the model parameter values that minimize

the deviation between real traffic and modeled traffic. The calibration of lane change models is more complex than the calibration of car-following models, which have only one output variable (acceleration) and a few input variables (speeds and positions of leader and follower). Lane change models, however, have more than one output variable (depending on the model, e.g., acceleration, lateral position, and time of the lane change) and more input variables (speeds and positions of the surrounding vehicles in the current lane and the target lane). To reduce this complexity, some studies rely on a less complex macroscopic calibration [4], while other studies observe the model parameters directly from empirical data instead of calibrating them [22]. Since our proposed model is based on a car-following model, we calibrate the model microscopically using the methodology for car-following model calibration, see [23, 24].

Traffic flow models must also be validated to show that they describe the characteristics of real traffic appropriately. The validation of lane change models can be performed at both the macroscopic and microscopic scales. Macroscopic traffic characteristics including flow, density, and mean speed describe overall traffic behavior. Criteria for validation used in the literature include the relationship between mean speed and flow [25]; speed contour plots, which visualize variations in mean speed over time and space [4]; or the distribution of flows over the lanes [4, 26, 27]. Microscopic traffic characteristics refer to the behavior of individual vehicles, for example, speed as well as gaps and headways between vehicles. In the context of on-ramps, criteria for validation include the gaps that drivers accept before they start merging [8, 13], the positions where lane changes occur, or the distribution of time headways during merging [8, 28].

The calibration of the model parameters and the validation of the models rely on empirical data. These data can either be macroscopic flows and mean speeds, e.g., derived from induction loops, or microscopic trajectories derived from floating car data or from drones or stationary cameras. Macroscopic data from induction loops are the simplest type of data. Although they only provide cross-sectional data, these data are useful to calibrate lane change models if the cross-sections are sufficiently close together [29] or if the traffic state between the cross-sections is interpolated [30, 31], for example, using the adaptive smoothing method [32]. Floating car data provide the trajectories of a sample of vehicles, and they enable analyses on the location and duration of lane changes and the speeds during lane changes [30]. However, they do not contain interactions with other vehicles, so the gap selection and the headways during merging cannot be analyzed. Trajectory datasets from drones or stationary cameras allow detailed analyses of these aspects. Some researchers collect their own data specifically for the analysis of lane changes at on-ramps [28, 29, 33], while many others still use the NGSIM dataset from 2006 [14, 31, 34, 35]. For all data sources, it is important that both free and congested traffic states are included to achieve a model that is valid for both

states.

In this paper, we derive a lane change model for freeway on-ramps based on a car-following model that uses the concept of desired time headways (Section 6.3). Since the lane change model is derived from a car-following model, the methodology for calibrating and validating the model at the microscopic scale can be adopted from car-following models (Section 6.4). We analyze the features of the model using sensitivity analysis, example cases, and traffic simulations (Section 6.5).

6.3 Model Derivation

We propose a model for lane changes at on-ramps that focuses on the longitudinal behavior, which means it is based on a car-following model with the following adaptations:

1. The merging vehicle (hereafter referred to as *merger*) may have more than one leader (see Figure 6.1(a): one on the on-ramp and one in the main lane). The car-following model calculates one acceleration value for each leader. The smaller value is the relevant one. In the following, we use the term *leader* for the leader in the main lane if not mentioned otherwise because this is the relevant leader in most cases.

2. While the merger is on the on-ramp, it can pass one or more vehicles in the main lane or be passed by them (see Figure 6.1(b)). Thus, the leader is not necessarily the current preceding vehicle, but the preceding vehicle after merging. The algorithm for selecting the leader will be presented in Section 6.3.5

3. The merger must reach a sufficient time headway (hereafter referred to as *headway*) to the leader only at the end of the on-ramp, while smaller and even negative headways are allowed at the beginning of the on-ramp, as shown in Figure 6.1(b). When the lane change starts, the headway must be at least zero, i.e., the merger must be behind the leader.

4. The follower in the main lane also has more than one leader: one in the main lane, which is also the leader of the merger, and the merger. The headway between the follower and the merger must also only be sufficient at the end of the on-ramp, and it must be at least zero when the lane change starts. Again, the car-following model calculates one acceleration value for each leader, and the smaller value is the relevant one.

While adaptation 1 can easily be achieved with any existing car-following model, adaptations 2, 3, and 4 are incompatible with existing car-following models because the models

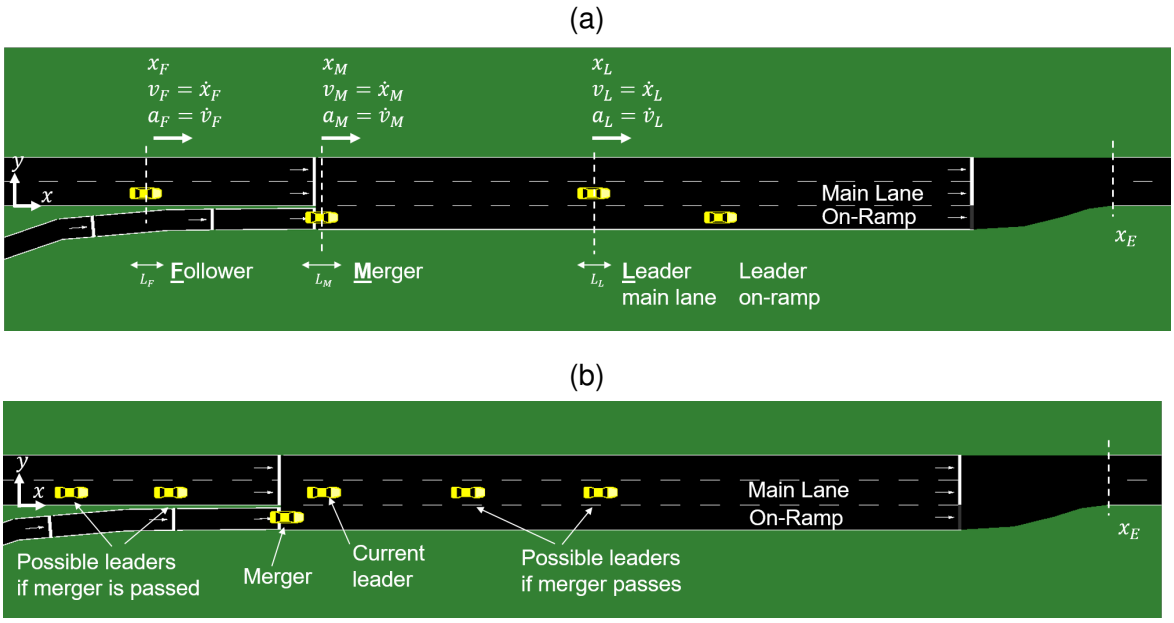

Figure 6.1: (a) Definition of leader, follower, and merger, (b) small headway between merger and current leader at the beginning of the on-ramp, and possible leaders if merger passes or is passed.

would predict unrealistically negative accelerations if the headway was small or negative. Therefore, we propose a new car-following model based on desired headways, which we describe in the following section. From this car-following model, we derive the lane change model for on-ramps.

6.3.1 Car-Following Model Based on Desired Time Headways

The proposed car-following model is based on the concept that the follower intends to achieve a desired headway T_{des} to the leader. The headway T at time t is defined as the net distance between leader and follower divided by the speed of the follower:

$$T(t) = \frac{\Delta x(t)}{v_F(t)} = \frac{x_L(t) - x_F(t) - (L_L/2) - (L_F/2) - \Delta x_{min}}{v_F(t)}, \tag{6.1}$$

where x is the position, v is the speed, and L is the length of a vehicle. Δx represents the net distance between leader and follower minus a minimum distance Δx_{min} at standstill. Δx_{min} is included here to make the model equations more comprehensible, although it is not included in the common definition of the net distance. Index L denotes the leader, and index F denotes the follower.

The follower accelerates with acceleration a_F such that it reaches the desired headway after time τ, which we refer to as *adaptation time*. To derive this acceleration, we use the following kinematic equations, assuming the leader has zero acceleration, which is a common simplification in existing car-following models, e.g., in the intelligent driver model (IDM) [36]:

$$x_F(t+\tau) = \frac{1}{2} \cdot a_F(t) \cdot \tau^2 + v_F(t) \cdot \tau + x_F(t) \tag{6.2}$$

$$v_F(t+\tau) = a_F(t) \cdot \tau + v_F(t) \tag{6.3}$$

$$x_L(t+\tau) = v_L(t) \cdot \tau + x_L(t) \tag{6.4}$$

After the adaptation time, the headway must be equal to the desired headway:

$$T(t+\tau) = \frac{\Delta x(t+\tau)}{v_F(t+\tau)} = \frac{x_L(t+\tau) - x_F(t+\tau) - (L_L/2) - (L_F/2) - \Delta x_{min}}{v_F(t+\tau)} = T_{des} \tag{6.5}$$

Inserting equations 6.2-6.4 into equation 6.5 yields:

$$\frac{v_L \cdot \tau + x_L(t) - (1/2) a_F(t) \cdot \tau^2 - v_F(t) \cdot \tau - x_F(t) - (L_L/2) - (L_F/2) - \Delta x_{min}}{a_F(t) \cdot \tau + v_F(t)} = T_{des} \tag{6.6}$$

Equation 6.6 can be solved for a_F:

$$a_F(t) = \frac{v_L(t) \cdot \tau + x_L(t) - v_F(t) \cdot (\tau + T_{des}) - x_F(t) - (L_L/2) - (L_F/2) - \Delta x_{min}}{(1/2)\tau^2 + \tau \cdot T_{des}} = \frac{v_L(t) \cdot \tau - v_F(t) \cdot (\tau + T_{des}) + \Delta x(t)}{(1/2)\tau^2 + \tau \cdot T_{des}} \tag{6.7}$$

The result of equation 6.7 is dominated by τ^2 in the denominator, which means smaller values of τ lead to larger absolute values of the acceleration. The adaptation time τ can thus be interpreted as the urgency with which the follower intends to reach the desired headway, where smaller values of τ represent a higher urgency. This urgency should depend on the current headway $T(t)$. If the current headway is small, the follower must urgently reach the desired headway to avoid a collision. If the current headway is large, the follower has sufficient time to reach the desired headway. For simplicity, we assume that τ is equal to the current headway. However, τ must have an upper bound because otherwise the absolute value of the acceleration would be very small if the headway is very large, which occurs for small speeds ($v_F \to 0$) or large distances ($\Delta x \to \infty$):

$$\tau(t) = \min(T(t), \tau_{max}), \tag{6.8}$$

v_{max}	Maximum desired speed	m/s
a_{max}	Maximum (positive) acceleration	m/s^2
a_{min}	Minimum (negative) acceleration	m/s^2
Δx_{min}	Minimum distance at standstill	m
T_{des}	Desired headway	s

Table 6.1: Parameters of the car-following model based on desired headways.

where the upper bound τ_{max} can be interpreted as the headway above which the leader does not influence the behavior of the follower. Since this parameter is only relevant in a few situations, it does not have to be calibrated. We select $\tau_{max} = 10s$.

To avoid physically impossible accelerations, a_F should be bounded by a minimum (negative) acceleration a_{min} and a maximum (positive) acceleration a_{max}. The acceleration is additionally bounded by $-v_F(t)/\tau$ to avoid negative speeds after the adaptation time and by $(v_{max} - v_F(t))/\tau$ to avoid speeds above the maximum desired speed v_{max}. As a result, the model equation of the car-following model based on desired time headways is as follows:

$$a_{F,DTH} = \max\left[\min\left(\frac{v_L(t)\cdot\tau - v_F(t)\cdot(\tau + T_{des}) + \Delta x(t)}{(1/2)\tau^2 + \tau\cdot T_{des}}, a_{max}, \frac{v_{max} - v_F(t)}{\tau}\right), a_{min}, -\frac{v_F(t)}{\tau}\right] \quad (6.9)$$

In summary, the car-following model has five parameters listed in Table 6.1.

These parameters have an intuitive physical meaning and can either be calibrated or directly observed or estimated from real traffic data. They are also similar to the parameters of other common car-following models, for example, the IDM with v_0, a, b, s_0, and T [36]. While the IDM uses v_0, a, and b in all driving situations, our model uses these parameters only to bound the acceleration (see equation 6.9).

6.3.2 Car-Following Model for Mergers at On-Ramps

To model the acceleration of the merger in the case of on-ramps, the car-following model presented in Section 6.3.1 is adapted. For now, we assume that the merger has already selected a leader behind which it will merge. The selection of the leader will be modeled in Section 6.3.5. The merger aims at reaching the desired headway until it reaches the end of the on-ramp, and it also aims at reaching a non-negative headway before it starts the lane change.

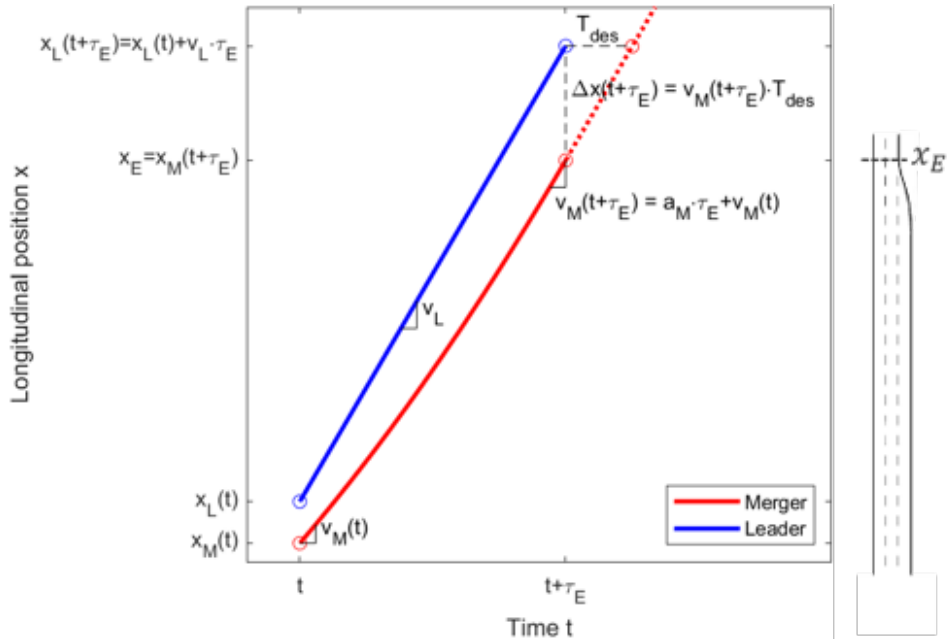

Figure 6.2: Time–space diagram with a merger (M) and its leader (L). The merger accelerates with a_M such that the net headway is equal to the desired headway T_{des} when it reaches the end of the on-ramp x_E after time τ_E. Note that the time–space diagram shows the gross distance and headway instead of the net distance and headway because it does not show the lengths of the vehicles.

First, we describe the former situation (desired headway until the end of the on-ramp), which is shown in Figure 6.2. The proposed car-following model can be applied in this situation by changing the definition of the adaptation time τ in equation 6.6. In the case of on-ramps, the adaptation time is the time until the merger reaches the end of the on-ramp, which we denote as τ_E. Thus, small headways or large speed differences between merger and leader at the beginning of the on-ramp do not result in extreme negative accelerations because there is enough time for the merger to reach the desired headway.

To derive the acceleration $a_{M,DesiredHeadway}$ of the merger, we use the same kinematic equations 6.2-6.4 as above, but using index M instead of F. The position of the merger after the adaptation time τ_E is equal to the position of the end of the on-ramp x_E. Since the time until the end of the on-ramp depends on the acceleration, equation 6.2 is first solved for a_M:

$$a_{M,DesiredHeadway}(t) = \frac{2\left(x_E - v_M(t)\cdot\tau_E - x_M(t)\right)}{\tau_E^2} \tag{6.10}$$

Equation 6.10 is then inserted for a_M into equation 6.6:

$$\frac{v_L(t)\cdot\tau_E + x_L(t) - \frac{1}{2}a_{M,DesiredHeadway}(t)\cdot\tau_E^2 - v_M(t)\cdot\tau_E - x_M(t) - \frac{L_L}{2} - \frac{L_M}{2} - \Delta x_{min}}{a_{M,DesiredHeadway}(t)\cdot\tau_E + v_M(t)} =$$

$$\frac{v_L(t)\cdot\tau_E + x_L(t) - (x_E - v_M(t)\cdot\tau_E - x_M(t)) - v_M(t)\cdot\tau_E - x_M(t) - \frac{L_L}{2} - \frac{L_M}{2} - \Delta xmin}{2\left[(x_E - v_M(t)\cdot\tau_E - x_M(t))/\tau_E\right] + v_M(t)} = T_{des}$$

$$\Leftrightarrow v_L(t)\cdot\tau_E^2 + \left(x_L(t) - x_E - \frac{L_L}{2} - \frac{L_M}{2} - \Delta x_{min} + T_{des}\cdot v_M(t)\right)\cdot\tau_E - 2\cdot T_{des}\cdot(x_E - x_M(t)) = 0 \tag{6.11}$$

This quadratic equation is solved for τ_E:

$$\tau_E = \frac{-x_L(t) + x_E + \frac{L_L}{2} + \frac{L_M}{2} + \Delta x_{min} - T_{des}\cdot v_M(t) \pm \sqrt{\left(x_L(t) - x_E - \frac{L_L}{2} - \frac{L_M}{2} - \Delta x_{min} + T_{des}\cdot v_M(t)\right)^2 + 8 v_L(t)\cdot T_{des}\cdot(x_E - x_M(t))}}{2 v_L(t)} \tag{6.12}$$

Only real and positive solutions of equation 6.12 are valid because the end of the on-ramp is reached in the future. If equation 6.12 has two real and positive solutions, the smaller one is relevant because it corresponds to the nearest moment in the future. This solution is then inserted into equation 6.10 to obtain the acceleration of the merger. If equation 6.12 has no real and positive solution, the resulting acceleration of the merger would be so small that it stops before the end of the on-ramp. In this case, it can be assumed that the merger stops at the end of the on-ramp. Equation 6.3 thus becomes:

$$\begin{aligned} v_M(t+\tau_E) = a_M(t)\cdot\tau_E + v_M(t) = 0 \\ \Leftrightarrow \frac{2\left(x_E - v_M(t)\cdot\tau_E - x_M(t)\right)}{\tau_E^2}\cdot\tau_E + v_M(t) = 0 \\ \Leftrightarrow \tau_E = \frac{2\left(x_E - x_M(t)\right)}{v_M(t)} \end{aligned} \tag{6.13}$$

For the latter situation (non-negative headway when the lane change starts), which is shown in Figure 6.3, the proposed car-following model can also be applied by changing the desired headway to zero ($T_{des} = 0$) and the time until the desired headway is reached to the time until the lane change starts. To finish the lane change at the end of the on-ramp at $t + \tau_E$, the lane change must start at $t + \tau_E - \tau_{LC}$, where τ_{LC} is the duration of the lane change. τ_{LC} is another parameter of the proposed lane change model for on-ramps in addition to the parameters of the car-following model introduced in Section 6.3.1. The time until the lane change starts is

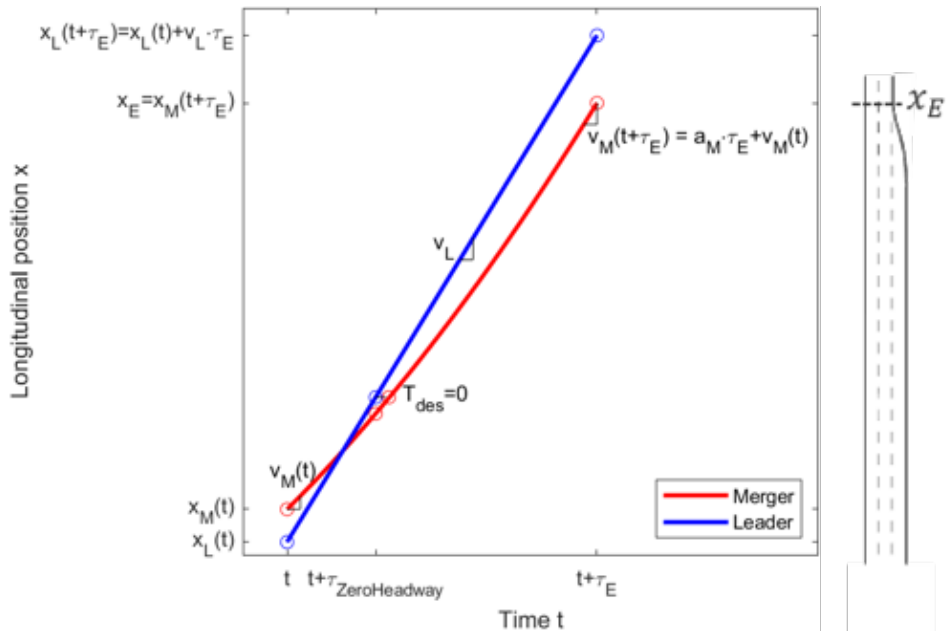

Figure 6.3: Time–space diagram with a merger (M) and its leader (L). The merger accelerates with a_M such that the net headway is zero when it starts the lane change after time $\tau_{ZeroHeadway}$. Note that the time–space diagram shows the gross headway, which is larger than zero, instead of the net headway because it does not show the lengths of the vehicles.

denoted as $\tau_{ZeroHeadway} = \tau_E - \tau_{LC}$. Inserting $T_{des} = 0$ and $\tau_{ZeroHeadway}$ instead of τ into equation 6.7 and adapting the indices, the acceleration of the merger is obtained:

$$a_{M,ZeroHeadway}(t) = \frac{(v_L(t) - v_M(t)) \cdot \tau_{ZeroHeadway} + \Delta x(t)}{(1/2)\tau_{ZeroHeadway}^2} \tag{6.14}$$

After the lane change has started, the merger also wants to maintain a non-negative headway. In this case, $\tau_{ZeroHeadway}$ can be set equal to the current headway.

The resulting acceleration of the merger is the minimum of the two accelerations mentioned above to ensure that the headway at the end of the on-ramp is at least the desired headway and that the headway at the start of the lane change is non-negative. Additionally, the bounds introduced in equation 6.9 are applied:

$$a_M(t) =$$

$$\max\left[\min\left(a_{M,DesiredHeadway}(t), a_{M,ZeroHeadway}(t), a_{max}, \frac{v_{max}-v_F(t)}{\tau_{ZeroHeadway}}\right), a_{min}, -\frac{v_F(t)}{\tau_{ZeroHeadway}}\right] \tag{6.15}$$

6.3.3 Lane Change Start

So far, we have focused on the longitudinal behavior of the merger. To model the lateral behavior, the most essential factor is the time when the lane change starts. In Section 6.3.2, we have assumed that the lane change starts at the latest possible time, that is, such that the lane change is completed when the merger reaches the end of the on-ramp. However, it is intuitive to assume that mergers start the lane change earlier if it is safe.

To quantify the level of safety, surrogate safety measures (SSMs) are suitable. For example, the *Deceleration Rate to Avoid a Crash* (DRAC) describes the required acceleration of the follower to reach a zero headway assuming that the leader does not change its speed, see [37]:

$$DRAC = \begin{cases} -\infty & \text{if } x_L - x_F - \frac{L_L}{2} - \frac{L_F}{2} \leq 0 \\ 0 & \text{if } x_L - x_F - \frac{L_L}{2} - \frac{L_F}{2} > 0 \text{ and } v_L \geq v_F \\ -\frac{(v_L - v_F)^2}{2(x_L - x_F - (L_L/2) - (L_F/2))} & \text{if } x_L - x_F - \frac{L_L}{2} - \frac{L_F}{2} > 0 \text{ and } v_L < v_F \end{cases} \tag{6.16}$$

If both the DRAC between the merger (index M instead of F in equation 6.16) and the leader and between the follower and the merger (index M instead of L in equation 6.16) are larger than some threshold $DRAC_{min}$, the lane change can start safely. In this case, the adaptation time τ becomes the time until the lane change is completed and not the time the merger reaches the end of the on-ramp.

Even if $DRAC \geq DRAC_{min}$ is not fulfilled until the latest possible lane change start time, the lane change can safely start because the car-following model for mergers (see Section 6.3.2) ensures that the headway between leader and merger is non-negative at this moment. To ensure that the headway between merger and follower is also non-negative, the follower must cooperate by decelerating in some cases. This cooperation will be described in Section 6.3.6.

In summary, the lane change model has the same five parameters as the car-following model (see Table 6.1) and two additional parameters (see Table 6.2). Compared to lane change models from the literature [4, 11, 12], the number of parameters in our model is small, which facilitates the calibration and the interpretability of the model parameters.

τ_{LC}	Lane change duration	s
$DRAC_{min}$	Threshold for lane change start	m/s^2

Table 6.2: Additional parameters of the lane change model.

6.3.4 Lateral Position During the Lane Change

After the lane change has started, the merger changes its lateral position from the center of the on-ramp to the center of the main lane. The lateral position during the lane change $y_M(t)$ follows some s-shaped curve (see Figure 6.4). Given that t_0 is the time when the lane change starts, $y = 0$ is the edge between the on-ramp and the main lane, and W_{Lane} is the lane width, the following boundary conditions for the lateral position and its first derivative $\dot{y}_M(t)$ apply:

$$y_M(t_0) = -\frac{W_{Lane}}{2} \tag{6.17}$$

$$\dot{y}_M(t_0) = 0 \tag{6.18}$$

$$y_M(t_0 + \tau_{LC}) = \frac{W_{Lane}}{2} \tag{6.19}$$

$$\dot{y}_M(t_0 + \tau_{LC}) = 0 \tag{6.20}$$

These boundary conditions ensure that the merger is in the center of the lane before and after the lane change (equations 6.17 and 6.19) and that the merger has no lateral movement before and after the lane change (equations 6.18 and 6.20).

The simplest solution for an s-shaped curve fulfilling these boundary conditions is the following third-order polynomial:

$$y_M(t) = \begin{cases} -\frac{W_{Lane}}{2} & t < t_0 \\ \frac{-2W_{Lane}}{\tau_{LC}^3}(t-t_0)^3 + \frac{3W_{Lane}}{\tau_{LC}^2}(t-t_0)^2 - \frac{W_{Lane}}{2} & t_0 \leq t \leq t_0 + \tau_{LC} \\ \frac{W_{Lane}}{2} & t > t_0 + \tau_{LC} \end{cases} \tag{6.21}$$

$$\dot{y}_M(t) = \begin{cases} 0 & t < t_0 \vee t > t_0 + \tau_{LC} \\ \frac{-6W_{Lane}}{\tau_{LC}^3}(t-t_0)^2 + \frac{6W_{Lane}}{\tau_{LC}^2}(t-t_0) & t_0 \leq t \leq t_0 + \tau_{LC} \end{cases} \tag{6.22}$$

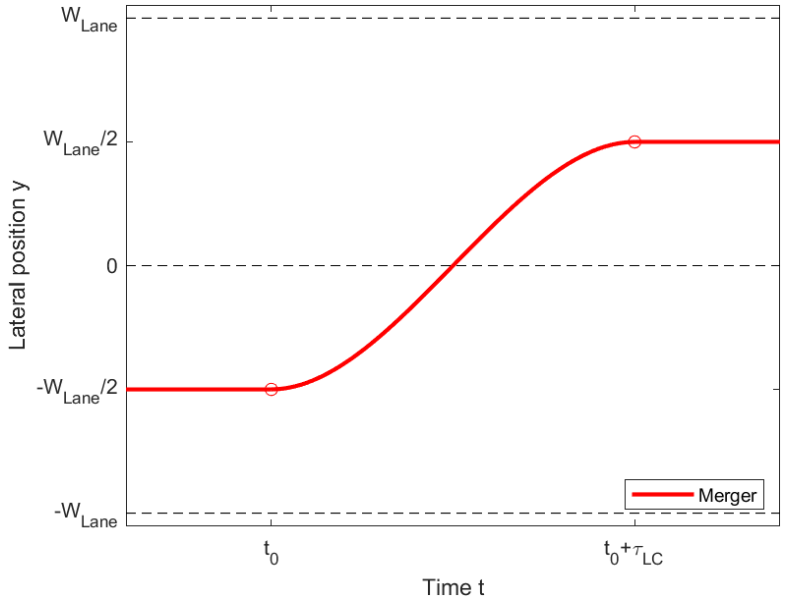

Figure 6.4: Lateral position of the merger. The lane change starts at t_0 and ends at $t_0 + \tau_{LC}$. Before and after the lane change, the merger drives in the center of the lane, and during the lane change, it follows an s-shaped curve.

6.3.5 Selection of the Leader

When a merger enters the on-ramp, there is usually more than one vehicle nearby in the main lane, which could be potential leaders of the merger. The merger selects a gap, which means it decides for one of these vehicles as a leader. This decision depends on its distances to the vehicles in the main lane, the gaps between them and their speeds. Although a human driver makes this decision intuitively, we aim to represent this decision in the lane change model using the concept of desired headways. To this end, we assume that the merger intends to reach the desired headway not only to the leader, but also to the follower. Accordingly, it must consider the follower even though this contradicts the concept of a car-following model, where only the leader determines the driving behavior. We argue that this modification is required to select the appropriate leader. The required acceleration to reach the desired headway to the leader has been derived in Section 6.3.2, while the required acceleration to reach the desired headway to the follower will be derived now.

When the merger reaches the end of the on-ramp x_E, the headway to the follower equals the desired headway T_{des}:

$$T_{des} = \frac{x_E - x_F(t + \tau_{E,Fol.}) - (L_M/2) - (L_F/2) - \Delta x_{min}}{v_F(t + \tau_{E,Fol.})}, \tag{6.23}$$

where $\tau_{E,Fol.}$ is the time until the merger reaches the end of the on-ramp, assuming that it accelerates such that it reaches the desired headway to the follower after $\tau_{E,Fol.}$. For simplicity, we assume that the follower in the main lane maintains its speed, which means that $v_F(t + \tau_{E,Fol.}) = v_F(t)$ and $x_F(t + \tau_{E,Fol.}) = v_F(t) \cdot \tau_{E,Fol.} + x_F(t)$. With this simplification, equation 6.23 can be solved for $\tau_{E,Fol.}$:

$$\tau_{E,Fol.} = \frac{x_E - x_F(t) - (L_M/2) - (L_F/2) - \Delta x_{min}}{v_F(t)} - T_{des} \tag{6.24}$$

This solution can be inserted into equation 6.10 to obtain the acceleration of the merger that is required to reach the desired headway to the follower in the main lane:

$$a_{M,Fol.}(t) = \frac{2\left(x_E - v_M(t) \cdot \tau_{E,Fol.} - x_M(t)\right)}{\tau_{E,Fol.}^2} \tag{6.25}$$

Note that $a_{M,Fol.}$ is a lower bound because larger accelerations lead to headways between merger and follower that are larger than the desired headway. a_M, on the other hand, is an upper bound because smaller accelerations lead to headways between leader and merger that are larger than the desired headway.

To select a leader, the merger evaluates $a_{M,i}$ and $a_{M,Fol.,i}$ for every hypothetical leader i and the corresponding follower. The smallest values of a_M and $a_{M,Fol.}$ are obtained for vehicles far behind the merger, and the largest values are obtained for vehicles far in front of the merger. The larger the difference between a_M and $a_{M,Fol.}$ for a given leader and follower, the larger the gap between leader and follower is. Therefore, the merger wants to select a gap for which the difference between a_M and $a_{M,Fol.}$ is large.

To reach the gap between a hypothetical leader and follower that is not the current leader and follower, the merger must pass a vehicle in the main lane or be passed by a vehicle in the main lane. Passing or being passed is only possible if it is completed before the merger must start its lane change. Completed means that the merger has a non-negative net distance to the hypothetical leader and follower. This condition can be represented by the following equations:

$$x_M(t + \tau_{Pass,i}) - x_i(t + \tau_{Pass,i}) - \frac{L_M}{2} - \frac{L_i}{2} - \Delta x_{min} \geq 0 \; \forall \; i \mid x_i(t) > x_M(t) \tag{6.26}$$

$$x_i(t + \tau_{Pass,i}) - x_M(t + \tau_{Pass,i}) - \frac{L_i}{2} - \frac{L_M}{2} - \Delta x_{min} \geq 0 \; \forall \; i \mid x_i(t) \leq x_M(t) \tag{6.27}$$

where $\tau_{Pass,i}$ denotes the available time for the merger to pass vehicle i or being passed by vehicle i:

$$\tau_{Pass,i} = \begin{cases} \tau_{E,i+1} - \tau_{LC} & x_i(t) > x_M(t) \\ \tau_{E,i} - \tau_{LC} & x_i(t) \leq x_M(t) \end{cases} \tag{6.28}$$

The difference between the two cases in equation 6.28 is that the merger has vehicle $i+1$ (the leader of vehicle i) as a leader if it passes vehicle i, whereas the merger has vehicle i as the leader if it is passed by vehicle i.

The positions at time $t + \tau_{Pass,i}$ can be computed assuming that the vehicles in the main lane maintain their speed (using equation 6.3 adjusting the indices) and that the merger accelerates with $a_{M,i}$ or $a_{M,i+1}$, depending on the case in equation 6.28, using equation 6.2 adjusting the indices. Only vehicles that can pass the merger or that can be passed by the merger before the lane change must start (equation 6.26 or 6.27) are considered as potential leaders. Of these potential leaders, the merger selects the one for which the corresponding leader and follower yield the largest difference between a_M and $a_{M,Fol.}$, i.e., it selects the largest reachable gap. If this difference is negative, the acceleration to reach the desired headway to the leader is smaller than the acceleration to reach the desired headway to the follower. In this case, the merger must rely on the cooperation of the follower, i.e., the follower must decelerate to enable the desired headway. The behavior of the follower in this case will be described in Section 6.3.6.

6.3.6 Car-Following Model for the Follower Behind a Merger

After the merger M has merged into the gap between leader L and follower F, M becomes the new leader of vehicle F. During the preparation and execution of the lane change, however, vehicle F has two leaders (L and M). The interaction between F and L is a normal car-following situation, so it can be described by the car-following model introduced in Section 6.3.1. For the interaction between F and M, the same concept as for the interaction between M and L can be applied. That means vehicle F intends to reach the desired headway to M until M has completed its lane change. Additionally, F intends to reach a non-negative headway until the latest possible time the merger starts its lane change. We assume that the drivers of vehicles in the main lane can perceive which gap M has selected for merging even before the lane change has started by estimating the acceleration of M. As a result, only the vehicle behind the gap that M merges into considers M as a leader and is defined as F. In conformity with the idea of car-following models, we assume that vehicle M only influences vehicle F if M is in front of F. That means if M passes F, it will influence F only after the passing maneuver is completed. The acceleration of F to reach the desired headway can be modeled by adapting equation 6.1. However, the simplification made in Section 6.3.2 that the

leader (in this case vehicle M) has zero acceleration is not valid because the acceleration of the merger significantly influences the future headway. Equation 6.6 therefore becomes:

$$\frac{\frac{1}{2}a_M(t)\cdot\tau^2 + v_M\cdot\tau + x_M(t) - \frac{1}{2}a_F(t)\cdot\tau^2 - v_F(t)\cdot\tau - x_F(t) - \frac{L_M}{2} - \frac{L_F}{2} - \Delta x_{min}}{a_F(t)\cdot\tau + v_F(t)} = T_{des} \quad (6.29)$$

To compute the acceleration to reach the desired headway after the lane change, $\tau = \tau_E$ is used. Solving equation 6.29 for a_F yields:

$$a_{F,DesiredHeadway}(t) = \frac{\frac{1}{2}a_M(t)\cdot\tau_E^2 + v_M(t)\cdot\tau_E + x_M(t) - v_F(t)\cdot(\tau_E + T_{des}) - x_F(t) - \frac{L_M}{2} - \frac{L_F}{2} - \Delta x_{min}}{\frac{1}{2}\tau_E^2 + \tau_E\cdot T_{des}} \quad (6.30)$$

To compute the acceleration to reach a non-negative headway when the lane change starts, $\tau_{ZeroHeadway} = \tau_E - \tau_{LC}$ and $T_{des} = 0$ are used. In this case, equation 6.29 yields:

$$a_{F,ZeroHeadway}(t) = \frac{\frac{1}{2}a_M(t)\cdot\tau_{ZeroHeadway}^2 + (v_M(t) - v_F(t))\cdot\tau_{ZeroHeadway} + x_M(t) - x_F(t) - \frac{L_M}{2} - \frac{L_F}{2} - \Delta x_{min}}{\frac{1}{2}\tau_{ZeroHeadway}^2} \quad (6.31)$$

The resulting equation for the acceleration of the follower including the appropriate bounds is:

$$a_F(t) = \max\left[\min\left(a_{F,DesiredHeadway}(t), a_{F,ZeroHeadway}(t), a_{max}, \frac{v_{max} - v_F(t)}{\tau_{ZeroHeadway}}\right), a_{min}, -\frac{v_F(t)}{\tau_{ZeroHeadway}}\right] \quad (6.32)$$

6.4 Model Calibration and Validation

In this section, we describe the trajectory data used for calibration and validation as well as the methodology to calibrate and validate the proposed lane change model.

	Duisburg dataset	**Cologne dataset**
Location	A59, Duisburg Meiderich, Germany	A4, Cologne Klettenberg, Germany
Number of lanes	2 + on-ramp	3 + on-ramp
Length of the on-ramp	ca. 100 m	ca. 200 m
Length of the road section	ca. 540 m	ca. 400 m
Speed limit	80 km/h	120 km/h
Total duration	38 min	102 min
Number of trajectories	2834 ($\approx$ 4475 vehicles per hour)	7039 ($\approx$ 4141 vehicles per hour)
Number of mergers	262 ($\approx$ 414 vehicles per hour)	581 ($\approx$ 342 vehicles per hour)

Table 6.3: Overview of the two trajectory datasets.

6.4.1 Trajectory Data

We use trajectory data from two different on-ramp locations with different infrastructure designs and traffic conditions. The main differences between the two locations are the number of lanes, the speed limit, and the length of the on-ramp (see Table 6.3). The first dataset was collected by our research group, including the authors of this paper, following the methodology described in [38] with some adaptations in the computer vision algorithms. The trajectories contain an on-ramp on the freeway A59 in Duisburg, Germany (see Figure 6.5). The trajectories have been gathered from drone videos recorded during the morning peak (06:30 to 07:15) in August 2022. The second dataset is part of the exiD dataset by Moers et al. [39]. The trajectories contain an on-ramp on the freeway A4 in Cologne, Germany. The data were recorded during the afternoon peak (approximately 14:00 to 17:00) in 2021. While the Duisburg dataset contains almost only congested traffic, the Cologne dataset contains mostly free-flow traffic with a short period of congested traffic. Both datasets are split into two equally long parts, one for calibration and one for validation.

6.4.2 Calibration Methodology

The aim of the model calibration is to obtain those values of the model parameters for which the prediction error is minimal. To achieve a model that accurately represents the driver

Figure 6.5: Screenshot of the drone video of freeway A59 in Duisburg, Germany. The on-ramp is at the bottom of the image (travel direction left to right).

behavior at the microscopic scale, we calibrate the model microscopically. Since our lane change model is based on the concept of a car-following model, we can adopt the methodology of car-following model calibration, which has been extensively discussed in the literature, see [23, 24]. Consequently, we define the prediction error as the deviation between the observed trajectories and the trajectories predicted by the model. We assume that the behavior of all drivers can be represented by the same model parameter values, i.e., we assume that the model is deterministic, which simplifies the calibration process.

We divide the calibration process into three different cases according to the three submodels described in Section 6.3: (1) mergers, (2) followers of mergers, and (3) vehicles with normal car-following behavior, i.e., all vehicles except the mergers and their followers. Although these submodels share the same model parameters, the values of these parameters may be different due to the different driving behaviors in each of these situations.

The model for mergers (submodel 1, Sections 6.3.2-6.3.5) consists of four different components (car-following, lane change start, lateral position, and leader selection). Since all model parameters affect more than one of these components, we calibrate the model in its entirety without separating it into its components. By minimizing the deviation between the observed and modeled trajectories, the best model parameter values for all components are obtained. For example, selecting the correct leader reduces the deviation in longitudinal direction, and predicting the correct lane change start time reduces the deviation in lateral direction.

Mergers whose leader or follower make a courtesy lane change are excluded from the calibration process. Mergers that change into the left lane directly after merging are also excluded.

To obtain the modeled trajectories, we select the time when a merger is at the start of the on-ramp as initial condition. We assume that the speed and position of the merger and the current

positions and speeds of all vehicles in the main lane are known. Based on this information, the model decides which leader is selected and whether the lane change is started or not and predicts the acceleration and the lateral position. The acceleration is used to compute the speed and position at the next time step. We assume that a time step of $0.1s$ is a good balance between computational efficiency and accuracy. At the next time step, this process is repeated with the predicted speed and position of the merger and the observed speeds and positions of the vehicles in the main lane. Thus, we neglect that the behavior of the mergers might influence the vehicles in the main lane to simplify the calibration. This process is repeated until the time when the merger reaches the end of the on-ramp. For each time step, the deviation between the predicted and the observed position is computed. This method is referred to as global calibration [23]. With the deviations, the root mean square error (RMSE) of the trajectory is computed:

$$RMSE_{Trajectory} = \sqrt{\frac{1}{n}\left(\sum_{i=1}^{n}(x_{Mod.} - x_{Obs.})^2 + \sum_{i=1}^{n}(y_{Mod.} - y_{Obs.})^2\right)}, \tag{6.33}$$

where n is number of time steps between the first and last position. $x_{Obs.}$ and $y_{Obs.}$ are longitudinal and lateral position observed. $x_{Mod.}$ and $y_{Mod.}$ are longitudinal and lateral position predicted by the model.

After the RMSE is computed for each trajectory individually, the total RMSE is computed as the root mean square of the individual RMSEs:

$$RMSE_{Total} = \sqrt{\frac{1}{n}\sum_{i=1}^{n}(RMSE_{Trajectory})^2}, \tag{6.34}$$

where n is the number of mergers in the trajectory datasets. To avoid parameter sets that lead to collisions between the merger and vehicles in the main lane, these parameter sets are penalized by multiplying the total RMSE with $(n_{Coll} + 1)$, where n_{Coll} is the number of collisions.

The total RMSE is minimized using the pattern search algorithm. To obtain realistic model parameters, the boundary conditions listed in Table 6.4 are applied. Since two datasets with different speed limits are used for the calibration, the maximum desired speed v_{max} is not calibrated. Instead, v_{max} is estimated based on the speed limits, which are $80km/h = 22.22m/s$ for the first dataset and $120km/h = 33.33m/s$ for the second dataset. For the second dataset, the maximum speed of trucks is set to $80km/h$ and the speed of buses is set to $100km/h$. For mergers that exceed the speed limit, the individual v_{max} is set to the maximum observed speed of this vehicle.

Model parameter	**Lower bound**	**Upper bound**
Maximum speed v_{max}	(Not calibrated)	(Not calibrated)
Maximum acceleration a_{max}	$1.0m/s^2$	$3.0m/s^2$
Minimum acceleration a_{min}	$-10.0m/s^2$	$-3.0m/s^2$
Minimum distance at standstill Δx_{min}	$1.0m$	$7.0m$
Desired headway T_{des}	$0.5s$	$2.0s$
Lane change duration τ_{LC}	$3.0s$	$6.0s$
Minimum DRAC to start lane change $DRAC_{min}$	$-1.5m/s^2$	$-0.1m/s^2$

Table 6.4: Lower and upper bounds of the model parameter values.

The calibration of the model for the followers of mergers (submodel 2, Section 6.3.6) is conducted in a similar way. Followers that make a courtesy lane change are not considered in the calibration process due to the focus on the car-following behavior. Followers that follow the merger with a headway larger than $3s$ are also not considered as they are likely not influenced by the merger. Since the followers do not change lanes themselves, the lane change duration τ_{LC} is not calibrated again; instead, the result of the calibration for mergers is used. The minimum DRAC to start the lane change is not contained in the model for the followers. The other model parameters are the same as for the mergers, and the same bounds (see Table 6.4) are applied. As an initial condition, we use the speed and position of the follower at the time when the merger is at the start of the on-ramp. We assume that the trajectory of the merger is known and that the behavior of the follower does not influence the behavior of the mergers. The trajectory of the follower is predicted by the model until the merger reaches the end of the on-ramp. The RMSE is defined as in equations 6.33 and 6.34, but without the term containing y because the lateral position of the follower is not relevant.

For the calibration of the regular car-following model (submodel 3, Section 6.3.1), the main difference to the first two cases is that we only consider vehicle pairs for which neither leader nor follower made a lane change in the whole road section included in the trajectory data. As an initial condition, we use the first available data point where both leader and follower are within the road section. The trajectory of the follower is predicted by the model until the leader leaves the road section. Parameter combinations that lead to a collision due to numerical instability if the leader suddenly brakes with a_{min} are excluded.

6.4.3 Simulation-Based Validation

To validate that the proposed model describes lane changes at on-ramps appropriately both at the microscopic and macroscopic scale, we set up traffic simulations of the two on-ramp locations described in Section 6.4.1. We use the open source traffic simulation software SUMO [40]. The car-following behavior and the lane change behavior at the on-ramps are modified according to the models presented in Section 6.3. The models are implemented in MATLAB [41], and the resulting vehicles' positions and speeds are transferred between MATLAB and SUMO with SUMO's traffic control interface (TraCI). Desired and courtesy lane changes are handled by SUMO itself. The traffic demand is taken from the trajectory data by aggregating the number of vehicles on the on-ramp and in the main lanes in intervals of 1 minute. For the first location (Duisburg), we distinguish four vehicle categories (car, van, truck, and bus), while the data for the second location (Cologne) only distinguish three vehicle categories (car, van, and truck). The maximum speed of the vehicles is set slightly above the speed limit ($86km/h$ for the first location with a speed limit of $80km/h$ and $130km/h$ for the second location with speed limit of $120km/h$), which corresponds to typical driving behavior in Germany. At the second location, buses and trucks have a lower maximum speed of $105km/h$ and $86km/h$, respectively. For simplicity, we assume that the other model parameters have the same values for all vehicle categories.

To achieve a small deviation between simulated and observed traffic on macroscopic scale, the simulation should yield the same amount of congested traffic (i.e., similar average speeds) as the trajectory data. However, the congested traffic in both trajectory datasets originates not only from the on-ramps but also from bottlenecks outside the range of the datasets. Since these bottlenecks are not contained in the simulation either, the amount of congestion occurring in the simulation would be smaller than in reality. To account for the bottlenecks in the simulation, the speed limit at the downstream end of the simulated road section is changed dynamically according to the observed average speed at the downstream end of the road section contained in the trajectory data.

6.5 Results and Discussion

In this section, we present the results of the model calibration and validation and discuss the capabilities and limitations of the model.

Parameter	Duisburg dataset	Cologne dataset
Maximum speed v_{max}	$80km/h$*	$120km/h$*
Maximum acceleration a_{max}	$1.00m/s^2$	$1.00m/s^2$
Minimum acceleration a_{min}	$-4.00m/s^2$	$-10.00m/s^2$
Minimum distance at standstill Δx_{min}	$2.48m$	$7.00m$
Desired headway T_{des}	$0.80s$	$0.65s$
Lane change duration τ_{LC}	$6.00s$	$6.00s$
Minimum DRAC to start lane change $DRAC_{min}$	$-1.50m/s^2$	$-0.10m/s^2$
RMSE calibration data	$3.60m$	$5.49m$
RMSE validation data	$3.16m$	$5.14m$

Table 6.5: Calibrated model parameters of the lane change model for mergers.
*Not calibrated

6.5.1 Calibration Results

Table 6.5 shows the calibrated parameters of the lane change model for mergers. The calibration yields reasonable values for both locations. The values of a_{max} are equal to the lower bound, which indicates that mergers do not require large accelerations to reach the desired headway. The values of τ_{LC} are equal to the upper bound, which indicates that the average lane change duration is larger than $6s$. However, it must be noted that the definition of the lane change start time is not straightforward in the trajectory data because vehicles do not drive exactly in the center of the lanes. The lower value of $DRAC_{min}$ for the Duisburg dataset shows that mergers accept riskier situations when they start their lane change. A possible explanation for this observation could be the smaller length of the on-ramp. In the Cologne dataset, the values of both a_{min} and Δx_{min} are equal to one of the bounds. This is presumably a calibration artifact due to the small speed variation in the data. The RMSE values for calibration and validation are in the same order of magnitude, which shows that the model is not overfitted to the data.

Table 6.6 shows the calibrated parameters of the model for the followers of mergers. The desired headway of the followers is larger compared to the mergers. However, the desired headway only refers to the end of the lane change, while smaller headways are possible during the lane change when the merger accelerates. The values of a_{max} and Δx_{min} are equal to the lower bounds, which indicates that the data do not contain situations where the follower

Parameter	Duisburg dataset	Cologne dataset
Maximum speed v_{max}	$80km/h^*$	$120km/h^*$
Maximum acceleration a_{max}	$1.00m/s^2$	$1.00m/s^2$
Minimum acceleration a_{min}	$-3.00m/s^2$	$-3.88m/s^2$
Minimum distance at standstill Δx_{min}	$1.00m$	$1.00m$
Desired headway T_{des}	$1.40s$	$1.02s$
RMSE calibration data	$3.97m$	$5.41m$
RMSE validation data	$3.99m$	$8.59m$

Table 6.6: Calibrated model parameters of the model for followers of mergers.

*Not calibrated

Parameter	Duisburg dataset	Cologne dataset
Maximum speed v_{max}	$80km/h^*$	$120km/h^*$
Maximum acceleration a_{max}	$1.00m/s^2$	$1.16m/s^2$
Minimum acceleration a_{min}	$-6.95m/s^2$	$-8.78m/s^2$
Minimum distance at standstill Δx_{min}	$1.00m$	$1.00m$
Desired headway T_{des}	$1.30s$	$1.12s$
RMSE calibration data	$6.71m$	$10.02m$
RMSE validation data	$6.31m$	$11.04m$

Table 6.7: Calibrated model parameters of the car-following model.

*Not calibrated

accelerated more or where the follower came to a standstill. For the Cologne dataset, the RMSE of the validation data is slightly larger than the RMSE of the calibration data. A possible explanation for this difference is that only the validation data contain congested traffic and that the model has been slightly overfitted to uncongested traffic. For the Duisburg dataset, there is no significant difference between the two RMSE values because both parts of the trajectory data contain congested traffic.

Table 6.7 shows the calibrated parameters of the car-following model based on desired headways. The values of T_{des} are similar to the values of T_{des} for the followers of mergers and they are larger than the values of T_{des} for the mergers. This difference shows that mergers intend to increase their headway after the merge when they approach regular car-following behavior. Thus, the model implicitly accounts for relaxation.

In general, the calibration results show that the microscopic calibration methodology, which is established for car-following models, is also applicable to lane change models. Nevertheless, it is important that the trajectory data used for calibration contain congested traffic conditions in order to obtain reasonable parameter values that are also valid for these conditions.

6.5.2 Sensitivity Analysis

To analyze how the choice of the parameter values affects the error of the calibration, we conduct a sensitivity analysis in which we vary the calibrated parameter values by $+10$ and -10% and compare the resulting prediction errors with the prediction error of the calibrated parameters. Ideally, the prediction error should increase in both directions if the parameters are successfully calibrated.

Table 6.8 shows that the errors change by less than 1% in most cases, which indicates that the calibration methodology is robust. This finding is particularly relevant for the practical application of the model in traffic simulations, in which it is not always feasible to thoroughly calibrate the parameters. In some cases, the error decreases if the calibrated value is varied. This occurs either if the varied value is outside the defined bounds or if the optimization algorithm converges to a solution slightly off the global minimum. Which parameter is the most sensitive depends on the model and on the dataset. Overall, a_{min} and Δx_{min} are the least sensitive parameters, and T_{des} and τ_{LC} are the most sensitive parameters.

Parameter		Duisburg dataset		Cologne dataset	
		RMSE change for calibrated value + 10%	**RMSE change for calibrated value -10%**	**RMSE change for calibrated value + 10%**	**RMSE change for calibrated value -10%**
Merger	Maximum acceleration a_{max}	$+0.26\%$	-0.35%*	$+5.94\%$	-5.46%*
	Minimum acceleration a_{min}	-0.01%	-0.02%	0.00%*	0.00%
	Minimum distance at standstill Δx_{min}	-0.15%	-0.05%	-0.21%*	-0.37%
	Desired headway T_{des}	$+1.55\%$	$+2.14\%$	-0.07%	$+0.58\%$
	Lane change duration τ_{LC}	$+1.68\%$*	$+6.54\%$	-4.66%*	$+3.28\%$
	Minimum DRAC to start lane change $DRAC_{min}$	0.00%*	0.00%	$+3.94\%$	0.00%*
Followers of mergers	Maximum acceleration a_{max}	$+0.21\%$	-0.25%*	$+1.75\%$	-2.22%*
	Minimum acceleration a_{min}	$+0.82\%$	-0.21%*	0.00%	0.00%
	Minimum distance at standstill Δx_{min}	$+0.10\%$	-0.04%*	$+0.07\%$	-0.04%*
	Desired headway T_{des}	$+1.46\%$	$+1.36\%$	$+0.75\%$	$+0.60\%$
Car-following	Maximum acceleration a_{max}	$+0.47\%$	-0.46%*	$+0.12\%$	$+0.16\%$
	Minimum acceleration a_{min}	$+0.01\%$	**	$+0.40\%$	**
	Minimum distance at standstill Δx_{min}	$+0.07\%$	-0.04%*	$+0.29\%$	-0.25%*
	Desired headway T_{des}	$+2.34\%$	**	$+6.11\%$	**

Table 6.8: Sensitivity analysis of the calibrated model parameters.

*The value lies outside the bounds for this parameter.

**Model becomes numerically unstable with these parameter values.

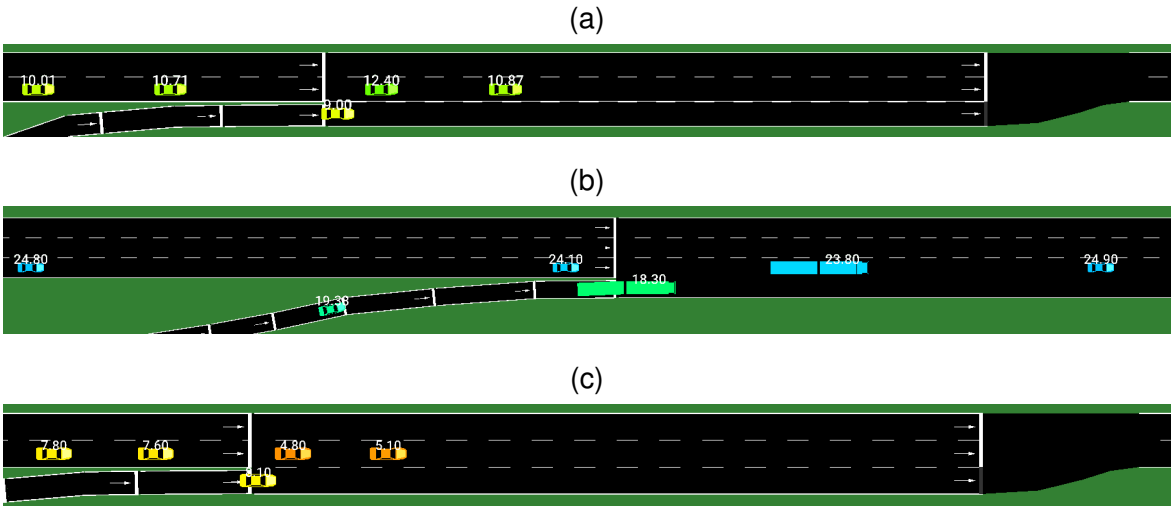

Figure 6.6: Example cases for merging at on-ramps. The color of the vehicles and the numbers above the vehicles indicate the current speed of the vehicles. (a) Case 1: merger is slower than main lane traffic and selects the current leader, (b) Case 2: merger is slower than main lane traffic and is passed, (c) Case 3: merger is faster than main lane traffic and passes.

6.5.3 Example Cases

To understand the behavior of the lane change model and to analyze its strengths and limitations, we extract three example cases from the trajectory data that represent typical merging situations:

1. Merger is slower than main lane traffic and selects the current leader
2. Merger is slower than main lane traffic and is passed
3. Merger is faster than main lane traffic and passes

Figure 6.6 and Table 6.9 show the positions and speeds of the merger and the three closest potential leaders and followers in the moment when the merger is at the start of the on-ramp. Table 6.9 also shows the results of the model in the three example cases.

Case	x_M	v_M	x_L	v_L	x_F	v_F	a_M	$a_{M,Fol.}$	Δa	τ_E	τ_{Pass}	x_M after pass	x_L after pass	x_F after pass	Passing possible	Selected leader
			282.5	10.7	262.0	10.0	-0.47	-0.09	-0.38	14.6	8.6	368.7	375.0	348.4	No	
1	308.6	9.0	315.4	12.4	282.5	10.7	0.45	0.13	0.31	10.5	-	-	-	-	-	Yes
			334.6	10.9	315.4	12.4	0.53	1.08	-0.55	10.2	4.2	350.5	379.8	366.9	No	
			103.5	24.1	2.5	24.8	0.18	0.16	0.01	13.2	7.2	259.0	277.5	182.1	No	
2	121.7	18.3	158.2	23.8	103.5	24.1	0.85	1.04	-0.19	11.5	5.5	-	-	-	-	Yes
			204.5	24.9	158.2	23.8	1.0	2.09	-1.10	11.2	5.2	230.0	333.7	281.2	No	
			293.1	7.6	278.7	7.8	-0.33	-0.09	-0.24	19.0	13.0	384.6	391.6	380.7	No	
3	307.6	8.1	312.5	4.8	293.1	7.6	-0.35	-0.06	-0.29	25.3	-	-	-	-	-	Yes
			325.9	5.1	312.5	4.8	-0.29	-0.21	-0.08	21.6	15.6	398.4	405.4	388.0	No	

Table 6.9: Initial conditions and results of the lane change model for the three example cases (see Figure 6.6).

In Case 1, the model predicts correctly that the merger selects the current leader because the merger cannot pass and cannot be passed (see Table 6.9). If the merger decided to be passed, it would have to decelerate with $a_M = -0.47m/s^2$ according to the model, and it would take $\tau_E = 14.6s$ to reach the end of the on-ramp ($x_E = 409m$). Since the lane change takes $\tau_{LC} = 6.0s$, the available time to be passed is $\tau_{Pass} = 8.6s$. After this time, the merger reaches $x_M = 368.7m$. Within the same time, the potential leader reaches $x_L = 375.0m$, so the gross gap is $6.3m$. Since both vehicles are approximately $5m$ long, the net gap between merger and potential leader is smaller than the minimum gap of $\Delta x_{min} = 2.48m$ (Duisburg dataset, see Table 6.5). This means the merger cannot be passed. If the merger decided to pass, it would have to accelerate with $a_M = 0.53m/s^2$. The merger would then reach $x_M = 350.5m$ within the available time to pass ($\tau_{Pass} = 4.2s$). However, the potential follower is still in front of the merger ($x_F = 366.9m$) after this time. This means the merger cannot pass either. As a result, the model predicts that the merger selects the current gap. Even if passing or being passed were possible, the merger would still select the current gap because it is the gap with the largest difference Δa between the required acceleration to stay behind the leader (a_M) and the required acceleration to stay in front of the follower ($a_{M,Fol}$).

Figure 6.7 (left) shows the predicted trajectory and the observed trajectory of the merger, leader, and follower in Case 1 during the whole merging process. It is evident that the calibrated value for the desired headway ($T_{des} = 0.80s$) is smaller than the observed desired headway, which results in a deviation in the longitudinal direction ($RMSE_X = 5.49m$). Since the model assumes the same parameter values for each driver, this deviation is inevitable. The lateral position, however, can be predicted very accurately in this example case ($RMSE_Y = 0.30m$). Furthermore, it is worth noting that both the predicted and the observed acceleration of the merger change along the on-ramp. If the assumption that the vehicles in the main lane maintain their speed was valid, the model would predict a constant acceleration along the on-ramp. However, both the leader and the follower continuously adapt their speed depending on their own leaders. As a result, the acceleration of the merger also adapts. The model is able to reflect this continuous adaptation.

In Case 2, the merger is very close to the current follower at the start of the on-ramp (see Figure 6.6(b)). Due to the speed difference to the current follower, the merger is not able to stay in the current gap. Instead, the current follower passes the merger and becomes its leader. According to the model, however, the merger cannot be passed within $\tau_{Pass} = 8.6s$ because the gross gap between merger and potential leader ($x_L - x_M = 18.5m$) is too small given the length of the merger (ca. $18m$) and the minimum gap ($\Delta x_{min} = 7.0m$ for the Cologne dataset) (see Table 6.9). The model instead predicts that the merger intends to stay in the current gap and accelerates with $a_M = 0.85m/s^2$. After approximately $4s$, the initial follower

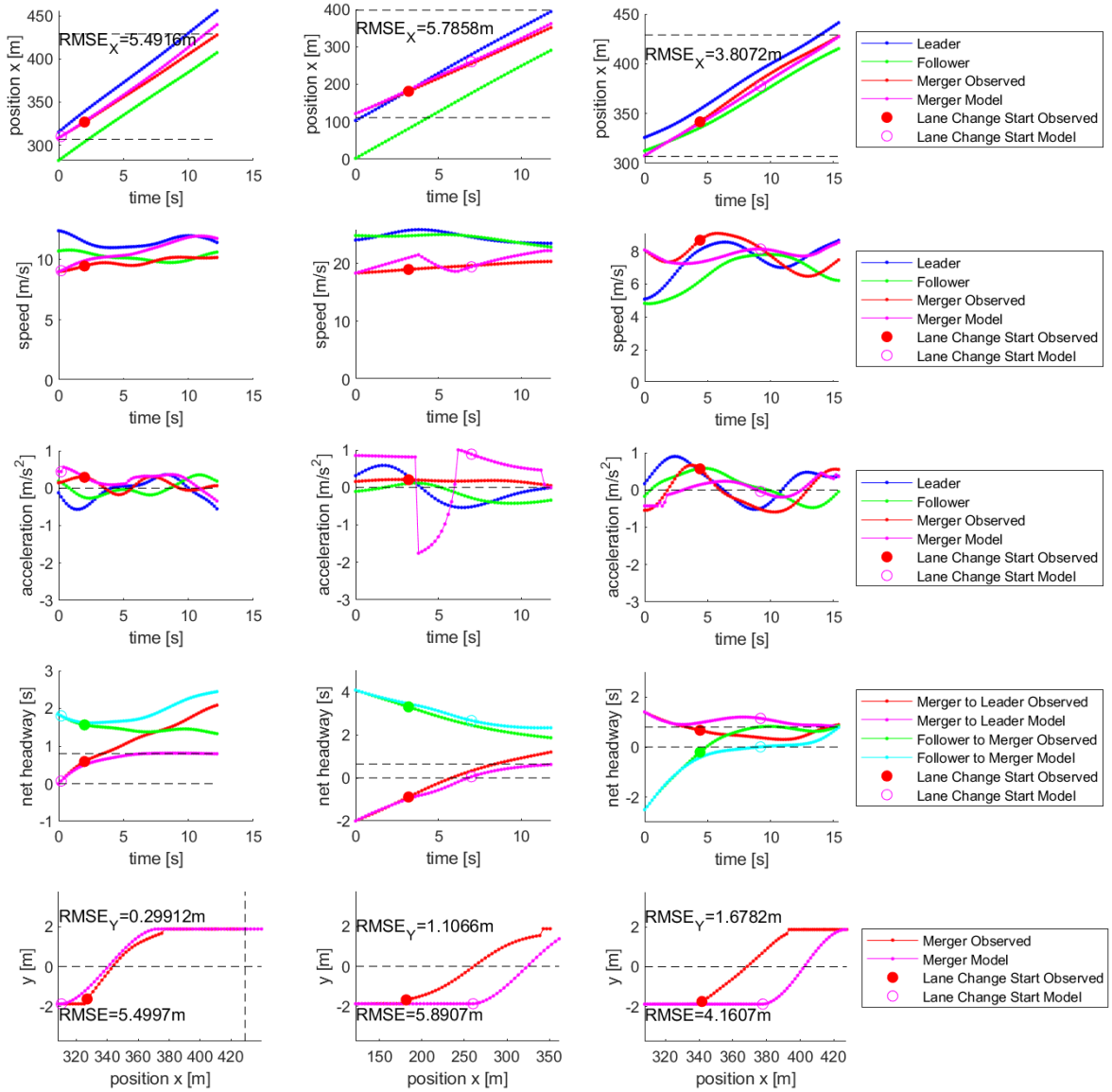

Figure 6.7: Trajectories of merger (observed and predicted by the model), leader, and follower in the three example cases shown in Figure 6.6.

passes the merger, which means that the current gap changes (see Figure 6.7 center). At this moment, the model predicts that the merger must stay in the new current gap. To stay behind the new leader, the merger must decelerate according to the model. This example shows that the model is able to correct its initially incorrect decision. However, this correction results in a sudden acceleration change. The RMSE in longitudinal direction ($RMSE_X = 5.79m$) is in the same order of magnitude as in the first example case, although the deviation in the acceleration is larger than in the first example case. The RMSE in lateral direction ($RMSE_Y = 1.11m$) is larger than in the first example case because the model predicts a later lane change start. Again, the assumption that the parameter values are the same for each driver affects the prediction accuracy of the model. For example, if Δx_{min} or τ_{LC} were smaller in this example case, the model would predict that the merger can be passed, and the deviation both in longitudinal and in lateral direction would be smaller.

In Case 3, the traffic in the main lane is congested and the merger has a larger initial speed than the traffic in the main lane (see Figure 6.6(c)). As a result, the merger passes its current leader, and the current leader becomes the follower. According to the model, however, passing is not possible because the gross gap between merger and potential leader ($x_L - x_M = 7.0m$) is too small given the lengths of the vehicles (ca. $5m$) and the minimum gap ($\Delta x_{min} = 2.48m$ for the Duisburg dataset) (see Table 6.9). Nevertheless, the merger passes the current leader after approximately $2s$ due to the small absolute value of a_M and the large speed difference between merger and current leader (see Figure 6.7 right). At this moment, the model predicts that the merger must stay in the new current gap. This leads to a discontinuity in the acceleration, but the discontinuity is much smaller than in example case 2. The RMSE in the longitudinal direction ($RMSE_X = 3.81m$) mainly results from the fact that the observed net headway between merger and leader is very small well after the lane change start. This unsafe behavior is not considered in the model. Instead, the model predicts that the net headway between merger and leader converges to the desired headway ($T_{des} = 0.80s$ for the Duisburg dataset) without falling below it. In return, the predicted net headway between merger and follower is smaller. However, it must be noted that we use the observed trajectory of the follower to compute the headway, which means the follower does not react to the modeled trajectory.

The three example cases show that the model has a good capability of predicting the correct leader even if the prediction is wrong at the start of the on-ramp. The reason behind this wrong prediction is the condition that the gap must be non-negative after passing (equations 6.26 and 6.27). This condition is necessary to prevent impossible passing maneuvers, but it also prevents some possible passing maneuvers because it might lead to safer merging behavior than observed in the trajectory data. If only the condition that the selected gap has the largest

difference between a_M and $a_{M,Fol}$ is considered, the model predicts the selected gap correctly in all three example cases. To analyze whether this observation holds for all observed merging maneuvers, we present a more generalized analysis of the leader selection in Section 6.5.4.1.

The three example cases also indicate that the model would make better predictions if other parameter values were used. However, the calibrated parameters are deterministic and represent average driving behavior. For future applications of the model in traffic simulations, stochastic parameters are expected to yield more realistic results.

6.5.4 Validation Results

For the validation results presented in this section, we use the part of the trajectory data presented in Section 6.4.1 that has not been used for calibration, as well as the results of the traffic simulations described in Section 6.4.3.

6.5.4.1 Leader Selection

To analyze how well the lane change model is able to predict which vehicle the merger selects as a leader, we use a confusion matrix (see Table 6.10). The model predicts a leader at every timestep until the lane change start, but the tables contain only the prediction at the start of the on-ramp (Table 6.10 top) and at the start of the lane change (Table 6.10 bottom). Table 6.10 confirms the observations made in Section 6.5.3 that the model is not always able to predict the selected leader correctly at the start of the on-ramp. Cases in which the merger passes are predicted as “no passing” or rarely as “merger is passed”. Cases in which the merger is passed are predicted correctly in the Cologne dataset, but rarely predicted as “no passing” in the Duisburg dataset. However, the model is always able to predict the selected leader correctly at the moment the lane change starts. This result shows that minimizing the RMSE in the longitudinal direction is a suitable approach to calibrate the leader selection component of the model. However, a major limitation of this analysis is that the trajectories of the potential leaders and followers do not adapt to the modeled trajectory of the merger. To overcome this limitation, we also analyze the number of passing mergers and mergers being passed in the simulations and compare these numbers with the trajectory data (see Section 6.5.4.3).

6.5.4.2 Lane Change Position

To validate the component of the model that predicts the lane change start time, we compare the observed and the modeled lane change positions (see Figure 6.8). Since the lane change start is not well defined for the trajectory data, we use the middle of the lane change as a

		Duisburg				**Cologne**		
		Observed				Observed		
Start of on-ramp	Model	Merger is passed	No passing	Merger passes	Model	Merger is passed	No passing	Merger passes
	Merger is passed	4.2%	4.2%	1.0%	Merger is passed	4.0%	—	—
	No passing	1.0%	76.7%	11.5%	No passing	—	88.0%	8.0%
	Merger passes	—	—	—	Merger passes	—	—	—
		Observed				Observed		
Start of lane change	Model	Merger is passed	No passing	Merger passes	Model	Merger is passed	No passing	Merger passes
	Merger is passed	5.2%	—	—	Merger is passed	4.0%	—	—
	No passing	—	82.3%	—	No passing	—	88.0%	—
	Merger passes	—	—	12.5%	Merger passes	—	—	8.0%

Table 6.10: Confusion matrix of the leader selection model. (Left column) Duisburg Dataset, (Right column) Cologne Dataset, (top) observed leader selection vs leader selection predicted at the start of the on-ramp, (bottom) observed leader selection vs leader selection predicted at the start of the lane change

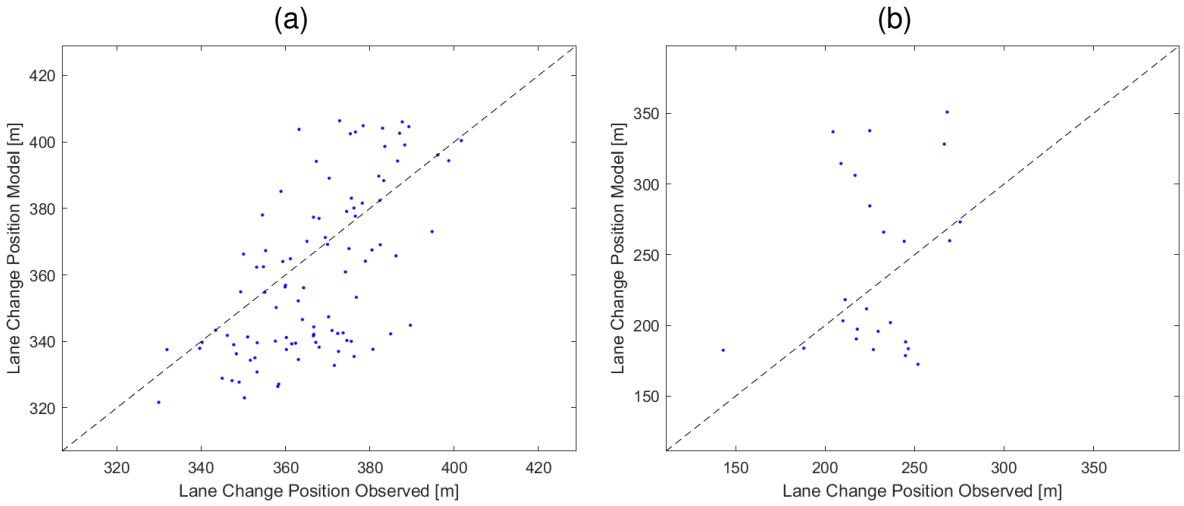

Figure 6.8: Comparison of the observed and modeled lane change positions. (a) Duisburg dataset, (b) Cologne dataset.

reference, that is, the moment when the center of the vehicle crosses the marking between on-ramp and main lane. Figure 6.8 shows that there is a good agreement between the observed and modeled lane change positions in the Duisburg dataset, while there is no clear correlation in the Cologne dataset.

Figure 6.8(b) indicates that the modeled lane change positions fall into two clusters, one cluster around $x \approx 200$ and the other cluster at $x > 260$. The reason for this behavior is that the merger can start the lane change in one of two cases. The first case is that the time until the end of the on-ramp equals the lane change duration ($\tau_E = \tau_{LC}$). These lane changes occur mostly toward the end of the on-ramp ($x > 260$). The second case is that it is safe to start the lane change earlier ($DRAC \leq DRAC_{min}$). Since the traffic density is low in the Cologne dataset, this condition is often fulfilled when mergers are at the start of the on-ramp, which leads to the cluster around $x \approx 200$. The observed lane change positions, however, are mostly between $x = 200$ and $x = 270$, which is between the two clusters. The most likely explanation for this deviation is the large length of the on-ramp in Cologne. Due to the length, mergers do not start the lane change early even it would be safe to do so. Instead, they remain on the on-ramp longer and reduce the speed difference to the vehicles in the main lane before they start the lane change. To reflect this behavior in the model, $DRAC_{min}$ would have to vary along the on-ramp so that mergers accept a larger accident risk toward the end of the on-ramp. However, this adaptation would increase the complexity of the model.

Selected gap	Duisburg		Cologne	
	Simulation	**Observed**	**Simulation**	**Observed**
Merger is passed	4 (1.5%)	8 (3.1%)	10 (1.7%)	13 (2.2%)
No passing	164 (62.1%)	198 (75.9%)	576 (97.0%)	555 (95.5%)
Merger passes	96 (36.4%)	55 (21.1%)	8 (1.3%)	13 (2.2%)

Table 6.11: Comparison between simulation and observed trajectory data with respect to passing maneuvers.

6.5.4.3 Microscopic Simulation Results

So far, we have compared observed trajectories with the corresponding modeled trajectories. While this approach is important to evaluate the model microscopically, it has several important limitations. One major reason for deviations between observed and modeled trajectories is the assumption that all drivers share the same model parameters. Another reason is the assumption that the follower of the merger does not adapt to the modeled trajectory of the merger. Furthermore, the behavior of the model cannot be analyzed in situations that are not included in the data. A traffic simulation can give insights into whether these limitations are relevant.

First, we analyze the number of mergers who pass or are passed by vehicles in the main lane. In the simulation, the follower of the merger adapts to the merger, which addresses one of the mentioned limitations. Table 6.11 shows that there is a good agreement between simulation and trajectory data for the Cologne dataset. There are slightly less passing maneuvers in the simulation than in reality, although the total number of passing maneuvers is small. The simulation of the Duisburg dataset contains considerably more situations where the merger passes vehicles in the main lane than the trajectory data. Whether the merger decides to pass depends mainly on the speed difference to the vehicles in the main lane. In the Duisburg dataset, the mean speed in the main lane is small, which means that mergers are usually faster than vehicles in the main lane when they enter the on-ramp. In reality, it can be observed that mergers already adapt to the speed in the main lane before they enter the on-ramp. This early adaptation cannot be fully captured in the simulation. As a result, the speed difference in the simulation is often larger than in reality, which leads to more mergers passing vehicles in the main lane. A possible solution to overcome this limitation is to analyze the speed of the mergers before the on-ramp to identify the location where the mergers start to adapt to vehicles in the main lane.

Another important aspect of the merging behavior is the headway between the merger and

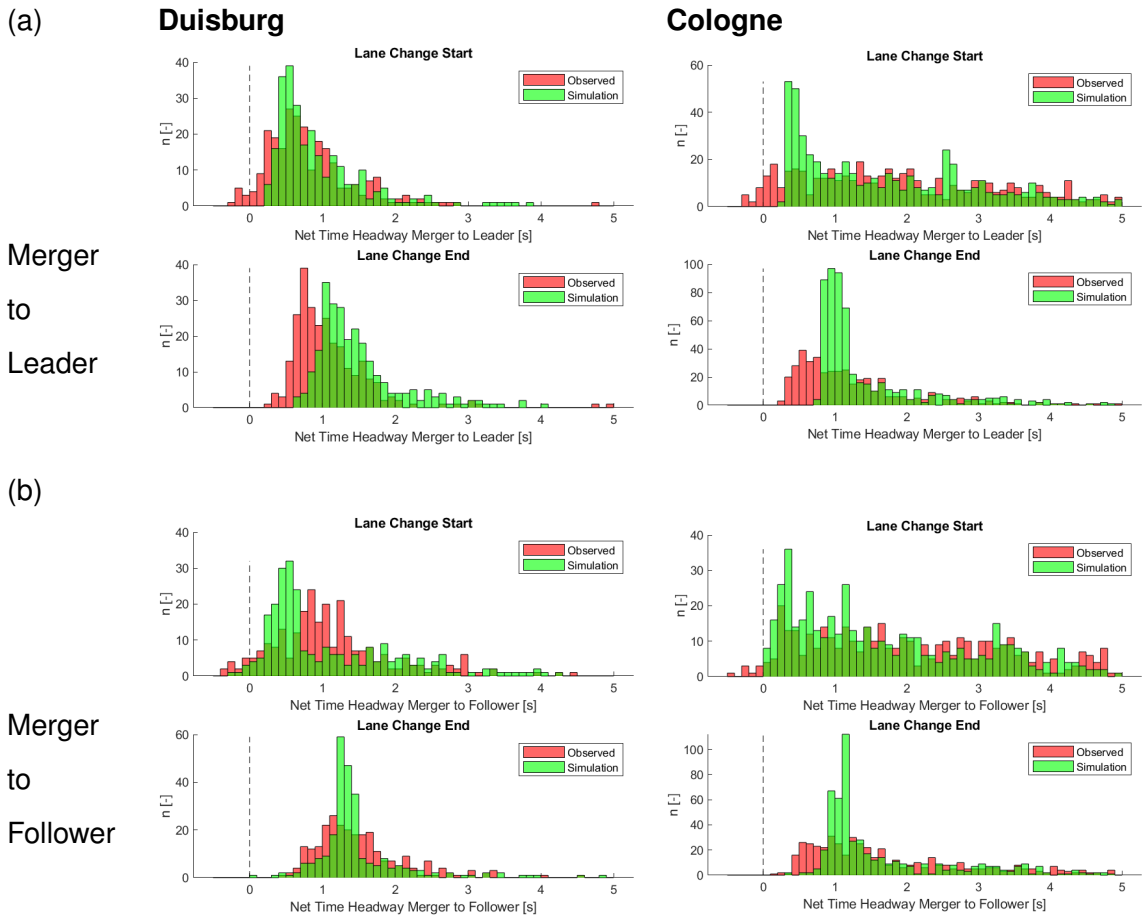

Figure 6.9: Distributions of headways at the start and at the end of the lane change. (a) Headway between merger and leader, (b) headway between merger and follower, (left) Duisburg dataset, (right) Cologne dataset.

the leader, which is controlled by the merger, and the headway between the merger and the follower, which is controlled by the follower. The most important difference between simulation and observation is that there are almost no negative headways at the start of the lane change in the simulation (see Figure 6.9). Negative headways are not inherently unsafe because the vehicles are not in the same lane yet and the headway usually increases after the lane change starts due to the speed difference between the two vehicles. Nevertheless, the model does not reproduce this risky behavior. To reflect this behavior, the model could be adapted by decreasing the lower bound of Δx_{min} to negative values, which would allow risky lane changes that start with negative gaps.

At the end of the lane change, there are some small headways in the data, which the model does not reproduce. As a result, the peak in the distribution in the simulation is at larger

headways. Since the model assumes the same value of T_{des} for all mergers, the variation of the headway at the lane change end is smaller than in reality. A more realistic distribution of net headways could be achieved by using stochastic values of T_{des}. Nevertheless, this deterministic model generates varying headways due to the varying boundary conditions, in particular speed changes of the leader during the merging process. Apart from these mentioned differences, the model is able to reproduce the headway distributions well.

The third aspect of merging behavior is the speed difference between merger and the vehicles in the main lane. In the trajectory data of the Duisburg dataset, most mergers are slightly slower than the leader, but slightly faster than the follower (see Figure 6.10(a)). This tendency is also visible in the simulation, although larger (absolute) speed differences occur more often. Together with the headway distributions, these results indicate that real drivers temporarily accept small headways if the (absolute) speed difference is small, while the model aims for larger headways, which can only be reached if the (absolute) speed difference temporarily increases.

For the Cologne dataset, the deviation between simulation and observation is smaller (see Figure 6.10(b)). While the simulation yields a larger variation of speed differences between merger and leader at the end of the lane change compared to the trajectory data, the opposite is true for the speed differences between merger and follower at the start of the lane change. These results must be interpreted cautiously due to the different lane change positions (see Section 6.5.4.2).

6.5.4.4 Macroscopic Simulation Results

The microscopic evaluations presented so far do not give insights whether the model is able to describe traffic flow at the macroscopic scale. To evaluate the capability to reproduce the formation and propagation of congestion waves, we compare the speeds in the main lane as a function of time and position (see Figure 6.11). Since there is only a short period of congestion in the Cologne dataset, only the Duisburg dataset is analyzed. In both speed contour plots in Figure 6.11, it is evident that the on-ramp acts as a bottleneck, which means that there are lower speeds before the on-ramp ($x < 300$) than behind the on-ramp ($x > 430$). Thus, the lane change model accurately describes the traffic flow characteristics of the on-ramp. However, the speeds in the simulation before and behind the on-ramp are slightly higher than in the data. This indicates that the car-following model overestimates the capacity of the freeway, which leads to less congestion. A possible explanation for these results could be the calibration methodology, in which we excluded a large proportion of the trajectories, mainly due to lane changes. It is conceivable that the trajectories used for calibration are not

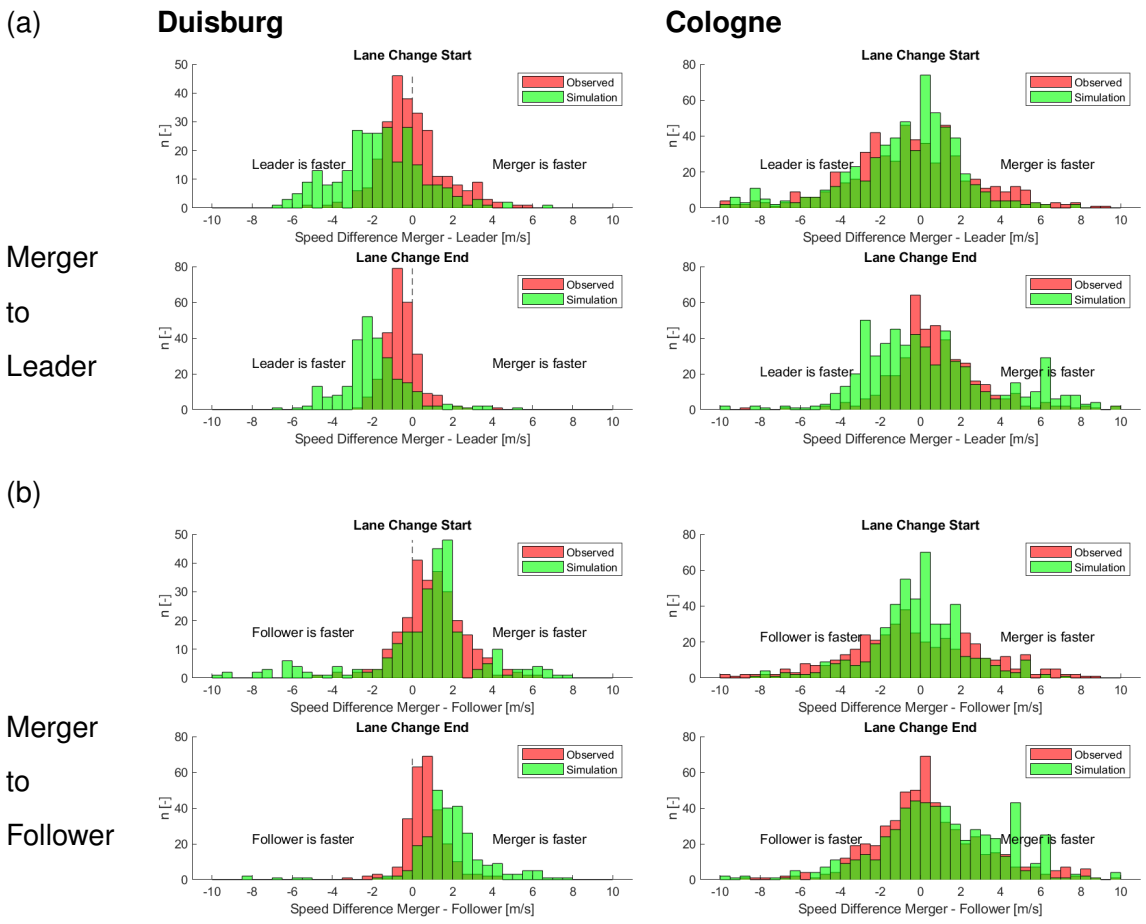

Figure 6.10: Distribution of speed differences at the start and at the end of the lane change. (a) Speed difference between merger and leader, (b) speed difference between merger and follower, (left) Duisburg dataset, (right) Cologne dataset.

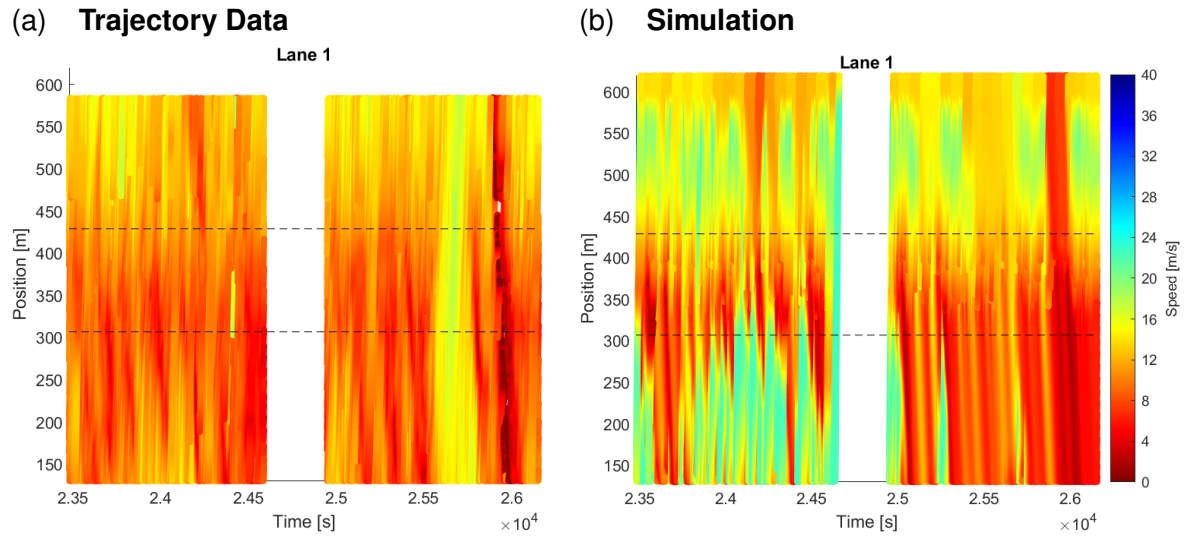

Figure 6.11: Speed contour plots for the main lane of the Duisburg dataset. (a) Trajectory data, (b) simulation. The dashed horizontal lines represent the start and end of the on-ramp.

representative in terms of the car-following behavior. To represent the car-following behavior around the on-ramp better, a macroscopic calibration might be more suitable.

Figure 6.12 shows that the speed–density relationships of the main lane and the on-ramp can be reproduced accurately in the simulation. Only the few data points in the Cologne dataset with small speeds cannot be found in the simulation. The reason behind this is again that the capacity of the car-following model is overestimated. As a result, the congestion that originates from a bottleneck downstream does not propagate realistically. Nevertheless, the speed–density relationships show that the lane change model can represent the traffic flow at the on-ramp well.

6.6 Conclusions

In this paper, we presented a lane change model for freeway on-ramps derived from a car-following model based on desired time headways. The model consists of three submodels, one for merging vehicles, one for the followers of merging vehicles, and one for all remaining vehicles with regular car-following behavior. The trajectory-based calibration methodology was adopted from car-following models as well. The seven parameters of the model have an intuitive meaning, which enables an evaluation of the calibrated parameter values. The

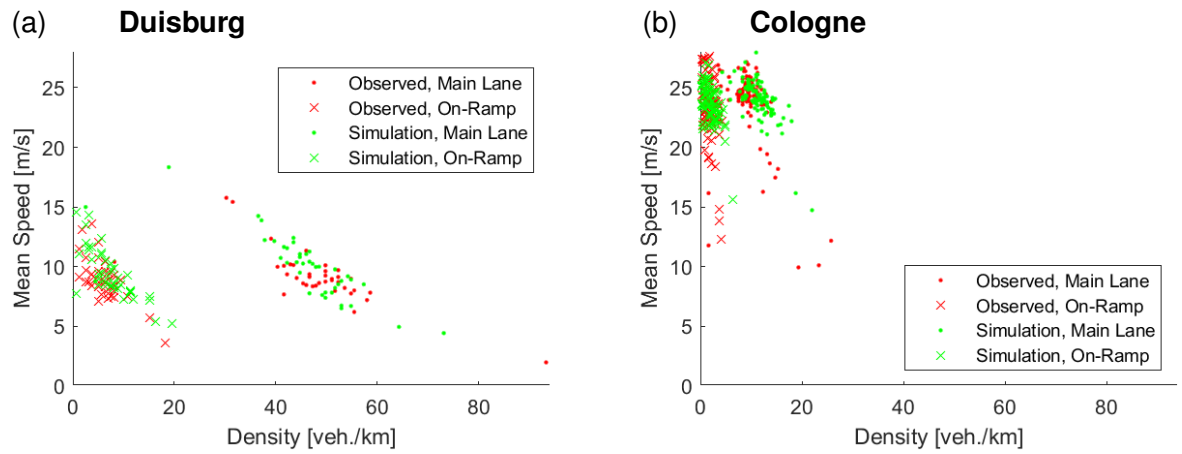

Figure 6.12: Speed–density relationship of main lane and on-ramp for the Duisburg dataset (a) and the Cologne dataset (b).

calibration results indicate that the parameter values are plausible and that the model predicts the trajectory of mergers with an RMSE of $3.6m$ in the dataset with congested traffic and a short on-ramp and $5.5m$ in the dataset with free-flow traffic and a longer on-ramp. The RMSE for the trajectory of the followers of mergers is in the same order of magnitude. The sensitivity analysis shows that parameter variation causes only a small increase in RMSE, indicating that the calibration is robust. A detailed analysis of three typical cases (merger selects current leader, merger is passed, and merger passes) demonstrates that, despite the small number of parameters, the model can accurately represent the longitudinal driver behavior of mergers and their followers in the main lane, as well as the decision of the merger to pass or be passed. The lateral driver behavior, mainly the positions of the lane changes, can be described well only for the location with a short on-ramp and with congested traffic. In microscopic simulations, the number of mergers passing a vehicle in the main lane is slightly overestimated, which likely results from mergers adapting their speed to traffic in the main lane before the on-ramp—a behavior not fully captured in the simulation. The distribution of net time headways and speed differences is accurately represented in the simulation, except in cases involving risky behavior with very small headways at the start of the lane change. The lane change model makes good predictions also at the macroscopic scale in terms of the speed–density relationships and the role of the on-ramp as a bottleneck. However, the results indicate that the car-following model overestimates the capacity of the freeway before and behind the on-ramp, which impairs the capability of the model to reproduce the propagation of congestion. The main goal of the novel car-following model presented in this paper was to apply it to the car-following behavior of merging vehicles and their followers. Further research

is required to improve the car-following model for regular car-following behavior.

For the validation of the model, a deterministic approach with the same parameter values for all drivers was used. Stochastic parameter values could further improve the results, in particular the headway distributions. However, a stochastic approach would require a more complex calibration methodology in order to identify the best parameter values for each individual driver.

With the three submodels, a complete traffic simulation of an on-ramp can be run, with the exception of desired and courtesy lane changes. Further research is recommended to evaluate whether the lane change model can be extended to these types of lane changes. We assume that the main concept of our lane change model, which is that the lane changing vehicle has two leaders and that it gradually reaches the desired headway after some time, is also applicable for desired and courtesy lane changes.

The validation results have shown that the model is suitable to assess on-ramps in terms of traffic flow. For example, the effect of the length of the on-ramp and the effect of different traffic volumes and different truck ratios can be analyzed. Whether the model is also able to assess on-ramps in terms of traffic safety, that is, the question whether the simulation yields a similar amount and similar spatial distribution of conflicts, is also a topic for further research. Since the model contains a SSM as a parameter, we expect that the model can also be optimized for traffic safety in addition to traffic flow in future research.

The model can also be used to assess traffic management measures related to on-ramps, for example, ramp metering. While current ramp-metering algorithms are mostly based on macroscopic parameters, our lane change model could be used to develop a microscopic ramp-metering algorithm.

While our model primarily describes human driving behavior, it also holds relevance in the context of connected and automated vehicles. Recent research explores how automated vehicles interact with human-driven vehicles, and which implications this mixed traffic has for both traffic flow and safety. To make valid predictions, models that capture the driving behavior of both humans and automated vehicles are essential.

Acknowledgments

The authors would like to thank Eszter Kalló, Michael Herty, and Niklas Kolbe from RWTH Aachen University for the valuable discussions throughout the project. The authors would also like to thank Mohamed Kastouri from RWTH Aachen University for his dedication in preparing and providing the trajectory data.

References

[1] V. Knoop. *Introduction to Traffic Flow Theory*. Delft University of Technology, 2nd edition edition, 2018.

[2] J. Erdmann. SUMO's Lane-Changing Model. 2015. URL `https://elib.dlr.de/102254/1/Springer-SUMOs_Lane_changing_model.pdf`.

[3] Z. Zheng. Recent developments and research needs in modeling lane changing. *Transportation Research Part B: Methodological*, 60(8):16–32, 2014. ISSN 01912615. doi: 10.1016/j.trb.2013.11.009.

[4] W. J. Schakel, V. L. Knoop, and B. van Arem. Integrated Lane Change Model with Relaxation and Synchronization. *Transportation Research Record: Journal of the Transportation Research Board*, 2316(1):47–57, 2012. ISSN 0361-1981. doi: 10.3141/2316-06.

[5] J. A. Laval and L. Leclercq. Microscopic modeling of the relaxation phenomenon using a macroscopic lane-changing model. *Transportation Research Part B: Methodological*, 42 (6):511–522, 2008. ISSN 01912615. doi: 10.1016/j.trb.2007.10.004.

[6] H. Kita. A merging–giveway interaction model of cars in a merging section: a game theoretic analysis. *Transportation Research Part A: Policy and Practice*, 33(3-4):305–312, 1999. ISSN 09658564. doi: 10.1016/S0965-8564(98)00039-1.

[7] J. Wang, R. Liu, and F. Montgomery. A Simulation Model for Motorway Merging Behaviour. In *Transportation and traffic theory*, pages 281–302. Elsevier, Amsterdam and Boston, 2005. ISBN 0080446809.

[8] A. van Beinum, E. Broekman, H. Farah, W. Schakel, F. Wegman, and S. Hoogendoorn. Critical Assessment of Microscopic Simulation Models for Simulating Turbulence around Motorway Ramps. *Journal of Transportation Engineering, Part A: Systems*, 146(2):501, 2020. ISSN 2473-2907. doi: 10.1061/JTEPBS.0000296.

[9] D. Chen and S. Ahn. Capacity-drop at extended bottlenecks: Merge, diverge, and weave. *Transportation Research Part B: Methodological*, 108:1–20, 2018. ISSN 01912615. doi: 10.1016/j.trb.2017.12.006.

[10] K. Chen, Z. Li, P. Liu, V. L. Knoop, Y. Han, and Y. Jiao. Evaluating the safety and efficiency impacts of forced lane change with negative gaps based on empirical vehicle trajectories. *Accident; analysis and prevention*, 203:107622, 2024. doi: 10.1016/j.aap.2024.107622.

[11] A. Kesting, M. Treiber, and D. Helbing. General Lane-Changing Model MOBIL for Car-Following Models. *Transportation Research Record: Journal of the Transportation Research Board*, 1999(1):86–94, 2007. ISSN 0361-1981. doi: 10.3141/1999-10.

[12] A. Kondyli and L. Elefteriadou. Modeling Driver Behavior at Freeway–Ramp Merges. *Transportation Research Record: Journal of the Transportation Research Board*, 2249 (1):29–37, 2011. ISSN 0361-1981. doi: 10.3141/2249-05.

[13] F. Marczak, W. Daamen, and C. Buisson. Merging behaviour: Empirical comparison between two sites and new theory development. *Transportation Research Part C: Emerging Technologies*, 36(4):530–546, 2013. ISSN 0968090X. doi: 10.1016/j.trc.2013.07.007.

[14] C. Ng, S. Susilawati, M. A. S. Kamal, and I. M. L. Chew. Development of a binary logistic lane change model and its validation using empirical freeway data. *Transportmetrica B: Transport Dynamics*, 8(1):49–71, 2020. ISSN 2168-0566. doi: 10.1080/21680566.2020.1715309.

[15] K. Kang and H. A. Rakha. Game Theoretical Approach to Model Decision Making for Merging Maneuvers at Freeway On-Ramps. *Transportation Research Record: Journal of the Transportation Research Board*, 2623(1):19–28, 2017. ISSN 0361-1981. doi: 10.3141/2623-03.

[16] C. F. Choudhury. *Modeling Driving Decisions with Latent Plans: Dissertation*. 2007.

[17] R. Delpiano, J. C. Herrera, J. Laval, and J. E. Coeymans. A two-dimensional car-following model for two-dimensional traffic flow problems. *Transportation Research Part C: Emerging Technologies*, 114:504–516, 2020. ISSN 0968090X. doi: 10.1016/j.trc.2020.02.025.

[18] W. Schakel, V. Knoop, M. Keyvan-Ekbatani, and H. van Lint. *Social Interactions on Multi-Lane Motorways: Towards a Theory of Impacts*. 2023. doi: 10.20944/preprints202305.0193.v1.

[19] C. Dong, H. Wang, Y. Li, X. Shi, D. Ni, and W. Wang. Application of machine learning algorithms in lane-changing model for intelligent vehicles exiting to off-ramp. *Transportmetrica A: Transport Science*, 17(1):124–150, 2021. ISSN 2324-9935. doi: 10.1080/23249935.2020.1746861.

[20] S. Mozaffari, M. A. Sormoli, K. Koufos, and M. Dianati. Multimodal Manoeuvre and Trajectory Prediction for Automated Driving on Highways Using Transformer Networks. *IEEE Robotics and Automation Letters*, 8(10):6123–6130, 2023. doi: 10.1109/LRA.2023.3301720.

[21] X. Wan, P. J. Jin, F. Yang, J. Zhang, and B. Ran. Modeling Vehicle Interactions during Merge in Congested Weaving Section of Freeway Ramp. *Transportation Research Record: Journal of the Transportation Research Board*, 2421(1):82–92, 2014. ISSN 0361-1981. doi: 10.3141/2421-10.

[22] G. Bham. A simple lane change model for microscopic traffic flow simulation in weaving sections. *Transportation Letters*, 3(4):231–251, 2011. ISSN 1942-7867. doi: 10.3328/TL.2011.03.04.231-251.

[23] M. Treiber and A. Kesting. Microscopic Calibration and Validation of Car-Following Models – A Systematic Approach. *Procedia - Social and Behavioral Sciences*, 80:922–939, 2013. ISSN 18770428. doi: 10.1016/j.sbspro.2013.05.050.

[24] M. Berghaus, E. Kallo, and M. Oeser. Car-Following Model Calibration Based on Driving Simulator Data to Study Driver Characteristics and to Investigate Model Validity in Extreme Traffic Situations. *Transportation Research Record: Journal of the Transportation Research Board*, 2675(12):1214–1232, 2021. ISSN 0361-1981. doi: 10.1177/03611981211032650.

[25] P. Hidas. Modelling lane changing and merging in microscopic traffic simulation. *Transportation Research Part C: Emerging Technologies*, 10(5-6):351–371, 2002. ISSN 0968090X. doi: 10.1016/S0968-090X(02)00026-8.

[26] A. van Beinum, H. Farah, F. Wegman, and S. Hoogendoorn. Driving behaviour at motorway ramps and weaving segments based on empirical trajectory data. *Transportation Research Part C: Emerging Technologies*, 92:426–441, 2018. ISSN 0968090X. doi: 10.1016/j.trc.2018.05.018.

[27] C. M. Weyland, M. V. Baumann, H. S. Buck, and P. Vortisch. Parameters Influencing Lane Flow Distribution on Multilane Freeways in PTV Vissim. *Procedia Computer Science*, 184 (1):453–460, 2021. ISSN 18770509. doi: 10.1016/j.procs.2021.03.057.

[28] W. Daamen, M. Loot, and S. P. Hoogendoorn. Empirical Analysis of Merging Behavior at Freeway On-Ramp. *Transportation Research Record: Journal of the Transportation Research Board*, 2188(1):108–118, 2010. ISSN 0361-1981. doi: 10.3141/2188-12.

[29] A. van Beinum, M. Hovenga, V. Knoop, H. Farah, F. Wegman, and S. Hoogendoorn. Macroscopic traffic flow changes around ramps. *Transportmetrica A: Transport Science*, 14(7):598–614, 2018. ISSN 2324-9935. doi: 10.1080/23249935.2017.1415997.

[30] M. A. Arman and C. M. J. Tampère. Empirical Study of Lane-Changing Maneuvers in a Weaving Area Based on Reconstructed Trajectories of Floating Car Data. *Transportation Research Record: Journal of the Transportation Research Board*, 303:30, 2023. ISSN 0361-1981. doi: 10.1177/03611981231179474.

[31] X. Chen, G. Qin, T. Seo, Y. Tian, and J. Sun. A Macro-Micro Approach to Reconstructing Vehicle Trajectories on Multi-Lane Freeways with Lane Changing.

[32] M. Treiber and D. Helbing. Reconstructing the Spatio-Temporal Traffic Dynamics from Stationary Detector Data. *Cooper@tive Tr@nsport@tion Dyn@mics*, 1:3.1–3.24, 2002.

[33] L. Klitzke, K. Gimm, C. Koch, and F. Koster. Extraction and Analysis of Highway On-Ramp Merging Scenarios from Naturalistic Trajectory Data. pages 654–660, 2022. doi: 10.1109/ITSC55140.2022.9922191.

[34] T. Toledo and D. Zohar. Modeling Duration of Lane Changes. *Transportation Research Record: Journal of the Transportation Research Board*, 1999(1):71–78, 2007. ISSN 0361-1981. doi: 10.3141/1999-08.

[35] E. Balal, R. L. Cheu, T. Gyan-Sarkodie, and J. Miramontes. Analysis of Discretionary Lane Changing Parameters on Freeways. *International Journal of Transportation Science and Technology*, 3(3):277–296, 2014. ISSN 20460430. doi: 10.1260/2046-0430.3.3.277.

[36] M. Treiber, A. Hennecke, and D. Helbing. Congested traffic states in empirical observations and microscopic simulations. *Physical review. E, Statistical physics, plasmas, fluids, and related interdisciplinary topics*, 62(2 Pt A):1805–1824, 2000. ISSN 1063-651X. doi: 10.1103/PhysRevE.62.1805.

[37] C. Fu and T. Sayed. Comparison of threshold determination methods for the deceleration rate to avoid a crash (DRAC)-based crash estimation. *Accident; analysis and prevention*, 153:106051, 2021. doi: 10.1016/j.aap.2021.106051.

[38] M. Berghaus, S. Lamberty, J. Ehlers, E. Kalló, and M. Oeser. Vehicle trajectory dataset from drone videos including off-ramp and congested traffic – Analysis of data quality, traffic flow, and accident risk. *Communications in Transportation Research*, 4:100133, 2024. doi: 10.1016/j.commtr.2024.100133.

[39] T. Moers, L. Vater, R. Krajewski, J. Bock, A. Zlocki, and L. Eckstein. The exiD Dataset: A Real-World Trajectory Dataset of Highly Interactive Highway Scenarios in Germany. In *2022 IEEE Intelligent Vehicles Symposium (IV)*, pages 958–964. IEEE, 04.-09.06.2022. ISBN 978-1-6654-8821-1. doi: 10.1109/IV51971.2022.9827305.

[40] P. A. Lopez, E. Wiessner, M. Behrisch, L. Bieker-Walz, J. Erdmann, Y.-P. Flotterod, R. Hilbrich, L. Lucken, J. Rummel, and P. Wagner. Microscopic Traffic Simulation using SUMO. In *2018 21st International Conference on Intelligent Transportation Systems (ITSC)*, pages 2575–2582. IEEE, 04.11.2018 - 07.11.2018. ISBN 978-1-7281-0321-1. doi: 10.1109/ITSC.2018.8569938.

[41] The MathWorks Inc. MATLAB version: 9.13.0 (R2022b), 2022. URL `https://www.mathworks.com`.

7 Conclusion

The overarching research question of this thesis was how trajectory data from different sources can contribute to a more accurate two-dimensional modeling of driver behavior. To address this, data from multiple sources were utilized, methods for improving data quality were introduced, and different types of traffic flow models were developed, calibrated, and validated.

A driving simulator study demonstrated that existing car-following models are not valid in safety-critical situations. Therefore, future research should focus on improving these models to better capture driver behavior in such scenarios. However, the study also showed that trajectory data from driving simulations are suitable for calibrating car-following models with individual parameter values. This insight can be built upon in future research to better represent traffic flow heterogeneity using stochastic car-following models. Since automated driving is expected to reduce behavioral heterogeneity, these models can help analyze the impact of increasing automation on the traffic flow.

Additionally, this dissertation demonstrated that trajectory data from real traffic can be used to control an adaptive speed reduction measure in real-time and to evaluate its effectiveness afterward using a speed prediction model. It is worth noting that, in this study, vehicle trajectories were captured using classical computer vision methods rather than neural networks, which have since become the state-of-the-art. As neural networks are expected to improve trajectory accuracy, their use will likely facilitate real-time applications. Future real-time applications could include adaptive traffic control systems, such as traffic signal optimization or ramp metering. However, the quality of trajectory data will continue to depend on camera perspectives and resolution, requiring ongoing quality evaluation and tailored data processing methods.

Regarding the use of trajectory data for developing and validating traffic flow models, this thesis found that drone-based trajectory data provide sufficient accuracy, provided that the data are thoroughly post-processed and checked for plausibility. The same applies to using trajectory data for deriving Surrogate Safety Measures to assess the crash risk of specific road sections.

Furthermore, a lane change model was developed to realistically describe driver behavior at freeway on-ramps. The model was derived using basic kinematic equations and calibrated

with trajectory data from real traffic. To validate the model and analyze its properties, additional data from traffic simulations were used. This model can make traffic simulations of freeway networks more realistic and improve predictions of interactions between human drivers and automated vehicles at freeway on-ramps. Moreover, future research could apply this model to develop new algorithms for ramp metering.

Although this thesis contributes to more precise two-dimensional driver behavior modeling, significant research gaps remain in this field. Despite the increasing presence of automated vehicles, this thesis focused on human driving behavior. This focus remains relevant since human drivers will continue to be part of road traffic for the foreseeable future. Understanding the interactions between human drivers and automated vehicles requires a deeper comprehension of human driving behavior, including its strengths and weaknesses regarding safety and efficiency. For this reason, this study deliberately refrained from using black-box machine learning models and instead relied on classical traffic flow theory. These models are based on relatively simple kinematic equations and they have interpretable parameters linked to real-world phenomena, enabling not only predictions but also a deeper understanding of human driving behavior.

Given the Vision Zero objective and the ongoing advancement of automated driving, there is an increasing demand for traffic safety while maintaining efficiency. As a result, future traffic flow models will increasingly focus on safety. This thesis takes a first step in this direction. The next steps involve further investigating the impact of driving behavior heterogeneity on safety and using traffic flow models to identify safety-critical situations and road designs in order to derive road designs and safety measures with reduced crash risks.